UNIVERSITY OF LIVERPOOL

Development of Small Intestinal Organoid Cultures for the Study of Enteric Pathogens

Thesis submitted in accordance with the requirements of the University of Liverpool for the degree of Doctor in Philosophy

by

Lisa Luu

September, 2017

Table of Contents

Abstract

The gastrointestinal tract is the major route of entry for enteric pathogens. Current models are not suited for the study of early invasion which limits the use of systems biology approaches to study host-pathogen interactions. Therefore, there is a demand to develop a suitable model to study early-stage host-pathogen interactions.

Recent developments in stem cell research have led to the establishment of "mini-gut" organoids that encapsulate the cellular diversity and structural arrangement of the small intestinal epithelium *in vivo.* Due to these features, they have been proposed as a promising tool for infection studies.

Several aspects of organoid optimization are required before exploiting this model for infection. Firstly, recent works have demonstrated the amenability of organoid cultures to be driven toward Paneth or goblet cell phenotype for the study of specialized host defence functions. However this model requires further validation. Secondly, luminal access is restricted, and infection can only be established via microinjection of pathogens. Lastly, mass spectrometry approaches have not yet been validated for use in these models.

This doctoral thesis addresses these issues by firstly validating the use of drug-skewed organoid models using quantitative label free mass spectrometry, and then by modifying cultures to establish differentiated and polarized murine epithelial monolayers with an accessible apical surface. This collagen-supported monolayer is exploited to study host-proteome changes during early infection with *Toxoplasma gondii* via quantitative label-free mass spectrometry.

Label-free mass spectrometry of Paneth and goblet-enriched organoids detected unique organoid proteome profiles that reflect the phenotype of these subpopulations as expected *in vivo*, and demonstrate the suitability of mass spectrometry to study changes in protein abundance in this model. Here, we also identified a protein, DNAJC3, enriched within Paneth cells which may play a role in specialized cell function or differentiation.

Modification of 3D organoid culture on collagen scaffolds has established a novel stem cell derived collagen-supported epithelial monolayer culture. Confocal microscopy demonstrated retention of differentiated features, such as the presence of Paneth and goblet cell sub-populations and apical polarization. Label-free mass spectrometry was used to detect the presence of intestinal epithelial cell markers in both 3D and collagen-supported epithelial sheets. The findings here demonstrate that many of the differentiated epithelial cell markers are detectable in the collagen-supported epithelial monolayer, and that this model can mimic the *in vivo* epithelial composition.

A series of pilot studies and time-course infection studies were performed to establish a working protocol to exploit the collagen-supported epithelial sheet for infection studies. Quantitative label-free mass spectrometry was exploited to examine host-proteome changes in response to infection with two strains of *Toxoplasma gondii*; Veg (type III, avirulent) and RH (type I, virulent). In agreement with current literature, we observed modulation of proteins associated with host cell cycling, apoptosis and lipid metabolism. Interestingly, we observed a lag in parasite replication compared to reported observations in cell line cultures and an aggregative behavior along epithelial sheet perimeters previously not reported. The findings in this chapter demonstrate the suitability of this model for infection studies, and highlights some parasite behaviours that are not observed in cell line models.

List of Tables

List of Supplementary Tables

List of Figures

List of Abbreviations

2D	2-Dimensional
3D	3-Dimensional
AF488	Alexa Fluor 488
AF647	Alexa Fluor 647
AMP	Anti-Microbial Peptides
BMI1	Polycomb Group Protein
BMP	Bone Morphogenesis Protein
CDC	Centres for Disease Control and Prevention
CHIR	CHIR 99021
Crypt	Crypt Columnar Base Units
DAPI	4',6-diamidino-2-phenylindole
DAPT	*N*-[(3,5-Difluorophenyl)acetyl]-L-alanyl-2-phenyl]glycine-1,1-dimethylethyl ester
DEFA	Alpha-Defensin
EDTA	Ethylenediaminetetraacetic acid
F-Actin	Filamentous Actin
FITC	Fluorescein isothiocyanat
FSA	Food Standards Agency
GRA	Dense Granules
IFN-γ	Interferon Gamma
IL	Interleukin
IWP-2	Inhibitor of WNT Production-2
LGR5	Leucine-Rich Repeat-Containing G-Protein Coupled Receptor 5
LYS	Lysozyme
MIC	Micronemal Protein
MMP7	Matrilysin 7
MUC2	Mucin-2
NAC	N-Aceytl L-Cysteine
NF-κB	Nuclear Factor Kappa-Light Chaing-Enhancer of Activated B Cells
PBS	Phosphate Buffer Solution
PFA	Paraformaldehyde
PV	Parasitophorous Vacuole
ROP	Rhoptry Protein
SAG	GPI-Anchored Surface Antigens
TLR	Toll-Like Receptor
UK	United Kingdom
USA	United States of America
WHO	World Health Organisation
Wnt	Wingless-Related MMTV Integrated Site
ZO	Zonula Occludens

Acknowledgements

This doctoral project would not have been possible without the support and guidance of a multitude of people. Firstly, I would also like to thank both the University of Liverpool and the Biotechnology and Biological Sciences Research Council (BBSRC) for funding this DTP project. Without their financial support, none of this would be possible.

Secondly, I'd like to express my gratitude to my supervisors, Dr Janine Coombes, Professor Paul Wigley and Professor Jonathan Wastling. Janine, you have been an amazing supervisor and you made me feel at ease from the very first day that I joined the project and became the first member of Team Coombes and Team Organoid. Thank you for everything you have taught me!

I'd like to thank everyone in both the Coombes' and Wastling group for your scientific discussion and support. Particularly, Dr Hayley Derricott and Dr Laetitia Petit-Jentreau for helping me shape this thesis to tell my story, and Dr Nadine Randle, Dr Stuart Armstrong and Dr Dong Xia for their proteomic genius and guidance. I will also be forever grateful to Professor Julian Hiscox who shared his resources with me for the analysis of proteome data.

Thank you to the technical team at UoL, especially Catherine Hartley who helped me immensely with cell and parasite culture, the Biological Specimens Unit (BSU) for taking such good care of our mice, and the Centre for Cell Imaging (CCI) for providing us with such a fantastic imaging facility. A huge thanks to my colleagues in IC2 (Tess, Jen, Elsa and Tasha) and my DTP cohort (Kerry, Jess and Edd) – you guys have made this experience so enjoyable.

Lastly, a massive thank you to my family and friends; my siblings, my parents, the Gao-Coleman's, Chan's, McDonald's and Melody for being so un-scientific that you allow me to clear my brain and momentarily forget about work! In particular, a huge thank you to my boyfriend Craig, who has been so supportive and understanding throughout this time.

Authors Declaration

The work presented in this thesis was performed solely by the author except where the assistance of other has been acknowledged.

Lisa Luu

September 2017

Chapter 1 – General Introduction

1.1 The Impact of Enteric Diseases

Food-borne illnesses have major impacts on both human and animal health and are a major cause of morbidity and mortality on a global scale (World Health Organisation, 2015). However, the global public health burden of food-borne diseases is not fully quantified. In 2006 the world health organisation (WHO) recognised the significance of food-borne diseases and launched an initiative to accurately estimate the global burden of food-borne diseases (Kirk et al., 2015; World Health Organisation, 2015). Since the establishment of this initiative, over 200 pathogens have been identified as causing food-borne disease in humans with varying symptoms and severity of disease (World Health Organisation, 2015). Of these 200 pathogens, 32 pathogens have been attributed as the cause of over half of all cases of food-borne disease (World Health Organisation, 2015). These 32 disease agents can be further characterised into either diarrhoeal disease-causing, invasive infectious disease-causing, enteric intoxications and helminthic agents (**Table 1**) (World Health Organisation, 2015). In 2010, these 32 pathogens were estimated to have caused 600 million incidences of food-borne diseases globally resulting in 420,000 deaths, with over 40% of cases of diseases reported in children under the age of 5 (World Health Organisation, 2015).

Table 1). Major Causes of Food-Borne Illnesses as Reported by WHO in 2015	
Diarrhoeal Disease Agents	
Norovirus	Virus
Campylobacter spp. Enteropathogenic *Escherichia coli* Enterotoxigenic *Escherichia coli* Shiga toxin-producing *Escherichia coli* Non-typhoidal *Salmonella enterica* *Shigella* spp. *Vibrio cholerae*	Bacteria
Entamoeba histolytica *Cryptosporidium* spp. *Giardia* spp.	Protozoa
Invasive Infectious Disease Agents	
Hepatitis A Virus	Virus
Brucella spp. *Listeria monocytogenes* (perinatal) *Listeria monocytogenes* (acquired) *Mycobacterium bovis* *Salmonella* Paratyphi *Salmonella* Typhi	Bacteria
Toxoplasma gondii (congenital) *Toxoplasma gondii* (acquired)	Protozoa
Enteric Intoxications	
Bacillus cereus *Clostridium botulinum* *Clostridium perfringens* *Staphylococcus aureus*	Bacteria
Helminths	
Echinococcus granulosus (cases seeking treatment) *Echinococcus granulosus* (cases not seeking treatment) *Echinococcus multilocularis* *Taenia solium*	Cestodes
Ascaris spp. *Trichinella* spp.	Nematodes
Clonorchis sinensis *Fasciola* spp. Intestinal flukes *Opisthorchis* spp. *Paragonimus* spp.	Trematodes

The incidence of food-borne diseases is globally variable with the highest burdens associated with low-income regions, namely Africa and South-East Asia (World Health Organisation, 2015). These infections are primarily associated with diarrhoheal disease agents, whereas in the USA the CDC reports that the most common causative agents are Norovirus, *Salmonella, Clostridium perfringens, Campylobacter* and *Staphylococcus aureus* (Centres for Disease Control and Prevention, 2017). The WHO reports that premature mortality can be attributed to diarrhoeal-causing agents, but infections with helminths such as *Taenia solium, Ascaris* spp and *Fasciola* spp, along with the protozoal parasite *Toxoplasma gondii* contribute to a large proportion of cases of long term morbidity as a result of food borne illness (World Health Organisation, 2015). The global burden of food-borne diseases in 2010 was estimated at 33 million disability-adjusted life years (DALYs), with over half of these attributed to diarrhoeal disease causing pathogens; Norovirus, *Campylobacter,* enteropathogenic and enterotoxigenic *E. coli, Vibrio cholera* and *Shigella*, causing 1-3 million DALYs each (World Health Organisation, 2015). Of the invasive infectious disease agents, *Salmonella* Typhi caused 3 million DALYs, with *Salmonella* Paratyphi and *Toxoplasma gondii* causing approximately 800,000 DALYs each (World Health Organisation, 2015).

Due to the large number of causative agents of food-borne disease, there are difficulties diagnosing disease. Many of these pathogens exhibit non-specific symptoms that are acute and self-limiting, so often patients do not seek medical care. However, in some cases, a lack of treatment and the development of chronic infection can lead to the development of complicated morbidities such as haemolytic uraemic syndrome, inflammatory bowel disease, organ failure, and in cases of congenital *Toxoplasmosis*, foetal neurological damage, visual impairment or sporadic abortions in sheep

(Montoya and Liesenfeld, 2004; Munday and Dubey, 1986; Rees et al., 2004; SYROCOT, 2007; Tarr et al., 2005). The development of chronic diseases can often be wrongly diagnosed and not attributed to the initial enteric infection. For these reasons, the numbers of cases reported by the WHO are considered conservative estimates. In reality, the true burden of food-borne illness may be much higher, especially in low-resource areas where diagnosis and reporting of diseases is not well documented.

The burden of these food-borne infections has economic impacts due to the cost of healthcare in both acute and chronic infections leading to a loss of workforce productivity, and the loss of agriculture productivity in cases of animal infections.

1.2 Enteric Diseases in Food-Producing Animals

To truly understand how to prevent the incidence of food-borne disease in humans, we must consider the role of zoonotic enteric infections in disease transmission, particularly in food-producing species. Enteric infections in food-animals are a common zoonotic risk of human enteric disease through the ingestion of contaminated meat and dairy products (Centres for Disease Control and Prevention, 2017; Kirk et al., 2015; World Health Organisation, 2015). In some cases, infections can be asymptomatic in livestock resulting in a lack of prompt pathogen detection and onward transmission throughout flocks and to the human population. In particular, *Campylobacter* spp. infections can asymptomatically infect broiler chickens making them an important reservoir for human infections through the consumption of undercooked meat products, and environmental contamination (Larson and Spickler, 2013). Due to close housing practices of food-producing animals, pathogen shedding

from a single animal can rapidly result in the spread of disease throughout a herd or flock of animals (Hollenbeck, 2016; Kleinlützum et al., 2013; Lupindu et al., 2015). This is reflected by the multitude of enteric pathogens contaminating food-products including *Listeria monocytogenes* in beef, *Salmonella* in stir fry products and turkey products, and *Escherichia coli* 0157 in cheese products as reported by the Food Standards Agency (FSA) (Food Standards Agency, 2017). Therefore, the incidence of disease in animals, especially food-producing animals, bears huge importance for the prevention of disease in humans.

The emergence of antimicrobial resistance means that these infections are becoming increasingly difficult to treat, and new treatments or vaccines are urgently required. Recently, resistance in several pathogens including carbapenem-resistant *Klebsiella pneumoniae*, fluoroquinoline-resistant *E. coli*, artemisin-resistant *Plasmodium faciparum* and multi-drug resistance in *Mycobacterium tuberculosis* have been identified as pressing threats to public health (Glasner et al., 2013; Pickering, 2004; Smith et al., 2013; WHO, 2014). To combat antimicrobial resistant strains, the development of novel vaccines and therapeutics are urgently required. To do this, a better understanding of the earliest post-infection events, such as pathogen-epithelial cell interactions and the initiation of mucosal immune responses is required. This requires species-appropriate sophisticated models of the intestinal epithelium.

1.3 The Gastrointestinal Tract as a Route of Infection

As food-borne pathogens are ingested into the host, the gastrointestinal (GI) tract is a major system in determining the outcome of infection. Following ingestion, enteric pathogens enter the host gastrointestinal tract, consisting of the stomach, small and

large intestines, colon and the rectum where initial invasion events may take place. Enteric pathogens differ in their host-pathogen interactions with some species exhibiting site-specific invasion patterns. For example, protozoal *Eimeria* spp exhibit a high degree of site specificity to invade distinct anatomical regions within the host intestine (Augustine, 2001). Similarly *Giardia* spp infect the duodenum and jejunum of the small intestine nut not the ileum (Wolfe, 1992). These site specific invasion strategies directly impact the host cell response to infection, as demonstrated by *Campylobacter jejuni* infection of human ileal and colon tissues *in vitro*, which induced different levels of IL-8 secretion in response to bacterial invasion (MacCallum et al., 2006).

Due to its anatomical location as one of the first sites to become exposed to the pathogen, the small intestine is considered a major route of infection. Following ingestion, pathogens reach the small intestine where initial invasion events may take place. Studying these early stage host-pathogen interactions are key for the identification of novel targets for the prevention of enteric disease within this organ. To do this, we must firstly understand the small intestinal homeostatic processes. Several aspects of intestinal biology will be discussed here; gut homeostasis and the renewal of the epithelium, the signalling pathways that drive this process, secretory cells of the intestine and their roles in host defence and the tight junctions of the epithelium for host defence.

1.3.1 Small Intestinal Epithelial Regeneration

The intestinal epithelium can be considered as the crypt domain, transit amplifying region and villus domain, all of which undergo continual regeneration as part of gut

homeostasis (**Figure 1** and **Figure 2**). The continual regeneration of the small intestinal epithelium is facilitated by the presence of intestinal stem cell populations which can be identified by specific markers leucine-rich repeat-containing G-protein coupled receptor 5 (LGR5+), polycomb group protein (BMI1+) and atypical homeobox protein (HOPX) (Barker et al., 2007; Montgomery and Breault, 2008; Yan et al., 2012).

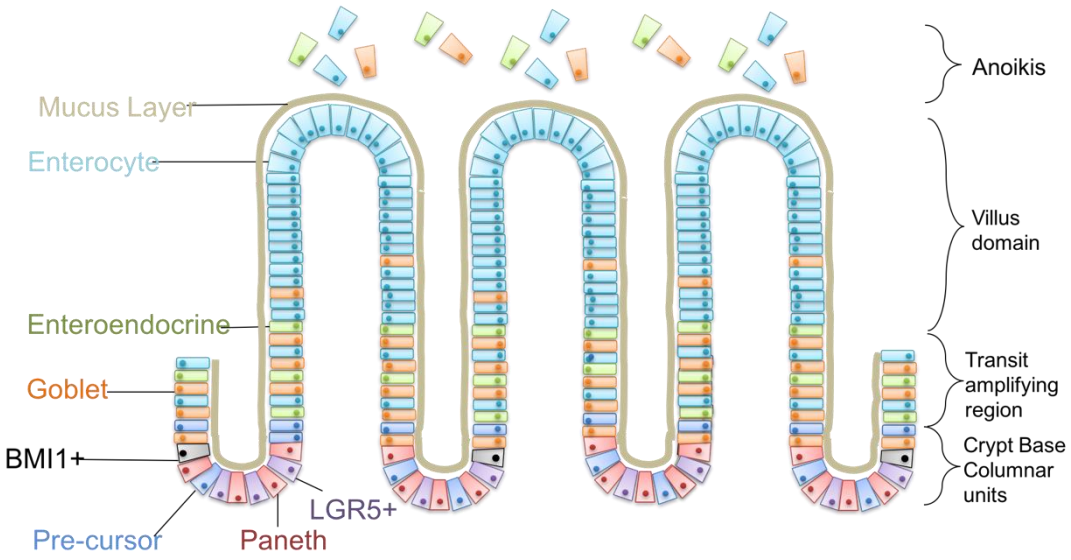

Figure 1) Anatomy of the small intestine

Self-regeneration of the small intestinal epithelium is primarily facilitated by the LGR5+ stem cell population at the base of the crypt base columnar units, which then proliferate and differentiate into each of the intestinal epithelial cell types (Paneth, goblet, enteroendocrine and enterocytes) within the transit amplifying region under exposure to different signalling cascades. As new cells are generated, the older cells are pushed further along from the base of the crypt columnar unit up into the villus tip where they are eventually shed into the lumen via a process called anoikis, with the exception of Paneth cells that migrate downwards toward the base of the crypt. Another stem cell population at the +4 location (BMI1+) can also give rise to all the differentiated epithelial cell types, however the regenerative role of this sub-population is not well understood.

Within the crypt domain lie two intestinal stem cell populations; LGR5+ cells at the base of the crypt, and BMI1+ cells at the +4 location relative to the crypt base (**Figure 1**) (Barker et al., 2007; Bevins and Salzman, 2011; Specian and Oliver, 1991; Yan et al., 2012; Zhu et al., 2013). The LGR5+ stem cells are thought to function as the main source of regeneration, whereas BMI1+ cells are quiescent (Dehmer et al., 2011; Yan et al., 2012; Zhu et al., 2013). However, the relationship between these sub-populations is not fully understood. It has been suggested that +4 cells expressing atypical homeobox protein (HOPX) can give rise to crypt base columnar cells, and that crypt base columnar cells can similarly generate HOPX-expressing +4 stem cells demonstrating a bidirectional relationship between these populations (Takeda et al., 2011). This suggests that the functional role of the two subpopulations may be determined upon the environmental cues to increase or suppress proliferation of either population. Furthermore, the expression of known stem cell markers LGR5 and BMI1, which were previously thought to be population-specific, are now known to be co-expressed within crypt base columnar cells (Itzkovitz et al., 2011). Clearly, the intestinal stem cell populations are not fully understood, however the mechanisms of homeostasis and epithelial regeneration have been identified.

$LGR5^+$ stem cells proliferate at the base of crypt columnar units, to push daughter cells upwards through the transit amplifying region where they terminally differentiate into distinct epithelial cell types; mucin-secreting goblet cells, hormone-secreting enteroendocrine cells or absorptive enterocytes (Garcia et al., 2009; He et al., 2004; Kuhnert et al., 2004; Milano et al., 2004; Nakamura et al., 2007; Turck et al., 2006; VanDussen et al., 2012; Walton et al., 2015; Zhang and Li, 2005). Through the action of LGR5+ cell proliferation, older cells are eventually pushed to the villus tip where

they undergo a form of programmed cell death, termed anoikis, and are sloughed off into the lumen and routinely removed with the mucus layer (Gilmore, 2005) (**Figure 1**). Unlike other epithelial cells, anti-microbial (AMPs) secreting Paneth pre-cursor cells migrate downwards towards the crypt base columnar units where they terminally differentiate and reside alongside $LGR5^+$ stem cells (Bry et al., 1994; Farin et al., 2012; Toshiro Sato et al., 2011).

Stem cell proliferation and differentiation are tightly controlled by several signaling pathways as part of normal gut homeostasis. Three pathways have been identified that determine the outcome of cell differentiation; Wingless-Related MMTV Integrated Site (Wnt), Notch and bone morphogenesis protein (BMP) signaling (**Figure 2**) (Fevr et al., 2007; He et al., 2004; Nakamura et al., 2007; Ormestad, 2006; Pin et al., 2012; Yang et al., 2001; Yin et al., 2014).

Within the intestine, Wnt signaling is highest within the crypt base columnar units and decreases towards the villus tip, whereas BMP signaling is the inverse, increasing toward the villus tip (**Figure 2**). Notch signaling can be observed throughout the transit amplifying region and at the border of the crypt base columnar units (**Figure 2**). Under these signaling pathways, intestinal stem cells terminally differentiate into four major epithelial cell types; absorptive enterocytes, or secretory Paneth, goblet or enteroendocrine cells to replenish the small intestinal epithelial cell population (**Figure 2 B**).

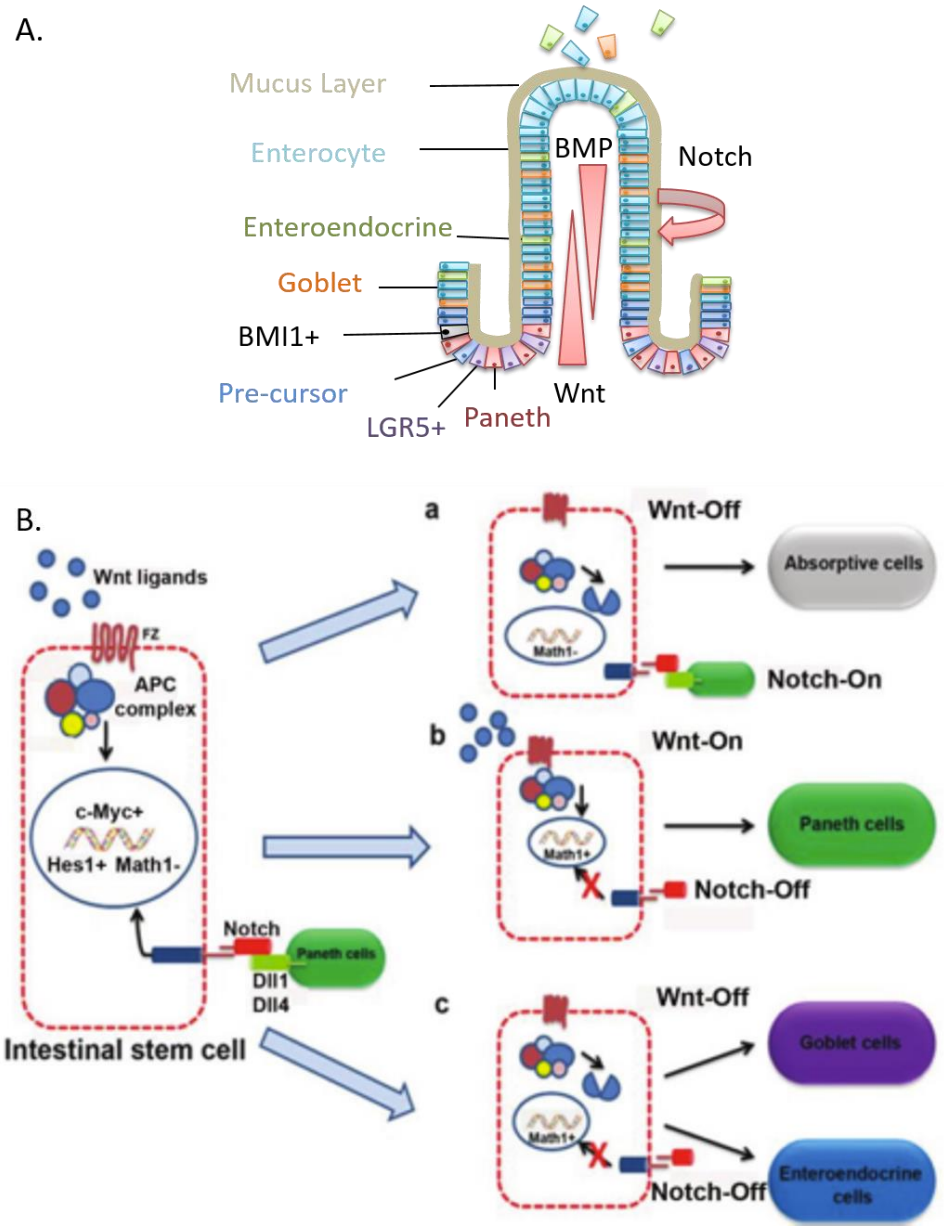

Figure 2) Intestinal stem cell signalling cascades, modulating self-renewal and cell differentiation

A) At the very base of the crypt in the absence of Notch signaling, lie Paneth cells that provide a source of Wnt signaling within the epithelium to maintain stem cell proliferation. Moving upward, Wnt signaling becomes weaker, allowing for the differentiation of epithelial cells within the transit amplifying region. Toward the tip of the villus BMP signaling is strongest, which inhibits cell proliferation and replication. B) Under the conditions in the small intestine, stem cells terminally differentiate into four major lineages of epithelial cells; absorptive enterocytes, or secretory cells Paneth, goblet and enteroendocrine cells (Clevers, 2006; Clevers and Nusse, 2012; Lazzeri et al., 2012; VanDussen et al., 2012).

1.3.2 Wingless-Related MMTV Integrated Site (Wnt) Signalling Modulates Cellular Proliferation

The Wnt signalling pathway plays a major role in the maintenance and activation of the intestinal stem cell population. There are 5 mammalian intestinal Wnt proteins, which upon binding to the Frizzled (FZ)/low density lipoprotein (LDL) receptor-related protein (LRP) complex, induces the inactivation of glycogen synthase kinase 3β (GSK3β), a major component of the β-catenin destruction complex (**Figure 3**) (Clevers and Nusse, 2012; Logan and Nusse, 2004). The inactivation of GSK3β leads to a de-phosphorylation and migration of β-catenin into the cell nucleus to interact with transcription factors (TCF) to activate target genes (**Figure 3**) (Clevers and Nusse, 2012; Nakamura et al., 2007; Toshiro Sato et al., 2011; Spence et al., 2010). Specifically, mutational activation of TCF4 induces adenoma formation, whereas it's removal results in the loss of the proliferative cell population (Korinek et al., 1998).

The presence of a Wnt signalling gradient originating in the crypt domain allows for the terminal differentiation of daughter cells within the transit amplifying region of the villus domains. An accumulation of β-catenin has been observed in the cells of the crypt columnar base units where the intestinal stem cells are located, and with a reduced effect in epithelial cells located towards the top of the crypt unit and within the villi forming a Wnt signalling gradient (Haegebarth and Clevers, 2009). Under normal gut homeostasis, newly produced daughter cells migrate from the crypt to the villus tip, however an exception to this rule are Paneth cells which migrate toward the source of Wnt signalling at the base of the intestinal crypt units. Studies of cell differentiation have determined that the Paneth cell population is critically dependent upon the presence of TCF4 activation for complete maturation and terminal differentiation in the small intestine (Es et al., 2005; Farin et al., 2012). *In vitro,* Paneth

cells provide essential niche signals including Wnt3a to LGR5+ stem cells which contributes to the maintanence of stem cell proliferation, and a Wnt gradient (Toshiro Sato et al., 2011).

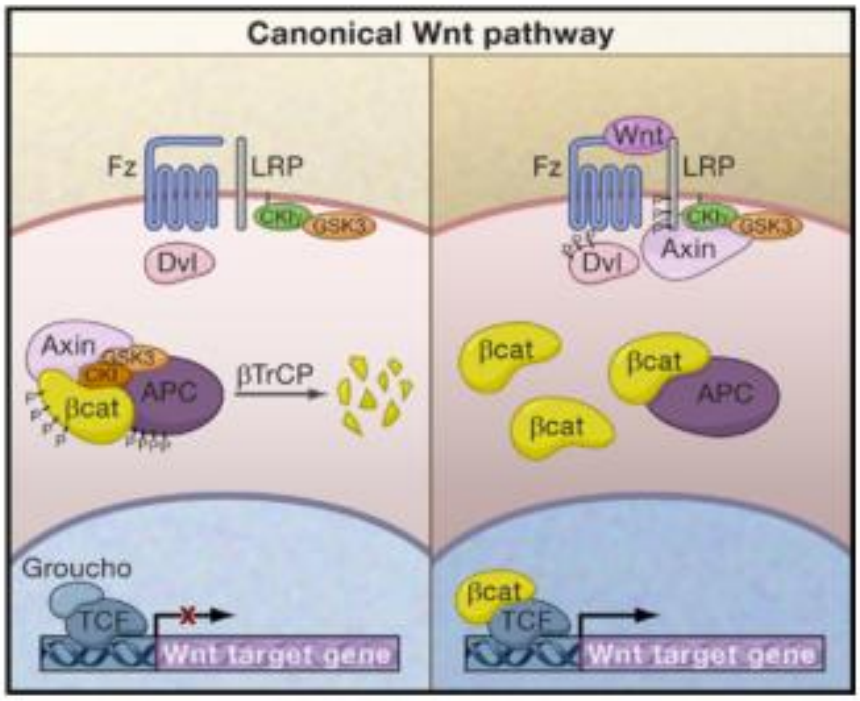

Figure 3) Canonical Wnt signalling pathway

(Left panel) In the absence of ligand, the frizzled (fz) receptor remains unbound and β-catenin is a target for ubiquitination and degradation by the proteasome. (Right panel) In the presence of ligand, binding to a Fz/LRP5/6 complex stabilizes β-catenin through the inactivation of GSK3β, resulting in the migration of β-catenin into the nucleus and activation of downstream transcriptional factors (Clevers, 2006; Clevers and Nusse, 2012)

Wnt signalling is regulated by the R-spondin family (RSPO) of secreted proteins (**Figure 4**). There are four known members of the R-spondin family with high shared homology and expression patterns. All four RSPO are ligands for the Wnt signaling receptor complex and are capable of activating the Wnt signalling pathway, with the highest potency attributable to RSPO2 and 3, followed by RSPO1 and poor activation

by RSPO4 (Kim et al., 2008). Currently, very little is known about the source of R-spondin *in vivo*, however there is evidence to suggest that the intestinal stroma may be a potential source of these proteins (Kang et al., 2016).

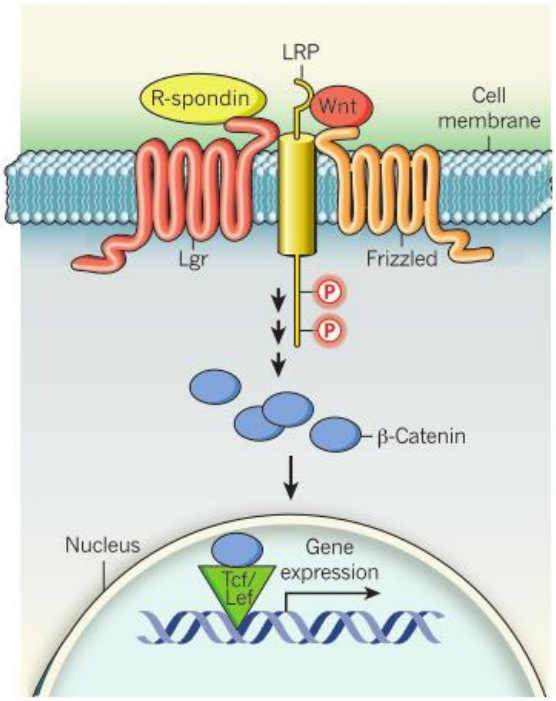

Figure 4) Co-operative signalling within stem cells

R-spondins activate membrane protein LGR, which is also a stem cell marker protein. LGR recruits the LRP-frizzled receptor complex, which binds to Wnt ligands, and reinforces Wnt signalling after phosphorylation of LRP. B-catenin is then stabilised and translocated to the nucleus, which induces gene expression (Birchmeier, 2011).

It is evident that Wnt signaling regulates the proliferative ability of stem cells, however the differentiation of other cell lineages requires a fine-tuned balance of additional signalling pathways.

1.3.3 The Notch Signalling Pathway Determines Secretory Cell Fate

Like Wnt signalling, Notch signalling occurs within the crypt domains, however, can also be detected in proliferating cells at the border of the crypt domain and the transit amplifying region (Tian et al., 2015).

Notch receptors are activated through binding with a neighboring cell presenting an appropriate ligand. The majority of Notch signalling is induced by a family of Delta, Serrate and Lag2 domain (DSL) ligands. Mammalian DSL ligands are classified into Delta-like (Dll1, Dll3 and Dll4) or Serrate (Jagged)-like (Jagged 1 and Jagged 2) (Kopan and Ilagan, 2009). The binding of these ligands induces a series of proteolytic cleavage steps in Notch, which ultimately releases the intracellular domain which functions as a biologically active signal transducer.

Upon ligand binding, the conformational change to the Notch receptor makes this complex susceptible to cleavage by an A-Disintegrin-And-Metalloprotease (ADAM). Notch cleavage generates a membrane-anchored extracellular fragment (NEXT), which is a substrate for γ-secretase. Γ-secretase then cleaves the Notch transmembrane domain to release an active form; Notch intracellular domain (NICD). NICD enters the nucleus associating with DNA binding CSL, which ultimately activates transcription (Kopan and Ilagan, 2009; Nakamura et al., 2007; VanDussen et al., 2012).

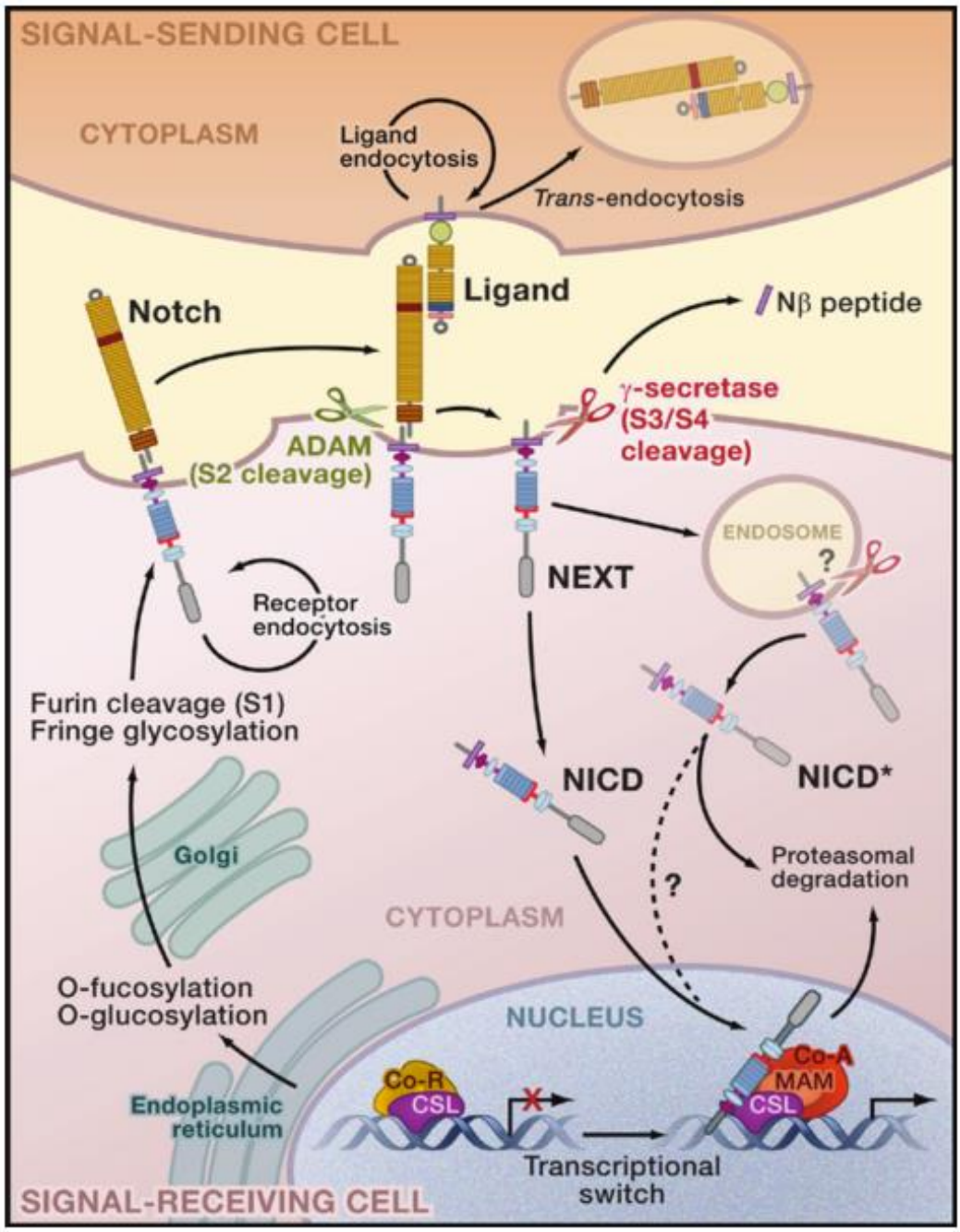

Figure 5) The Notch signalling pathway

Upon activation of this signalling pathway, Notch proteins are cleaved by ADAM metalloproteases to generate a Notch extracellular truncation (NEXT) fragment. NEXT is cleaved by γ-secretase, releasing the Notch intracellular domain (NICD) which enters the cell nucleus to associate with DNA-binding CSL. This association leads to an activation of down-stream transcription involved with suppression of secretory cell lineages (Kopan and Ilagan, 2009; Nakamura et al., 2007; VanDussen et al., 2012).

The presence or absence of active Notch signaling determines the fate of secretory cell lineages within the small intestine, and several genes have been identified that regulate this process basic helix-loop-helix (bHLH) transcription factors (*Hes1*) and atonal homolog 1 (*Atoh1*) (Schonhoff et al., 2004; VanDussen et al., 2012). Under active Notch signaling, progenitor cells follow the absorptive enterocyte cell lineage, however in the absence of Notch signaling, progenitor cells differentiate along the secretory cell lineage at the expense of absorptive cell differentiation (**Figure 6**) (Jensen et al., 2000; Tian et al., 2015; VanDussen et al., 2012).

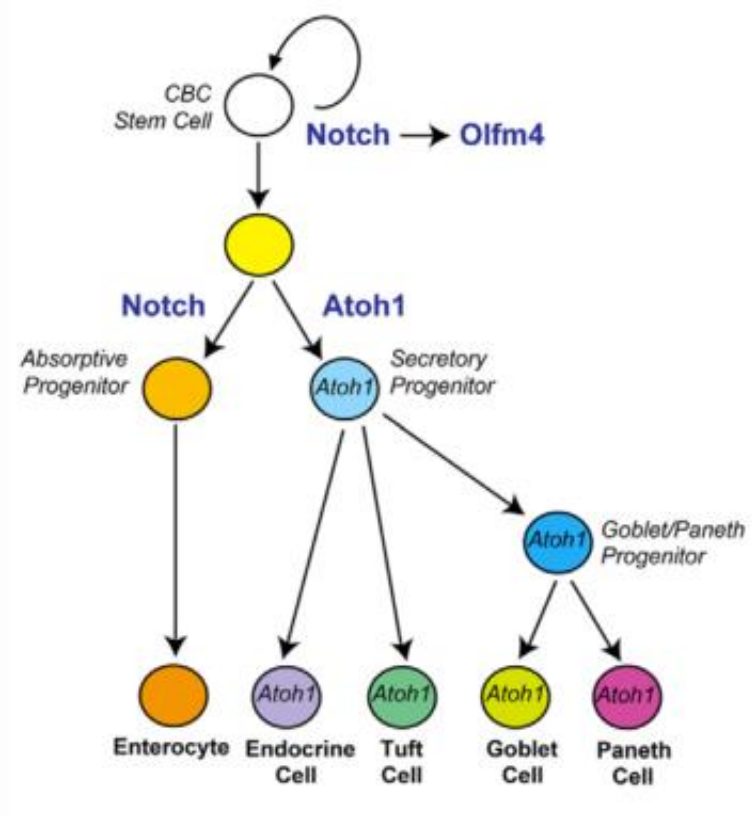

Figure 6) Notch signalling regulates secretory cell homeostasis

Notch signalling directly targets stem cells to activate olfactomedin-4 (OLFM4) transcription to maintain stem cell proliferation and promotion of cell survival. Notch acts to promote absorptive cell lineage through suppression of *ATOH1* transcription. Later, Notch indirectly segregates Paneth and goblet cell lineage to generate a mature Paneth cell phenotype, however this mechanism is not fully understood (VanDussen et al., 2012)

Disrupting Notch signalling with a γ-secretase inhibitor DAPT, blocks the conversion process of the Notch receptor into its transcriptionally active form, which results in a loss of proliferating LGR5+ stem cells within crypt domains, and an increased proportion of secretory cell types (VanDussen et al., 2012). Notch signalling must therefore act by suppressing the differentiation of secretory cells leading to the sporadic distribution of these cell types within the small intestine *in vivo* (Schonhoff et al., 2004; Tian et al., 2015; Yin et al., 2014).

The determination of secretory cell fate is not regulated by Notch signalling alone. Blocking of Notch signalling, and attenuation of Wnt signalling increases the number of goblet cells and suppressed stem cell proliferation, and there is evidence to suggest an upregulation of Wnt underlies secretory cell amplification when Notch signalling is removed (Tian et al., 2015).

1.3.4 Bone Morphogenesis Protein Signalling (BMP) Represses Cell Replication

Bone morphogenesis proteins (BMP) are involved with tissue re-modelling and regeneration. There are currently over 20 known BMPs classified as a subset of transformation growth factor beta (TGFβ) proteins (Zhang and Li, 2005). There are three type 1 BMP receptors; ALK2, ALK3 (BMPR1A) and ALK6 (BMRPR1B), and one type 2 BMP receptor, (BMPRII) (Zhang and Li, 2005). The BMP signalling cascade can be trigger by BMPRII in combination with any type 1 receptor, leading to different downstream processes dependent upon the stem cell niche (**Figure 7**) (Miyazono et al., 2005; Wang et al., 2014; Zhang and Li, 2005).

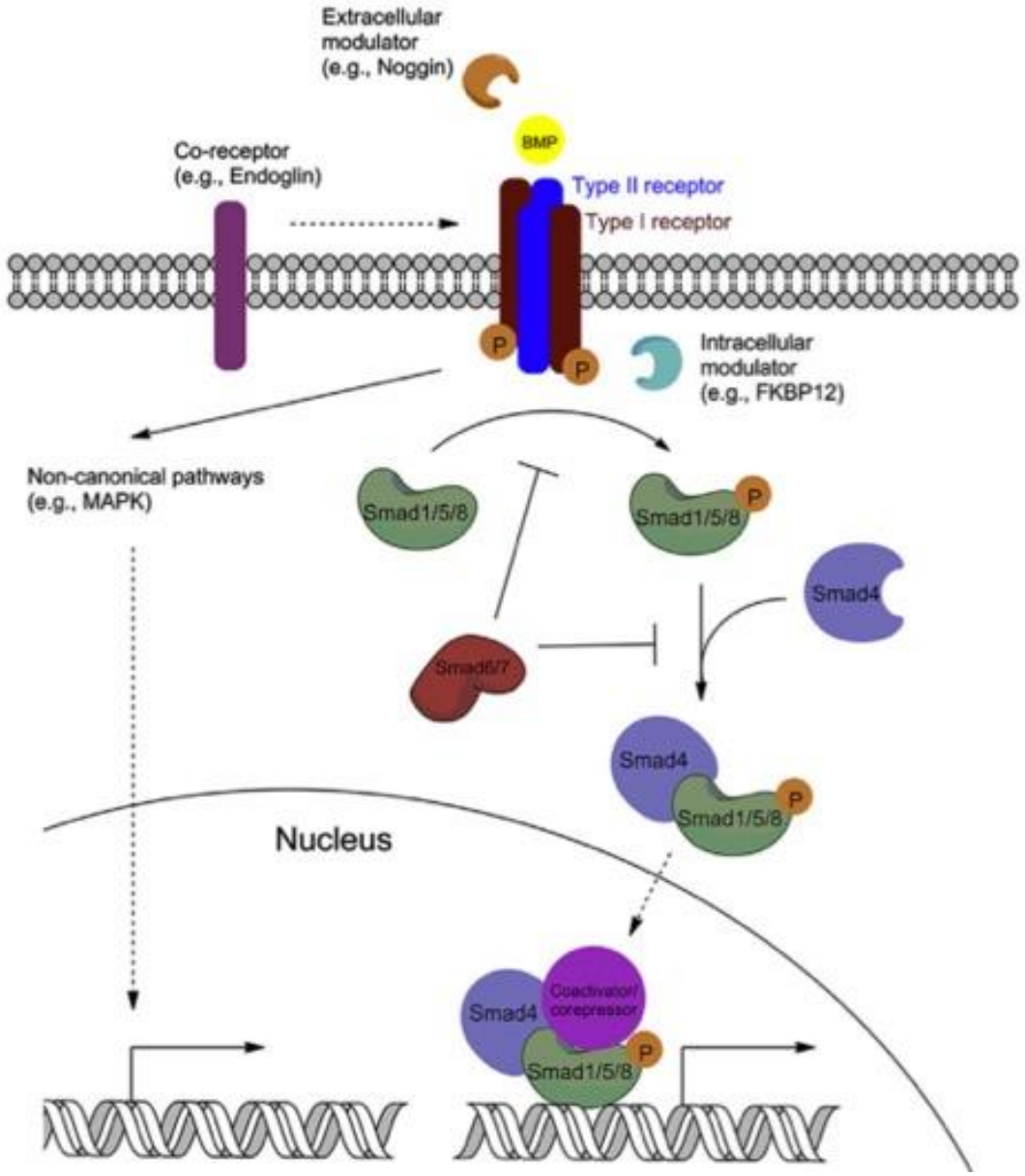

Figure 7) BMP signalling pathway via canonical Smad-dependent and non-canonical pathways

During canonical activation, binding to type I or type II serine/threonine kinase receptors by BMP ligands forms a complex. The constitutively active type II reporter transphosphorylates the type I receptor, which phosphorylates R-smads (smad1/5/8). Phosphorylated R-smads associate with smad-4 and translocates into the nucleus. Here, the complex associates with co-activators or –repressors to regulate gene expression (Wang et al., 2014).

Within the small intestine, BMP signalling occurs primarily in the mesenchymal cells neighbouring villus epithelial cells and is regulated by noggin to suppress Wnt β-catenin signalling (He et al., 2004). The suppression of Wnt represses stem cell proliferation and replication (Haramis et al., 2004; He et al., 2004). The suppression of "stemness" allows for the terminal differentiation of epithelial cells through the transit amplifying region.

To date, the interactions between signalling pathways, remains to be fully clarified and the role of these following injury or invasion by enteric pathogens are still unknown. In tandem, these signalling cascades give rise to differentiated epithelial cell types which are important for small intestinal functions in both nutrient absorption and host defence against invading pathogens.

1.4 Secretory Epithelial Cells Play a Significant Role in Host Defence

As the site of initial exposure, the small intestine must defend against invading pathogens whilst maintaining a balance of healthy gut microbiota. To do this, it relies on the presence of differentiated secretory cells that each have distinct roles in host defence, the immune system and nutrient absorption.

1.4.1 Goblet Cells Renew the Mucus Barrier

The first line of intestinal defence is the presence of a highly-glycosylated mucus barrier loosely adhered above the epithelial cell layer (**Figure 1**). This mucus layer traps and physically separates invading microorganisms from the underlying epithelial cells to protect the host, and like the epithelium itself, is routinely renewed to facilitate microbial clearance (Ermund et al., 2013a, 2013b; Rodriguez-Pineiro et al., 2013).

The regeneration of the mucus layer is driven by the presence of goblet cells sporadically distributed along the intestinal epithelium. These specialised secretory cells continually replenish the mucus layer through secretion of mucus components such as mucin-2 and trefoil factor 3 (Birchenough et al., 2015; Ermund et al., 2013a, 2013b; Hansson, 2012; Johansson et al., 2013; Pelaseyed et al., 2014; Rodriguez-Pineiro et al., 2013). In addition to contributing to a physical barrier against invading pathogens, mucus components themselves play roles in activation of host immune response to infection. For example, deficiency of trefoil factor 2 , a gastrointestinal secretory protein, is reported to protect host cells from low-dosage infection of *Toxoplasma gondii* (McBerry et al., 2012). Here it is reported that trefoil factor 2 plays a role in mucosal barrier function and the release of type I cytokines during oral infection (McBerry et al., 2012). More recently, Wlodarska *et al.,* 2014 demonstrated that disruption to normal goblet cell function in mice leads to deficient microbial clearance within the gut, resulting in persistent *Citrobacter rodentium* and *Salmonella enterica* infections, which demonstrates the importance of this secretory cell lineage for host intestinal defence (Johansson and Hansson, 2014; Wlodarska et al., 2014).

1.4.2. Paneth Cells Secrete Antimicrobial Peptides

As well as goblet cells, Paneth cells also play a significant role in host defence. Some enteric pathogens have evolved mechanisms to exploit or avoid the mucus barrier to establish infections. Upon reaching the epithelial cells, microbial stimulation causes Paneth cells of the crypt domains to secrete AMPs such as lysozyme and alpha-defensins into the crypt lumen to regulate intestinal ecology (Clevers and Bevins, 2013; Elphick and Mahida, 2005; Farin et al., 2014; Fernandez et al., 2008; Peeters and Vantrappen, 1975; Wilson, 1999). In particular, Paneth cell AMPs are important

for the regulation of bacterial pathogens such as *Salmonella* and *Shigella* (Fernandez et al., 2008; Salzman et al., 2003a, 2003b).

Defects in either of these differentiated cell types can lead to significant disease thus play an important role in maintaining gut homeostatic processes and protection against invading pathogens.

1.5. Tight Junctions of the Epithelium Inhibit Pathogen Invasion

The intestinal epithelium acts as a barrier between microbes in the lumen and the host mucosal immune system in the underlying lamina propria. Maintenance of a secure barrier is heavily dependent upon the presence of tight junctional proteins (**Figure 8**) (France and Turner, 2017).

Paracellular permeability is regulated through protein complexes known as tight junctions which reside just beneath the apical surface of adjacent cells (**Figure 8**). Epithelial permeability is variable throughout the small intestine dependent upon the tight junctional complex which consists of three families of proteins; occludin, claudin and junctional adhesion molecules (JAM) (Citi and Cordenonsi, 1998; Wells et al., 2014). Beneath tight junctions lie adherens junctions, desmosomes and gap junctions to regulate intracellular signalling and cell-cell adhesion (**Figure 8**) (France and Turner, 2017; Wells et al., 2014). The presence of these tight junctional complexes compartmentalises the luminal contents from the underlying *lamina propria* to support epithelial polarisation (Oshima and Miwa, 2016).

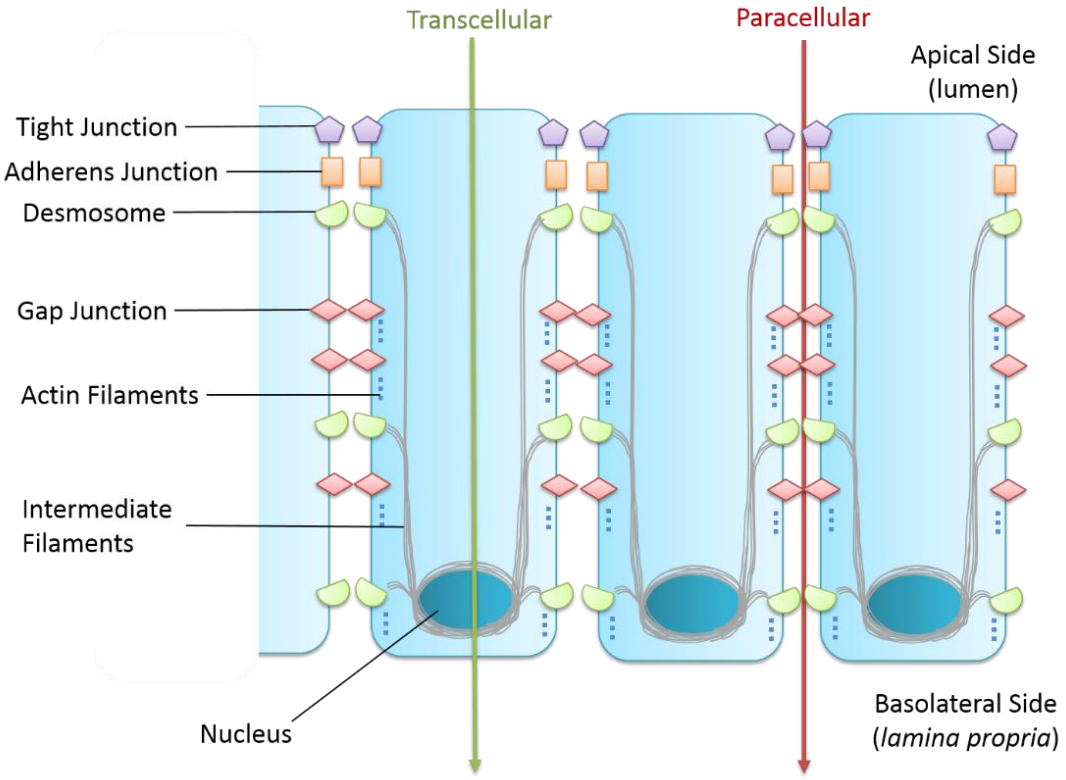

Figure 8) A simple schematic representing the arrangement of epithelial cell junctions. Tight junctions form at the apical junction and laterally connect neighbouring epithelial cells. Tight junctions allow for paracellular selection of small molecules. Adherens junctions and desmosome regulate cell-cell adhesions and intracellular signalling to maintain epithelial integrity. Gap junctions and desmosomes associate the remaining lateral membranes. Intermediate filaments dock into desmosomes whereas actin filaments attach to tight junctions and adherens junctions [Figure is modified and adapted from (Guttman and Finlay, 2009; Wells et al., 2014)].

Although tight junctions can restrict microbial access to the underlying *lamina propria* some enteric pathogens have evolved mechanisms to disrupt tight junctions during invasion including using tight junctions as receptors for attachment and invasion, or by disrupting normal tight junction protein expression and localisation (Muza-Moons et al., 2004; Roxas et al., 2010; Simonovic et al., 2000). Tight junctional alterations caused by bacterial invasion results in a disruption in ion and water transport across the epithelial membrane, which presents as classical acute gastroenteritis symptoms such as diarrhoea. A prime example of this can be observed

during infections with either enterohaemorrhagic *Escherichia coli* (EHEC) or enteropathogenic *E. coli* (EPEC). Both EHEC and EPEC utilise a type-three secretion system (T3SS) to inject effector proteins into the host cytoplasm and re-arranges the host cytoskeleton to disrupt intercellular tight junctions (Muza-Moons et al., 2004; Roxas et al., 2010; Simonovic et al., 2000).

Similarly, *Salmonella* spp induce host cell membrane ruffling, leading to actin re-arrangement and engulfment of the bacteria by the host cell to establish infection. Exposure to extracellular *Salmonella* also induces tight junctional disruption, which presents with a lower transepithelial resistance and increased permeability *in vitro* (Boyle et al., 2006; Collazo and Galán, 1997; Kohler et al., 2007). Both these bacteria are well characterised, however in the majority of cases it is unknown how host-pathogen interactions at the epithelial surface lead to successful invasion.

For the purposes of preventing the incidence of enteric diseases, it is imperative to study the invasion events within the small intestinal interface. Identification of key molecular pathways could lead to the development of novel therapeutics.

1.6 Polarisation of the Intestinal Epithelium

Intestinal epithelial cells are polarized: the apical surface faces the lumen of the intestine, and the basal surface faces the lamina propria. Epithelial polarization is maintained through the exclusive targeting of proteins to either the apical or basolateral sides, and this separation is maintained by tight junctions (Abreu, 2010). An important feature of epithelial polarisation is the regulation of surface protein expression on the relevant interface. For the study of infections and host-pathogen interactions, the

regulation of pattern recognition receptors (PRRs), such as toll-like receptors (TLRs) are important.

The localization of toll-like receptors (TLRs) have been studied in both human and murine tissues revealing that TLR expression can be spatially restricted to either the apical or basolateral surfaces of the epithelium depending on the epithelial cell type, location along the intestinal tract, and the cell developmental stage (Abreu, 2010). This polarized expression of TLRs may help the host to respond appropriately to commensal and pathogenic microbes. Interestingly, stimulation of the same TLR at either the apical or basolateral surface has distinct outcomes. Basolateral stimulation of TLR9 results in textbook activation of the NF-κB pathway, whereas apical stimulation inhibits this pathway and reduces responsiveness to subsequent TLR stimulation. In addition to polarized expression of TLR, host cell receptors utilized by pathogens for invasion may also show polarized patterns of expression. It is therefore important that any models of the small intestinal epithelium are correctly polarized, and that pathogens of interest are applied to the apical surface, as they would during the progression of natural infections.

1.7 Existing Models of Intestinal Biology

To study the intestine, a suitable model that fully mimics the intestinal epithelium is required. Existing intestinal infection models can be split into several types each with their own advantages and limitations (**Table 2**):

1. ***In vitro* immortalised cell line cultures**; a cheap and convenient method of studying host-pathogen interactions, however these models may be physiologically irrelevant as they lack cell diversity and structural complexity which severely limits their ability to accurately mimic and recapitulate the *in vivo* environment.

2. ***In vitro* 3D explant models**: more physiologically relevant models than cell line cultures as these incorporate the cellular diversity and structural architecture of small intestinal tissues *in vivo.* However, models developed from donor tissues can be highly variable and explant models are restricted in duration of study due to poor tissue viability.
3. ***In vivo* models:** are the most biologically relevant as they incorporate host innate and adaptive immune responses to infection, however in some instances may be unsuited for the purposes of studying infections. Smaller models (rodent and avian) are routinely exploited for infections studies, however the use of species-specific pathogens within these models creates a species incompatibility. *In vivo* models of larger animal species could be used, however the cost and technical difficulties of these is a major limiting factor. Furthermore under the NC3R's recommendations, we should be aiming to replace the use of animals in research for alternative models to reduce the numbers of animals in research.

Table 2) Common models of the intestine, their uses and limitations

Origin	Features	Uses	Limitations	References
***In vitro* cell lines**: immortalised cell line cultures provide a cheap and convenient method of studying host-pathogen interactions, however lack cell diversity and the structural architecture of the small intestine so are physiologically inaccurate. Cell lines are often used to study host-pathogen cell interactions and bacterial pedestal formation.				
CaCo2 Human Colon Colorectal Epithelial Cells	Polarised with apical microvilli, tight junctions and intestinal hydrolase enzyme activity	Can be co-cultured with raji B cells on transwell inserts to generate microfold cells. This model identified *E.coli* targeting of M cells for translocation across the epithelium.	Enterocytes may more closely represent foetal and not adult enterocytes. Colonic epithelial cells do not represent small intestinal epithelium	(Roberts et al., 2010; Sambuy et al., 2005)
HeLa (I407) Human Cervical Adenocarcinoma Epithelial Cells	Jejunum and ileum of 2 month old embryo, contaminated with HeLa cell markers	Previously used to study the internalisation of *Salmonella* and *Yersinia.*	Non-polarised cells which are not representative of the gastrointestinal epithelium. Also known to over-take other cell cultures *in vitro* and therefore pose a risk of contamination.	(Devenish and Schiemann, 1981; Gianella et al., 1973; Kihlstrom, 1977)
HT-29 Human Colorectal Adenocarcinoma	Morphology can be induced to enterocyte differentiation to form polarised epithelial with brush border	Widely used for adherence and invasion assays.	Colonic epithelial cells do not represent small intestinal epithelium.	(Cohen et al., 1999; Martin et al., 2004)

Table 2 Continued) Common models of the intestine, their uses and limitations				
Origin	**Features**	**Uses**	**Limitations**	**References**
MDCK Canine Kidney Epithelial Cells	Apico-basolateral polarity and tight cell junctions	Previous uses include: adherence, invasion and transcytosis of bovine *E. coli* through monolayer cultures, and *Salmonella* migration through MDCKs grown on transwell membranes.	Lack of validated canine antibodies available. Cells are renal in origin and may not accurately mimic small intestinal interactions.	(Dukes et al., 2011; Finlay et al., 1988; Korth et al., 1994; Tafazoli et al., 2003)
T84 Human Colon Carcinoma Epithelial Cells	Contains goblet-like cells and forms polarised monolayers	T84 has been used to study intestinal epithelial integrity and IFN-γ signalling.	Shown to be more susceptible to infection by enteroaggregative *E. coli* strain 042 than CaCo2 cells and so findings are not comparable between studies.	(McCool et al., 1990; Nataro et al., 1996)
IEC-6 Rat Small Intestine Epithelial Cells	Small intestinal in origin making it more suited than colonic epithelial cell lines	Has been previously used to study transmigration of *Toxoplasma gondii* and wound healing	In comparison to human cell line cultures, IEC6 is relatively uncharacterized. It is unknown what cell types are present within this model	(Jones et al., 2016)

Table 2 Continued) Common models of the intestine, their uses and limitations				
Origin	**Features**	**Uses**	**Limitations**	**References**
***In vitro* 3D models:** these models are favourable over monolayer cultures are they introduce more complexity to produce more physiologically relevant findings. However models utilising live tissues are subject to donor variability, and poor availability of animal tissues may hinder the study of zoonotic infections.				
Scaffold Models	Immortalised CaCo2 or primary cells cultured on villus hydrogel structures	Culture on scaffold forms polarised epithelial monolayer with brush border phenotype at the villus tip.	Models exploiting CaCo2 cells lacks diversity. Primarily developed for drug permeability and has not been optimised for infection.	(Nakase et al., 2006; Yu et al., 2012)
***Ex vivo* tissues**	Human or animal biopsies/tissues	More complex than monolayer cultures as they contain structural complexity and cellular diversity.	Tissue thickness limits the use of traditional microscopy techniques. Tissues deteriorate and are not able to be cultured long term due to poor oxygenation.	(Bansal et al., 2009; Grivel and Margolis, 2009)
Precision-cut intestinal slices (PCIS)	Viable explants of tissues *ex vivo*	More complex than monolayer cultures containing structural complexity and cellular diversity. Can be sliced thinly to extend tissue viability allowing the use of imaging techniques.	PCIS requires using specialist slicing equipment. Optimised for the study of drug transport and toxicology and not infection. Tissue viability limited to 24 hours.	(de Graaf et al., 2010; de Kanter et al., 2005; Fahy et al., 2013; van de Kerkhof et al., 2005)

Table 2 Continued) Common models of the intestine, their uses and limitations				
Origin	**Features**	**Uses**	**Limitations**	**References**
Ussing chamber	Stripped intestinal mucosae mounted in chambers with stirring conditions.	More complex than monolayer cultures as they contain structural complexity and cellular diversity.	Used primarily for the study of intestinal permeability and not infections. Not optimised for imaging techniques and short term viability comparable to PCIS.	(Ungell et al., 1998; Van De Kerkhof et al., 2006)
Gut-on-Chip	CaCo2 induced on micro-fluidic chip forming 3D villus structures	Polarised and differentiated epithelial layer in 3D conformation. Incorporates dynamic flow of microfluids.	Developed primarily for the study of intestinal permeability and not yet fully evaluated for infection studies. Unknown what cell types are present.	(Kim and Ingber, 2013)
Organoids	Stem cell derived model	"Mini-guts" containing differentiated epithelial cells in 3D conformation. Can also be developed using tissues from stem cells from other anatomical sources to generate region specific cultures (jejunal, ileal) or organ specific cultures (e.g. colon, rectum)	Access to lumen is restricted and requires the use of microinjection equipment.	(Sato et al., 2009; Wilson et al., 2014; Zhang et al., 2014)

Table 2 Continued) Common models of the intestine, their uses and limitations				
Origin	**Features**	**Uses**	**Limitations**	**References**
***In vivo* models:** these models form the gold standard for study of host-pathogen interactions as they are physiologically and incorporate host immune and systemic responses to infection, however are not suited for optimised for studying early stage infections by confocal imaging or proteomic approaches				
Ileal loop model	Ligation of ileum through surgical means under anesthesia to study host response to infection	Treatments can be replicated within the same animal maximizing outputs. Identified M cells as the target for *Salmonella typhi* strain 10007	Requires animal husbandry facilities and project licenses. Limitations of 24 hour experiments.	(Kohbata et al., 1986)
Whole animal models	Infection of whole animals by oral gavage, or intraperitoneal injection	Include systemic and host immune response to infections. Can produce transgenic murine models to study immune responses to pathogen infection.	Difficult to obtain approval for large animal studies which is required to species-specific pathogens/host adaptations. Not optimised for early stage invasions. Method of infection may not always mimic the natural oral route of infection.	

1.7.1 *In vitro* Monolayers Lack Structural Complexity

Existing 2D *in vitro* models of the gastrointestinal epithelium have been significant for the study of gastrointestinal pathogens. A notable example of such a model is the CaCo2 cell-line, which when grown as a monolayer show polarised morphology with tight junctions between adjacent cells, and microvilli on the apical surfaces (Sambuy et al., 2005). Conventionally, these are used for the study of basic attachment and invasion assays and have been invaluable in furthering our understanding about the mechanisms involved in bacterial invasion in pathogens such as *Escherichia coli, Salmonella* spp, and *Clostridium difficile.*

Immortalised cell lines were previously favoured for the study of infections due to the ease of sub-culturing and reproducibility of these cell lines, however it has since been established that repeated passage can lead to structural changes within the model (Lu et al., 1996). Firstly, it was observed that regions of CaCo2 cells at high passage number formed multiple cell layers rather than monolayers as observed in early passage number cells (Lu et al., 1996). Secondly, it was reported that high passage number cells exhibit an enhanced trans-epithelial electrical resistance (TEER) when compared to those of a lower passage, potentially due to the stacking of multiple cells (Lu et al., 1996). Thirdly, high passage number cells show a significantly higher rate of proliferation in comparison to low passage number CaCo2 cells. Finally, the expression of small intestinal hydrolase enzymes are altered in high passage number CaCo2 cell lines which may affect cell functionality (Sambuy et al., 2005). Although CaCo2 cells are a heterogenous mix of cells, over time through repeated passage, sub-populations of enterocytes become dominant within the culture resulting in the changes described (Briske-Anderson et al., 1997; Lu et al., 1996; Senarathna and

Crowe, 2015; Siissalo et al., 2007). Furthermore, the maintenance of CaCo2 across different laboratories has likely led to the selection of different sub-populations and ultimately variation within the cell line, resulting in the reporting of contrasting experimental findings (Briske-Anderson et al., 1997; Sambuy et al., 2005).

In addition to the morphological changes acquired through long term passage, monolayer cultures are considered too simplistic and unable to fully mimic the *in vivo* cellular physiology. Traditionally immortalised cell lines contain one dominating cell type, in the case of CaCo2, enterocytes. Characterisation of CaCo2 cell lines have suggested that long term culture may have induced a foetal and not adult enterocyte phenotype (Sambuy et al., 2005). As foetal cell responses differ to mature cell response, this is likely to result in misleading observations during infection studies.

A lack of secretory cell types in cell lines also limits their use in recapitulating the *in vivo* epithelium. A method of co-culture with raji B cells has demonstrated that CaCo2 cells are able to be further differentiated into M cells, however using co-culture techniques does not generate cell lines cultures containing Paneth or goblet cells that are important for host defence.

The limitations described above result in host-pathogen interactions that do not occur as they do naturally. For example, *in vivo* enteropathogenic *E. coli* (EPEC) localises specifically with intestinal epithelial cells, however *in vitro* the host cell specificity is ablated and EPEC also interacts with non-intestinal epithelial cells (Law et al., 2013). Thus, immortalised cell lines will not produce physiologically accurate representations of complex gastrointestinal pathogen infections of the epithelium

1.7.2 Scaffold Models Lack Cell Diversity

In terms of structural arrangement, 3D scaffold models are advantageous when compared to immortalised cell lines. Hydrogel structures moulded to accurately replicate the shape and size of human small intestinal villi are used as a scaffold to overlay immortalised cells such as the CaCo2 cell line (Yu et al., 2012). This model, characterised by confocal imaging, describes variable enterocyte maturation along the villus length with polarized cells at the top of the villus tip exhibiting brush border characteristics, and less mature enterocytes at the villus base (Yu et al., 2012). However, due to its dependence on an immortalised cell line, this model is likely to succumb to the formation of multiple cell layers which again affects the permeability of the culture and altered epithelial integrity (Yu et al., 2012). More importantly, this model still lacks Paneth and goblet cell types involved with host, as these cell types are absent in the CaCo2 cell line (Yu et al., 2012). Currently, primary cells have not been cultured in this way, but could offer a suitable model to study intestinal biology if the structural arrangement mimics the *in vivo* environment.

Existing scaffold models have primarily been developed for the study of drug permeability and has not been utilised for infection studies. However the characteristics described above make this model less desirable for infection studies, and an alternative model may be more appropriate.

1.7.3 Explant/Tissue Based *In vitro* Models Have Short Term Viability

In vitro explant tissue-based models incorporate all the differentiated epithelial cell types, as well as the complex structural architecture *in vivo,* making them an attractive *in vitro* alternative to study host-pathogen interactions. However, many of these

models were primarily designed and optimised for the study of intestinal permeability, and may not be suitable for infection studies.

A major drawback of using explant and tissue-based models is the rapid tissue degeneration of this tissues leading to short viability. Recently, modifications have been described to generate precision cut intestinal slices (PCIS) to produce thin transverse sections of intestinal tissues (de Graaf et al., 2010; de Kanter et al., 2005). Using this method, oxygenation of the tissues are improved to prolong it's viability for up to 24 hours. Modification of these methods through the integration of more sophisticated perfusion systems may further improve tissue viability, however these are challenging to implement and the benefits are not yet fully understood.

Ultimately, this technique is still heavily reliant on experimental animals or biopsies for donor tissues. The repeated use of experimental animals is unfavoured, and donor biopsies often introduce biological variation into experiments. The rapid degeneration of intestinal tissues and dependence on repeated animal use or donors makes explant models undesirable for the study of host pathogen interaction studies.

1.7.4 *In vivo* Models are Not Suited for Short Term Infection Studies

Due to the limiting factors of *in vitro* models, it is still necessary to utilise *in vivo* experimentation to accurately mimic host-pathogen interactions of enteric pathogens. There are currently two *in vivo* models of enteric disease; ileal loop models and whole animal models.

Ileal loop models involve surgical ligation of ileum tissues to form multiple loops within a single animal and pathogens or treatments are then injected into the intestinal lumen for study (Kohbata et al., 1986). A unique feature of this model is that several

treatments can be administered as these ileal loops are separated by ligation, which allows for the study of multiple conditions in one biological donor, and consequently the collection of experimental data is restricted to the intestinal tissues. The use of this model is also generally limited to a maximum of 24 hours and requires the use of live animals under anesthesia which requires surgical expertise and careful monitoring for animal welfare purposes (Kohbata et al., 1986).

In contrast, whole animal models involve studying the whole animal response to infection following either oral gavage or injection (intravenous or intraperitoneal), which allows researchers to study multiple tissues of interest or bodily fluids, generating multiple sets of experimental data in the process. With the development of new technologies, the production of knockout or gene silenced models make *in vivo* models indispensable. However, several challenges arise when considering whole animal models for the study of early stage host-pathogen interactions.

Firstly, oral gavage of animal models is technically challenging due to difficulties with administering standardized pathogen doses, as well as in culturing the relevant invasive life stages for oral infection. Therefore, many studies of *in vivo* enteric infection are established through intraperitoneal injection which does not mimic the natural route of infection. Secondly, during early host invasion, enteric pathogens often infect small regions of the small intestine which are difficult to identify and study *in vivo.* Similar to explant tissues, live imaging of *in vivo* models is limited due to rapid tissue degeneration, which is further complicated by the thickness of native tissues. Thirdly, systems biology approaches are not suited for *in vivo* intestine models. Due to the large volume of uninfected cells present *in vivo*, small changes in protein abundance in foci of infection may be masked. The signal-to-noise ratio is favoured

toward the more numerous non-infected cells within the gut, meaning that subtle changes exhibited by infected cells may be missed.

In addition to these issues, generally *in vivo* models are often rodent based which is unsuitable for the study of pathogens with species-specific adaptations. This species mis-match produces physiologically irrelevant host-pathogen interactions which do not mimic the response in the natural hosts. An example of this is the limitation of study of *Listeria monocytogenes.* The bacterial surface proteins required for invasion are poorly recognized by murine cells, so establishing infection requires a high bacterial dose administered intravenously which bypasses the natural route of infection (Hoelzer et al., 2012; Pizarro-Cerda et al., 2015). The administration of infectious dose via this method does not mimic the natural progression of infection where systemic symptoms may not appear until several weeks after initial bacterial exposure (Hoelzer et al., 2012; Pizarro-Cerda et al., 2015). Consequently, the study of *Listeria* in murine models may poorly mimic human infection.

Alternatively, larger models of farm or companion animals for the study of infections are not as feasible as small murine models of infection. Acquiring ethical approval for these studies is challenging due to potential animal welfare issues, and the cost of establishing animal housing facilities is limiting. Furthermore *in vivo* models require repeated animal use which we should be aiming to reduce, for both ethical and welfare reasons. For these reasons, *in vitro* models may provide an advantageous means of studying host-pathogen interactions over *in vivo* models. With these limitations in mind, there is a clear need for the modification and improve current *in vitro* techniques for the study of infection within the small intestine as an alternative to simplistic 2D models and *in vivo* models that are both routinely used in this context.

1.7.5. 3D Organ Models Form a New Generation of Enteric Models

Due to the limitations of classic enteric models, there has been an increased interest in the development of novel enteric models. In recent years, two promising new models have been developed; gut-on-chips and stem cell derived organoid models.

Microfluidics and organ-on-a-chip approaches are upcoming engineering technologies developed for the study of drug toxicity and permeability that integrate small volumes of fluids to fabricate functional units of organs (Kim and Ingber, 2013; Kim and Takayama, 2015). Gut-on-chips feature CaCo2 cells continuously perfused in chambers to induce morphogenesis of 3D villus structures forming a polarised, differentiated epithelial monolayer (Kim and Ingber, 2013). It is unknown how the establishment of gut-on-chip models is affected by sub-clones of CaCo2 cells and whether this introduces variability between different laboratories. However due to the limitations of CaCo2 cells as a monolayer, it would not be surprising if this model was subject to some challenges. Furthermore, the colonic origin of CaCo2 cells is likely to generate differentiated epithelial cells that do not mimic the small intestinal epithelial cells *in vivo*. As we know that CaCo2 enterocytes are more likely to mimic foetal enterocytes, and are colonic in nature, this model requires further characterisation before its use in host-pathogen interactions can be introduced. For these reasons, the organoid model will more likely become a more promising tool for the study of enteric pathogens.

1.8. An Introduction to Small Intestinal Stem Cell-Derived Organoids

Since the identification of LGR5+ stem cells within the small intestine (Barker et al., 2007), we have seen the establishment of "organoid" cultures. These "mini-guts" are stem cell derived 3D models representative of the intestine that incorporates all the major differentiated cell types and complex structural architecture found in vivo (Sato et al., 2009) (**Figure 9**). Prior to the establishment of organoid cultures, there has never been a long-term in vitro culture system to maintain the crypt-villus physiology observed in vivo, making these an exciting prospect for the future of intestinal biology.

1.8.1 The Generation of Organoid Cultures

To generate organoid cultures, the LGR5+ stem cells must be isolated, either as single cells or within crypt base columnar units. Firstly, small intestinal tissues are flushed and cut into small sections, then are subjected to several cycles of dissociation through shaking in PBS/EDTA. Each dissociation cycle gently removes the mucus, followed by the villi to eventually generate a crypt-enriched fraction. The crypts are then briefly quantified and concentrated via centrifugation. Crypts are then plated within Matrigel® at 10 crypts/µL and overlaid with organoid media containing growth factors r-spondin-1, epidermal grown factor (EGF) and noggin that are known to modulate intestinal signalling pathways involved with normal gut homeostasis (Mahé et al., 2014; Sato et al., 2009).

Within 4-6 days in Matrigel®, stem cells within crypt units proliferate and differentiate into terminal epithelial cell types to form spheroid structures with clearly defined villus and crypt domains that are representative of the complex architecture observed *in vivo* (**Figure 9**) (Sato et al., 2009). The presence of stem cells within organoid crypt domains drives self-renewal and cell proliferation under intestinal homeostatic

signaling cascades as described *in vivo*. By days 7-9, the organoid cultures can be passaged by syringing to generate fragments, and re-plating into fresh Matrigel®.

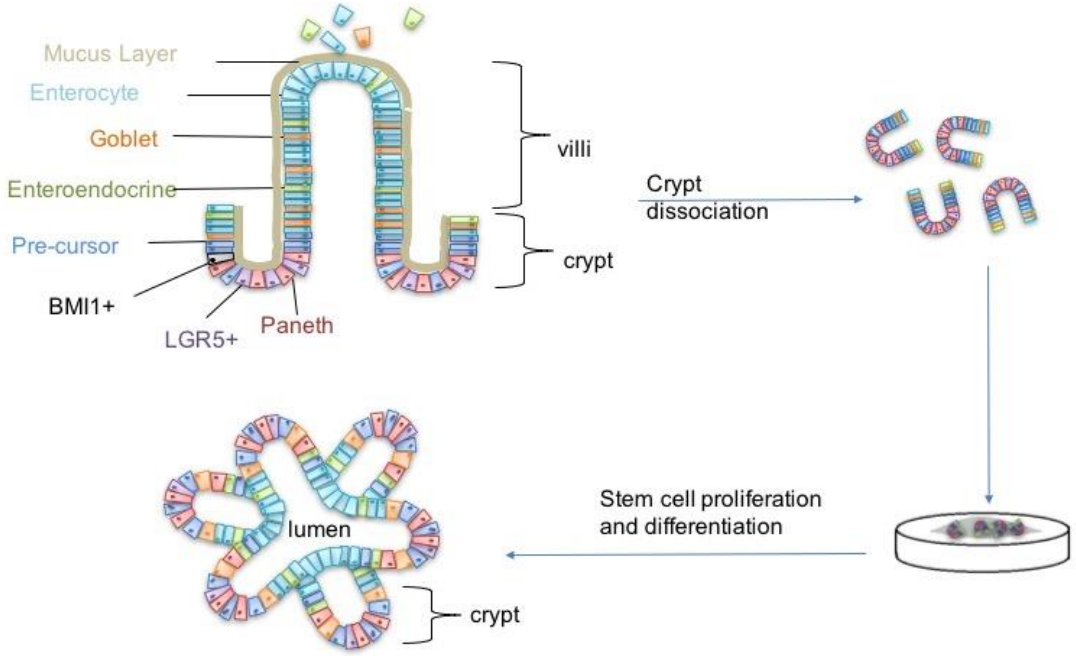

Figure 9) Intestinal crypt dissociation and organoid culture.

Small intestinal tissue (murine or human) is flushed with PBS. Incubation of tissues in a series of EDTA followed by PBS washes fractionates the tissues to sequentially remove mucus, villi and crypts into enriched fractions. The optimal enriched crypt fraction is concentrated via centrifugation and crypt units embedded into Matrigel®. Media containing R-spondin, Noggin and EGF is overlaid onto Matrigel® domes. Cellular proliferation and differentiation occurs to generate multilobular "organoid" cultures with an enclosed lumen. Figure generated from published organoid culture protocols (Andersson-Rolf et al., 2014; Sato et al., 2009).

In addition to the advantages of the self-renewal abilities of organoid models, their microscopic size is much smaller than whole gut tissues that currently pose a challenge when identifying foci of infection. For this reason, organoids are advantageous over *in vivo* models as they can be easily visualised by confocal imaging. Moreover, unlike tissue biopsies, organoid models are not as susceptible to degradation and therefore have a longer durability which opens the potential of studying multiple time courses during an infection.

Currently the organoid culture technique has been mainly utilised by culturing murine small intestinal stem cells and human tumour cells for the purposes of studying cancer development and drug development (Ranga et al., 2014; T Sato et al., 2011). Organoid culture technology has also been expanded and exploited to generate other types of epithelial organoids of the gastrointestinal tract including stomach organoids (gasteroids), small intestinal organoids (enteroids) and colon organoids (colonoids) (Stelzner et al., 2012).

1.8.2 Organoids Have Not Been Fully Utilised For Infection Studies

To date, with the exception of a few studies, there has been limited work on developing organoid cultures for the purposes of studying intestinal pathogens (Macartney et al., 2000; Wilson et al., 2014; Yin et al., 2015; Zhang et al., 2014). Due to their closed conformation, luminal access is severely restricted. Preliminary work in this area have demonstrated that infection of the intestinal organoid cultures is achievable through the use of a microinjection system to apply bacterial and viral pathogens directly into the luminal interface of the organoids (Finkbeiner and Spence, 2013; Wilson et al., 2014; Zhang et al., 2014). Using PCR, immuno-staining and western blotting, organoids have been utilised to investigate morphological and chemical changes occurring during infections (Finkbeiner and Spence, 2013; Wilson et al., 2014; Zhang et al., 2014). Through these methods, the bacterial restrictive abilities of alpha-defensins has been successfully studied within a sealed anatomical region. Furthermore, organoids can be cultured from reporter mice strains making them a promising tool for the generation of *in vitro* reporter models (Wilson et al., 2014). Currently, the use of organoid cultures for infection within its infancy and further

expansion into this field would provide a promising tool for the study of host-pathogen interactions.

More recently organoid cultures have been established in various animal species including cats, dogs, cows, horses, pigs, sheep and chickens (Powell and Behnke, 2017) as well as organoids produced from various anatomical regions within the gastrointestinal tract (Klotz et al., 2012). The generation of animal small intestinal organoids provides a solution to the current species mis-match which occurs through use of murine *in vivo* models and animal pathogens. The ability to generate organoids of food producing animals makes this model an attractive prospect for the study of zoonotic enteric pathogens, and to elucidate species specific pathways that we can exploit for the development of novel vaccines and therapeutics. For the reasons above, these organoid cultures have the potential to propel the field of intestinal biology forward.

1.9. Enteric Protozoan Parasites

Protozoa are a diverse group of eukaryotic unicellular protists. The classification of protozoa has been difficult and so the majority of species identification performed is dependent upon morphological characteristics. Over 50,000 species of protozoa have been described geographically worldwide. The protozoa group can be divided into flagellates, amoeboids, ciliates and sporozoans, many of which are free-living organisms with sizes ranging from 10 to 50µm in size.

This group of organisms infects a wide range of human and animal hosts to varying degrees. Pathogenic protozoa are commonly transmitted via the consumption of contaminated food and drink. However, this is more frequently observed in developing countries due to the poor sanitation and occurrence of microbial contamination.

Consequently, these diseases are often neglected and receive less interest than bacterial diseases.

Many protozoal pathogens have been implicated in both human and veterinary disease. Examples of these include *Eimeria* spp, *Entamoeba* spp, *Cryptosporidium* spp, *Giardia* spp, *Toxoplasma* spp and *Neospora* spp (Fayer et al., 2000; Fletcher et al., 2012; Kaltungo and Musa, 2013; Nichols, 2000; Stark et al., 2009). These infections may be asymptomatic in agricultural animals, which eventually leads to unintentional onward transmission throughout herds or flocks of animals. In other instances, disease in farm animals results in a loss of milk and meat yield, and thus a loss in agricultural productivity. However, the primary concern is the zoonotic risk of transmission to humans upon consumption of contaminated meat products.

The ability to study these diseases in both human and animal models will further our understanding of key host-pathogen interactions to identify molecular signaling pathways to develop novel therapeutics. A significant group of protozoa with relevance to both human and veterinary health are the Apicomplexa.

1.9.2 Unique Features of Apicomplexa

This phyla of parasitic alveolates are named as such due their polarised phenotype and the presence of shared unique features. Apicomplexa are obligate intracellular parasites that invade host cells and establish a parasitophorous vacuole for replication using shared morphological structures, many of which are found in the apical complex. The apical complex contains an apical polar ring, and several secretory organelles; micronemes (MICs), rhoptries (ROPs) and dense granules (GRAs) (**Figure 10**).

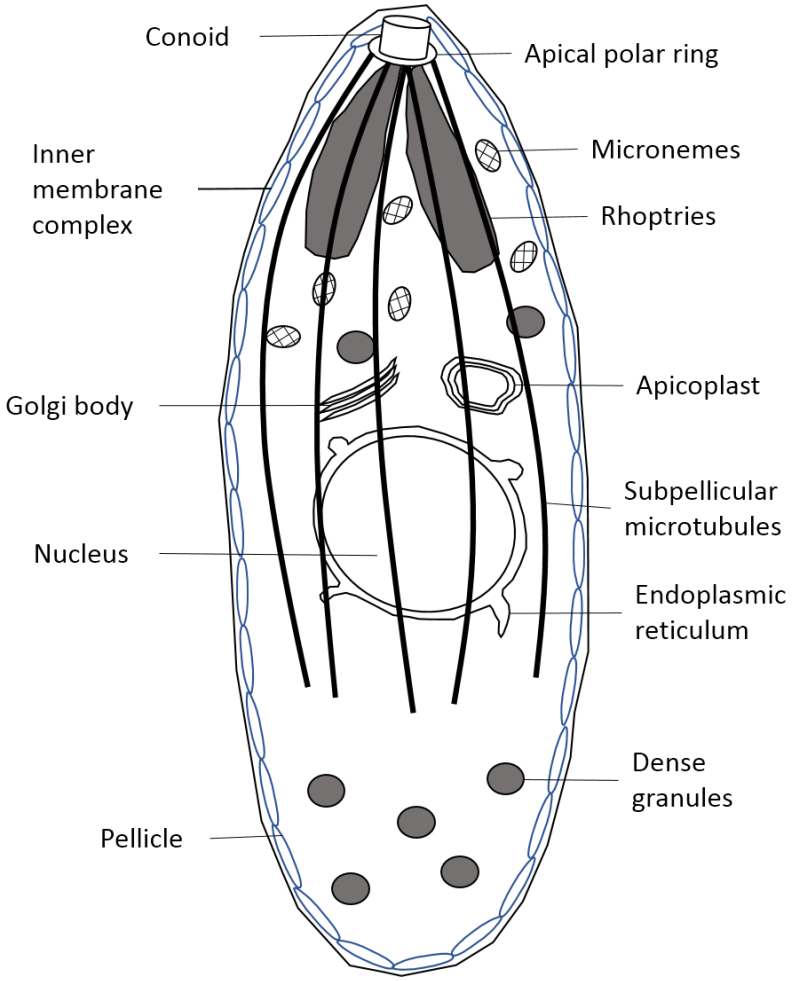

Figure 10) Structural Characteristics of Apicomplexan Parasites

Apicomplexa are polarised cells containing unique organelles. Rhoptries, micronemes and dense granules are secretory organelles required for motility, host cell invasion and the establishment of a parasitophorous vacuole. Adapted from (Morrissette and Sibley, 2002)

The apical pole serves as a microtubule-organising centre (MTOC), and some apicomplexa also contain conoids that are composed of spiral filaments which is thought to be mechanically involved with host cell invasion. The secretory organelles are crucial for parasite motility, host cell invasion and the establishment of parasitophorous vacuoles. Another unique feature of this phyla is the apicoplast, a chloroplast-like organelle. Apicoplast are contained within an inner membrane

complex (IMC) composed of pellicles that are also associated with cytoskeletal constructs such as actin, myosin, intermediate filaments and microtubules (**Figure 10**).

Comparison of apicomplexan cytoskeleton against eukaryotic models reveal interesting features. The survival of Apicomplexa parasites is attributed to the presence of subpellilcular microtubules that exhibit heightened stability to withstand unusual pressure and temperature conditions (Morrissette and Sibley, 2002). The subpellilcular microtubules run through the cytosolic face of the parasite pellicle, and span approximately 2/3 of the parasite length to the region just below the nucleus to regulate apical polarity (**Figure 10**) (Morrissette and Sibley, 2002). The arrangement of these microtubules is variable within the phylum and are specific to different life stages for host cell invasion and parasite replication. However extracellular life stages of apicomplexan parasites appear to contain two forms of microtubules; the subpellicular and spindle microtubules to facilitate with extracellular survival and function (Morrissette and Sibley, 2002).

Apicomplexa also share a substrate-dependent "gliding motility" for tissue migration and host cell invasion, which is made possible by a glideosome located between the IMC and parasite plasma membrane (PPM) (**Figure 11 A**). Structural proteins of the apicomplexa have been identified for gliding motility named gliding-associated proteins (GAPs); GAP40, GPA45 and GAP50 that are thought to maintain the integrity of parasite pellicle during gliding and invasion (Bargieri et al., 2014). The pairing of a myosin light chain through GAPs forms a class XIV myosin (MYOA) to generate moving force (**Figure 11 A**). The interaction of the actin-myosin motor to the plasma membrane adhesions forms short actin filaments (F-actin) (Bargieri et al., 2014; Drewry and Sibley, 2015; Jewett and Sibley, 2003; Morrissette and Sibley, 2002).

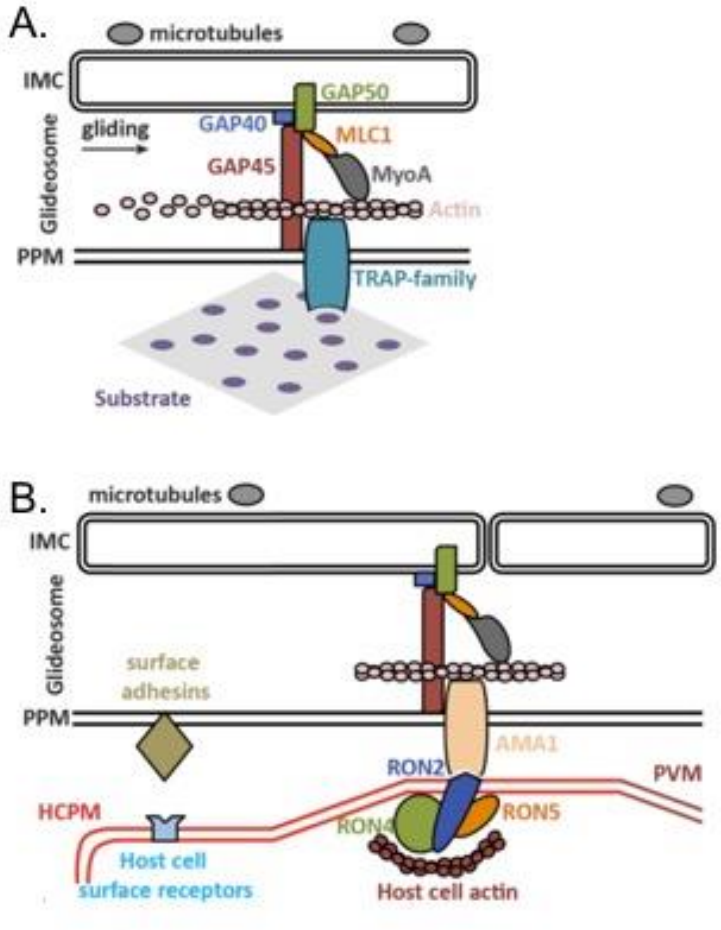

Figure 11) Molecular mechanism of apicomplexan gliding motility and host cell invasion

(A) A parasite motor (glideosome) is located between the parasites inner membrane complex (IMC) and plasma membrane (PPM). The action of parasite motility is mediated through binding of the ectodomain of transmembrane TRAP-family proteins, to a solid substrate as the cytoplasmic tail of the protein links to the parasite motor. The integrity of the glideosome is regulated by the gliding-associated protein 45 (GAP45), which anchors to the PPM and IMC via GAP40 and GAP50 at either end. Binding of GAPs, the IMC and actin is mediated by myosin A (MyoA) and the MyoA light chain (MLC1). Capping of the TRAP-family protein by myosin-actin consequently generates a moving force to provide movement of the parasite cell. (B) Upon adhesion to host cell plasma membrane (HCPM) by parasite surface adhesins and host cell surface receptors, parasite apical membrane antigen 1 (AMA1) and rhoptry neck protein 2 (RON2) are inserted into host cells and associates with RON4 and RON5 to form a junction. Host actin recruited to the parasite junction links the parasite to host cell cytoskeleton. The forward propulsion of parasites provided by the glideosome towards the interior of the host cell forms a parasitophorous vacuole (PVM). Images from (Bargieri et al., 2014).

Apical deployment of these adhesins results in a forward movement from the apical end to induce parasite internalization (**Figure 11**). Upon identification of host cells,

Apicomplexa attach and invade these targeted cells via an attachment cascade regulated by the secretory organelles (Drewry and Sibley, 2015; Jewett and Sibley, 2003; Morrissette and Sibley, 2002).

The mechanisms by which apicomplexan parasites invade host cells varies between species due to their stage specific adaptations. Due to their ability to invade almost all mammalian cell types, *Toxoplasma gondii* is considered the most successful invasive enteric protozoan. For this reason, *T. gondii* will be the focus of this doctoral thesis for the discussion of apicomplexan invasion strategies and as a model parasite for development of a suitable model.

1.10 An Introduction to *Toxoplasma gondii*

Since its discovery in the early 1900s, *T. gondii* has been heavily studied. Despite this, there are still several aspects of this parasite's life cycle that elude our understanding. The definitive host for Toxoplasma are members of the *Felidae* family, and an array of mammalian species of intermediate host, including humans, mice, birds and food-producing farm animals have been identified (Bonapaz et al., 2010; Dubey et al., 2002; Esteban-Redondo and Innes, 1997; Guo et al., 2015; Hutchinson et al., 2011; Limon et al., 2017; Tenter et al., 2000).

The geographical presence of human *Toxoplasmosis* has been reported with variable rates of infection estimted; 9% in the USA, 30% in the UK and up to 50-80% in Central and South America (Hill and Dubey, 2002; McAuley, 2014; NHS, 2015). The majority of *T. gondii* infections are asymptomatic or cause only mild flu-like symptoms, however the acquisition of infection by immuno-suppressed individuals or during early pregnancy can have severe consequences. Alternatively, if an infected person subsequently becomes immunocompromised, parasite re-activation can result

in the development of neuro- or ocular toxoplasmosis leading to long term morbidities (Carruthers and Suzuki, 2007; Hill and Dubey, 2002).

Although the majority of cases of severe disease involve immunocompromised patients, infection of immune competent hosts can alter brain function. The formation of neuronal tissue cysts has been reported to alter the behaviour of infected rodents and is thought to increase the likelihood of parasite transmission to the definitive feline host (Gatkowska et al., 2012). It has been suggested that the formation of brain cysts results in neuronal atrophy in these mice and an enhanced dilation of ventricles in the brain. Comparatively, examination of the human schizophrenic patients have highlighted reduced grey matter in infected patients when compared to non-infected patients associated to a loss of brain parenchyma. These findings have led to the theory that the development of brain cysts during infection has implications for the manipulation of behaviour in infected hosts (Berenreiterová et al., 2011; Torrey and Yolken, 2003).

Acquisition of infection during pregnancy results in congenital toxoplasmosis. The risk of congenital toxoplasmosis is variable in relation to the stage of pregnancy that infection is acquired, with the lowest rates of foetal transmission reported during the first trimester which increases as pregnancy proceeds (McAuley, 2014). Animal studies have demonstrated that initial infection occurs within the uterus which eventually migrates to the foetus through multiple mechanisms (Jones et al., 2016; McAuley, 2014). Congenital toxoplasmosis has a wide range of clinical presentations, and is inversely related to the gestational age of infection, with more severe clinical disease if acquired during the first trimester (McAuley, 2014). These manifestations include birth defects, anaemia, seizure, developmental delay and sporadic abortion in

both humans and animal species impacting both human and animal health (Gilbert et al., 2006; Kravetz and Federman, 2005; McAuley, 2014).

In humans, the threat of congenital toxoplasmosis is primarily the highest when the mother is previously uninfected, however in farm animals the subsequent chronic infection and transmission within flocks is problematic. Importantly, the acquisition of toxoplasmosis results in chronic latent infection in animal species resulting in subsequent transmission to offspring, posing both a risk of repeated animal abortions and onward human transmission upon entering the food chain. For these reasons, the development of more effective treatments, or vaccines for the prevention of disease is desirable.

1.10.1 Existing Therapeutics against *Toxoplasma gondii* Infection

To date, several drugs have been used for the treatment of *Toxoplasma* infections, such as; pyrimethamine, sulfadiazine, spiramycin, azithroymycin, clindamycin, minocycline, dapson and rifabutin. The most effective treatment against *Toxoplasma* generally involves the administration of pyrimethamine in combination with other drugs (Alday and Doggett, 2017; Derouin et al., 1991; Köksal et al., 2016). However, overuse of the same drugs for prevention of malaria in pregnancy have increased drug resistance in other apicomplexan pathogens and in *Toxoplasma* mutants *in vitro*, posing a threat to the future use of these therapies (Gatton et al., 2004; Köksal et al., 2016). Furthermore, the drugs mentioned here are not effective against slow growing bradyzoites, which limits the treatment options for immune-suppressed patients at risk of re-activation of infection (Köksal et al., 2016).

Currently only one commercial vaccine, Toxovax®, has been licensed for veterinary use (MSD Animal Health, 2017). However Toxovax® is not suitable for widespread

use as it is a live-attenuated vaccine and risks the development of adverse effects. Moreover, this vaccine is expensive to purchase and has a short shelf-life making it less attractive. Although many efforts have been made to further the development of an alternative vaccine, multiple challenges are inhibiting progress. The use of inactivated or killed antigens are unable to produce effective immune progression, whereas live attenuated vaccines are able to do so but have the potential to revert to pathogenicity (Liu et al., 2012). Currently, a lack of effective vaccine candidates is restricting the progression within this field, especially due to the multi-stage lifecycle of this pathogen. Stage specific parasite proteins limits protection and thus it is likely that an effective vaccine will have to be developed using a multi-antigenic approach (Liu et al., 2012). For these reasons, we must understand the host-pathogen interactions during invasion to identify key targets for the development of novel vaccines or therapeutics.

1.10.2 Clonal Lineages of *Toxoplasma gondii*

North American and European *T. gondii* strains can be defined as three clonal lineages; type I, II and III with direct association of genotype and disease pathogenicity (Howe et al., 1995). A distinct difference between these clonal strains is their migratory ability. *In vitro* type I strains show enhanced migration in comparison to type II and III strains. These type I parasites exhibit long-distance migration behaviour in the MDCK cell line as well as *ex vivo*. This is also reflected *in vivo*, where type I RH strain migrate more efficiently to the spleen compared to less virulent strains (Saeij et al., 2005). This migration is associated with clonal pathology. Type I strains are generally highly virulent in mice (Fuentes et al., 2001; Howe et al., 1995). Type II strains are associated with clinical human infections and are thought to cause re-activation of

chronic disease in immunosuppressed or immunocompromised patients, and are also associated with congenital infections in Europe and North America (Carneiro et al., 2013; Howe et al., 1995).

Although these clonal lineages are widely accepted, regional differences in the dominant circulating genotype and presence of atypical genotypes are exception to these rules. Genotyping of isolated strains demonstrate a complex relationship of infection, with animal *Toxoplasma* strains being isolated from congenitally infected infants (Carneiro et al., 2013). The current source of these infections are not yet understood and further investigation into fully characterizing isolated parasites will help us to understand these interactions and parasite virulence.

Ultimately, studying the phenotype of highly virulent strains comparatively with non-virulent strains may help to identify key mechanisms in relation to the progression of parasitemia and pathogenicity to prevent disease transmission.

1.10.3 Life Cycle of *Toxoplasma gondii*

There are three extracellular infectious stages of *T. gondii*; tachyzoites, bradyzoites (found in undercooked meat) and sporozoites (found within oocysts that are shed into the environment) (**Figure 12**). *Toxoplasma* bradyzoites and sporozoites are acquired orally through the ingestion of contaminated food or water as tissue cysts or oocysts, respectively (Bonapaz et al., 2010; Cook et al., 2000; Dubey et al., 2002; Esteban-Redondo and Innes, 1997; Guo et al., 2015; Limon et al., 2017). Following ingestion, in both definitive Felidae and intermediate hosts, pH changes within the digestive tract break down the walls of ingested oocysts or tissue cysts to release bradyzoites or sporozoites in the small intestinal lumen (**Figure 12**). Here, parasites invade the intestinal epithelial cells to infect host cells.

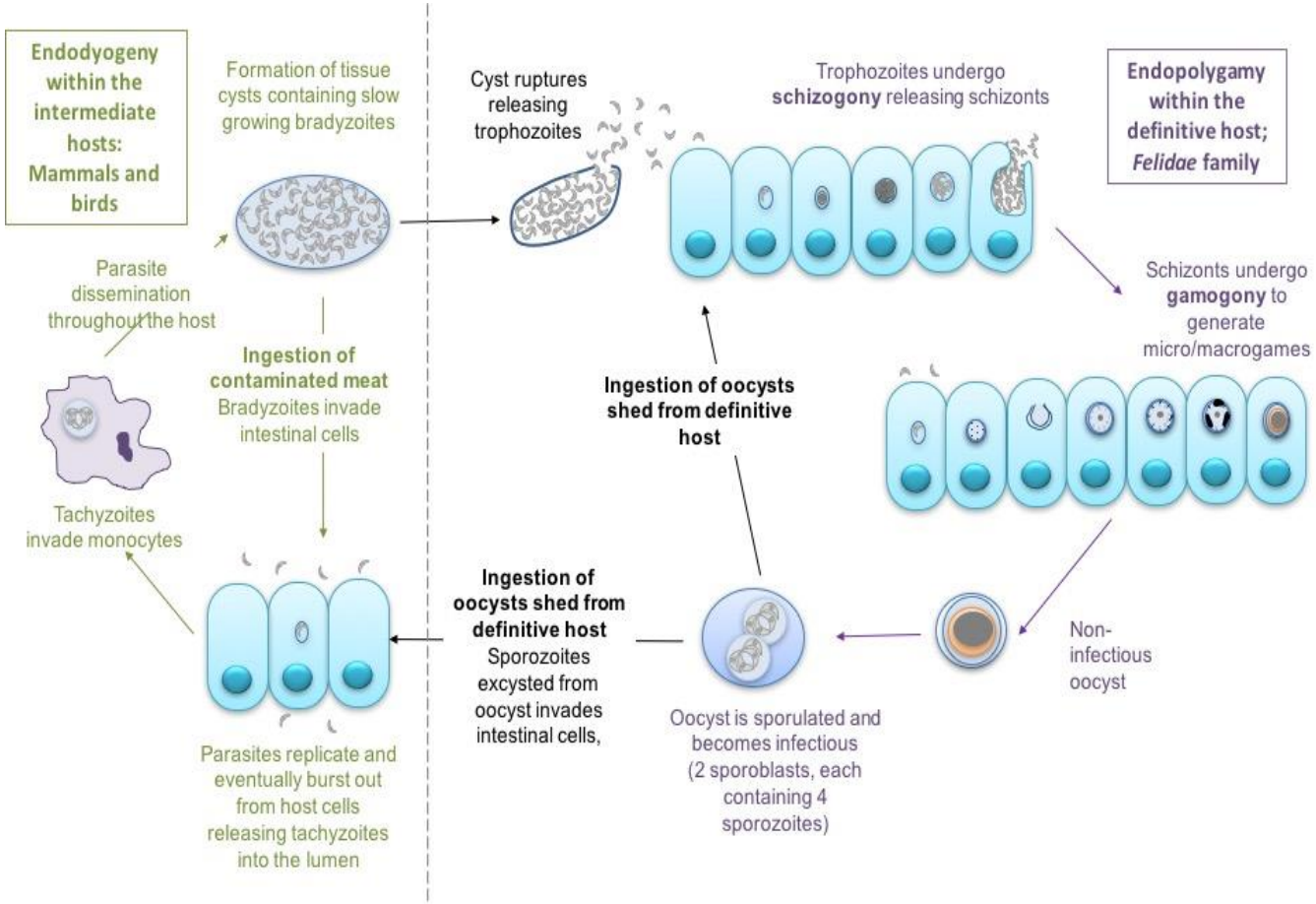

Figure 12) Toxoplasma life cycle

The definitive host for *Toxoplasma* has been identified as the members of the *Felidae* family. Upon ingestion of tissue cysts in mice or birds, parasites are released to infect intestinal cells where they undergo schizogony and gamogeny forming oocysts. Shedding of oocysts results in environmental contamination which further infects intermediate hosts. In intermediate hosts, parasites invade intestinal cells, replicate, burst out of host cells and disseminate to other tissues. Here they form tissue cysts which are ingested in contaminated meat products. [Figure is modified and adapted from (Robert-Gangneux and Dardé, 2012)].

At this stage, the *T. gondii* life cycle differs in the definitive host and intermediate hosts (Black and Boothroyd, 2000; Robert-Gangneux and Dardé, 2012). Within the epithelial cells of the definitive host, invaded parasites undergo a series of processes called endopolygamy (schizogony followed by gamogeony) to produce gametocytes. Macro and micro-gametes fuse to form an oocyst (zygote). An oocyst wall forms around the parasite, and the infected cells burst to release oocysts into the small intestinal lumen which are later shed into feline faeces to contaminate the environment (**Figure 12**) (Black and Boothroyd, 2000; Robert-Gangneux and Dardé, 2012).

Upon ingestion of bradyzoites or oocysts by the intermediate hosts, parasites invade the intestinal epithelial cells and undergo replication by endodyogeny until the host cell bursts to release highly invasive tachyzoites (**Figure 12**) (Black and Boothroyd, 2000; Robert-Gangneux and Dardé, 2012). The tachyzoite stage parasites then re-infect epithelial cells and monocytes. Within monocytes, the parasites exploit the systemic system to disseminate throughout the host and target the lymph node, brain and other tissues (**Figure 12**) (Black and Boothroyd, 2000; Robert-Gangneux and Dardé, 2012). Within host tissues and in response to host immune responses, tachyzoites convert into slow growing bradyzoites to form tissue cysts, and so the cycle continues (**Figure 12**) (Black and Boothroyd, 2000; Robert-Gangneux and Dardé, 2012).

1.11 *Toxoplasma* Effector Molecules for Invasion

Toxoplasma has a wide host range, and can infect virtually all mammalian and avian cells, a feature allowing for its biological success for invasion. Initial invasion events

occur within the small intestine following the release of free parasites from cysts or oocyst. Invasion of host cells is mediated by several proteins that act sequentially; SAGs, MICs, ROPs and GRAs (**Figure 13**). Invasion of host cells can be considered as multiple stages; attachment, formation of a moving junction, rhoptry discharge and finally invasion.

The surface of *Toxoplasma* parasites contain GPI-anchored surface antigens (SAGs) and SAG-related sequence (SRS) proteins. Over 150 of these genes have been identified, however expression of these proteins appears to be life-stage specific. On invasive and proliferative tachyzoites, SAGs 1-3 and SRS 1-3 comprise the dominant phenotype and are thought to be involved with host cell attachment. The abundance of parasite SAGs positions has been theorised to allows for the parasite to glide along the target host cell to identify optimal binding sites during initial invasion (Carruthers and Boothroyd, 2007; Smith, 1995).

After initial invasion, an adhesion event occurs specifically involving the apical pole of *T. gondii*. Due to the widespread distribution of SAG proteins, it was determined that they were not responsible for this apical attachment. Alternatively, this led to the study of MICs. There are approximately 15 MICs that have been identified, many of which are observed to be apically secreted during attachment. MIC2 and MIC3 have since been identified as a crucial secretory adhesion for host cell binding, and likely work synergistically to form a tight attachment to host cells (Carruthers and Sibley, 1997; Garcia-Réguet et al., 2000; Huynh and Carruthers, 2006). This process of attachment also involves another micronemal protein, apical membrane antigen (AMA1). Although the interaction of AMA1 is not fully understood, they are thought to interact with rhoptry neck (RON) proteins prior to the secretion of ROPs.

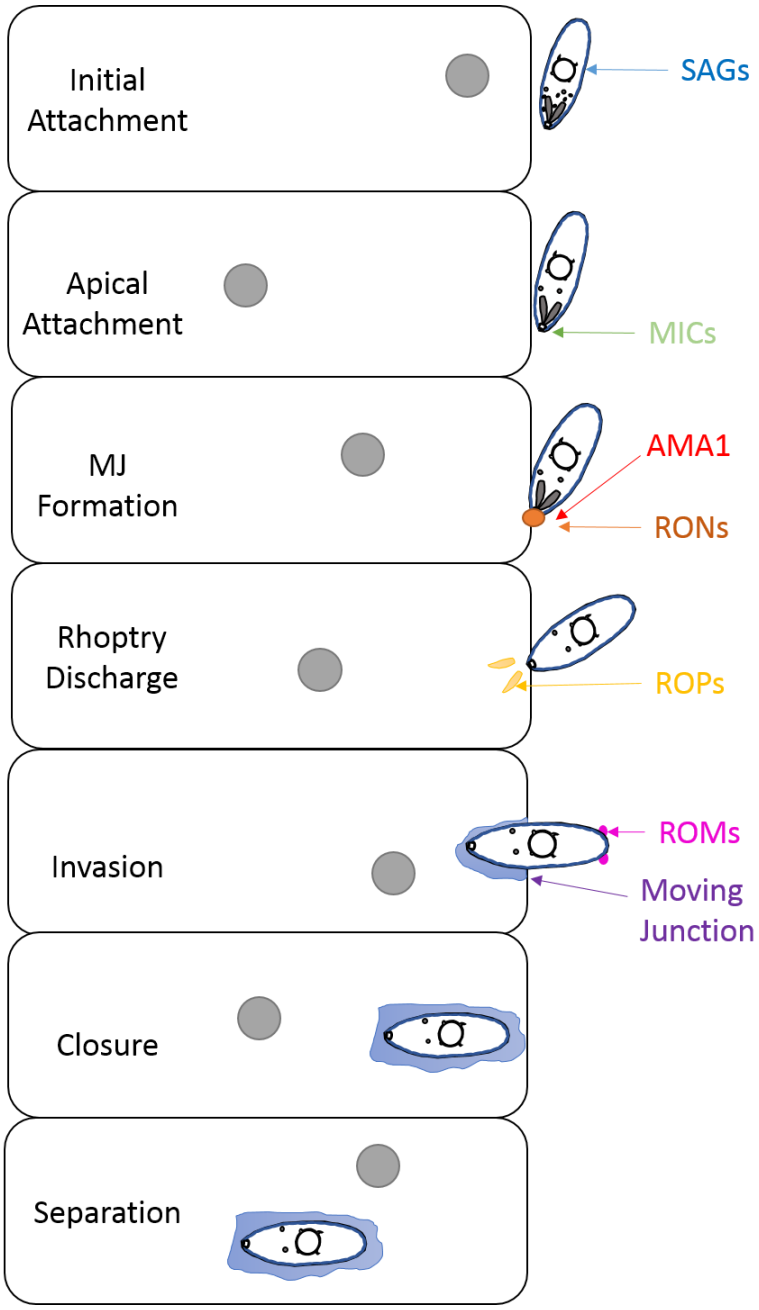

Figure 13) Invasion of Host Cells by Toxoplasma gondii

Initial attachment involves the parasite surface receptor SAG proteins (blue), followed by a calcium-dependent deployment of MICs (green) during apical attachment. At this point, the moving junction is formed by the release of RONs (orange) associated with microneme-derived AMA1 (red) forming a tight interface with a ring-like structure on the host cell surface. ROPs (yellow) are discharged at the invasion site into host cytoplasm. Parasites then invades host cells by pulling transmembrane MICs and the AMA1-RON ring to invaginate the plasma membrane for the creation of a parasitophorous vacuole. Parasites then traverse the host cell membrane in an unknown mechanism and undergo cell closure and separation. Modified from (Carruthers and Boothroyd, 2007).

As these secretory proteins reach the parasite surface, RONs form a stable connection with AMA1 to generate a moving junction (MJ) (Aikawa et al., 1978; Singh et al., 2010). The MJ and apicomplexan gliding motility shares the same actin-myosin motor, which has allowed for the identification of relevant proteins in host cell attachment (Harding et al., 2016). RON2, RON4 and RON8 have been identified to play significant roles in firm attachment to the host cell, potentially in a two-step process (Lebrun et al., 2005; Straub et al., 2011). AMA1 depleted parasites exhibit compromised invasion with no effect on initial attachment, but with inhibition of ROP secretion (Mital et al., 2005). Complete removal of AMA1 suggest that this protein is critical for invasion, but not essential (Egarter et al., 2014). Thus, the complete role and function of AMA1 for host cell invasion is still not understood.

As the invasion process continues, *Toxoplasma* hijacks the host organelles and cytoskeleton as the MJ migrates towards the posterior end of the parasite to form a parasitophorous vacuole (PV) border. *T. gondii* then utilises their actin-myosin motor supported by the IMC, to actively penetrate and become internalised within host cells. At this stage, ROPs are secreted into the PV including ROP1, ROP4, ROP16 and ROP18 which signals the end of early stage invasion (Butcher et al., 2011; Carey et al., 2004; Carruthers and Sibley, 1997; El Hajj et al., 2007).

Within the PV, GRAs are secreted to modify the structural environment and the PV membrane acts as a sieve for the diffusion of host small molecules, regulated by GRAs 17 and 23 (Gold et al., 2015). Within the PV, GRAs 2, 4 and 6 form the intervacuolar membrane (IVM) which is thought to provide a supporting scaffold for the PV and partake in nutrient trafficking (Labruyere et al., 1999; Mercier and Cesbron-Delauw, 2015). GRA7 is reported to be phosphorylated upon invasion of host cells and

associates with ROPs 2 and 4, and is thought to stabilise the PV (Clough and Frickel, 2017; Dunn et al., 2008). Other GRAs are reported within the PV and IVN however the role of these are not well understood.

Under the protection of the PV, *T. gondii* replicate by a process of internal budding to create two daughter cells (Goldman et al., 1958). Here the IMC plays an additional role in cell division, and an enrichment of IMC3 can be observed in daughter complexes (Gubbels et al., 2004; Morrissette and Sibley, 2002). The expression of IMC genes is coordinated and coincides with *T. gondii* budding (IMC1, 3-6, 8-11, 13 and 15) however IMC 7 and 12 have the opposite expression, and IMC14 exhibits a 1 hour lag (Anderson-white et al., 2012). Consequentially, a subset of IMCs have been attributed to each stage of replication (Anderson-white et al., 2012). Repeated cycles of parasite division form clusters of rosettes within host cells that eventually become overloaded and burst to release parasites back into the intestinal lumen (Gregg et al., 2013).

1.12 Manipulation of Host Cell Responses by *T. gondii*

As *Toxoplasma* is an obligate intracellular parasite, the success of host cell invasion is crucial for parasite survival and subsequent dissemination throughout the host. The successful infection of host immune cells poses a challenge to the parasite as these host cells possess antimicrobial machinery. To ensure survival, *Toxoplasma* must manipulate host cell signalling and immune response to evade immunity.

Host immunity is stimulated by pathogen-associated molecular patterns (PAMPs) that stimulate host pattern receptors such as TLRs. The activation of TLR (except TLR3) initiates intracellular signalling cascades via the common adapter myeloid differentiation factor 88 (MyD88). During *Toxoplasma* infection in MyD88 deficient

mice, IL-12 and IFN-γ response is impaired, suggesting that TLRs are important for the correct recognition of *Toxoplasma* and initiation of host immune response.

Our understanding of how the parasite manipulates host cells is still only partially understood, however a few processes have been described. Upon infection, *Toxoplasma* is known to block apoptotic processes, disrupt host cell transcription factors including signal transducer and activator of transcription 1 (STAT1) and NF-κB, which in turn inhibits the production of IL-12 and TNF-α.

STAT family proteins induce a broad range transcriptional program and are modulated differently according to the parasite clonal lineage. All strains appear to inhibit the dissociation of STAT1 from nuclear DNA to prevent future-reactivation of host cell response (Rosowski et al., 2014). During normal STAT1 activation, STAT1 undergoes nuclear cytoplasmic cycling. Following DNA binding and activation, STAT1 is dissociated with nuclear DNA, dephosphorylated and exported back into the cytoplasm where it can be re-activated to induce downstream responses to host cell infection. Other STAT members STAT3 and STAT6 must also undergo cycling of DNA to fulfil their full transcriptional functions. During infection, the ablation of a STAT1 response is thought to benefit parasite survival as $STAT1^{-/-}$ mice show enhanced susceptibility to infection (Rothfuchs et al., 2006).

In contrast to STAT1 activation, host cell STAT3 and STAT6 activation is regulated by *Toxoplasma* ROP16 in a strain-specific manner. During host cell invasion, *Toxoplasma* ROP16 is injected into the host cell cytosol, and localises to the host cell nucleus where it can modulate host cell signalling pathways and suppress macrophage pro-inflammatory responses (IL-12 production). Types I and III strains of *Toxoplasma* are potent activators of STAT3, whereas type II strains are incapable of sustaining

activation. Deletion of ROP16 converts type I parasites into high inducers of IL-12p40 and eliminates the parasite's ability to block nitric oxide production. Interestingly, ROP16$^{-/-}$ parasites exhibited increased replicative behaviour both *in vivo* and *in vitro*, which is attributed to STAT6-mediated activation of arginase-1, an essential amino acid nutrient required for parasite survival and for host cell production of nitric oxide (Butcher et al., 2011; Laliberte and Carruthers, 2008; Ong et al., 2010).

Toxoplasma ROP16 modulation of IL-12p40 is significant for parasite survival, as the IL-12 IFN-γ pathway has repeatedly been demonstrated to play a critical role in control of *Toxoplasma* infections. The recognition of parasite factors via TLRs activates the NF-κB pathway to induce IL-12 production by dendritic cells and macrophages (Dupont et al., 2013). IL-12 in turn activates the production of IFN-γ by T cells and natural killer (NK) cells (Dupont et al., 2013). Mice lacking IFN-γ, the IFN-γ receptor of IL-12p40 show enhanced susceptibility to infection (Jankovic et al., 2002; Rothfuchs et al., 2006).

NF-κB is an important part of host response to *T. gondii*, and is one of the key pathways modulated following invasion. Again, there are differences in the way each clonal lineage of *T. gondii* manipulates the host response. Type II strains drive translocation of NF-κB to the nuclei of myeloid cells, resulting in the secretion of high levels of IL-12, whereas type I strains inhibit NF-κB pathway translocation (Rosowski et al., 2011). In type II parasites, the dense granule protein 15 (GRA15) is responsible for driving NF-κB translocation (Rosowski et al., 2011), whereas the type I allele of the rhoptry protein (ROP18) inhibits the NF-κB pathway (Du et al., 2014).

Clearly, the modulation of host cell response to infection is variable across parasite lineages, and understanding these processes are critical to identifying mechanisms to tackle infections in the future.

1.13. Interactions between *Toxoplasma gondii* and the Intestinal Epithelium

Following oral ingestion, *Toxoplasma* traverses the intestinal epithelium to disseminate deep into host tissues reaching immunologically privileged sites to cause severe pathology. Several known interactions occur during invasion; disruption of tight junctions, host cell cytokine production, and release of Paneth cell defensins. However, our knowledge of the specific molecular pathways governing the interaction between *T. gondii* and the intestinal epithelium are still extremely limited.

1.13.1 Disruption of Intercellular Tight Junctions

During early stage invasion, *Toxoplasma* concentrate at intercellular junctions and potentially exploit a paracellular route of migration to traverse the intestinal epithelium. Further work dissecting the mechanisms underlying transepithelial migration have identified a crucial interaction of *Toxoplasma* MIC2 with host cell intercellular adhesion molecule 1 (ICAM-1) which is up-regulated during infection (Barragan et al., 2005). Infection of Madin Darby Canine Kidney monolayers by type I RH strain tachyzoites for 6 hours report that migration can occur without disrupting the epithelial barrier integrity (Barragan et al., 2005), however live cell imaging of YFP-expressing RH bradyzoite infection of rodent intestinal epithelial cells demonstrate a disruption to the tight junctional complex component, occludin (Weight et al., 2015). Here, infection altered the distribution of occludin which led to fractured tight junctional complexes and observable occludin within the host cell cytosol (Weight et al., 2015). This finding is in agreement with a more recent study of CaCo2

monolayers infected by RH-derived 2F1 strain for 24 hours, which induced co-localisation of tight junction proteins occludin and zonula-occludens 1 (ZO-1) which manifested as a discontinuous pattern and resulted in decrease transepithelial electrical resistance (TEER) (Briceño et al., 2016). Importantly, the parasite counterpart in this interaction is not yet known.

In response to stimulation, the intestinal epithelium releases mediators to attract and activate immune cells. *In vitro,* enterocyte cell lines respond to *Toxoplasma* infection by release of CCL2 (MCP-1), CXCL2 (MIP-2) and CXCL10 (IP-10) (Mennechet et al., 2002). Co-incubation of enterocytes with primed intraepithelial lamina propria $CD4^+$ T cells enhances this response by producing CCL5 (RANTES), CCL2, CCL7 (MCP-3) and CXCL10 following *Toxoplasma* infection (Mennechet et al., 2002). *In vivo,* 8-day orally infected mice show significantly up-regulated expressed of CCL2, CCL3, CCL5, CXCL2, CXCL9 and CXCL10 in the small intestine (Gopal et al., 2011; Mennechet et al., 2002). Receptors for some of these chemokines (for example CCL2 and CCL5) have been shown to play important host protective roles in *T. gondii* infection through induction of appropriate immune responses. Understanding what drives production of these chemokines in the intestinal epithelium following *T. gondii* infection, what other signals the epithelium may transmit to the immune system, and whether the parasite can manipulate these pathways, may allow for the design of novel adjuvants or therapeutics.

1.13.2. TLR-9 Mediated Release of Paneth Cell Defensins

Oral infection with *T. gondii* stimulates IFN-β production via TLR9, resulting in the release of α-defensins. *In vitro* studies have shown that both α- and β-defensins can reduce the infectivity of *T. gondii,* though the precise mechanism remains unclear.

Additionally, α-defensin production may be linked to the production of host-protective chemokines by the intestinal epithelium. Interestingly, Type I strains may be capable of down-modulating the production of host β-defensins to enhance invasion and survival, though the parasite effector proteins mediating these effects remain to be identified.

Here, it is evident that many aspects of the intestinal epithelial response to *T. gondii* are poorly understood. The generation of a suitable model could facilitate the progress within this field of study by identifying key host-pathogen interactions. These findings also re-iterate the importance of generating a suitable model that retains an apically polarised phenotype to mimic the *in vivo* mechanisms of infection.

1.14 The Need for Proteomic Studies of Host-Pathogen Interactions

Generally, the observations reported about *Toxoplasma* invasion have been largely discovered using reductionist and hypothesis-driven experimental design. However recent developments in the field of genome sequencing, transcriptomic and proteomic approaches will be crucial for identifying the host-pathogen interactions during infection. Unlike traditional studies, systems biology gather experimental data in a hypothesis-generating approach through assessment of whole complex systems.

Currently, *Toxoplasma* host-pathogen interactions has relied heavily on transcriptomic approaches, however the relationship between transcripts and their respective protein abundance is not clear. It has been estimated that only approximately half of transcripts detected by transcriptomic approaches correlate with a significant change in protein abundance (Ghazalpour et al., 2011). Unsurprisingly, studying the proteome changes during *Toxoplasma* infection has reported additional findings not observed using

transcriptomic, microarray or serial analysis of gene expression (SAGE) techniques (Xia et al., 2008). Thus the use of proteomic systems biology approaches may be favoured over microarray or transcriptomic technologies to identify key mechanisms for further study.

Proteomic techniques have been used to compare parasites of different developmental stages (Z. X. Wang et al., 2017) and parasite strains of clonal lineages (Zhou et al., 2017) to elucidate some of the underpinning parasite biology that is important for understanding the mechanisms of parasite growth and replication. However, one of the current limitations of utilizing proteomic approaches for the purposes of studying host cell responses to early stage infection is a lack of appropriate intestinal model. Existing cell line models, as discussed previously, can't recapitulate the host cell responses of the *in vivo* epithelium which makes them an unsuitable model. Studies have utilised cell lines to study infections, but generally these experiments require almost 100% parasitisation to compensate for the signal-to-noise ratio of uninfected cells (Al-Bajalan et al., 2017; Guiton et al., 2017). From a physiological standpoint, these models do not represent a natural infection where parasites form small, discrete foci of infection in relatively low abundance (Coombes et al., 2013). Thus the findings performed in cells lines *in vitro* with high parasitic loads are likely to be not comparable to the *in vivo* progression of infection. For these reasons, there is a demand for the establishment and optimisation of an *in vitro* alternative for study of these events in order to identify targets for the development of novel therapeutics.

1.15 Research Aims and Objectives

A lack of suitable *in vitro* model and the identification of LGR5+ stem cells has driven the establishment of stem-cell derived 3D intestinal models. However limitations with

accessing the luminal space in organoid cultures poses challenges for studying host-pathogen interactions within this model. For this reason, this doctoral project aims to evaluate the use of organoid cultures as a model for intestinal biology, and to optimise organoid models specifically for the study of enteric pathogens using the successful protozoan parasite *T. gondii* to validate the model. The project can be separated into three separate aims as described below.

<u>*Aim number 1:*</u> *Generate organoid models enriched for particular epithelial cell types, and validate their use as a potential novel infection model using mass spectrometry-based label-free quantitative proteomics*

Objectives:

a) Demonstrate that organoids are amenable to manipulation to drug skewing to generate high purity cultures with a major dominating intestinal epithelial cell type and confirm changes with confocal and imaging
b) Validate the changes observed via mass spectrometry by comparing proteomic profiles of each high purity culture with known markers of differentiated cell types within the intestinal epithelium
c) Identify novel proteins belonging to specific differentiated intestinal epithelial cell types

<u>*Aim number 2:*</u> *Modify existing organoid culture protocols to develop a semi-monolayer model with an accessible luminal surface for the application of parasites*

Objectives:

a) Establish a culture protocol to generate organoids with an open luminal surface

b) Characterise the differentiation status, polarisation and integrity of the semi-monolayer model using confocal microscopy and proteomic approaches

Aim number 3: *Using T. gondii as a model pathogen, optimize methods for the infection of collagen-supported epithelial sheets, and study the host response to infection using mass spectrometry-based label-free quantitative proteomics*

Objectives:

a) Perform pilot infections with *T. gondii* to provide proof-of-concept evidence to support the use of the modified model as a tool to study host-pathogen infections
b) Quantify infection with *T. gondii* via confocal imaging and determine time points for proteomic experiments
c) Evaluate host response to two strains of *T. gondii* at early stage invasion and during parasite replication via mass spectrometry-based label-free quantitative proteomics

Together, these aims will examine the feasibility of utilising organoids for infection, and will explore the use of these models to study basic host-pathogen interactions within the small intestinal epithelium.

Chapter 2 – Materials and Methods

2.1 Murine Small Intestinal Organoid Culture

All mice used within this study were maintained in accordance with the Animals Scientific Procedures Act 1986 (ASPA) under the PPL of "cull for tissue".

Drug skew treatments of organoid cultures described in chapter 3 was performed by Zoe Matthews in University of East Anglia using PGK-Cre on C57/BL6 background with no Cre activation i.e. wild type C57/BL6 mice.

With the exception of the work mentioned above, throughout this study unless otherwise stated, female specific-pathogen free, C57B1/6J strain, aged between 6-12 weeks (Charles River, Margate, United Kingdom) were culled by cervical dislocation schedule 1 procedure. Dissections of mice were performed in the Biological Specimens Unit (BSU) of the University of Liverpool. Biological samples were transported to IC2 (Liverpool Science Park) for further processing in PBS on ice.

2.1.1 Crypt Isolation and Murine Organoid Culture

Cold PBS without Ca^{++} or Mg^{++} (Sigma Aldrich, Dorset, United Kingdom) was used throughout the isolation process unless stated otherwise. Murine jejunum and ileum were transferred PBS where abdominal fat was carefully removed. Small intestinal (SI) tissues were cut longitudinally and washed thrice in PBS. SI tissues was cut into $0.5cm^2$ sections and transferred to fresh PBS for transport.

Tissue pieces were incubated in 15mL of 30mM EDTA dissociation buffer for 5 minutes at room temperature (**Table 3**). SI were transferred to fresh PBS and shaken for approximately 15 seconds. PBS fraction was examined by light microscopy to

check for epithelial dissociation. Incubation in EDTA and PBS shaking was repeated a further 3 times to further dissociate villus to generate a crypt-rich solution (**Figure 14**). Crypt solutions were filtered through a 70µm cell strainer into a falcon tube to remove remaining villus fragments. Crypt density was estimated by performing a rough count of 20µL of the filtered solution. Crypts were concentrated by centrifugation at 300*xg* for 10 minutes at 4 degrees, and re-suspended at a density of 10 crypts/µL into Matrigel® (Corning). Matrigel® solution was plated onto pre-warmed 48-well plates containing 9mm round coverslips in 30µL domes and allowed to polymerise for 30 minutes at 37^{o}C and 5% CO_2.

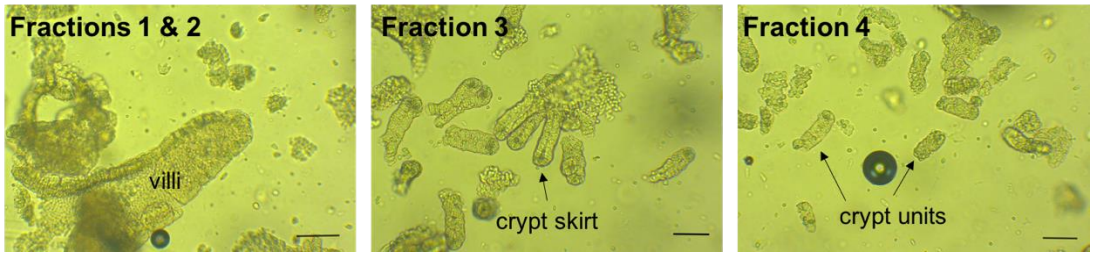

Figure 14) Dissociation of small intestinal tissues remove mucus, villus and eventually crypt units

During the first two cycles of 30mM EDTA incubation, the luminal debris, mucus contents and large villus structures are dissociated from small intestinal tissues. Within the third cycle of EDTA incubation, crypt columnar units begin to dissociate from the base of the villus as clumps that resemble a "crypt skirt". Small intestinal crypts are identifiable by their elongated shape and the presence of granular Paneth cells. By the fourth round of dissociation, crypt columnar units are removed singularly to generate a crypt rich fraction which can be concentrated and embedded into Matrigel® for culture. Scale bars = 100µm

Complete organoid media was prepared according to published protocol (Sato et al., 2009), however the media was unusually yellow in colour and was unable to sustain organoid growth during initial attempts (**Table 3**). To address this, I tested the addition of either NAC or HEPES to correct the pH of the medium. As a result, I found that the addition of HEPES to a final concentration of 0.1M was suitable for organoid culture

and was thus added to the media each time. Complete media changes were performed every 4 days (Sato *et al.*, 2009).

Table 3. Recipes of buffers and medium required for establishing murine organoids

	Volume	**Stock concentration**	**Final concentration**
EDTA Dissociation Buffer			
0.5M EDTA (Corning, ThermoFisher)	900µL	0.5M	30mM
PBS	14.1mL	-	-
Complete Organoid Media (per 1mL)			
Advanced Reduced Serum Dulbecco's Modified Eagle Medium (Gibco™, ThermoFisher)		-	-
Human R-Spondin 1 (PeproTech)	5 or 10µL*	100µg/mL	1µg/mL but reduced to 500ng/mL after first passage*
Murine Noggin (PeproTech)	10µL	10µg/mL	100ng/mL
Human EGF (PeproTech)	10µL	5µg/mL	50ng/mL
B27 Supplement (Gibco™, ThermoFisher)	20µL	50X	1X
N2 Supplement (Gibco™, ThermoFisher)	10µL	100X	1X
Penicillin/Streptomicin (Sigma)	10µL	-	1%
N-Acetyl L-Cysteine (NAC)+ Included in the original recipe but was later replaced with HEPES+	10µL	100mM	1mM
HEPES (Sigma)	10µL	1M	10mM

2.1.2 Organoid Passage

At days 7-9 of culture, established organoids were routinely passaged by mechanical disruption. Organoid media was removed via pipetting and Matrigel® domes were washed gently with PBS to remove residual media. Matrigel® domes were disrupted by repeated pipetting with 500µL of cold PBS (using a P1000 pipette) and transferred to a fresh tube. Organoid solutions were syringed through a 27G needle into a 15mL conical tube, and the volume was topped to 10mL with cold PBS. Fragmented organoid cultures were concentrated down at 300*xg* for 10 min at 4ºC, and re-plated in fresh Matrigel® as described above. Generally, organoids were passaged at a 1:3 or 1:4 ratio dependent upon density.

2.1.3 Drug Skew Treatments of Murine Small Intestinal Organoids

Drug skew treatments in chapter 3 were performed by Zoe Matthews at the University of East Anglia. Organoids were established, as above, and overlaid with drug skew media consisting of Dulbecco's Modified Eagle Media (DMEM) containing 500ng/ml R-spondin (R&D Systems), 50ng/ml EGF (Peprotech) and 100ng/ml noggin (Peprotech), as described by Sato et al, 2009. Media was replaced on days 2, 5 and 7 post-isolation to introduce 3µM CHIR99021 (Tocris) and 10µM DAPT (Tocris) for Paneth cell; 2µM IWP-2 (Tocris) and 10µM DAPT for goblet and enteroendocrine cells (Yin *et al.*, 2013). Drug skewed organoids were not passaged, but were fixed for confocal imaging or prepared for proteomics at day 8.

2.2 Establishment of Epithelial Sheet Cultures on Collagen Gels

For the development of organoid models on collagen gels, murine organoids were first established in Matrigel®. At day 7 organoids were fragmented and passaged onto

either bovine (type I) or rat tail (type I) collagen gel domes in 48-well tissue cultures plates containing sterile 9mm coverslips. Collagen gels were prepared as described below.

2.2.1 Preparation of Collagen Gels

Type 1 bovine collagen gels were prepared to a final concentration of 1.5mg and 2mg/mL using a modified version of a previously described protocol (Sixt and Lämmermann, 2011) (**Table 4**). Briefly, 7.5% sodium bicarbonate solution ($NaHCO_3$, sterile-filtered) (Sigma Aldrich, Dorset, United Kingdom) and sterile water were added to 10X Minimal Essential Medium (Eagle) (MEM) with Earle's salts, without, L-glutamine and sodium bicarbonate (Sigma Aldrich) and thoroughly mixed. Purecol® (3mg/mL) (Advanced Biomatrix, San Diego, USA) was added to the MEM/sodium bicarbonate solution and pH strips were used to test pH levels of the gel solution.

Table 4) Recipes for 10 wells of either 1.5mg/mL or 2mg/mL bovine type I collagen gels

	Final collagen concentration 1.5mg/mL	Final collagen concentration 2mg/mL
10x DMEM (µL)	40.00	40.00
Water (µL)	137.6	70.94
7.5% $NaHCO_3$ (µL)	22.40	22.40
Collagen (3mg/mL) (µL)	200.00	266.66

Type 1 rat-tail collagen gels (Life Technologies, Warrington, United Kingdom) were prepared following manufacturer's instructions to a final concentration of 1.5mg/mL

and 2mg/mL using the volumes below (**Table 5**). NaOH and water was added to 10X MEM and pipetted carefully to ensure thorough mixing. Rat tail collagen (3mg/mL) was added to the MEM solution and pH strips were used to test pH levels.

Table 5) Recipes for 10 wells of either 1.5mg/mL or 2mg/mL rat tail type I collagen gels

	Final collagen concentration 1.5mg/mL	Final collagen concentration 2mg/mL
10x DMEM (µL)	40.00	40.00
Water (µL)	190.00	123.33
1M NaOH (µL)	10.00	10.00
Collagen (3mg/mL) (µL)	200.00	266.66

Both types of collagen gels were formed by pipetting 30µL of mixture into 48-well plates onto 9mm coverslips followed by incubation at 37ºC and 5% CO_2 for a minimum of 30 min to allow for gel polymerisation.

2.2.2 Seeding Organoid Fragments onto Collagen Gels

Day 7 murine organoid cultures were fragmented through pipetting and syringing, concentrated down and re-suspended in PBS. Fragment solutions were then overlaid onto polymerised collagen gels. Success in the initial attempts to culture monolayers were limited by the poor adherence of organoid fragments onto the collagen gels which were due to two reasons; the shape of the dome causing fragments to slip off resulting in a pool of fragments not adhered to the collagen, and the incubation time of fragments to allow adherence without drying the cells out which led to poor viability of cells.

To address this issue, subsequent collagen gels were pipetted as previously, however they were smoothed out using a P200 pipette tip in order to generate a flatter surface to prevent organoid fragments from sliding off the gel and pooling around the base of the dome. This in turn allowed for more organoid fragments to be associated with the collagen gels.

To access the duration of incubation for adherence to the collagen gel, I aimed to identify a balance between feasibly applying the fragments in a small volume, without the samples drying out too quickly. Two volumes of PBS containing fragments were attempted and evaluated (5µL and 10µL) along with two types of pipette tips; small bore (1-10µL tip) and medium bore (10-200µL tips).

Here, I determined that using 1-10µL tips were unsuitable for re-plating organoids as the bore of the tip was too narrow to allow the organoid fragments to be dispensed without touching/compromising the surface of the gel. Comparatively, using the larger tip, I could pipette the organoid fragments above the gel and allow gravity to pull the suspension downwards onto the collagen gel without damaging it. Similarly, using the larger volume of 10µL was beneficial as the large volume allowed for more coverage of the collagen gel, whereas re-plating using 5µL volume yielded fragments concentrated in one region of the gel. For this reason, subsequent monolayer establishment was performed using organoid fragments re-suspending in 10µL PBS, and pipetted using 10-200µL tips.

Organoids incubated for 15 minutes in 37^{o}C and 5% CO_2 and complete media was added to cultures for 8 days, with a complete media change on day 4.

2.3 *Toxoplasma gondii* Culture

Two clonal strains of *T. gondii* are used within this thesis; RH strain (type I, virulent) and Veg strain (type III, avirulent). Both strains of *T. gondii* were cultured in immortalised adherent Vero cells derived from African green monkey kidney epithelial cells.

Vero and *T. gondii* RH and Veg were cultured in T-25 vent-lidded flasks with basal media Dulbecco's Modified Eagle's Medium with high glucose supplemented with 5% foetal bovine serum and 1% Penicillin/Streptomycin, and incubated at 37^{o}C in a 5% CO_2 atmosphere.

2.3.1 Vero Cell Culture

Confluent Vero cells were sub-cultured every 7 days. Cell supernatant was discarded, and cell monolayer as rinsed thrice with 3mL PBS to remove residual serum that inhibits trypsin function. To detach cells from the flask, 1mL of Trypsin-EDTA (Gibco) was added and cells were incubated for 5 min at 37^{o}C in a 5% CO_2. Progression of detachment was examined by light microscopy and cells were re-incubated for a further 5 min if required. To neutralise trypsin activity, 4mL of complete media was added to cells and 10µL of cell suspension was added to 10µL of trypan blue (Thermofisher) for counting using a Neubauer chamber. New flasks were seeded at 4 x 10^5 cells/flask.

2.3.2 *Toxoplasma gondii* Culture

Following an overnight incubation, culture medium was replaced on Vero cells, and a cryovial of frozen parasite tachyzoites were added. Infected Vero cell cultures were examined daily using an inverted light microscope to monitor parasite growth. Within

approximately 5-7 days, 75% of Vero cells were infected with regions of parasites egress observed. At this point, 10µL of supernatant was taken to count parasites within the culture. To maintain parasite cultures, *T. gondii* RH and Veg were passaged onto new flasks at 3×10^3 and 1×10^4 per flask respectively. Parasite passage was routinely performed every 7 days, onto 24 hour incubated 14 cells.

2.3.3 Parasite Purification from Vero Cells

For infection assays, parasites were grown until over 75% of Vero cells were infected and parasites were beginning to egress. Infected veros were removed from flasks using a cell scraper and transferred to a 50mL conical tube. Parasites were concentrated down at 400*xg* for 10 min and cell pellet was re-suspended in 10mL of PBS. The cell suspension was syringed thrice with a blunt ended needle to disrupt Vero cell structure and release intracellular tachyzoites. The cell and parasite suspension was concentrated down again at 400*xg* for 10 min and the cell pellet was re-suspended in 5mL of PBS.

A PD-10 desalting column (GE HealthCare Life Sciences, Buckinghamshire, United Kingdom) was equilibrated by releasing and discarding the storage fluid. The column was then washed twice with 5mL PBS, and the flow through discarded. The parasite cell suspension was added to the column, collecting the flow through. An additional 5mL of PBS was added to flush the column. Parasite counts were then performed on 10µL of PBS, the desired number of parasites were concentrated down by centrifugation and re-suspended in complete organoid media.

2.4 *Toxoplasma gondii* Infection Assay

Media was removed from day 7 collagen-supported epithelial sheets, and media containing parasites was applied directly onto cultures, then incubated at 37^{o}C and 5% CO_2.

For initial infections, epithelial sheets were allowed to incubate with parasites for set time periods and samples were fixed with 4% PFA (Life Technologies) in PBS for 60 minutes at room temperature.

For optimisation of the infection protocol, we introduced centrifugation following exposure to parasites. Infected monolayer cultures were either not centrifuged, or centrifuged (at 100*xg* for 1 min) prior to incubation. Cultures were fixed and stained for confocal imaging.

To assess the role of mucus during the initial stages of infection, we introduced a pre-treatment with a mucolytic N-Acetyl L-Cysteine (NAC) (Sigma Aldrich). At day 7, media was replaced with organoid media containing 0mM, 2mM, 5mM or 10mM NAC, and sheets were incubated for 60 minutes. Mucolytic media was removed after incubation and replaced with complete media containing *T. gondii* tachyzoites. Samples were fixed for confocal imaging. For each infection within this thesis, a non-infected control was also prepared for comparison.

2.5 Antibody Staining and Confocal Imaging

For chapters 4 and 5, all staining of organoid and epithelial sheet samples were performed on 9mm coverslips in 48-well plates. Organoids samples used in chapters 4 and 5 were fixed with 4% paraformaldehyde (PFA) in PBS for 60 minutes at room temperature. All staining steps were performed on a rocker.

To stain epithelial sheets, samples were washed thrice with washing buffer; PBS with 1% donkey serum and 0.1% Triton X-100. Samples were incubated for 1 hour at room temperature in blocking buffer. Primary antibodies were made up in blocking buffer; PBS with 10% donkey serum and 1% Triton X-100, and incubated on epithelial sheets for 1 hour at room temperature. Epithelial sheets were then washed thrice with washing buffer. Secondary antibodies, epithelial stains and DAPI were made up in washing buffer, and incubated on epithelial sheets for 2 hours at room temperature. Epithelial sheets were washed thrice in PBS and extracted from 48-well plates on coverslips.

To stain 3D organoids, samples were washed for 2 hours with washing buffer at room temperature, with buffer changed every 20 min. Organoid samples were incubated with blocking buffer for 4 hour, then primary antibodies were incubated in blocking buffer overnight at 4^{o}C. Samples were washed thrice with washing buffer, and secondary antibodies, epithelial stains and DAPI were incubated for 2 hours at room temperature. Organoid samples were washed thrice in PBS and extracted from 48-well plates on coverslips.

To prevent damaging epithelial sheets and organoid samples during mounting, 7mm diameter O-rings were attached to glass slides using rubber adhesive (Halfords). Hydromount (Scientific Laboratory Supplies, Nottingham, United Kingdom) was

pipetted into O-rings, and the sample was inverted onto the Hydromount solution for preservation. Stained samples were stored in the dark at 4^{o}C until confocal imaging.

For characterisation of collagen sheets, organoids and epithelial sheets were stained with phalloidin, and a combination of either lysozyme or mucin-2 (**Table 6**).

To visualise tight junctions, epithelial sheets were stained with e-cadherin, CD326 EpCam or ZO-1 (**Table 6**). For infections, epithelial sheets were stained with phalloidin and anti-SAG1 (**Table 6**).

Secondary antibodies used were either donkey anti-mouse Alexa Fluor 488 (AbCam, Cambridge, United Kingdom), donkey anti-rabbit FITC (Stratech Scientific Ltd, Suffolk, United Kingdom), or donkey anti-rabbit TRITC (Stratech). All samples were stained with DAPI for nuclear visualisation.

All images reported in chapters 4 and 5 were acquired in the Centre for Cell Imaging within the Institute of Integrative Biology, University of Liverpool. Confocal images were acquired using Zen Black software (Zeiss) on a Zeiss LSM880 upright confocal microscope with laser lines Diode (405), Argon (488), DPSS-5610 (561) and HeNe633 (633) and W-Plan Apochromat 40x/1.0 Dic (water immersion) objective (Zeiss) or Plan-Apochromat 63x/1.0 oil DIC M27 (oil immersion) objective (Zeiss) lenses.

Table 6) Antibodies and stains used for confocal imaging in chapters 4 and 5.			
Product	**Host**	**Manufacturer**	**Target**
Stains			
Phalloidin conjugated to rhodamine	N/A	Life Technologies	F-actin
Phalloidin conjugated to AF647	N/A	Life Technologies	F-actin
DAPI	N/A	Life Technologies	Nucleus
Primary Antibody			
Chromogranin A	Rabbit	Insight Biotechnology	Enteroendocrine Cells
E-cadherin (24E10)	Rabbit	BD Transduction Laboratories	Tight Junctions
Epithelial Cell Adhesion Molecule (CD326 EpCam)	Mouse	Affymetrix eBiosciences	Tight Junctions
GRA7	Rabbit	Gift from David Sibley (Washington University)	Dense Granule 7 of *T. gondii*
Lysozyme (BGN/06/961)	Mouse	AbCam	Lysozyme (Paneth cells)
Mucin-2 (H-300)	Rabbit	Insight Biotechnology	Mucin 2 (goblet cells)
SAG-1 (TP3)	Mouse	Abcam	Surface antigen protein of *T. gondii*
Zonular Occludens 1 (ZO-1)	Rabbit	Abcam	Tight junction Protein
Secondary Antibody			
Anti-rabbit TRITC	Donkey	Stratech Scientific Ltd	N/A
Anti-rabbit FITC	Donkey	Stratech Scientific Ltd	N/A
Anti-mouse AF488	Donkey	AbCam	N/A

2.6 Quantification of Confocal Images using Imaris

All images quantified for characterisation and infection were processed using Imaris x64 v9.0.1 image analysis software (BitPlane). In all cases, automated cell counting was manually checked for accuracy of quantification.

In chapter 4, total cell numbers and numbers of differentiated cells were acquired using the "spots" function on Imaris (**Figure 15**). The "spots" function on Imaris detects fluorescent signals from any chosen source channel and assigns a spot which can be automatically quantified within the software. To calculate the total number of cells within an image, the spots function was used to quantify nuclear staining by detecting DAPI fluorescence. Using the default settings (minimum diameter: 4.15µm), followed by manually adjusting the detection threshold, it was possible to generate an overlay of "spots" that was representative of the cells within the image (**Figure 15 B**).

The detection of differentiated cells was also quantified using the "spot" function by detection of mucin-2 (goblet cell marker) via FITC fluorescence (**Figure 15 C**) or lysozyme (Paneth cell marker) via AF488 fluorescence. All "spots" were manually checked for accuracy of the fluorescent detection and edited as appropriate. The number of goblet and Paneth cell populations within our monolayer culture was calculated as a proportion of the total number of cells available within the field of view.

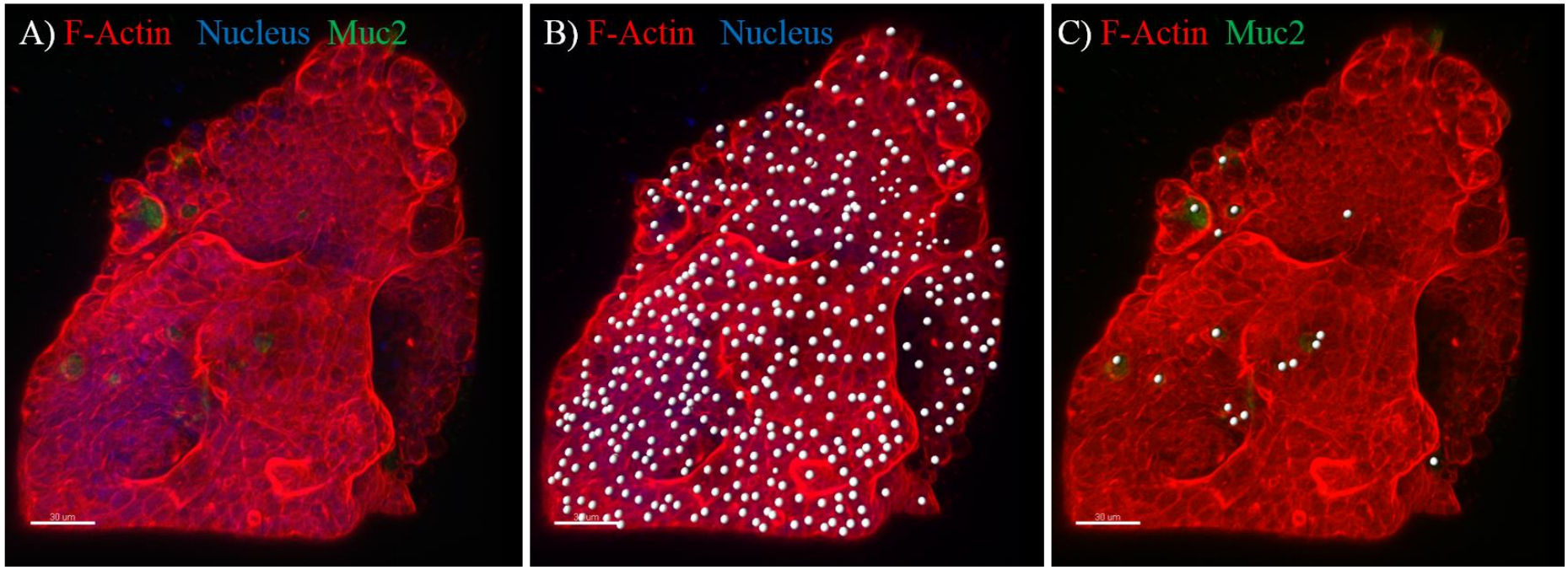

Figure 15) Quantification of differentiated cell markers using "spots" on Imaris

Confocal images acquired to check the differentiation status of epithelial sheets were quantified using Imaris image analysis software. (A) Whole epithelial sheets were overlaid with "spots" against DAPI fluorescence for total cell quantification (B), FITC for goblet cell quantification (C). Image C depicts the accuracy at which "spots" functions can identify fluorescence, and demonstrates the need for manual adjustment of "spots" to improve accuracy of quantification. Scale bars = 30µm.

Due to their 3D conformation, the "spots" function was not as easily applied to Matrigel®-grown organoids. For this reason, quantification of goblet and Paneth cells was performed on a single z-stack slices using the same methods as described above. Quartile and median slices of any given organoid were used for quantification, and an average of the three slices were taken.

In chapter 5, infected samples were quantified using both "spots" and "surfaces" functions in Imaris. As described, total cell counts were obtained against DAPI fluorescent channel detection, and total *Toxoplasma* counts were obtained against AF488 fluorescent channel detection with a maximum diameter of 6µm (**Figure 16 A-C).** Next, to distinguish between intra- and extra-cellular parasites within the image, the "surfaces" function was utilised to generate an iso-surface of the F-actin epithelial stain (**Figure 16 D**). Within this surface, it was possible to detect overlapping AF488 fluorescence of intra-cellular parasites and generate a duplicated channel which was allocated the colour yellow (**Figure 16 E**). Using this newly generated channel, "spots" were then used to quantify the number of intracellular parasites.

In all cases, the automated "spots" were manually checked for accuracy. In some circumstances, the duplicated channel of intra-cellular parasites was not 100% precise, and so the "ortho-slice" function was used to examine the distribution of parasites that were identified along the edges of the surface. Using the counts obtained for total cell number, total parasite number and intracellular parasite number, the infection and invasion rates were calculated.

.

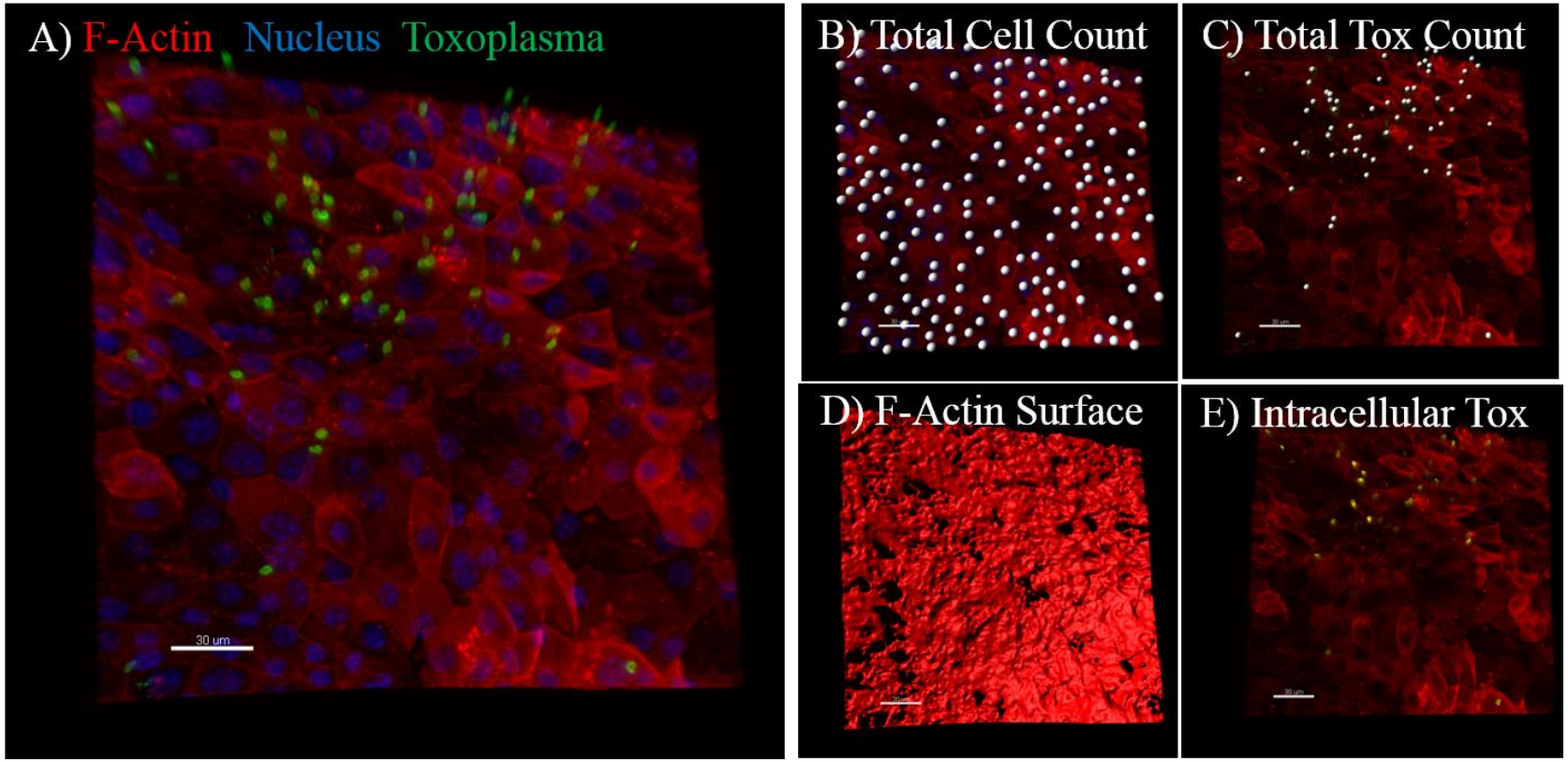

Figure 16) Quantification of parasite infection and invasion of epithelial sheets using "spots" and "surfaces" on Imaris

(A) Confocal images of infected epithelial sheets were analysed via a combination of "spots" against (B) DAPI for total cell counts and (C) *T. gondii* by SAG-1 staining via AF488 fluorescence for parasite counts. (D) An "isosurface" was generated to match the F-actin staining, which was then used to mask intracellular parasites, and generate a duplicated channel of fluorescence (E) to identify parasites within the epithelial sheet. Scale bars = 30 µm

2.7 Sample Preparation for Mass Spectrometry

2.7.1 Matrigel®-Grown Organoid Sample Preparation for Proteomics

In chapter 3, drug skewed organoids and non-treated controls were established as described in section 2.1.3. At day 8, media was removed and Matrigel® domes were washed with PBS. Matrigel® was gently disrupted by pipetting with large bore tip. Samples were washed thrice with PBS by centrifugation at 300*xg* for 5 min. Samples were stored as a dry pellet at -80ºC. For chapter 4, day 7 wild type organoid cultures were washed as described above, and stored as a dry pellet at -80ºC. Three biological replicates of both drug skewed and wild type organoids were prepared for chapter 3 by Zoe Matthews (UEA).

In chapter 4, organoids were cultured until day 7 and dissociated from Matrigel® as described above. Three biological replicates of murine organoids were pelleted for proteomic comparison with collage grown epithelial sheets.

2.7.2 Optimisation of Epithelial Sheet Purification from Collagen Gels

In chapter 4, epithelial sheets were cultured for proteomics. Unlike Matrigel®, collagen gels are not easily dispersed through pipetting, so the separation of the epithelial sheet is more complex. Here, a protocol was established that uses collagenase to break the peptide bonds in the supporting collagen gel matrix, and release the epithelial sheets.

Manufacturer protocols of collagenase enzymes suggest a working concentration of 1mg/mL, however due to the sensitivity of intestinal epithelial cells several concentrations of collagenase were tested on collagen gels without epithelial cells first.

2mg/mL rat tail collagen gels were plated in 30µL domes onto coverslips, and allowed to polymerise for 60 min at 37ºC and 5% CO_2. Gels were transferred to Eppendorf tubes and submerged in an equal volume of either 0.1mg/mL, 0.2mg/mL, 0.5mg/mL or 1mg/mL type VIII collagenase from *Clostridium histolytica* (Sigma) and incubated for 30 min at 37ºC. After 15 min, the gels were gently pipetted with a large bore pipette. After a total incubation of 30 min, samples were checked by eye. At this point, if large pieces of gel were still visible by eye, then samples were re-incubated with pipetting every 10 min until fully dissolved. An equal volume of DMEM was added to neutralise collagenase enzyme activity. From this assay, it was determined that 0.1mg/mL of collagenase with 30 min incubation was sufficient to dissolve a 30µL dome of 2mg/mL rat tail collagen gel. This was then repeated with epithelial sheets to check whether the addition of PBS washes was sufficient to remove residual collagenase from the sample.

Two biological replications of epithelial sheets, each with 5 wells, were grown on 2mg/mL rat tail collagen. Media was removed and gels were washed with PBS to remove residual media. Gels were transferred to an Eppendorf tube and equal volumes of 0.1mg/mL of two different type VIII collagenases (Sigma) were added. Samples were incubated for 30 min at 37ºC with pipetting at 15 min. Sample suspension was visualised by eye to confirm the dissolving of collagen gels, and media was added to neutralise collagenase activity. Samples were washed thrice with PBS by centrifugation at 300*xg* for 5 min each. Samples were stored at -80º and checked for sample degradation and thorough removal of collagenase by running on a 12% 1D gel.

10µL of each sample were diluted in a 1:1 ratio with 2x laemmli buffer (Sigma) and denatured at 100ºC for 10 min on a heat block. 5µL of CSL-BBL protein standard

(Geneflow Ltd) and 10µL of denatured samples were loaded into a 12% SDS gel (**Table 7**).

Samples were run on the 1D gel for 50 min at 200V, 260mA and 100W using an electrophoresis power supply – EPS 601 (GE Healthcare). In addition to collagenase-treated epithelial sheet samples, one aliquot of each collagenase was also included as controls. The gel was then stained with PageBlue Protein Staining Solution (ThermoFisher) to visualise protein bands.

Table 7) 1D 12% mini-gel recipe for protein quality checks		
	Resolving Gel	**Stacking Gel**
Acrylamide/bisacrylamide	4mL	0.65mL
4x Resolving gel buffer (1.5M Tris pH 8.8)	2.5mL	---------
4x Stacking gel buffer (0.5M Tris pH 6.8)	--------	1.25mL
10% SDS	50µL	50µL
milliQH_2O	3.4mL	3.025mL
Mix first four ingredients and add the last two when ready to pipette the gel		
10% Ammonium Persulphate (100mg in 1mL)	75µL	25µL
TEMED	7.5µL	2.5µL*
**Increase to 5µL to reduce setting time*		

Manufacturer product information sheets predict that the collagenase used contains at least 7 different proteases of varying sizes within a range of 68-130kDa. Epithelial sheet samples contained high molecular weight bands (**Figure 17** – lanes 1 and 2) whereas collagenase only samples contained multiple protein bands at a variety of molecular weights ranging from ~30kDa to ~120kDa (**Figure 17**– lane 3 and 4).

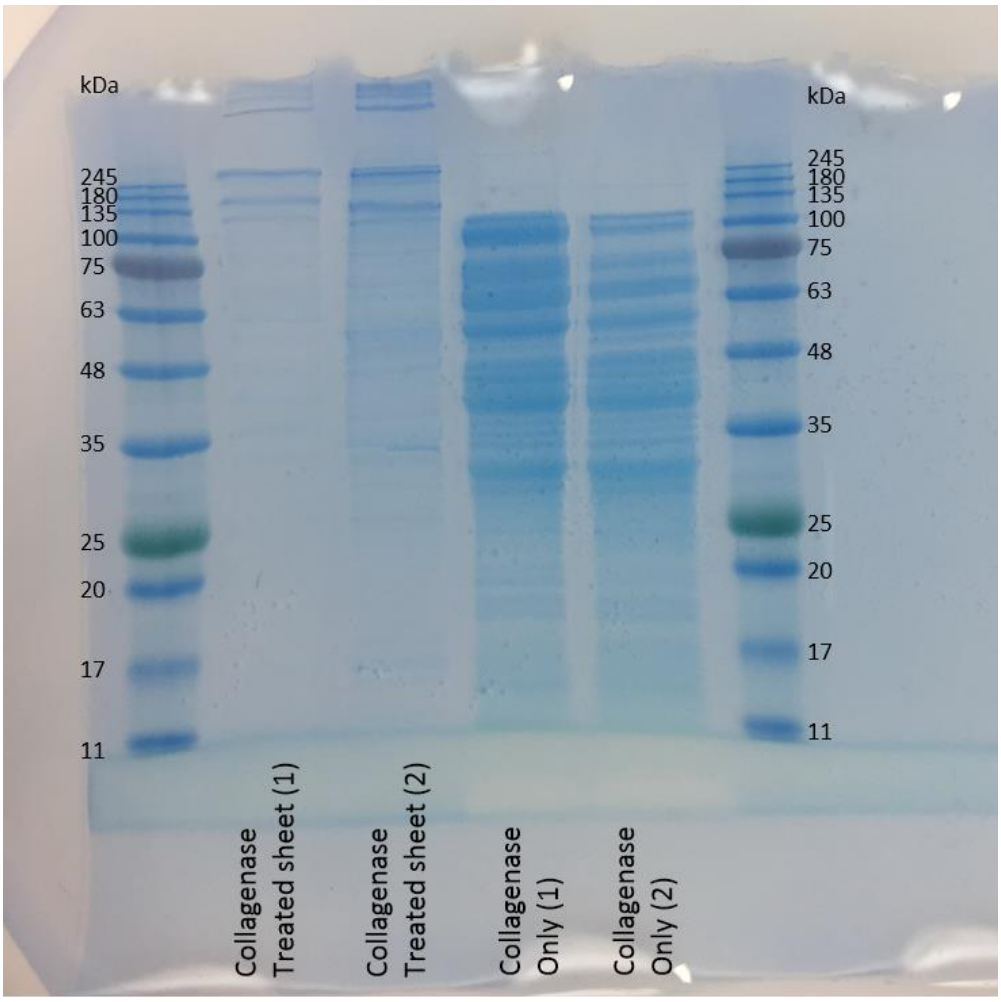

Figure 17) Collagenase treatments at 30 min for 37oC and 5% CO2 successfully separates epithelial sheets from collagen gels and removal of collagenase is successful through PBS washing.

Day 7 epithelial sheets were collagenase treated for 30 min at 37°C and 5% CO_2. Samples were washed thrice in PBS and run on a 12% 1D gels. Epithelial sheet samples (lanes 1 and 2) contain heavy molecular weight bands, one of which is approximately 180kDa, whereas collagenase only samples contained multiple protein bands with varying weights. Bands found in collagenase only samples were absent from washed epithelial sheets, indicating the absence of collagenase remnants following PBS washes.

The absence of protein bands within the range of ~30kDa and ~120kDa in epithelial sheet samples indicates the successful removal of collagenase from samples during the PBS wash steps. Henceforth, epithelial sheet and collagen gel separation for mass spectrometry sample preparation was performed using 0.1mg/mL for 30 min at 37ºC and 5% CO_2, as successful removal was confirmed here.

2.7.3 Protein Digest for Mass Spectrometry

Samples in chapter 3 were prepared for proteomics by Stuart Armstrong using the following protocol. Buffer (50mM ammonium bicarbonate, 0.2% w/v Rapigest, Waters) was added to washed organoid samples before sonication using sonicating water-bath (Jencons) for 3 x 10 minutes on ice. Samples were then heated at 80^0C for 10 minutes. Protein content was determined using the Coomassie plus protein assay kit (Pierce) according the manufacturer's instructions. Protein content was normalised between samples using 50mM ammonium bicarbonate. Protein were then reduced with 3 mM dithiothreitol (Sigma) at 60^0C for 10 minutes then alkylated with 9 mM iodoacetimde (Sigma) at room temperature for 30 minutes in the dark. Proteomic grade trypsin (Sigma) was added at a protein: trypsin ratio of 50:1 and samples incubated at 37^0C overnight. Rapigest was removed by adding TFA to a final concentration of 1% (v/v) and incubating at 37^0C for 2 hours. Peptide samples were centrifuged at 12,000g for 60 min (4^0C) to remove precipitated Rapigest.

Samples used in chapters 4 and 5 were all digested using the same protocol as above by myself.

2.8 NanoLC MS ESI MS/MS Analysis

All peptide mixtures within this thesis were run through the mass spectrometer by Dr Stuart Armstrong. Protein data for chapter 3 was generated using the following protocol.

Peptide mixtures (2µl) were analyzed by on-line nanoflow liquid chromatography using the nanoACQUITY-nLC system (Waters MS technologies, Manchester, UK) coupled to an LTQ-Orbitrap Velos (ThermoFisher Scientific, Bremen, Germany) mass spectrometer equipped with the manufacturer's nanospray ion source. The analytical column (nanoACQUITY UPLCTM BEH130 C18 15cm x 75µm, 1.7µm capillary column) was maintained at 35^0C and a flow-rate of 300nl/min. The gradient consisted of 3-40% acetonitrile in 0.1% formic acid for 150 min then a ramp of 40-85% acetonitrile in 0.1% formic acid for 5min. Full scan MS spectra (m/z range 300-2000) were acquired by the Orbitrap at a resolution of 30,000. Analysis was performed in data dependant mode. The top 20 most intense ions from MS1 scan (full MS) were selected for tandem MS by collision induced dissociation (CID) and all product spectra were acquired in the LTQ ion trap.

For chapters 4 and 5, peptides were analysed by on-line nanoflow LC using the Ultimate 3000 nano system (Dionex/Thermo Fisher Scientific). Samples were loaded onto a trap column (Acclaim PepMap 100, 2 cm × 75 µm inner diameter, C18, 3 µm, 100 Å) at 5 µl min−1 with an aqueous solution containing 0.1 %(v/v) TFA and 2% (v/v) acetonitrile. After 3 min, the trap column was set in-line an analytical column (Easy-Spray PepMap® RSLC 50 cm × 75 µm inner diameter, C18, 2 µm, 100 Å) fused to a silica nano-electrospray emitter (Dionex). The column was operated at a constant temperature of 35°C and the LC system coupled to a Q-Exactive mass spectrometer

(Thermo Fisher Scientific). Chromatography was performed with a buffer system consisting of 0.1 % formic acid (buffer A) and 80 % acetonitrile in 0.1 % formic acid (buffer B). The peptides were separated by a linear gradient of 3.8 – 50 % buffer B over 90 minutes at a flow rate of 300 nl/min. The Q-Exactive was operated in data-dependent mode with survey scans acquired at a resolution of 70,000 at m/z 200. Up to the top 10 most abundant isotope patterns with charge states +2 to +5 from the survey scan were selected with an isolation window of 2.0Th and fragmented by higher energy collisional dissociation with normalized collision energies of 30. The maximum ion injection times for the survey scan and the MS/MS scans were 250 and 50ms, respectively, and the ion target value was set to 1E6 for survey scans and 1E5 for the MS/MS scans. MS/MS events were acquired at a resolution of 17,500. Repetitive sequencing of peptides was minimized through dynamic exclusion of the sequenced peptides for 20s.

For all chapters, Thermo RAW files were imported into Progenesis LC–MS (version 4.1, Nonlinear Dynamics). Runs were time aligned using default settings and using an auto selected run as reference. Peaks were picked by the software and filtered to include only peaks with a charge state of between +2 and +6. Peptide intensities were normalised against the reference run by Progenesis LC-MS and these intensities are used to highlight differences in protein expression between control and treated samples with supporting statistical analysis (ANOVA p-values) calculated by the Progenesis LC-MS software. Spectral data were transformed to .mgf files with Progenesis LC–MS and exported for peptide identification using the Mascot (version 2.3.02, Matrix Science) search engine. Tandem MS data were searched against the bovine predicted proteome (Uniprot release 2013_09). Mascot search parameters were as follows;

precursor mass tolerance set to 10ppm and fragment mass tolerance set to 0.05 Da. One missed tryptic cleavage was permitted. Carbamidomethylation (cysteine) was set as a fixed modification and oxidation (methionine) set as a variable modification. Mascot search results were further processed using the machine learning algorithm Percolator. The false discovery rate was < 1%. Individual ion scores > 13 indicated identity or extensive homology ($p < 0.05$). Protein identification results were imported into Progenesis LC–MS as .xml files.

2.9 Protein Analysis

2.9.1 Ingenuity Pathway Analysis® (IPA)

Proteomics data from chapters 3 and 5 were analysed using Ingenuity Pathway Analysis (IPA®, QIAGEN Redwood City, www.qiagen.com/ingenuity). Detected proteins were identified by matching mass spectrometry data against reviewed proteome sequences, which were downloaded from a publically accessible database (UniProt). Core analysis has multiple methods of putting proteomics data into context by summarising canonical pathways, diseases and functions, and networks of the input proteins.

For chapter 3, core analysis of each dataset were performed on IPA, with the following exclusion criteria; minimum of one peptide used for quantification, $\log_2$ fold change > 1 and q value < 0.05. For chapter 5, core analysis of each dataset were performed on IPA, with the following exclusion criteria; minimum of one peptide used for quantification, $\log_2$ fold change > 1 and p value < 0.05. The $\log_2$ fold change criteria was used here as it is widely considered as a representation of a biologically relevant change in terms of differential abundances in protein expression.

2.9.2 Protein Atlas

In chapter 3, highly up-regulated proteins within drug skewed organoids were cross-checked for cell distribution on The Human Protein Atlas (www.proteinatlas.org V13). The Human Protein Atlas is a free online database of immuno-histological and immunofluorescent confocal microscopy images showing the spatial distribution of proteins in normal and cancerous human tissues, as well as 46 different human cell lines. Protein localisation was investigated to identify any proteins highly up-regulated that were specific to one or more of the differentiated intestinal epithelial cell types.

2.9.3 Venny 2.1

In chapters 3 and 5, comparison of protein lists was performed on Venny 2.1 (http://bioinfogp.cnb.csic.es/tools/venny/index.html) (Oliveros, 2007). Venny is a free online interactive resource that compares up to four lists and generates the appropriate venn diagrams for visualisation. Using this tool, the associated common and unique proteins found within and across samples were identified for further analysis.

2.9.4 PANTHER GO Protein Classification

In chapters 5, gene ontology of proteins detected in non-infected, 24 hour infected and deactivated parasite spiked samples were analysed using online gene classification system PANTHER (www.pantherdb.org) (Mi et al., 2013). Protein IDs were uploaded and functional classification analysis was performed. Associated molecular functions and biological processes data were exported and visualised graphically to compare the lists of proteins identified in each sample.

Chapter 3 – Proteomic Profiling of High Purity Drug Skewed Organoid Cultures

3.1. Introduction

The gastrointestinal tract is a major route of entry for pathogens. A lack of suitable intestinal models has led to the establishment of *in vitro* organoid models. "Mini-gut" organoid models recapitulate the complex 3D structure and cellular composition of the intestinal epithelium *in vivo*, and are promising tools for the study of host-pathogen interactions at the luminal surface. In particular, the presence of fully differentiated epithelial cell populations, such as Paneth or goblet cells, offers the opportunity to study the host-defensive properties of these particular cells. However, the natural occurrence of these cell types in organoid cultures are low, which when combined with the small size of organoid cultures, severely limits the volume of biologically relevant material for functional analysis. This is particularly relevant for global profiling or systems analysis, which require large volumes of starting material to generate sufficient depth of coverage.

More recently, there has been growing interest in manipulating regulatory signalling pathways to generate "skewed" organoid cultures enriched for specific epithelial cell populations such as Paneth and goblet cells. Several compounds have been identified and tested for this purpose. Specifically DAPT, a γ-secretase inhibitor modulates Notch signalling to drive differentiation toward the secretory cell lineage, and in combination with either CHIR99021 (CHIR) or IWP-2 can drive differentiation towards Paneth cell or goblet/enteroendocrine phenotype respectively (Chen et al., 2009; Peignon et al., 2011; Yin et al., 2014).

In terms of intestinal infection, generating organoids enriched for Paneth or goblet cells lends itself to investigating host defence mechanisms specific to these cell types. Paneth cells secrete antimicrobial peptides (AMPs) such as defensins, lysozyme and Reg3

proteins in response to microbial stimulation (Bevins and Salzman, 2011; Cadwell et al., 2008; Clevers and Bevins, 2013; Elphick and Mahida, 2005; Farin et al., 2014; Fernandez et al., 2008; Peeters and Vantrappen, 1975; van Es and Clevers, 2014; Wilson, 1999), and goblet cells renew a mucus layer that physically separates invading pathogens and the underlying epithelial cells (Ermund et al., 2013a, 2013b; Rodriguez-Pineiro et al., 2013). Furthermore, goblet cells in particular have been shown to be important for the host immune response through the unique generation of goblet cell associated antigen passages (GAPs), which allow luminal antigens to be delivered to the underlying dendritic cells within the lamina propria (McDole *et al.,* 20012). Disruption to the secreted products of either Paneth or goblet cell population alters microbial clearance, making both of these important for host cell defence (Ganz et al., 2003; Loonen et al., 2014; Sommer et al., 2014).

Disruption to Paneth cell AMPs alters host susceptibility to enteric infections. Deficiency of REG3$\gamma^{-/-}$ results in mucus re-distribution, increased bacterial contact with epithelial cells and elevated expression of inflammatory markers (Loonen et al., 2014). Deficiency of lysozyme-M$^{-/-}$ results in the development of severe pathology in response to non-pathogenic bacterial infection in comparison to wild type mice (Ganz et al., 2003). These studies demonstrate the importance of AMPs for bacterial clearance. Disruption to the mucus barrier proteins also alters host susceptibility to enteric infections. For example, MUC2$^{-/-}$ mice are more susceptible to infection by *Citrobacter rodentium* (Bergstrom et al., 2010). The mucus barrier is highly glycosylated, and the disruption of this process in mice affects gut microbial ecology and alters the microbiome composition (Sommer et al., 2014).

In addition to their role in host defence, specific epithelial sub-populations are targeted during invasion. *Salmonella enterica* serovar Typhimurium inhibits Paneth cell AMP expression during infection (Salzman et al., 2003a). *Listeria monocytogenes* and *Escherichia coli* exploit goblet and microfold (M) cells (respectively) to establish infection (Nikitas *et al.,* 2011; Roberts *et al.,* 2010). Observations of colonic goblet cell depletion during *Citrobacter rodentium* infection have also been reported, indicating a bacterial advantage to the modulation of goblet cell function, however these mechanisms are not fully understood (Bergstrom et al., 2008).

An *in vitro* model that contained a high proportion of a specific epithelial cell lineage would allow the molecular mechanisms underlying the preferential invasion or cell modulation of these cell types to be studied in more detail. Understanding host-pathogen interactions with specific cell types will allow us to identify key pathways to target for drug and vaccine development.

Molecular approaches have been used to quantify changes in gene expression following drug-skewing of organoids, however proteomic approaches have not yet been exploited for this purpose (Farin et al., 2012; Koo et al., 2012; Milano et al., 2004; Vandussen et al., 2014; Yin et al., 2014). Due to poor correlation in mRNA levels and protein expression (de Sousa Abreu et al., 2009), it is vital to establish a proteome profile of these cultures to determine if we can detect canonical features of Paneth and goblet cells which can be used to study the host defence functions during infection.

The aim of this chapter is to establish drug skewed organoid cultures and demonstrate the ability to evaluate these organoids via quantitative label-free mass spectrometry. In collaboration with the University of East Anglia (UEA) and the Wileman Autophagy group, the objectives of this chapter are to:

a) Demonstrate that organoids are amenable to manipulation with drugs to generate Paneth and goblet/enteroendocrine enriched cultures
b) Identify changes in protein abundance of enriched organoid cultures via mass spectrometry
c) Identify novel proteins belonging to specific differentiated intestinal epithelial cell types

3.2 Materials and Methods

Biological samples were cultured and imaged by Zoe Matthews (UEA), mass spectrometry was performed by Dr Stuart Armstrong as part of a core facility (Centre for Pathogen Proteomics, University of Liverpool). Analysis of mass spectrometry data using Ingenuity Pathway Analysis, mining of the Human Protein Atlas, and comparative analysis with *in vivo* datasets was performed by Lisa Luu (**Figure 18**).

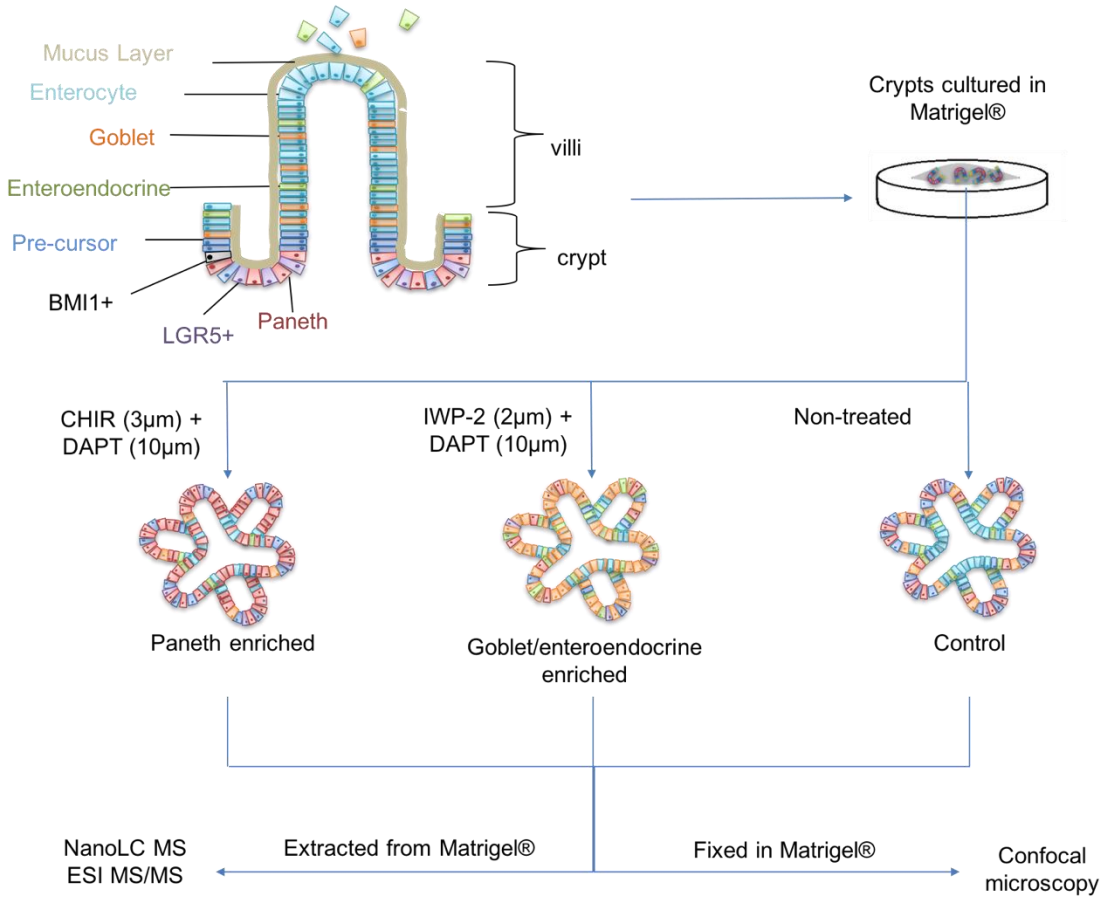

Figure 18) Workflow for the establishment of murine drug-treated organoids

To generate organoid cultures, crypt cells are isolated from the small intestine of mice and embedded into Matrigel®. Combinations of drugs are administered on days 2, 5 and 7 to divert organoids down specific differentiation pathways and generate high purity cultures. Following approximately 8 days, organoids are either fixed for staining and confocal imaging, or extracted from Matrigel®, pelleted and frozen down for mass spectrometry analysis.

3.2.1 Murine Stem Cell-Derived Organoid Culture and Drug-Skew Treatment

Murine organoids were established and drug treated by Zoe Matthews (UEA) described in Chapter 2.1.3. Organoids were treated with DAPT in combination with CHIR or IWP-2, on days 2, 5 and 7 to drive differentiation toward Paneth or goblet cell lineages, respectively. On day 8, organoids were either fixed in ice cold methanol containing 9% formaldehyde at -20^{o}C for 1 hour, or pelleted down and frozen for proteomic analysis.

3.2.2 Sample Preparation for Proteomics

Organoids were stained and imaged by Zoe Matthews (UEA) to confirm the enrichment of drug skewed organoid cultures, and samples were then processed for mass spectrometry by Dr Stuart Armstrong (Core Pathogen Proteomics) as described in Chapter 2.7. The increased abundance of Paneth, goblet and enteroendocrine cell markers was not quantified via confocal microscopy, however a significant up-regulation of these targets were visually overwhelming and confirm an increased population of Paneth, goblet and enteroendocrine sub-populations within their respective enriched culture. The data collected via confocal microscopy is not presented here, as it forms a part of Zoe Matthew's PhD thesis.

Organoid pellets were sonicated to release proteins, protein content was determined using the Coomassie plus protein assay kit (Pierce). Protein content was normalised across samples and reduced with 3mM dithiothreitol (Sigma). Samples were alkylated with 9mM iodoacetimide (Sigma) and then trypsinated at a ratio of 50:1 at 37^0C overnight. Detergent was then removed by the addition of TFA to 1% (v/v) and peptide mixtures were centrifuged to remove precipitated detergent.

3.2.3 NanoLC MS ESI MS/MS Analysis

Peptide mixtures (2µl) were analyzed by on-line nanoflow liquid chromatography using the nanoACQUITY-nLC system (Waters MS technologies, Manchester, UK) coupled to an LTQ-Orbitrap Velos (ThermoFisher Scientific, Bremen, Germany) mass spectrometer equipped with the manufacturer's nanospray ion source, and RAW data were analysed by Dr Stuart Armstrong as described in Chapter 2.8.

3.2.4 IPA® Protein Analysis

Detected proteins were identified by matching mass spectrometry data against reviewed proteome sequences, which were downloaded from a publically accessible database (UniProt). Data were analysed through the use of QIAGEN's Ingenuity® Pathway Analysis (IPA®, QIAGEN Redwood City). Core analysis of each dataset were performed on IPA, with the following exclusion criteria; minimum of one peptide used for quantification, $\log_2$ fold change < 1 and q value > 0.05, to identify enriched networks following treatment of each organoid culture.

3.2.5 Functional Annotation Clustering

Functional annotation clustering was performed on statistically significant proteins using online resource DAVID Bioinformatics (Da Huang et al., 2009) to determine the biological function of proteins found to be up- or down- regulated in goblet or Paneth skewed cultures.

3.2.6 Protein Atlas

Statistically significant differentially expressed proteins within each data set were cross-checked for cellular location against human intestinal tissues using Protein Atlas (www.proteinatlas.org V13). Protein atlas is a free online database of immunohistological and immuno-fluorescent confocal microscopy images showing the spatial distribution of proteins in normal and cancerous human tissues, and 46 different human cell lines. Protein localisation of highly up-regulated proteins was investigated to identify cell-specific protein expression. Known markers of Paneth and goblet cells were used as anatomical references.

3.2.7 Comparison of Goblet Cell Proteomics with Published Mucus Component Study

Proteomic profiles of our goblet and enteroendocrine organoid cultures were cross-compared with a published database of mucus components to validate our findings and to examine whether the goblet cells within organoid cultures can correctly mimic what has previously been observed in mucus taken from small intestinal tissues.

3.3 Results

3.3.1 Mass Spectrometry Identified Unique Proteins within Each Treatment Group

Organoids were treated with either DAPT/CHIR or DAPT/IWP-2 to generate enriched Paneth or goblet cell organoid cultures, respectively. Drug skew success was confirmed by Zoe Matthews (UEA) using confocal microscopy. Although the confocal images were not quantified or presented here, the confirmation of successful drug skew was observable in the images with a striking increased abundance of Paneth, goblet and enteroendocrine cell markers (from Zoe Matthews via personal communication).

Within enriched, drug-skewed organoids, we detected 1574 proteins in Paneth-skewed cultures, and 1471 proteins in goblet/enteroendocrine-skewed organoid samples. To identify highly up- or down-regulated proteins in drug-skewed organoids relative to untreated controls, an exclusion criteria of; >2 unique peptides for quantification, $\log_2$ fold change > +/- 1 and q value < 0.05 was used.

Based on this criteria, we identified proteins with changed abundances following drug skew treatment. In Paneth-enriched organoids, 36 proteins had increased abundance and 65 proteins had decreased abundance when compared to un-untreated controls (**Figure 19**). In goblet/enteroendocrine-enriched cultures, 55 proteins had increased abundance and 153 proteins had decreased abundance compared to un-treated controls (**Figure 19**).

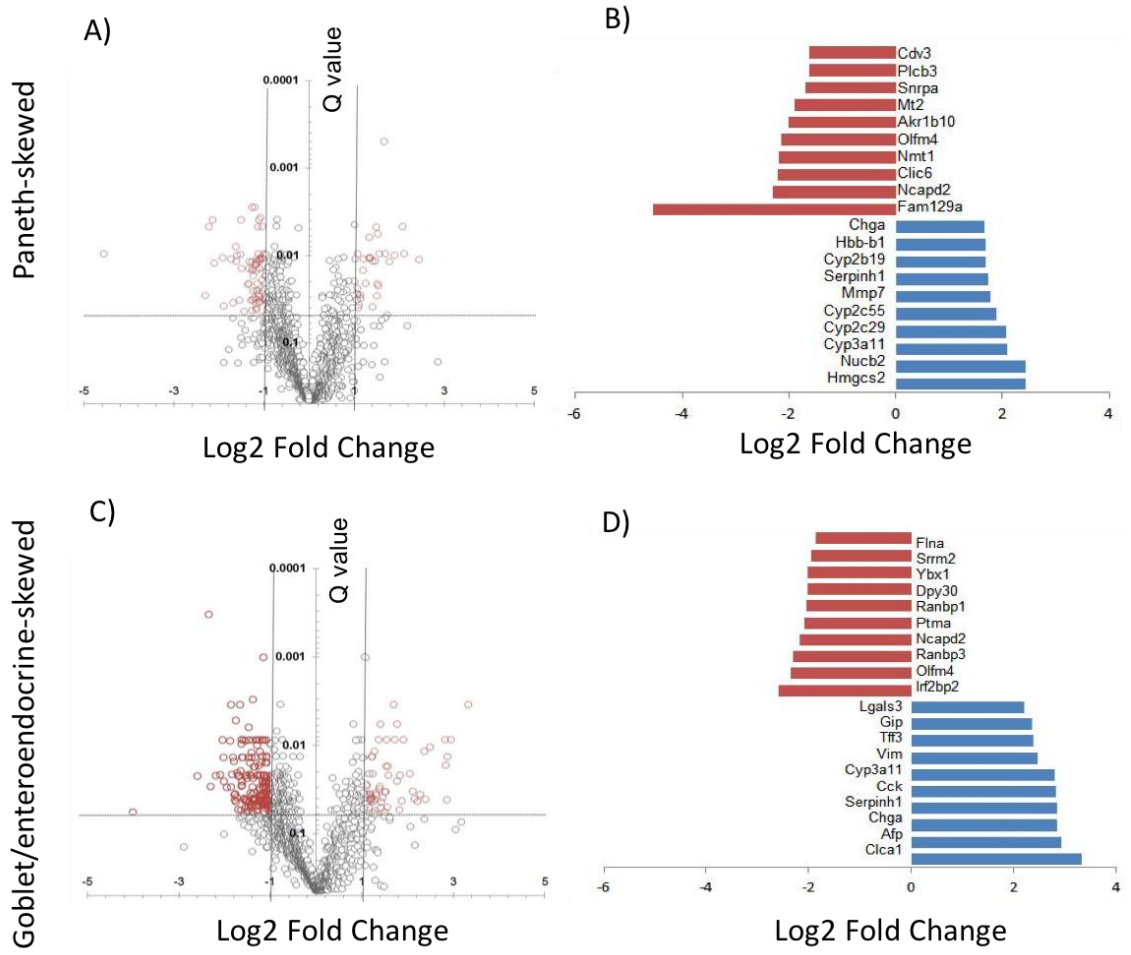

Figure 19) Quantitative label-free proteomics of drug-skewed organoid cultures reveals altered patterns of protein expression

Organoids were treated with DAPT/CHIR or DAPT/IWP-2 to promote differentiation towards the Paneth and goblet cell lineages, respectively. (A) Volcano plot depicting changes in protein expression between control and Paneth-skewed organoids compared to non-infected controls (B) Top 10 proteins up- and down-regulated in Paneth-skewed organoids (C) Volcano plot depicting changes in protein expression between control and goblet/enteroendocrine-skewed organoids compared to non-infected controls. (D) Top 10 proteins up- and down-regulated in goblet/enteroendocrine-skewed organoids.

3.3.2. Proteomic Analysis of CHIR and DAPT Treated Cultures Show an Increased Abundance of Known Paneth Cell-Associated Protein, Matrilysin (MMP7)

Drug skew with DAPT and CHIR skews intestinal epithelial cell differentiation along the Paneth cell lineage. Here, we determined if observed changes in protein abundance in DAPT/CHIR-treated organoids were biologically characteristic of Paneth cells.

A known marker of Paneth cells, matrilysin (MMP7) required for the activation of Paneth cell defensins, was highly up-regulated in DAPT/CHIR organoids (log fold change = 1.78, q value = 0.00093, Supplementary Table 1 Appendix A). Within these cultures, we also observed an increased abundance of several alpha-defensin proteins (DEFA); DEFA4, DEFA5, DEFA7, DEFA20, DEFA22 and DEFA24, although none of these were statistically significant (data not shown).

Additionally, we observed an increased abundance of proteins associated with other secretory epithelial cell types including nucleobindin-2 (NUCB2 - also known as nesfatin-1) (log fold change = 2.43, q value = 0.00076, Supplementary Table 1 Appendix A), chromogranin-A (CHGA) (log fold change = 1.66, q value = 0.00000, Supplementary Table 1 Appendix A) and secretogranin-1 (CHGB) (log fold change = 1.35, q value = 0.00013, Supplementary Table 1 Appendix A). MMP7 up-regulation was specific to DAPT/CHIR treatment (Supplementary Table 3 Appendix A), whereas NUCB2, CHGA and CHGB up-regulation was also observed in DAPT/IWP-2 treated organoids which is consistent with the shared secretory lineage of goblet, enteroendocrine and Paneth cells (Supplementary Table 7, Appendix A).

In tandem with an increase in secretory proteins, a down-regulation of a known intestinal stem cell marker, olfactomedin-4 (OLFM4) was observed, suggesting a loss of stem cell

phenotype as epithelial cells are directed along the Paneth cell lineage (log fold change = -2.14, q value = 0.00004, **Figure 19 B and D**; Supplementary Table 1 Appendix A).

Network analysis of all proteins detected indicate an enrichment of proteins associated with cellular development, cellular growth and proliferation (**Figure 20**). Of the 35 proteins displayed in this network, 6 were significantly up-regulated (red), 7 were significantly down-regulated (green) and 4 were detected but changes in protein abundance were not statistically significant (**Figure 20**). Here, only MMP7 up-regulation was unique to DAPT/CHIR treatment, and multiple other proteins were commonly up- or down-regulated in DAPT/IWP-2 organoids (Supplementary Tables 7 and 8, Appendix A).

To identify proteins within our dataset that may be specific to the Paneth cells lineage, we attempted to stain murine organoids and murine small intestinal tissues with antibodies against two of the highly up-regulated proteins; KIAA1324 and DNAJC3. However the antibodies tested were not fully validated for use against murine targets, and thus these attempts were unsuccessful. Due to the lack of availability of validated antibodies, we utilised the online tool, The Human Protein Atlas as an alternative method to examine protein localization within the small intestine. Here we identified Paneth cells as granular cells at the base of intestinal crypts, and used lysozyme (LYS) and alpha defensin 5 (DEFA5) staining patterns as a reference (**Figure 21 A and B**). Staining patterns of proteins increased in abundance after DAPT/CHIR drug skew was compared to the LYS and DEFA5 references to identify those that were restricted to, or enriched within Paneth cells.

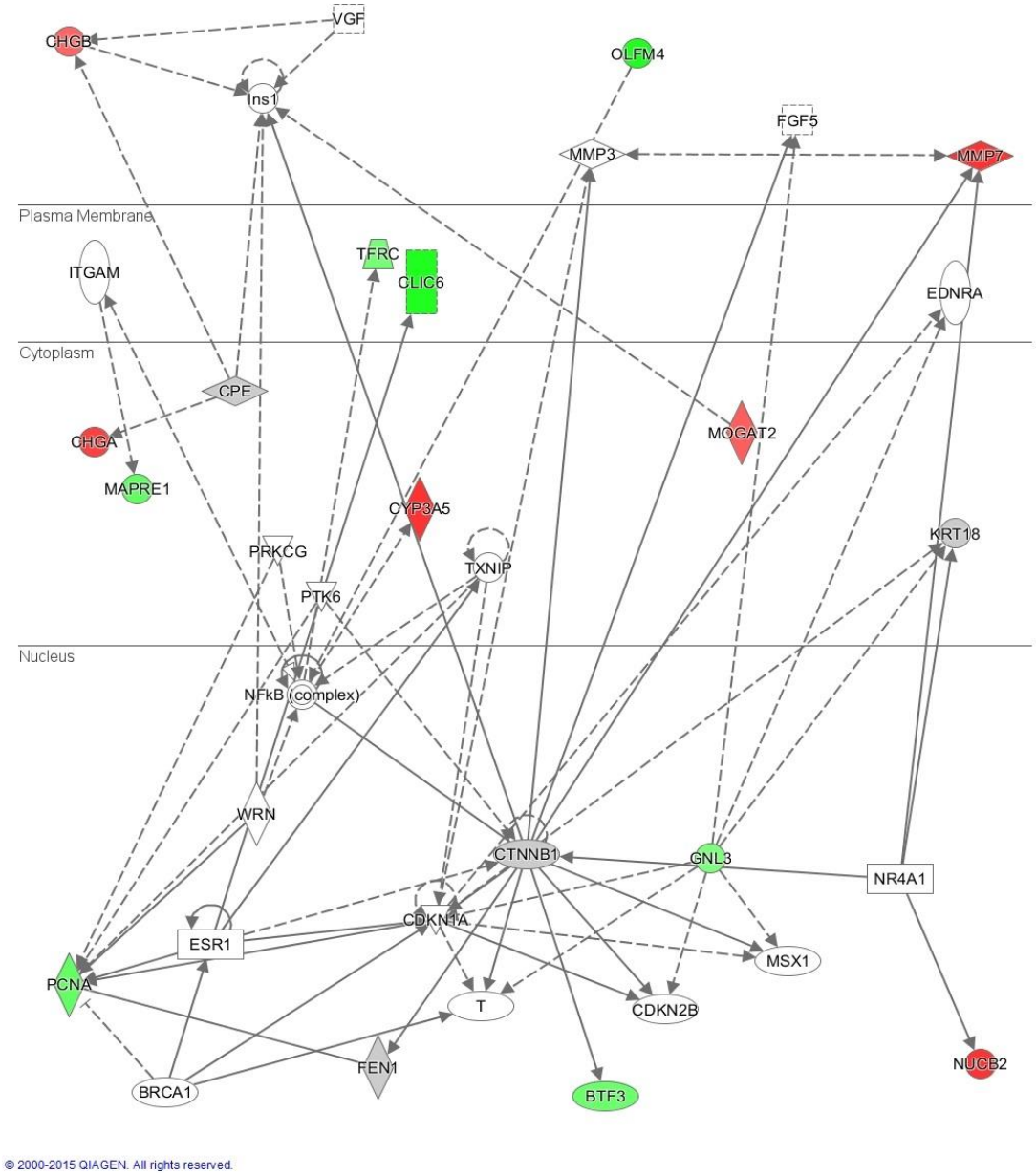

Figure 20) Differentially-expressed proteins in DAPT/CHIR-treated samples are involved with cellular development, cellular growth and proliferation

Network analysis of proteins exhibiting significant changes in protein abundance following treatment with DAPT/CHIR identified a protein network for cellular development, cellular growth and proliferation as highlighted on Ingenuity Protein Analysis software. Grey-shaded molecules indicate proteins that were detected within our dataset but not statistically significant, red-shaded molecules indicate up-regulated proteins and green-shaded molecules indicate down-regulated proteins. This protein network displays an up-regulation in known secretory proteins CHGA and CHGB and an up-regulation in a Paneth cell associated protein MMP7, along with a down-regulation in a known intestinal stem cell marker, OLFM4.

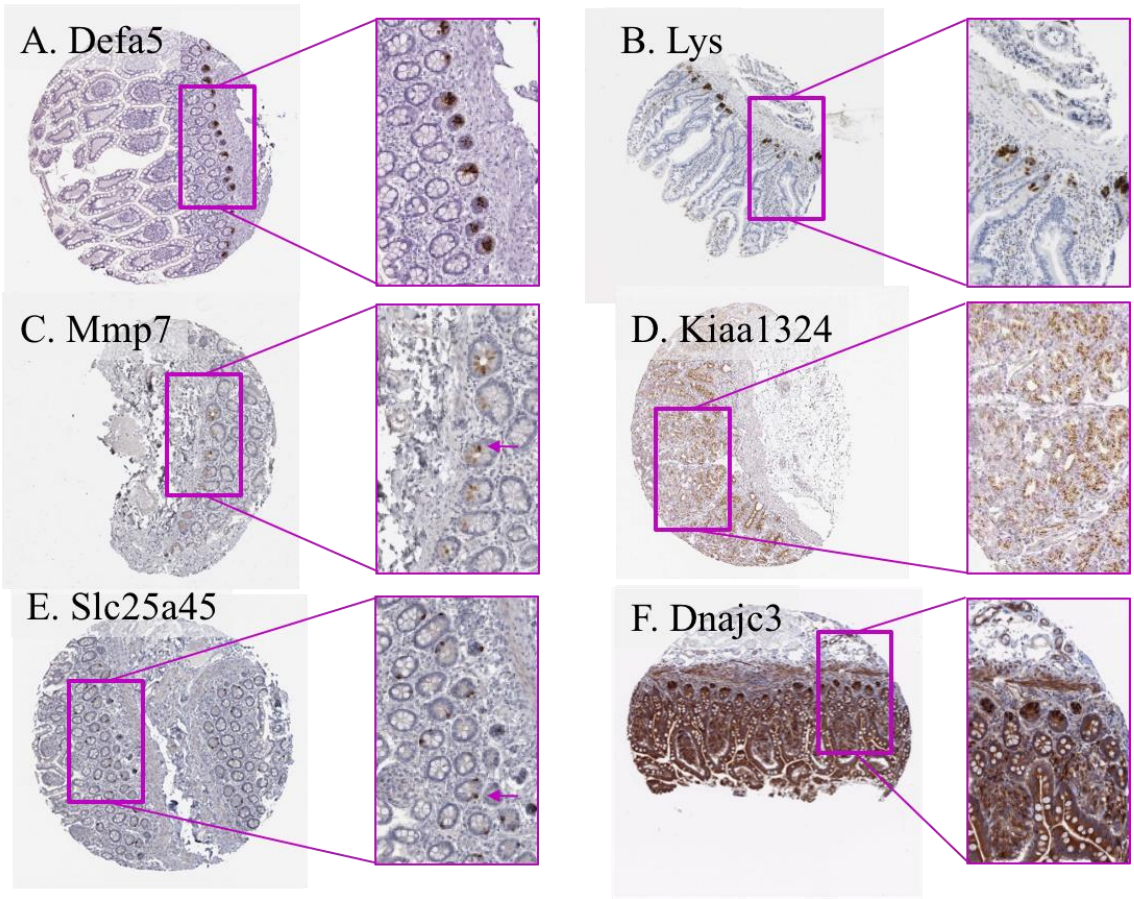

Figure 21) Expression of a sub-set of up-regulated proteins in DAPT/CHIR treated organoids is enriched within Paneth cells of the small intestinal crypt

Protein localisation was examined using online tool, The Human Protein Atlas. Known Paneth cell markers (A) DEFA5 and (B) LYS were used to identify granular Paneth cells at the base of small intestinal crypts as an anatomical reference. Protein expression patterns of up-regulated proteins (C) MMP7, (D) KIAA1324, (E) SLC25A45 and (F) DNAJC3 are localised within Paneth cells, identifying them as potential novel markers.

Of the 36 proteins up-regulated, MMP7, KIAA1324, SLC25A45 and DNAJ3 expression was restricted to, or enriched within Paneth cells (**Figure 21 C – F**). With the exception of MMP7, the role of these proteins in Paneth cell development and function, if any, is not yet understood. Of these proteins, MMP7 and DNAJC3 were uniquely up-regulated by DAPT/CHIR treatment whereas KIAA1324 and SLC25A45 were also up-regulated in DAPT/IWP-2 treated organoids, revealing a potential role of DNAJC3 in Paneth cell development or function (Supplementary Tables 3 and 7, Appendix A).

3.3.3 Proteomic Analysis of IWP-2 and DAPT Treated Cultures Show an Increased Abundance of Known Goblet Cell and Enteroendocrine Cell Proteins

Goblet cells secrete mucus components to regenerate a protective mucus layer that physically separates the host intestinal epithelium and invading pathogens. Enteroendocrine cells secrete hormones for digestion to aid in nutrient absorption across the epithelium. Drug skew with DAPT and IWP-2 skews intestinal epithelial cell differentiation along the goblet and enteroendocrine cell lineage. Here, we determined if observed changes in protein abundance in DAPT/IWP-2-treated organoids were biologically characteristic of goblet and enteroendocrine cell phenotype.

Multiple major mucus components were up-regulated following DAPT/IWP-2 skew; calcium-activated chloride channel regulator (CLCA1) (log fold change = 3.328, q value = 0.00347, Supplementary Table 2 Appendix A), anterior gradient protein 2 (AGR2) (log fold change = 1.857, q value = 0.04257, Supplementary Table 2 Appendix A), trefoil factor 3 (TFF3) (log fold change = 2.383, q value = 0.04095, Supplementary Table 2 Appendix A) and zymogen granule membrane protein 16 (ZG16) (log fold change = 2.270, q value = 0.03616, Supplementary Table 2 Appendix A). Furthermore, several known enteroendocrine cell markers were up-regulated; alpha-fetoprotein (AFP) (log fold change = 2.939, q value = 0.00866, Supplementary Table 2 Appendix A), cholecystokinin (CCK) (log fold change = 2.828, q value = 0.01682, Supplementary Table 2 Appendix A), and gastric inhibitory polypeptide (GIP) (log fold change = 2.360, q value = 0.01173, Supplementary Table 2 Appendix A). In addition to an increase in proteins associated with secretory cell lineages, a down-regulation of stem cell markers was observed; OLFM4 (log fold change = -2.337, q value = 0.02152, Supplementary Table 2 Appendix A) and SPARC-related modular calcium-binding protein (SMOC2) (data not shown) which indicate a loss of stem cell phenotype as a result of driving goblet/enteroendocrine

cell differentiation. Here, CLCA1, AGR2, TFF3, ZG16, AFP, CCK and GIP were all uniquely up-regulated in DAPT/IWP-2 treated organoids (Supplementary Table 5, Appendix A) and confirm the success of direct differentiation toward goblet and enteroendocrine phenotype.

Network analysis of all proteins detected indicate an enrichment of proteins associated with enteroendocrine development and function network (**Figure 22**). Of the 35 proteins displayed within this network, 9 were significantly up-regulated (red), 8 were significantly down-regulated (green), and 3 were detected but changes in protein abundance was not statistically significant (grey) (**Figure 22**).

Many of the known goblet cell markers that were uniquely up-regulated can also be observed within this network suggesting a dominant enrichment of goblet-associated proteins as well as enteroendocrine system-related proteins (**Figure 22**). However, some proteins here were also up-regulated in DAPT/CHIR treated organoids; CHGA, CHGB, KIAA1324 and 2-acylglycerol O-acyltransferase 2 (MOGAT2).

To identify other proteins within our dataset that may be specific to goblet cell differentiation or function, we utilised the online tool, The Human Protein Atlas. Firstly using histochemical staining patterns of MUC2 as a reference, and the presence of apical mucin granules we identified goblet cells (**Figure 23 A and B**). We then used this anatomical location to examine the expression of proteins with higher abundances in DAPT/IWP-2 organoid samples.

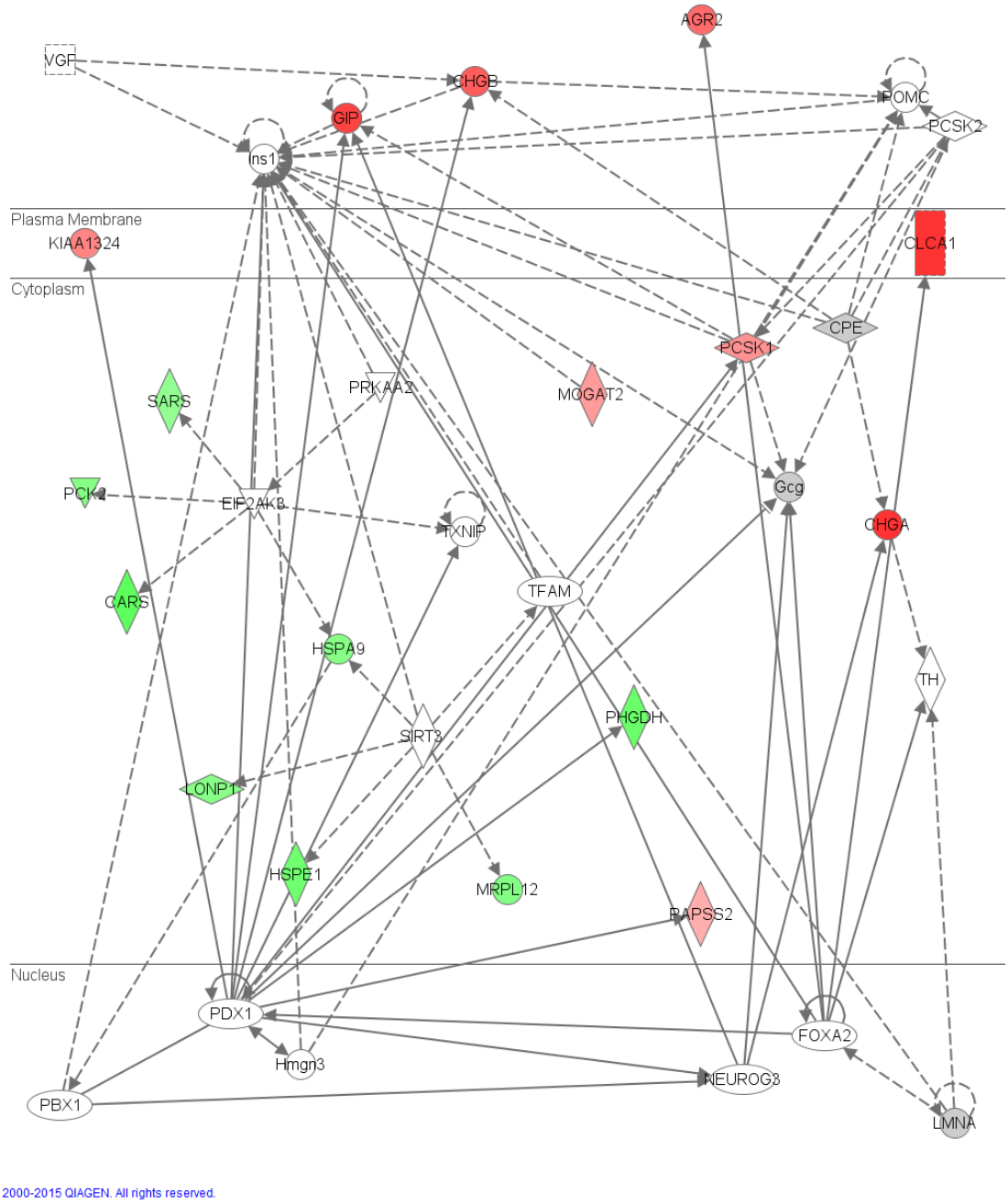

Figure 22) Differentially-expressed proteins in DAPT/IWP2-treated samples are involved with enteroendocrine system development and function.

Network analysis of proteins exhibiting significant changes in protein abundance following treatment with DAPT/IWP-2 identified a protein network for enteroendocrine system development and function as highlighted on Ingenuity Protein Analysis software. Grey-shaded molecules indicate proteins that were detected within our dataset but not statistically significant, red-shaded molecules indicate up-regulated proteins and green-shaded molecules indicate down-regulated proteins. This protein network displays an up-regulation in known goblet cell and enteroendocrine associated proteins CLCA1, AGR2, GIP and CHGA.

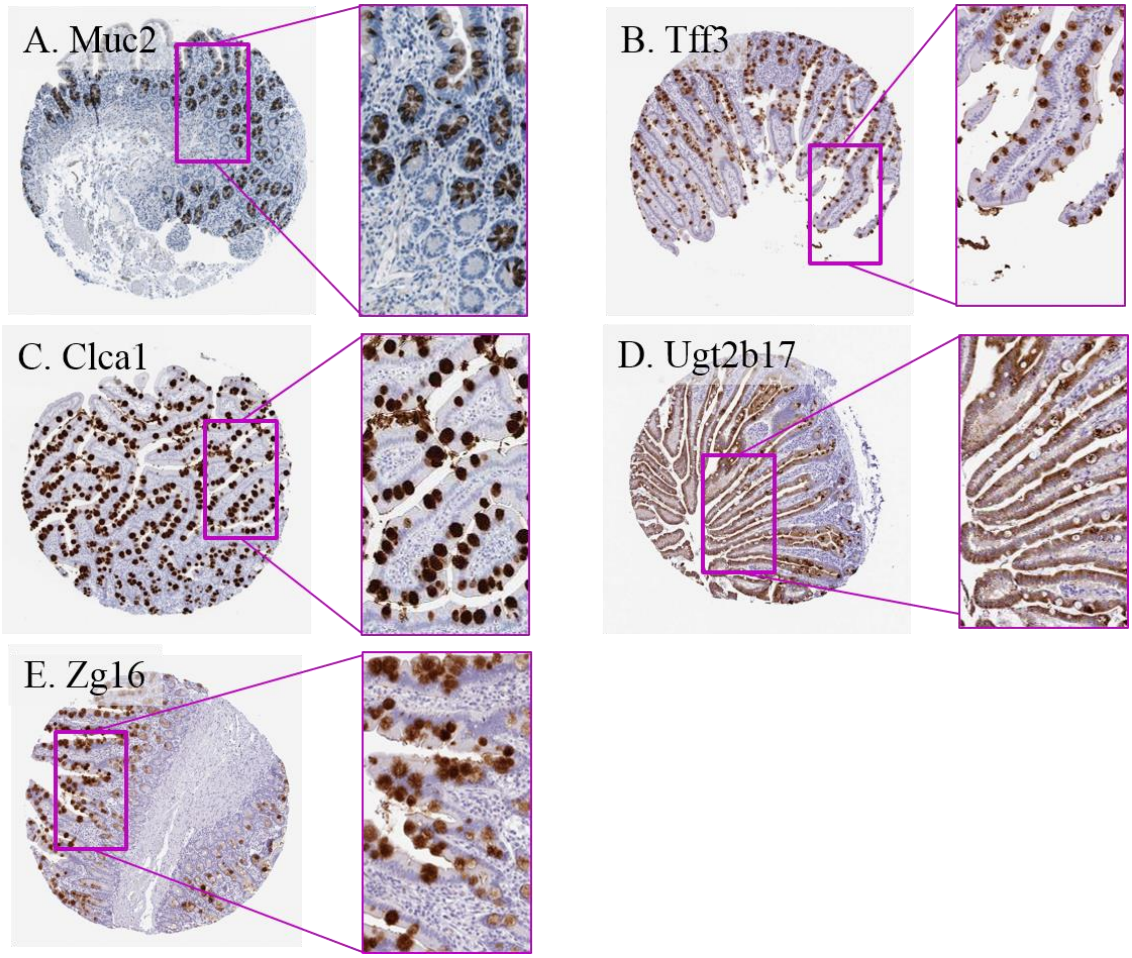

Figure 23) Expression of a sub-set of up-regulated proteins in DAPT/IWP-2 treated organoids is localised within goblet cells of the villus tissues

Protein localisation was examined using online tool, The Human Protein Atlas. Known goblet cell markers (A) MUC2 and (B) TFF3 were used to identify goblet cells containing apical mucin granules. Protein expression of up-regulated (C) CLCA1, (D) UGT2B17 and (E) ZG16 are localised within goblet cells.

Of these proteins found more abundantly in DAPT/IWP-2 organoids, TFF3, CLCA1, ZG16 were localised within goblet cells and UDP glucuronosyltransferase family 2 member B17 (UGT2B17) was localised within a subset of goblet cells (**Figure 23 B - E**). All three of these proteins were uniquely up-regulated in DAPT/IWP-2 treated organoid cultures (Supplementary Table 5 Appendix A).

To validate our findings and show that high purity goblet/enteroendocrine mixed cell cultures can mimic the *in vivo* environment, we compared up-regulated proteins with those detected within mucosal scrapings of murine gastrointestinal tracts in a study investigating the composition of gut mucus (Rodriguez-Pineiro et al., 2013).

Of the 56 statistically significant up-regulated proteins within our goblet and enteroendocrine mixed cultures, 14 are reported to be found within murine *in vivo* gastrointestinal scrapings as detected by mass spectrometry (Rodriguez-Pineiro *et al.*, 2013) (Table 8). Of these common proteins, 10 were uniquely up-regulated in DAPT/IWP-2 and not in DAPT/CHIR treated organoids (highlighted with an asterix in **Table 8**), indicating that the changes in protein abundance in the former more closely represent murine gastrointestinal mucus scrapings than the latter.

Table 8) 14 proteins detected in DAPT/IWP-2 organoids, common to Rodriguez-Pineiro et al., 2013 studying murine gastrointestinal mucus composition

Protein Identifier	Description	Q Value	P Value	Log Ratio Change	Regions of small intestine previously detected
Q9D7Z6*	Calcium-Activated Chloride Channel Regulator 1 (CLCA1)	0.00347	0.00004	3.334	duodenum, ileum
P20152*	Vimentin (VIM)	0.01043	0.00053	2.48	all
Q8K0C5*	Zymogen Granule Membrane Protein 16 (ZG16)	0.03616	0.01062	2.27	all
P16110*	Galectin 3 (LGALS3)	0.04314	0.01623	2.20	all
O88312*	Anterior Gradient Protein 2 Homolog (AGR2)	0.04257	0.01533	1.86	all
Q64133	Amine Oxidase [Flavin-Containing] A (MAOA)	0.00578	0.00009	1.75	all
Q62425	NADH Hydrogenase [Ubiquinone] 1 Alpha Subcomplex Subunit 4 (NDUFA4)	0.01732	0.00175	1.51	all
P97742*	Cartinine O-Palmitroyltransferase 1, Liver Isoform (CPT1A)	0.03385	0.00810	1.49	all
Q9CQX2	Cytochrome B2 Type B (CYPB5B)	0.04134	0.01455	1.26	all
Q61847*	Meprin A Subunit Beta (MEP1B)	0.03891	0.01211	1.19	all
Q64521*	Glycerol-3-Phosphate Dehydrogenase, Mitochondrial (GPD2)	0.04085	0.01386	1.18	all
Q64464*	Cytochrome P450 3A13 (CYP3A13)	0.02908	0.00612	1.10	all
P21447	Multidrug Resistant Protein 1A (ABCB1A)	0.00101	0.00000	1.07	all
O88428*	Bifunctional 3'-Phosphoadenosine 5'-Phosphosulfate Synthase 2 (PAPSS2)	0.03487	0.00896	1.03	all

* Proteins uniquely up-regulated in DAPT/IWP-2 treatment

3.3.4 The Shared Secretory Lineage of Paneth and Goblet Cells is Reflected in the Proteome of Drug Skewed Organoids

Having identified unique proteins in both Paneth and goblet/enteroendocrine skewed organoids, we also observed a subset of 18 up-regulated proteins that were shared in both treatment groups groups (Supplementary Tables 7 and 8, Appendix A).

Within this group we report an increased abundance of proteins associated with secretory cell lineage; CHGB, SERPINH1, CHGA, NUCB2, MAOA, MOGAT2, several cytochromes; CYP2B19, CYPB10, CYP2C29, CYP3A11 and several solute carrier family proteins; SLC22A18, SLC25A45 and SLC27A4 (Supplementary Tables 7 and 8, Appendix A). The shared increased abundance of secretory cell proteins is likely due to the shared secretory cell lineage of these populations.

Using the same techniques as previously, we compared the staining pattern of these shared proteins with goblet and Paneth cell localisation on the Human Protein Atlas. Here we observed that, three of the proteins most changed in abundance were localized in enteroendocrine and Paneth cells; CHGA, CHGB and NUCB2 (**Figure 24**). The function of these shared proteins for secretory cell differentiation is currently unknown.

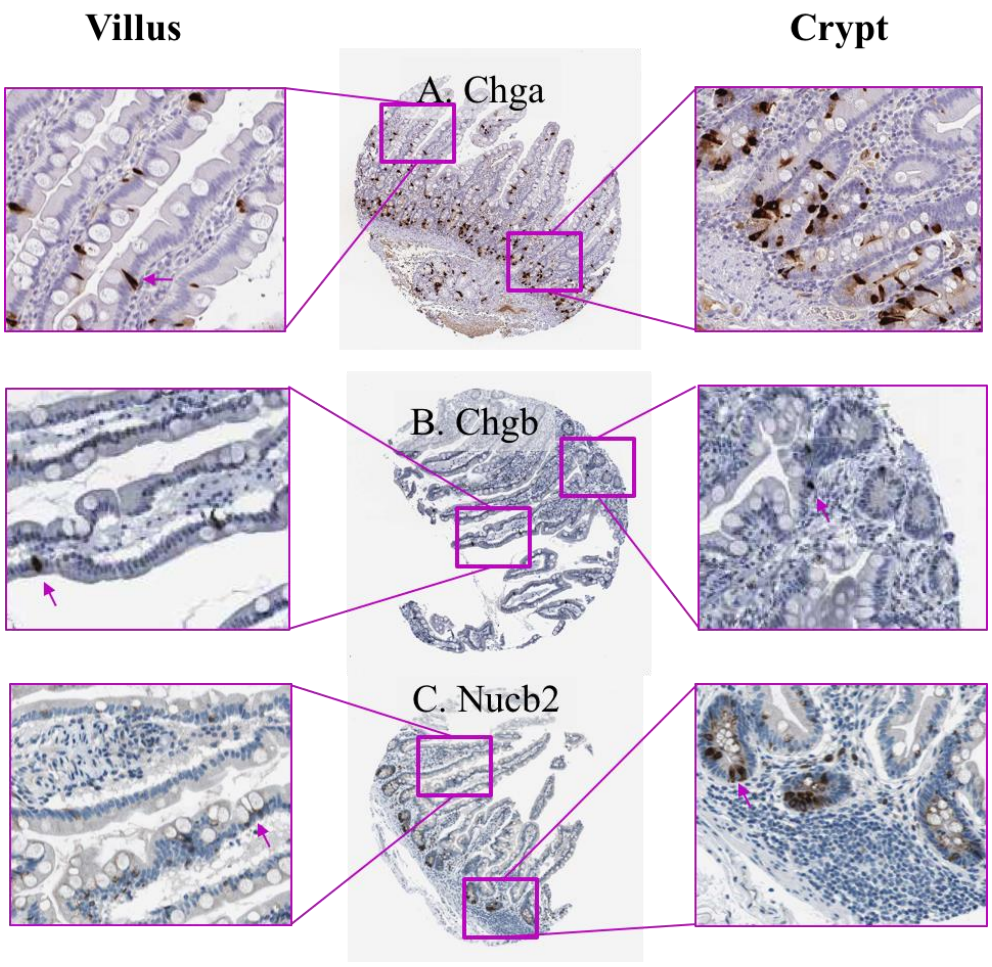

Figure 24) Expression of a sub-set of up-regulated proteins in both DAPT/IWP-2 and DAPT/DHIR treated organoids is localised within Paneth and enteroendocrine cells of the small intestinal epithelium.

Protein localisation was examined using online tool, The Human Protein Atlas. Using the same reference images as previously, we identified that (A) CHGA, (B), CHGB and (C) NUCB2 are localized within enteroendocrine and Paneth cells.

3.4 Discussion

Organoids are promising tools for the study of infection. However, due to the limited volume of experimental material, the study of host defensive functions of Paneth cells and goblet cells is severely limited.

In this chapter, we validated drug-skewed organoids to be used to study Paneth and goblet cell functions in host-defence via quantitative label free mass spectrometry. Established murine organoid cultures were drug-skewed to drive differentiation along specific secretory cell lineages. Using confocal and proteomic approaches, we demonstrate that these *in vitro* organoid cultures share characteristics of Paneth and goblet cells *in vivo* and are amenable to mass spectrometry analysis.

Previous studies have demonstrated that small molecule manipulation of cell signalling pathways can divert cellular differentiation toward specific cell lineages as determined by IHC and gene expression assays (transcriptomics) (Farin et al., 2012; Koo et al., 2012; Milano et al., 2004; Vandussen et al., 2014; Yin et al., 2014). To date, proteomic approaches have not been exploited to study organoid cultures, and as the correlation between mRNA expression and protein expression has been proven to be low in some instances, it is crucial to study the proteomic profile develop a better understanding of the underlying proteome in differentiated intestinal organoid cultures (Steiling *et al.,* 2009). Furthermore, here we demonstrate that drug-skewed organoids provide sufficient material to apply mass spectrometry techniques for the analysis of Paneth and goblet cells in organoid cultures.

Paneth-skewed organoids were produced by addition of DAPT/CHIR treatment to established murine organoids, and then analysed by label-free mass spectrometry for Paneth cell features. Paneth cells contain AMPs such as lysozyme and alpha-defensins. Alpha-defensin pre-cursors are constitutively produced, however are only activated through cleavage by MMP7 allowing for their secretion into the crypt lumen in response to antimicrobial stimulation (Weeks et al., 2006; Wilson, 1999). Here, mass spectrometry detected an increased abundance of several alpha-defensin proteins

although these were not statistically significant, and no observable change in the abundance of other AMPs were found. The production of other AMPs is not constitutive, and requires the sensing of commensal flora (Foureau et al., 2010; Menendez et al., 2013; Peeters and Vantrappen, 1975; Walker et al., 2013). A lack of microbial stimulation in this model could explain why other AMPs were not observed to be significantly increased in abundance here. Prediction of cleavage sites after trypsination (using Peptide Cutter - http://web.expasy.org/peptide_cutter/) on the alpha defensin protein sequence (taken from UniProt) indicate that trypsination may result in peptide sequences sizes that are not within the detectable range for this method of mass spectrometry (800Da – 3000Da), highlighting a limitation of the sole use of this method of protein detection.

Further examination of all up-regulated proteins in Paneth-skewed versus control organoids reveal several potential novel markers of Paneth cells. Using online tool, The Human Protein Atlas, localisation of up-regulated proteins was compared to expression patterns of known Paneth cell markers. MMP7, KIAA1324, SLC25A45 and DNAJC3 were identified to be specifically expressed or enriched within Paneth cells. KIAA1324 (also known as EIG121), up-regulates autophagy pathways (Deng et al., 2010). Murine knockout models of *atg16l* autophagy gene exhibit abnormal Paneth cell protein secretion, demonstrating that autophagy is essential for maintaining Paneth cell function (Bevins and Salzman, 2011). SLC25A45 is a fatty acid transport protein, however relatively little is known about this member of the SLC25 family. An up-regulation of SLC25A45 mRNA is reported during hyperthyroidism, however the physiological role of this protein in the intestine is unknown. It's localisation to Paneth cells may suggest a role in innate defence (Gutierrez-Aguillar and Baines, 2013; Ramadoss et al., 2014). DNAJC3 (also known as $p58^{IPK}$) plays a role in the unfolded

protein response during endoplasmic reticulum stress (Roobol et al., 2015; Van Huizen et al., 2003) and is activated during viral infection, inducing cell death and inflammation as part of host cell response (Goodman et al., 2009). The up-regulation of these proteins in DAPT/CHIR treated organoids, and the evidence of Paneth cell-specific localisation may suggest that these proteins play a role in Paneth cell function. Functional studies are required to further evaluate the role of these proteins in Paneth cell function, either for host immune defence or for maintenance of the intestinal stem cell population.

Gastrointestinal goblet cells are responsible for mucus secretion onto the intestinal epithelia, generating a protective mucosal layer that acts as a physical barrier to regulate the exposure of the host immune system to antigenic material (Specian & Oliver, 1991; Zarepour *et al.*, 2013). The composition of mucus varies throughout the gastrointestinal tract, and the major mucus protein component in the small intestine is mucin-2 (MUC2) (Zarepour *et al.*, 2013). An increase in MUC2-positive cells was observed following DAPT/IWP-2 treatment by confocal imaging (reported by Zoe Matthews), however the changes in MUC2 protein abundance was not significant by q value (false discovery rate). Here we could report that an increased abundance of mucin-2 was observed if we base this observation on the reported p-value, however this method is less robust and does not take into account multiple testing.

Proteins increased in abundance in DAPT/IWP-2 samples in relation to non-treated controls were compared with published murine gastrointestinal mucus scraping proteome data, to validate that DAPT/IWP-2 skewing results in an epithelial phenotype representative of *in vivo* mucus composition. A subset of proteins were commonly identified in murine gastrointestinal mucus samples and DAPT/IWP-2

treated organoid samples. These include several known mucus-related proteins CLCA1, ZG16, AGR2 and TFF3 that were within the top 20 up-regulated proteins (Pelaseyed *et al.,* 2014; Rodriguez-Pineiro *et al.,* 2013; Taupin & Podolsky, 2003). The similarities between the *in vitro* skewed organoids with *in vivo* mucus components proteome profile support the finding that DAPT/IWP-2 treated organoids can mimic *in vivo* mucus production.

Further examination of up-regulated proteins in goblet/enteroendocrine samples compared to untreated controls reveals a potential marker of goblet cells. Using online tool, The Human Protein Atlas, localisation of up-regulated proteins was compared to expression patterns of known goblet cell markers. CLCA1 and UGT2B17 were identified to be specifically expressed within goblet cells. CLCA1 is a known mucus component and has previously been identified as a goblet-specific marker. More recently, studies of CLCA1 deficient mice suggest that the removal of this protein has no effect on mucus synthesis, structure or barrier function within the colon (Erickson et al., 2015). UGT2B17 is an enzyme associated with elimination of toxic xenobiotics (Wang et al., 2012). A down-regulation of ovine mucosal UTGB17 transcripts in response to nematode infection has been reported (Knight et al., 2011), however it's exact role in the development of goblet cells and host response to infection is currently unknown. The physiological importance of this protein during infection requires further examination, however its localisation specifically within goblet cells may allow it to be used as a specific cell marker.

Enteroendocrine cells constitute a small population of the intestinal epithelial cell layer, and are essential for regulating digestion, metabolism and gut motility through the secretion of various hormones such as serotonin, insulin and secretin

(Gunawardene *et al.,* 2011; Herzig, 1998; *Li et al.,* 2011; Nagatake *et al.,* 2014). Currently, the inter-relationship between various enteroendocrine cell lineages is poorly understood and difficulties remain with identifying differentiated enteroendocrine cell types, however several markers have been established (Cirillo *et al.,* 1995; Furness *et al.,* 2013; Gunawardene *et al.,* 2011; Liu *et al.,* 2001; Nagatake *et al.,* 2014; Roth *et al.,* 1990). Amongst these known proteins associated with the endocrine phenotype, CHGA, AFP, CKK and GIP have all been shown to be highly up-regulated within our cultures. CHGA has previously been detected as up-regulated (by ~14 fold) following the same treatment in a study utilizing microarray technology performed by Yin *et al.,* 2014.

In addition to determining unique protein changes within each treatment group, a sub-set of proteins were identified that were commonly up- or down-regulated in both enriched organoid cultures (Table 3, Appendix A). Of these proteins, CHGA, CHGB and NUCB2 were localised in enteroendocrine-like cells in both crypt and villus domains.

These three proteins highlighted are known to be involved with enteroendocrine functions, and were therefore not expected to be differentially up-regulated in DAPT/CHIR Paneth skewed organoids. CHGA is an established enteroendocrine marker and a previous study has reported an increased in CHGA mRNA expression following DAPT/CHIR, which appears to be largely due to the addition of Notch signalling inhibitor DAPT (Yin et al., 2014). Our findings here obtained through proteomic approaches, agree with findings from qPCR and microarray experiments in a similar model. CHGB is often co-localised with CHGA, and is an important protein in secretory granule biogenesis (Huh *et al.,* 2003; Portela-Gomes *et al.,* 1997). It has

been hypothesised that CHGB has a secondary function and can bind calcium, potentially playing a role in protein transport (Schmidt *et al.,* 2011). *In vivo* studies show that $CHGB^{-/-}$ mice exhibit lower levels of hormone secretion by pancreatic islets (Obermuller *et al.,* 2010). However the effect of knocking out this protein has not yet been extensively studied within the intestine (Portela-Gomes *et al.,* 1997), and therefore its role in the gastrointestinal tract is not yet fully understood. Further studies investigating the role of CHGB in the secretory cells of the intestinal epithelium may help to further understand gut homeostasis and its role in the development of secretory epithelial cells. NUCB2 has recently been reported to be present within enteroendocrine cells and plays a role in the regulation of glucose homeostasis (Ramesh et al., 2015)

In addition, several other proteins were identified as potentially important for the function of either goblet or Paneth cells as they were up-regulated in both treated organoid cultures when compared to untreated controls; sulhydryl oxidase 1 (QSOX1) and SLC family proteins, SLC22A18, SLC25A45 and SLC27A4 (Supplementary Table 3, Appendix A). QSOX1 has previously been detected within colonic mucus and functions to establish disulphide bonds which are important for the formation of fibronectin within extracellular matrix networks (Ilani et al., 2013; Williams et al., 1983). Oxidation of disulphide bonds are important for the correct folding of secretory proteins, specifically the C- and N- terminus of MUC2 contain disulphide bonds (Godl et al., 2002). In rat tissues, QSOX1 protein expression has been specifically localised within epithelial secretory cell types (Tury *et al.,* 2005). Thus this protein is likely to be important for the correct formation of a protective mucus barrier or function of secretory cells within the small intestine. The solute carrier (SLC) family proteins are important for absorption, distribution, metabolism and elimination processes

(Gutierrez-Aguillar and Baines, 2013; Palmieri, 2004). Broadly, within the intestine, these proteins regulate small molecule transport across the epithelium to facilitate communication between the host and the microbiome (Wu et al., 2013). The known functions of the SLC family member proteins up-regulated in secretory cell populations here is unknown, and further investigation is required to determine the role of these proteins during host immunity.

Detection of common proteins in both Paneth and goblet cells may infer that the drug skew treatments were not successful in generating enriched organoid cultures, although this is not reflective of organoids as visualised by confocal imaging. More likely is that the similarities in up-regulated proteins observed in both treatment groups is due to the shared secretory cell lineage of Paneth, goblet and enteroendocrine cells. The determination of secretory cell fate is modulated by the Notch signalling pathway through suppressive action (Vandussen et al., 2014; VanDussen et al., 2012; Yin et al., 2014). In both DAPT/CHIR and DAPT/IWP-2 treatments, the Notch signalling pathway is inhibited to allow cells to differentiate along the secretory cell lineage (Yin et al., 2014). It is possible that the proteins up-regulated in both treatment groups are regulated solely through this pathway, and so the inhibition of Notch signalling results in an increase of these secretory associated proteins. As mentioned above, an increased level of CHGA mRNA has previously been reported in DAPT/CHIR treated organoids (Yin et al., 2014), which suggests that the drug treatments have worked as previously described in the literature. Currently, very little is currently known about the relationship between the various secretory cell types within the small intestinal epithelium. Further profiling of these drug treated cultures at timed intervals may provide us with more information regarding the changes in protein expression throughout the process of terminal differentiation.

To summarise, the data here demonstrates that mass spectrometry can be applied to intestinal stem cell derived organoid to examine changes in protein abundance. Distinct profiles of known cell markers can be observed within treatment groups by mass spectrometry which agrees with previous studies utilising microarray and imaging techniques (Koo *et al.*, 2011; Milano *et al.*, 2004; Yin *et al.*, 2013). Furthermore, *in vitro* goblet/enteroendocrine enriched organoid cultures are capable of generating proteins similar in composition to murine gastrointestinal mucus *in vivo.*

The ability to detect markers Paneth and goblet cell markers via proteomic approaches demonstrate the suitability of this model to study the functional roles of these cell types *in vitro*. This model bypasses the limitations of existing models by inducing an enriched phenotype providing sufficient biological material to examine during enteric infection.

Chapter 4 – Development of a Collagen-Supported Epithelial Sheet Model

4.1 Introduction

Due to the limitations of existing intestinal epithelial models for infection studies (Chapter 1), we are interested in adapting intestinal organoid models to study host-pathogen interactions at the epithelial surface. These models are considered a promising tool to propel to field of intestinal infection biology forward, but have not yet been adequately optimized for this purpose.

4.1.1 Establishment of Intestinal Organoids

Identification of $LGR5^+$ stem cells within the small intestine (Barker et al., 2007), has allowed for the establishment of organoid cultures (Sato et al., 2009). Crypt columnar base units containing $LGR5^+$ stem cells cultured in the presence of Wnt agonist R-spondin 1, epidermal growth factor (EGF) and noggin produce a 3D model of the intestine (Sato et al., 2009). Following crypt isolation, $LGR5^+$ stem cells of the crypts terminally differentiate into Paneth, goblet, enteroendocrine and tuft cells within distinct crypt-villus domains to form a fully differentiated *in vitro* model of the gut (Sato et al., 2009). Prior to the development of organoid cultures, there was never a long-term *in vitro* culture system that maintained the crypt-villus physiology observed *in vivo*, making organoid models an exciting prospect for the future of intestinal biology research.

4.1.2 Current Uses of Organoid Cultures

To date, organoids have been exploited for regenerative medicine, nutrient transport and cancer studies (Neal and Kuo, 2016; Zachos et al., 2016; Zietek et al., 2015). With the exception of a few studies, there has been limited work on developing organoid cultures for the purposes of studying intestinal pathogens (Macartney et al., 2000; Saxena et al., 2016; Wilson et al., 2014; Zhang et al., 2014). Although small intestinal organoid cultures have been proposed as a useful tool for the study of intestinal infections, the organoid model still poses challenges and bears its own limitations.

4.1.3 Organoids as Infection Models

In order to accurately reflect *in vivo* physiology during an infection, it is important to study the host-pathogen interactions at the luminal interface where the pathogen would naturally be exposed to the host. Existing organoid culture methods yield 3D closed conformation structures with an enclosed lumen surrounded by multiple crypt-villus domains, making the luminal surface difficult to access without disrupting epithelial structure and integrity. The direct application of parasites is therefore impractical without specialised equipment such as a micro-injector (Wilson et al., 2014).

The development of an organoid model specifically for the study of enteric pathogens would aid in the study of protozoan parasites, as our current ability to investigate enteric protozoan infection is severely limited. As stem cells can be isolated from the small intestine, large intestine or the colon, these new models will allow for protozoan infections to be studied at different anatomical locations within the gut to mimic the diverse infection strategies employed by a diverse group of parasites (Klotz et al., 2012).

Protozoa have not yet been studied within organoid models and there is still a lack of understanding of the mechanism involved in early stage invasion of the intestinal epithelium. Unlike bacteria and viruses which have been successfully micro-injected into organoid models to establish infection (Wilson et al., 2014), due to their large size there are technical challenges involved with micro-injecting protozoan parasites onto the luminal interface within a 3D model.

4.1.4 Modification of Organoid Culture

An alternative method of utilising small intestinal stem cell-derived organoid cultures is to modify current culture conditions to generate a 2-dimensional (2D) semi-monolayer culture grown either on transwell membranes or on an alternative gel matrix (Jabaji et al., 2013; Moon et al., 2013; Y. Wang et al., 2017). Unlike 3D organoids which are embedded in Matrigel®, these modified methods involve seeding established Matrigel®-grown organoids onto the surface of alternative matrices. The open conformation of semi-monolayer cultures exposes the luminal surface of the intestinal epithelium and would allow for direct overlay of gastrointestinal pathogens. However, unlike previously established organoids grown in Matrigel®, culture of murine organoids on collagen gels remains largely unexplored with only one research group briefly utilising this culture method, though not fully validating or optimising it for infection studies (Jabaji et al., 2013).

To act as a suitable *in vitro* intestinal model, two particular features of the intestinal epithelial must be retained; the presence of major epithelial cell types involved with immune defence, and the polarization of the epithelium for the recognition of pathogens.

Traditionally, *in vitro* monolayer cell line cultures are susceptible to de-differentiation with passage (Briske-Anderson et al., 1997; Sambuy et al., 2005). There is also evidence to suggest that cell densities are altered in transwell-supported monolayers making it a less reliable model than a collagen-based matrix model (Moon et al., 2013). However, the differentiation status of the cells within collagen grown semi-monolayer cultures and the functionality of this model are currently undefined. Whilst promising, the suitability of this monolayer model as an *in vitro* alternative to *in vivo* whole animal experimentation or 3D explant tissues for infections requires further validation.

Ultimately the translation of these culture techniques will lead to the development of *in vitro* models for the study of early stage infection events, which are severely lacking at present. Organoid models have been demonstrated to be amenable to genetic manipulation, allowing for the role of specific molecular pathways in the response to infection to be studied (Andersson-Rolf et al., 2014; Powell and Behnke, 2017).

4.1.4. Aim and Objectives

The aim of this chapter is to modify existing organoid culture protocols to develop a novel model for the study of enteric infections.

Objectives:

a) Establish a culture protocol to generate collagen supported epithelial sheets, and extend the protocol to generate livestock models.
b) Determine if collagen supported epithelial sheets contain major epithelial cell types with host defensive functions
c) Determine if the epithelium is appropriately polarised in collagen supported epithelial sheets

4.2 Materials and Methods

4.2.1. Collagen Gel Preparation

Type 1 bovine and rat tail collagen gels were prepared to a final concentration of 1.5mg/mL as described in Chapter 2.2.1. Collagen gels were pipetted in 30µL domes into 48-well plates containing 9mm coverslips, and incubated at 37ºC and 5% CO_2 for a minimum of 30 min to allow for gel polymerisation.

The integrity of collagen gels were evaluated after 60 min of polymerisation, and after the removal of favourable conditions. A suitable density of collagen was then identified to be used as a scaffold for organoid fragments. This was then tested with the addition of organoid fragments, to assess structural integrity throughout the culture of epithelial sheets and collagen gel contraction.

4.2.2 Matrigel Grown Murine Small Intestinal Culture

Murine small intestinal organoids were established after crypt isolation and cultured in Matrigel® using a modified culture technique (Sato et al., 2009) as described in 2.1.

Murine crypt units were isolated and embedded in Matrigel®. Matrigel preparations were polymerised for 30 min at 37ºC and 5% CO_2. Advanced Reduced Serum Dulbecco's Modified Eagle Media (DMEM) containing 500ng/ml R-spondin (Peprotech), 50ng/ml EGF (Peprotech), 100ng/ml noggin (Peprotech), 1X B27 supplement (Life Technologies, 1X N2 supplement (Life Technologies), 1% Penicillin/Streptomycin (Sigma) and 10µM HEPES (Sigma) was overlaid onto polymerised domes. Complete media changes were performed every 3-4 days (Sato *et al.,* 2009).

4.2.3 Generation of a Monolayer Epithelial Model

Day 7 Matrigel®-grown organoids were fragmented by pipetting with PBS and syringing through a 27G needle. Excess Matrigel® containing cellular debris was removed through centrifugation at 300*xg* for 10 min at 4°C.

The organoid pellet was re-suspended in PBS and organoid fragments were pipetted directly onto polymerised collagen domes. Fragments were allowed to adhere to gels during 15 min incubation at 37°C and 5% CO_2 atmosphere and complete media was added to cultures for 8 days, with a complete media change on day 4.

Light microscopy images were acquired using a Zeiss Axiovert inverted microscope (Carl Zeiss, Cambridge, United Kingdom) and processed using Zen Blue 2.0 software (Carl Zeiss). For confocal imaging, day 8 epithelial sheets were washed with PBS then fixed with 4% paraformaldehyde (PFA) (Life Technologies) (in PBS) for 20 min at room temperature and stored in PBS at 4°C until staining.

Pilot studies were performed to demonstrate that monolayer culture protocols are translatable to other species of organoid cultures. Bovine organoids (grown by Dr Hayley Derricott) were fragmented via pipetting, and concentrated down with centrifugation at 50*xg* for 3 min 4°C. The organoid pellet was plated onto collagen gels as described above, and allowed to adhere for 15 min at 37°C and 5% CO_2 atmosphere. Bovine organoid media consisting of 1:1 of IntestiCult® (StemCell Technologies, Cambridge, United Kingdom), and Wnt3a-conditioned media (HEK293 cell line was generously gifted from Dr Carrie Duckworth, University of Liverpool) containing 1µg/mL R-spondin 1, 100ng/mL noggin, 100ng/mL EGF, 1.5µM CHIR99021 (Tocris), 5µM Y27632 (Tocris), 5µM SB202190 (Tocris), 250nM A8301 (Tocris) and 100µg/mL Primocin (InvivoGen, Toulouse, France) was overlaid onto cultures. Media

was changed every 3 days. Sheets were then fixed with PFA, and stained for intestinal epithelial cell markers.

4.2.4 Antibody Staining and Confocal Imaging

To confirm differentiation, epithelial sheets were stained as described in chapter 2.5 with mouse monoclonal antibody to lysozyme (BGN/06/961, AbCam, Cambridge, United Kingdom) or rabbit polyclonal antibody tomucin-2 (H-300, Insight Biotechnology, Middlesex, United Kingdom) antibodies. Secondary antibodies used were either donkey anti-mouse Alexa Fluor 488 (AF488) (AbCam, Cambridge, United Kingdom), donkey anti-rabbit FITC (Stratech Scientific Ltd, Suffolk, United Kingdom), or donkey anti-rabbit TRITC (Stratech Scientific Ltd). Nuclei were stained with DAPI (Life Technologies). F-actin was labelled using phalloidin conjugated to Alexa Fluor 647 (AF647) or Rhodamine (Life Technologies).

For evaluation of polarisation and cell-cell adhesions, epithelial sheets were stained with rabbit monoclonal antibody to e-cadherin (Clone 24E10, New England BioLabs, Hertfordshire, United Kingdom) or mouse anti-CD326 Epcam (Affymetrix eBiosciences, Altrincham, United Kingdom) and nuclei stained with DAPI.

Confocal images were acquired using Zen Black software on a Zeiss LSM880 upright confocal microscope using laser lines Diode (405), Argon (488), DPSS-5610 (561) and HeNe633 (633) and W-Plan Apochromat 40x/1.0 Dic (water immersion) or Plan-Apochromat 63x/1.0 oil DIC M27 (oil immersion) objective lens (all Zeiss).

4.2.5. Quantification of Confocal Images for Cellular Differentiation

All images for quantification were processed using Imaris x64 v8.0.1. Image analysis software (BitPlane, Oxford Instruments, Zurich, Switzerland).

Quantification of differentiated epithelial sub-populations in epithelial sheets and 3D organoids was performed as described in Chapter 2.6 and Figure 15 using the inbuilt "spots" function. For 3D organoids, the lower quartile, median and upper quartile z-stack was used for quantification.

4.2.6 Collagenase Treatments for Collagen Gel Separation

For proteomics experiments, epithelial sheets were required to be separated from collagen gels. Optimisation of this process was performed as described in Chapter 2.7.2 to obtain an optimal concentration of collagenase enzyme. During sample collection for proteomics, epithelial sheets were washed twice PBS and transferred to 1.5mL Eppendorf tubes. Samples were submerged with 0.1mg/mL collagenase (Sigma) and incubated at 37^{o}C and 5% CO_2. At 15 min incubation, a P1000 was used to gently disrupt the collagen gels and the solutions were incubated for a further 15 min.

After 30 min incubation, an equal volume of complete media was added to collagenase solution to neutralize enzyme activity. Samples were washed three times with PBS by centrifugation at 300*xg* for 5 min each. Samples were stored as dry pellets at -80^{o}C. Three biological replicates of day 7 collagen-grown epithelial sheets were prepared for proteomics experiments.

4.2.7 Matrigel®-grown Organoid Preparation for Proteomics

Murine organoids were established as described above, at day 7 media was removed and Matrigel® domes were washed with PBS. Matrigel® domes were gently disrupted by pipetting with a large bore tip (P1000). Samples were washed three times with PBS by centrifugation at 300*xg* for 5 min each. Samples were stored as dry pellets at -80^{o}C.

Three biological replicates of day 7 Matrigel®-grown organoids were prepared for comparison to collagen-supported epithelial sheets.

4.2.8 Peptide Digest and NanoLC MS ESI MS/MS Analysis

Sample peptide digest was performed as described in Chapter 2.7. Organoid and epithelial samples were sonicated in 2mM ammonium bicarbonate, 0.1% w/v Rapigest (Waters, United Kingdom). Protein content was determined using the Coomassie Plus protein assay (Pierce, Thermofisher), and normalised as required. Samples were reduced with 3mM dithioreitol, alkylated with 0mM iodoacetimide and trypsinated at a ratio of 50:1. Samples were run on 12% mini-gel to confirm successful peptide digest and Rapigest was removed via the addition of 1% (v/v) trifluoroacetic acid (TFA). Peptide samples were centrifuged at 12,000*xg* for 60 min at 4^{o}C to remove precipitated Rapigest, re-suspended in 0.1% TFA in 3% acetonitrile and stored at 4^{o}C prior to loading. Peptide mixtures (2µl) were analyzed by Dr Stuart Armstrong as described in Chapter 2.8. Raw data files were processed in Progenesis LC-MS (Version 4.1, Nonlinear Dynamics) as described in Chapter 2.8.

4.3 Results

Due to limitations associated with existing *in vitro* and *in vivo* small intestinal infection models, there is a demand to generate a novel model incorporating differentiated epithelial cell types that is susceptible to infection at the luminal surface. Previous studies suggested that passage of established 3D organoid cultures onto an alternative collagen matrix could generate semi-monolayer epithelial sheets however, they have not yet been validated for infection studies. Within this chapter, we have described the

generation of collagen-supported epithelial sheets and demonstrated several desirable characteristics that make this model suitable for infection studies.

4.3.1 Rat Tail Collagen Gels Successfully Sustain Epithelial Sheet Growth

The first objective of this chapter was to optimise culture conditions for the generation of semi-monolayer epithelial sheets with an accessible lumen. We compared cultures grown on bovine type 1 collagen and rat tail type 1 collagen to identify a suitable substrate for the generation of these epithelial sheets.

Firstly, we assessed the structural integrity and polymerisation of 1.5mg/mL and 2mg/mL type 1 bovine and rat tail collagen gels. Collagen gels were prepared as described in Chapter 2.2 and allowed to polymerise for a minimum of 30 min at 37ºC and 5% CO_2, before being removed from the incubator and left at room temperature for 15 min (the approximate time taken to passage organoids onto the gels). Gels were re-incubated for a further 30 min and the structural integrity of the gels were examined. It was observed that gels at 1.5mg/mL were noticeably less stable than 2mg/mL gels, particularly, the bovine gels began to de-polymerise and lose their solid form. Therefore, further optimisation was carried out on rat tail collagen gels prepared to a final concentration of 2mg/mL

Next we incorporated the organoids onto collagen gels as described in Chapter 2.2, to determine the ability of 2mg/mL collagen gels to sustain epithelial cell growth (**Figure 25**). Briefly, 3D organoids were fragmented by syringing and re-plated onto polymerized 2mg/mL collagen gels and overlain with complete organoid media.

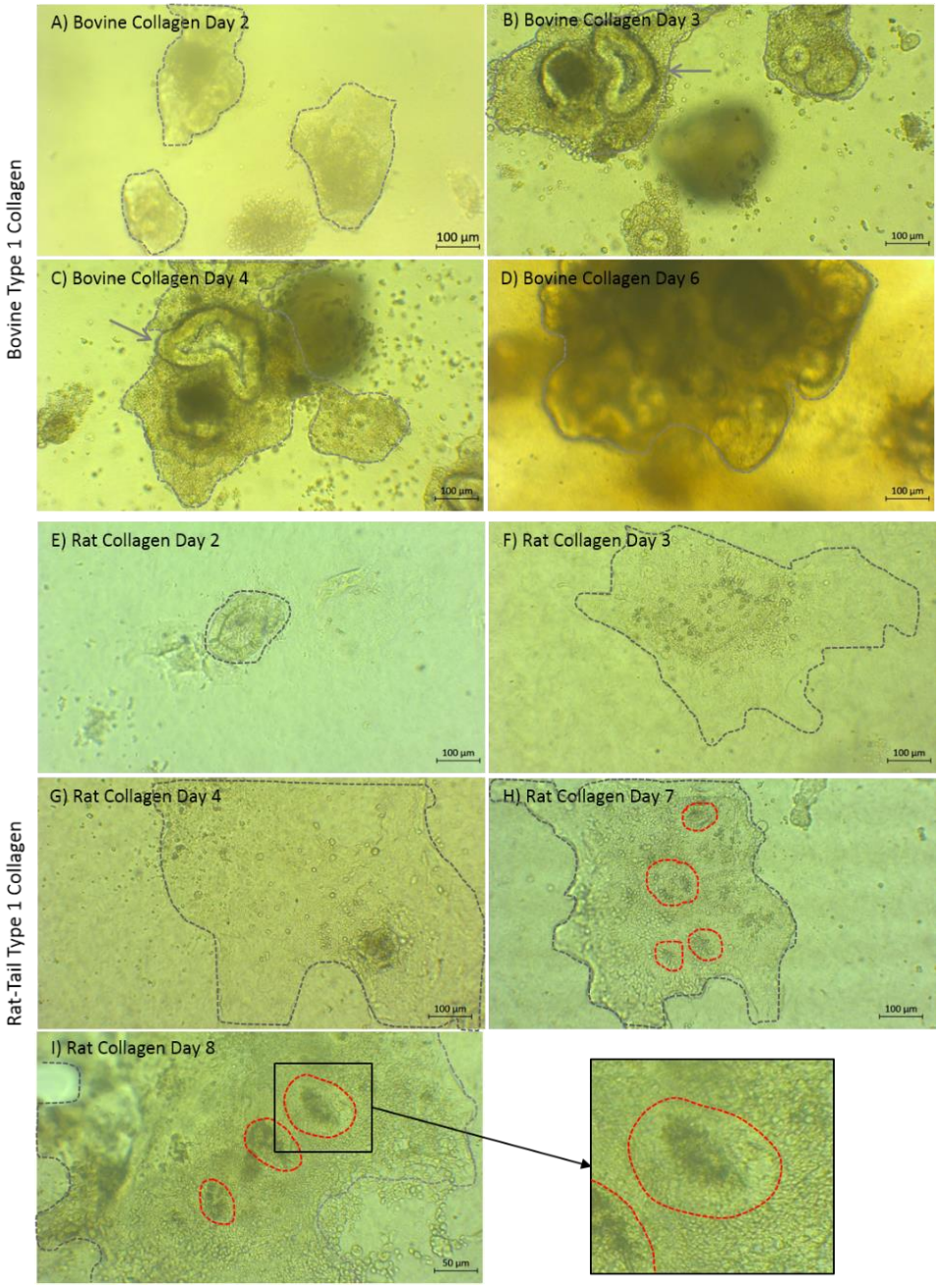

Figure 25) Rat tail collagen gels successfully sustains semi-monolayer epithelial sheets. Organoid fragments were applied to collagen gels during passage, and cultured for 8 days. Light microscopy shows morphological differences between organoid fragments grown on (A-D) bovine type 1 collagen gels and (E-I) rat tail type 1 collagen gels. Within 2 days of culture, organoid fragments begin to spread across the surface of both types of gel (A and E). 3D structures are retained on bovine gels (B) whereas this phenotype is lost on rat tail collagen gels by day 3 (F). Further growth is observed at day four on both types of gel (C and G), By day 6, fragments on bovine gels cease to develop further and remain in a 3D phenotype (D), whereas cultures on rat tail collagen develop to form an epithelial monolayer with cobblestone phenotype (H and I). At days 7 and 8 (H and I), areas of non-uniformity were evident (highlighted by red dashed lines) within the epithelial sheets. These were later identified by confocal imaging to contain Paneth cells. Scale bars = 100µm, except (I) where scale bar = 50µm.

Within two days in culture, organoids began to undergo morphological changes on both bovine and rat-tail collagen gels (**Figure 25, A and E**). Unlike 3D organoid cultures embedded within Matrigel®, fragments grown on collagen gels began to spread outward across the surface of the gel forming a more flattened 2D phenotype (**Figure 25, A and E**).

After three days in culture, organoids grown on bovine collagen gels appear to have retained more of their 3D structure (**Figure 25 B**) compared to those grown on rat tail collagen gels where the fragments were fully At day four, although there were signs that the organoids grown on bovine collagen gels were spreading, these cultures still retained 3D structures (as indicated by the arrow (as indicated by the arrow **Figure 25 C**) whereas on rat tail collagen gels, the organoid fragments continued to spread further outwards forming a larger epithelial sheet (**Figure 25 G**).

At day six, organoids grown on bovine collagen gels show no further changes (**Figure 25 D**) whereas at days seven and 8, organoids passaged onto rat tail collagen gels formed a semi-monolayer large epithelial sheet with cobblestone phenotype that lack the 3D crypt-villus type structures seen on bovine gels (**Figure 25 H and I**).

In the later stages of growth, organoids grown on rat tail collagen exhibited regions of non-uniformity with respect to cell size and density, as indicated by the red dashed circles in **Figure 25** (H and I). These regions were visualised by confocal imaging and will be discussed in section 4.3.2.

Comparison of bovine and rat tail collagen gels determined a suitable composition of collagen for the modification of close conformation organoid culture techniques to open conformation epithelial sheets suitable for infection studies. Structurally, bovine collagen gels were more susceptible to de-polymerisation following their removal

from incubation at 37ºC and 5% CO_2, whereas rat tail collagen gels retained their structural integrity even after removal from incubation. Furthermore, retention of 3D structures on bovine collagen gels is not desirable when considering a monolayer culture. Rat tail collagen grown organoid fragments generated large epithelial sheets with cobblestone phenotype, that were similar to previously published results by Jabaji *et al.,* 2012. For these reasons, only organoid cultures on rat tail collagen gels were further evaluated for sustainability as an infection model.

4.3.2 Epithelial Sheets Retain Differentiated Status *In vitro*

The second aim of this chapter was to determine the differentiation status of collagen-supported epithelial sheets via confocal imaging and proteomic approaches. Traditional *in vitro* cultures are susceptible to de-differentiation, and due to their importance during host immune response against invading enteric pathogens, the presence of Paneth and goblet cells is a desirable trait for intestinal epithelial models.

Here, we characterised the epithelial sheet and evaluated the presence or absence of differentiated epithelial cell types within the culture via confocal imaging and mass spectrometry. Monolayer epithelial sheets were cultured for 7 days, and either fixed for confocal imaging or processed for mass spectrometry. Three replicates for confocal imaging were used for quantification, and three biological replicates of 5-well pooled samples of both collagen-supported epithelial sheets and Matrigel® grown organoids were prepared for mass spectrometry.

Both Paneth and goblet cells were shown to be present in epithelial sheets after 8 days in culture **(Figure 26** and **Figure 27**), confirming the retention of epithelial cell differentiation of this 2D monolayer culture in short term culture.

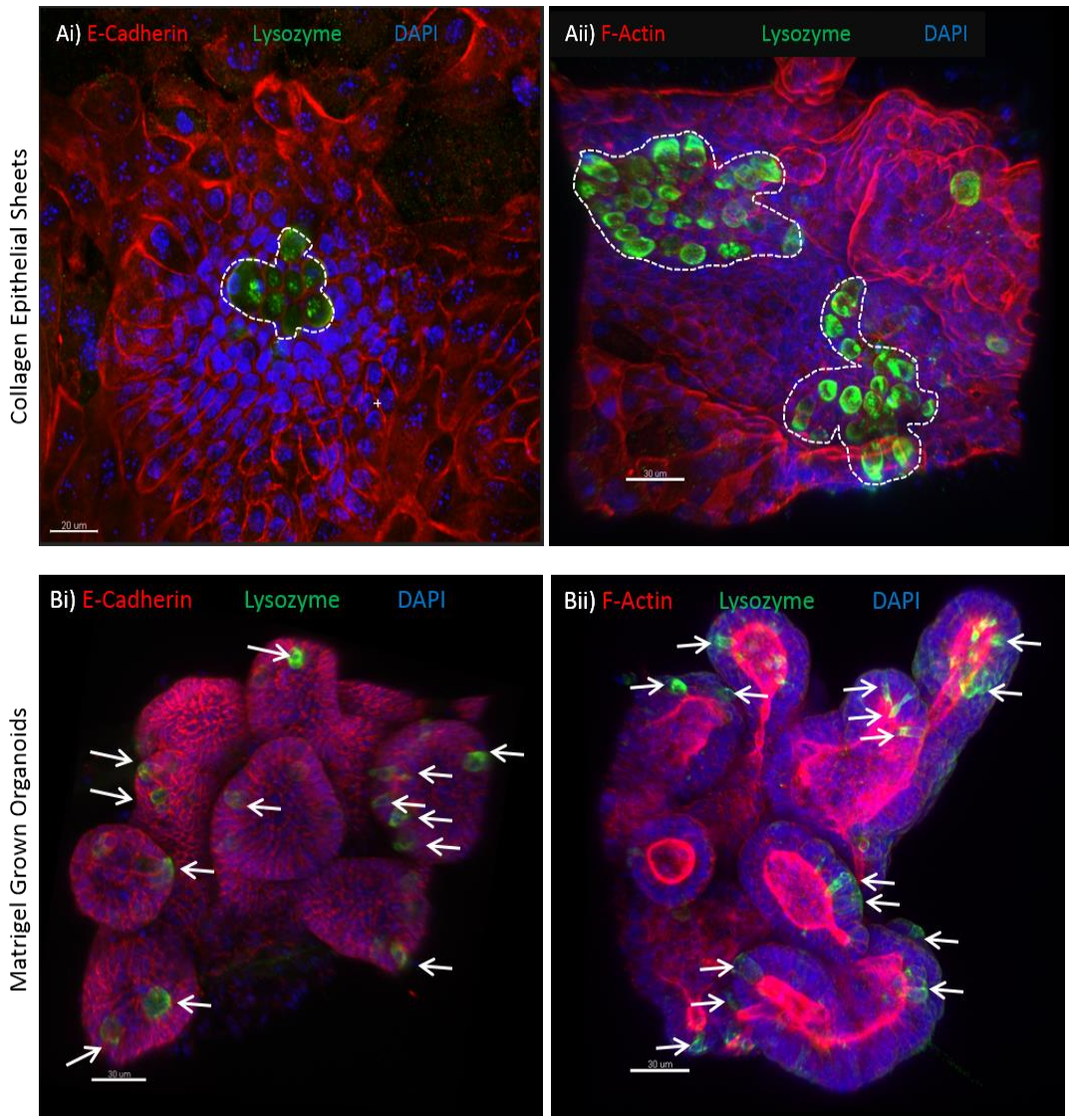

Figure 26) Characterisation of collagen epithelial cultures via confocal imaging confirms the presence of Paneth cells.

Collagen-supported epithelial sheets and Matrigel® embedded organoids were fixed and processed for confocal imaging. Paneth cells are identified via anti-lysozyme (green) antibody staining, accompanied by nuclear stain DAPI (blue) and either anti-E-cadherin (red) antibody or F-actin (red) staining. Paneth cells are present in both (A) collagen-supported epithelial sheets in clusters as highlighted by the dashed lines, and (B) Matrigel® controls some of which are highlighted by white arrows. Images are representative of three experimental replicates. Scale bars = 30µm, except for Ai where scale bar = 20µm.

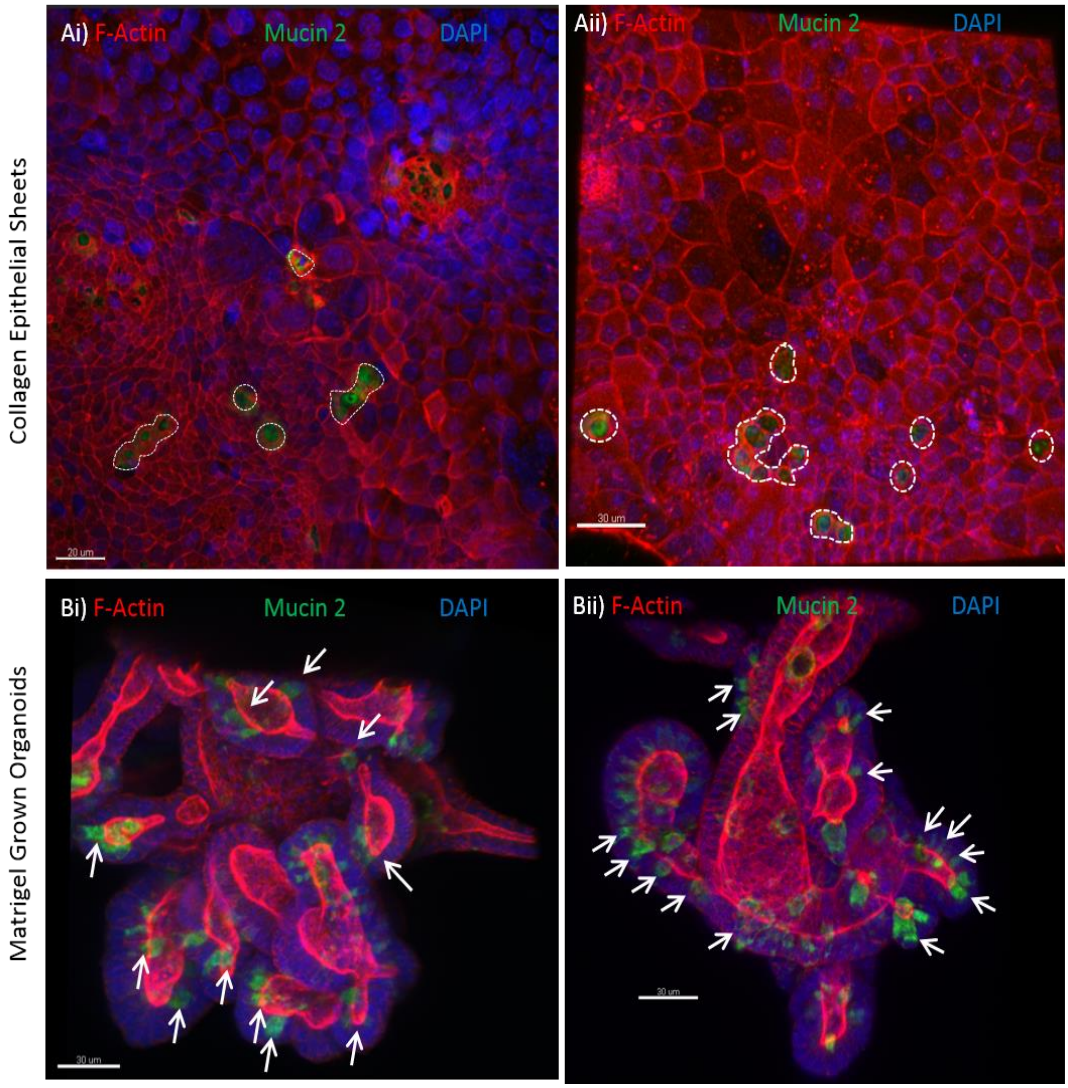

Figure 27) Characterisation of collagen epithelial cultures via confocal imaging confirms the presence of goblet cells.

Collagen-supported epithelial sheets and Matrigel® embedded organoids were fixed and processed for confocal imaging. Goblet cells are identified via anti-mucin-2 (green) antibody staining, accompanied by nuclear stain DAPI (blue) and F-actin (red) staining. Goblet cells are present in both (A) collagen-supported epithelial sheets in clusters as highlighted by the dashed lines, and (B) Matrigel® controls, some of which are highlighted by white arrows. Images are representative of three experimental replicates. Scale bars = 30µm, except for Ai where scale bar = 20µm.

Paneth cells are present and arranged in micro-domain clusters within the central regions of the monolayer culture (as indicated by regions surrounded by dashed lines in **Figure 26 A**), whereas in Matrigel® grown organoids, Paneth cells are distributed within crypt domains although not often neighbouring one another (highlighted by arrows in **Figure 26 B**). This is reminiscent of their distribution *in vivo* where Paneth cells are found clustered at the base of crypt columnar base units.

In contrast, goblet cells in monolayer cultures are more sporadically dispersed and appear to be distributed throughout the epithelial sheets (indicated by regions surrounded by dashed lines **Figure 27 A**). Similarly goblet cells in Matrigel® grown organoids are distributed throughout the whole organoid structure. These arrangements are comparable to *in vivo* goblet cell distribution, where goblet cells can be found throughout the transit amplifying region and within villus structures

Automated cell quantification, using Imaris image analysis software, was used to estimate overall epithelial cell counts and generate a percentage of differentiated epithelial cell populations based on DAPI nuclear staining and differentiated cell staining. Based on three experimental replicates, we have determined that the Paneth and goblet cell populations constitute approximately 7.34% and 7.26% in Matrigel® grown organoids, and 3.31% and 1.89% in collagen grown sheets, respectively (**Figure 28**). The population differences are significant for both Paneth ($p = 0.0355$ and goblet cells ($p = 0.0068$) by an unpaired t-test.

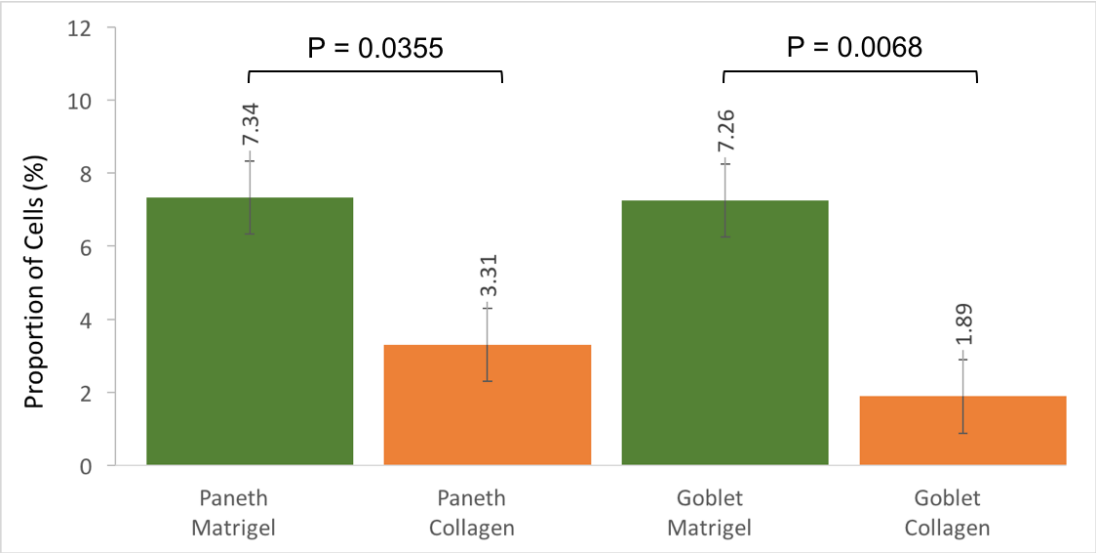

Figure 28) Paneth and goblet cell populations form a higher proportion of the whole cell population in Matrigel® grown organoids than collagen-supported epithelial sheets

Confocal microscopy and Imaris analysis software was used to quantify the Paneth and goblet cell populations in Matrigel® grown organoids and collagen-supported epithelial sheets. Comparison of Paneth cell populations in Matrigel grown organoids vs collagen-supported epithelial sheets via students t-test show a significant difference ($p = 0.0355$) in the numbers of this cell type between the two cultures. Similarly, comparison of goblet cell populations in Matrigel grown organoids vs collagen-supported epithelial sheets via students t-test show a significant difference ($p = 0.0068$) in the numbers of this cell type between the two cultures. Together, these indicate that Matrigel® grown organoids contain a higher proportion of Paneth and goblet cells that collagen-supported epithelial monolayer cultures. Passage numbers of organoids used for quantification were 4, 10 and 16. Data is representative of three technical replicates.

4.3.3. Mass Spectrometry Protein Detection in 3D Organoids vs Monolayer Epithelial Sheets

To evaluate the presence of other epithelial cell types within our culture, we exploited label-free mass spectrometry to compare the proteins detected in epithelial sheets with Matrigel® grown organoids. Of the proteins detected in these samples, we searched for known intestinal epithelial markers and confirmed the expression of multiple

proteins associated with differentiated epithelial cell types of the small intestine. Our results indicate the presence of Paneth cells, goblet cells, enterocytes, stem cells and microvilli within the epithelial sheet model.

Five Paneth cell products were detected; alpha-defensin 2, 5, 20, 24 and lysozyme C-1 (Ayabe et al., 2002; Lisitsyn et al., 2012; Peeters and Vantrappen, 1975; Salzman et al., 2010, 2003a), however their presence was not uniform across both sample types (**Table 9**). Alpha-defensin 5, in particular, was not detected in Matrigel® grown organoids, but was detected in collagen-supported epithelial sheets (**Table 9**).

Seven goblet cell markers and mucus components were detected; alpha-enolase, anterior gradient protein 2 homolog, chloride intracellular channel protein 1, mucin 2, mucin 13, trefoil factor 3 and zymogen granule membrane protein 16 (Lenaerts et al., 2007; Rodriguez-Pineiro et al., 2013; Roussa et al., 2010; Taupin and Podolsky, 2003) (**Table 9**). The first three of these proteins were detected in all samples, whereas the latter 4 were not. In particular, trefoil factor 3 was detected in Matrigel® grown organoids, but not in collagen-supported epithelial sheets (**Table 9**).

Two enterocyte markers were detected; intestinal fatty acid-binding protein and villin-1 (Hodin et al., 1997; Kanda et al., 1996; Rusu et al., 2005; Sommer and Mostoslavsky, 2014) (**Table 9**). The expression of both proteins was found across all samples (**Table 9**).

Table 9) Intestinal epithelial differentiation marker proteins present in epithelial sheets and Matrigel® grown organoids detected by mass spectrometry, based on three biological replicates per group

ID	Protein Name	Description	Collagen	Matrigel®
P28309	Alpha-defensin 2	Paneth cell markers (secreted anti-microbial peptides)	✓✓✕	✓✓✓
P28312	Alpha-defensin 5		✓✓✓	✕✕✕
Q45VN2	Alpha-defensin 20		✓✓✕	✓✓✓
Q5G865	Alpha-defensin 24		✕✓✓	✓✓✕
P17897	Lysozyme C-1		✓✓✓	✓✓✓
P17182	Alpha-enolase	Goblet cell markers (components of mucus)	✓✓✓	✓✓✓
O88312	Anterior gradient protein 2 homolog		✓✓✓	✓✓✓
Q9Z1Q5	Chloride intracellular channel		✓✓✓	✓✓✓
Q80Z19	Mucin-2 (Fragments)		✓✕✕	✕✓✓
P19467	Mucin-13		✓✕✕	✓✓✓
Q62395	Trefoil factor 3		✕✕✕	✓✕✓
Q8K0C5	Zymogen granule membrane protein 16		✓✓✓	✕✓✕
P55050	Fatty acid-binding protein, intestinal	Enterocyte markers	✓✓✓	✓✓✓
Q62468	Villin-1		✓✓✓	✓✓✓
Q3UZZ4	Olfactomedin-4	Intestinal stem cell marker	✓✓✓	✓✓✓
P16014	Secretogranin-1	Enteroendocrine cell marker	✓✕✕	✓✓✓
P26040	Ezrin	Epithelial organisation and villus morphogenesis	✓✓✓	✓✓✓
Q3V0K9	Plastin-1	Intestine specific actin bundling protein of micro-villi	✓✓✓	✓✓✓

Additionally, stem cell protein olfactomedin-4 (Grover et al., 2010) was detected in all samples, indicating a presence of intestinal stem cells within the culture, and enteroendocrine cell marker secretogranin-1 (Wang et al., 2004) was present in all Matrigel® organoid samples, and one collagen grown epithelial sample. Two proteins associated with villus morphogenesis were detected in both sample types; ezrin and plastin-1 (Revenu et al., 2012; Shinomiya, 2012; Sumigray and Lechler, 2012; Wald et al., 2005) (**Table 9**).

These subsets of proteins described above, indicate the presence of Paneth cells, goblet cells, enterocytes and stem cells within this epithelial model.

4.3.3 Epithelial Sheets Exhibit Basolateral E-Cadherin and Strong Apical F-Actin staining

Having confirmed the retention of epithelial cell differentiation after 8 days *in vitro*, next we evaluated the polarisation status of the epithelial sheets by confocal microscopy. As the intestinal epithelium *in vivo* is polarised and is the site of enteric pathogen invasion, *in vitro* models must also mimic this feature to accurately simulate early stage infection events which involves pathogen recognition on this surface.

Here we evaluate polarization of the epithelial sheet by examining the distribution of a basolateral marker protein, e-cadherin and F-actin which is concentrated on apical surfaces (**Figure 29**).

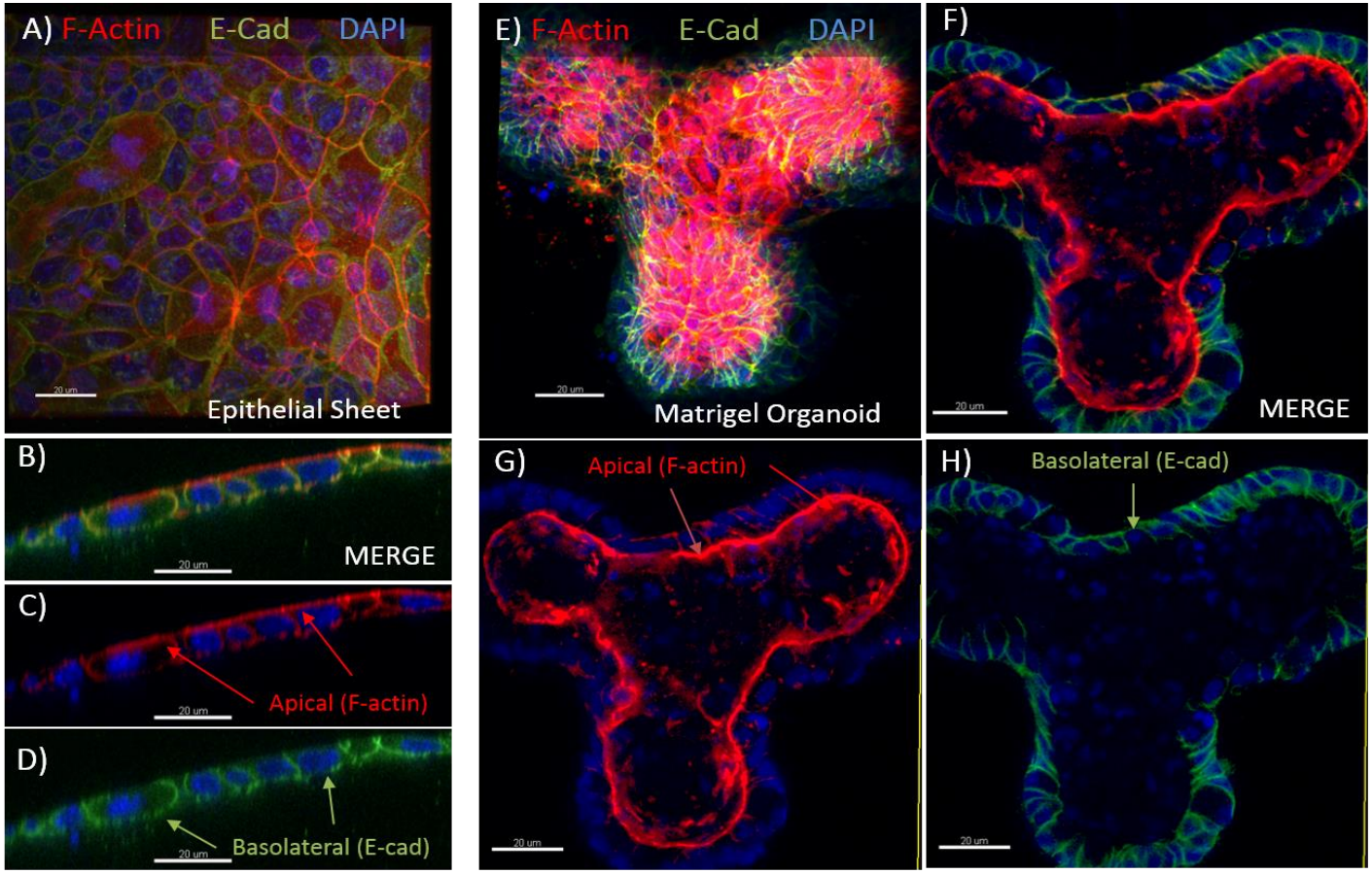

Figure 29) Collagen-supported epithelial sheets express specifically localised basolateral E-cadherin and enriched apical F-actin staining

Epithelial sheets were cultured, fixed and processed for confocal microscopy. (A) 3D view of collagen-supported model stained for f-actin and e-cadherin. (B) Transverse view of collagen-supported model (0.264µm section). Collagen-supported model is polarized as demonstrated by apical enrichment of F-actin (C) and basolateral localization of e-cadherin (D). (E) 3D view of organoid stained for f-actin and e-cadherin. (F) Transverse view of organoid model (0.470µm section). 3D organoid model is polarized as demonstrated by apical enrichment of f-actin (G) and basolateral localization of e-cadherin (H).Scale bars = 20µm.

Confocal microscopy was exploited to examine the localized expression of e-cadherin and f-actin staining in collagen grown epithelial (**Figure 29**). Here we report enrichment of f-actin expression upon the apical surface and basolateral localization of e-cadherin in both 3D organoids, and in collagen-supported epithelial sheets (**Figure 29**). This is further supported by the presence of integrin-beta 1, a protein involved in maintaining cell polarization (Yu et al., 2005) , which was detected in all three collagen grown epithelial samples by label free mass spectrometry.

Having confirmed the polarisation status of this epithelial sheet model, next we evaluated the presence of cell-cell adhesions for the maintenance of epithelial barrier integrity.

4.3.4. Staining for EpCam Demonstrates the Presence of Cell-Cell Adhesions

Selective permeability across the intestinal epithelium *in vivo* regulates gut biological functions and protects against pathogen invasion. To determine the structural integrity of collagen-supported epithelial sheets, here we examined the localisation of epithelial adhesion molecule (EPCAM) and evaluated the presence of junction-associated proteins by label-free mass spectrometry.

Confocal imaging confirmed the presence of cell-cell adhesions as denoted by EPCAM staining (**Figure 30**) and e-cadherin (**Figure 25)** staining on lateral surfaces. *In vivo*, epithelial sheet integrity is maintained by the presence of several complexes as described in Chapter 1.6; tight junctions, adherens junctions and desmosome. Particularly, EPCAM co-localises with tight junction protein claudin-7 to regulate cell-cell adhesions (Ladwein et al., 2005), and its presence in collagen-supported models demonstrates the presence of cell-cell adhesions.

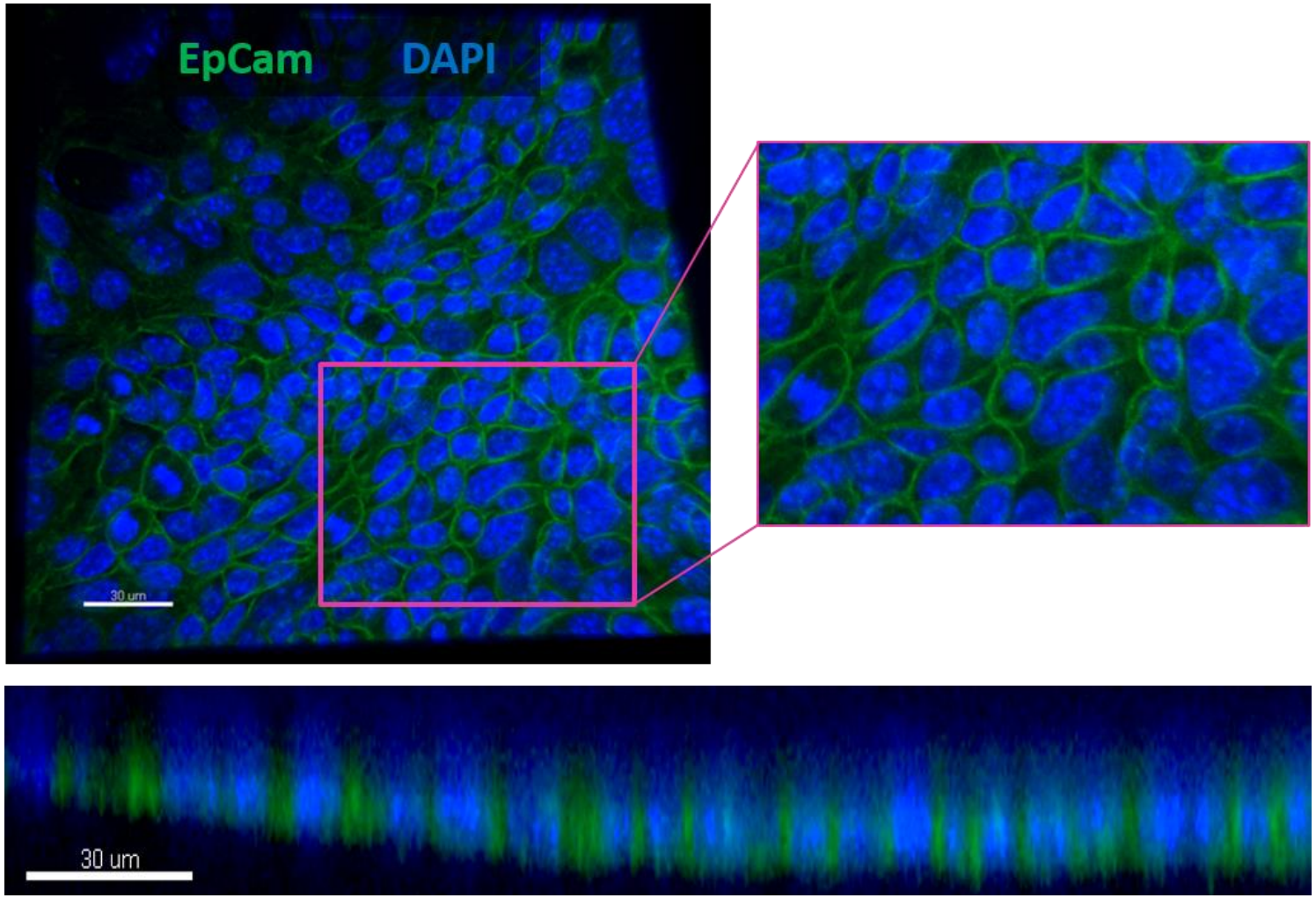

Figure 30) Collagen-supported epithelial sheet staining for EpCam confirms the presence of cell-cell adhesions. Epithelial sheets were cultured, fixed and processed for confocal microscopy. Intercellular localisation of EpCam demonstrates the presence of cell-cell adhesion complexes within the collagen grown epithelial model. Scale bar = 30µm.

4.3.5 Detection of Junctional Proteins by Label-Free Quantitative Proteomics

Next, we evaluate the presence of the proteins involved in the formation of these complexes by label-free mass spectrometry. Proteins involved in the formation of tight junctions, adherens junctions and desmosomes were detected within collagen-supported epithelial sheets.

Five adherens junction proteins were detected; cadherin-1 (e-cadherin), cadherin-17, catenin alpha-1, catenin delta-1 and epithelial cell adhesion molecule (EpCam) in all samples with the exception of catenin alpha-1 which was detected in only one of the Matrigel® grown samples (Anderson and Van Itallie, 2009; Coopman and Djiane, 2016; Su et al., 2008; Takeichi, 2014; van Roy and Berx, 2008) (**Table 10**).

Six hemidesmosome/desmosome proteins were detected in collagen grown sheets, but not in Matrigel® grown organoids; desmoglein 2, desmocollin-2, desmoplakin, integrin alpha-6, integrin beta-4 and plectin (Coch and Leube, 2016; Giuffrida et al., 2014; Ku et al., 1999; Mercurio et al., 2001; Stepp et al., 1990; van Roy and Berx, 2008) (**Table 10**).

Three tight junction proteins were detected, although not consistently in collagen-supported epithelial sheets; junctional adhesion molecule A, tight junction protein ZO-1 and tight junction protein ZO-2 (Arrieta et al., 2006; Citi and Cordenonsi, 1998; Giuffrida et al., 2014; Mandell and Parkos, 2005). These three proteins were all absent from Matrigel® grown organoid samples (**Table 10**). Here we also attempted to confirm the presence of tight junctions by staining for ZO-1. The antibody used was not reactive to the target protein in either epithelial sheets or Matrigel® control suggesting an antibody failure and not a lack of ZO-1 protein.

Table 10) Intestinal epithelial tight junction proteins present in epithelial sheets and Matrigel® grown organoids detected by mass spectrometry, based on three biological replicates per group.

ID	Protein Name	Description	Collagen	Matrigel®
P09803	Cadherin-1 (E-cadherin)	Adherens Junction Proteins	✓✓✓	✓✓✓
Q9R100	Cadherin-17		✓✓✓	✓✓✓
P26231	Catenin alpha-1		✓✓✓	✕✕✓
P30999	Catenin delta-1		✓✓✓	✓✓✓
Q99JW5	Epithelial cell adhesion molecule		✓✓✓	✓✓✓
O55111	Desmoglein-2	Hemidesmosome/ desmosome proteins	✓✓✕	✕✕✕
P55292	Desmocollin-2		✓✕✕	✕✕✕
E9Q557	Desmoplakin		✓✓✓	✕✕✕
Q61739	Integrin alpha-6		✓✓✓	✕✕✕
A2A863	Integrin beta-4		✓✓✓	✕✕✕
Q9QXS1	Plectin		✓✓✓	✕✕✕
O88792	Junctional adhesion molecule A	Tight junction protein	✕✓✕	✕✕✕
P39447	Tight junction protein ZO-1		✓✕✕	✕✕✕
Q9Z0U1	Tight junction protein ZO-2		✓✓✓	✕✕✕

In addition to detecting the presence of junctional associated proteins, we evaluated the presence of known structural proteins relevant to the *in vivo* small intestinal epithelium (**Table 11**). Five intestinal epithelial cytoskeletal keratins were detected; 7, 8, 18, 19 and 20 (Helenius et al., 2016; Ku et al., 1999). All of these were detected in all samples, with the exception of cytoskeletal keratin 20, which was detected in all but one Matrigel® sample (**Table 11**).

Table 11) Intestinal epithelial structural marker proteins present in epithelial sheets and Matrigel® grown organoids detected by mass spectrometry, based on three biological replicates per group.

Q9DCV7	Keratin, type II cytoskeletal 7	Component of intermediate filament	✓✓✓	✓✓✓
P11679	Keratin, type II cytoskeletal 8		✓✓✓	✓✓✓
P05784	Keratin, type I cytoskeletal 18		✓✓✓	✓✓✓
P19001	Keratin, type I cytoskeletal 19		✓✓✓	✓✓✓
Q9D312	Keratin, type I cytoskeletal 20		✓✓✓	✓✓✕

The presence of these known intestinal structural proteins indicate that collagen-supported epithelial sheets contain the same structural proteins as Matrigel® grown organoid cultures.

4.3.6 Differentiated Bovine Epithelial Sheets Can Be Cultured On Collagen Gels

The final aim of this chapter, was to demonstrate that the epithelial sheet protocol described above can be translated to generate models from other mammalian species. The availability of large mammal intestinal models is limited, particularly in food-

producing animals such as cows, pigs and sheep. To address this, Dr Hayley Derricott (Department of Infection Biology, University of Liverpool) has developed 3D organoid cultures derived from bovine and porcine small intestinal tissues. Here, using these 3D bovine organoids, I have demonstrated that the modified collagen-supported epithelial culture technique can be translated to generate bovine epithelial sheets. Collagen gels were prepared as previously, and bovine Matrigel®-grown organoids were harvested and re-plated on top. Bovine organoid media was added to collagen gels and cell adherence and growth was monitored.

Two days post passage, bovine organoids begin to show signs of flattening and remodelling to accommodate the collagen gel (**Figure 31 A**). By day 4, the bovine organoid fragments begin to spread across the surface of the collagen gel (**Figure 31 B**). By day 7, larger epithelial sheets have formed, although these still retain some 3-dimensionality (**Figure 31 C)**. The bovine epithelial sheets here have spread to a size comparable to the murine epithelial sheets described in **Figure 25**.

To determine the differentiation status of bovine epithelial sheets, samples were fixed and stained for markers associated with fully differentiated epithelial cell types. Confocal imaging confirms the presence of enteroendocrine cells (**Figure 31 D**). Attempts to stain for goblet cells and Paneth cells was also performed but were unsuccessful. This was limited by a lack of commercially available validated antibodies against bovine targets. Furthermore, the presence of bovine Paneth cells is disputed and has previously not been detected in bovine organoids (data not shown).

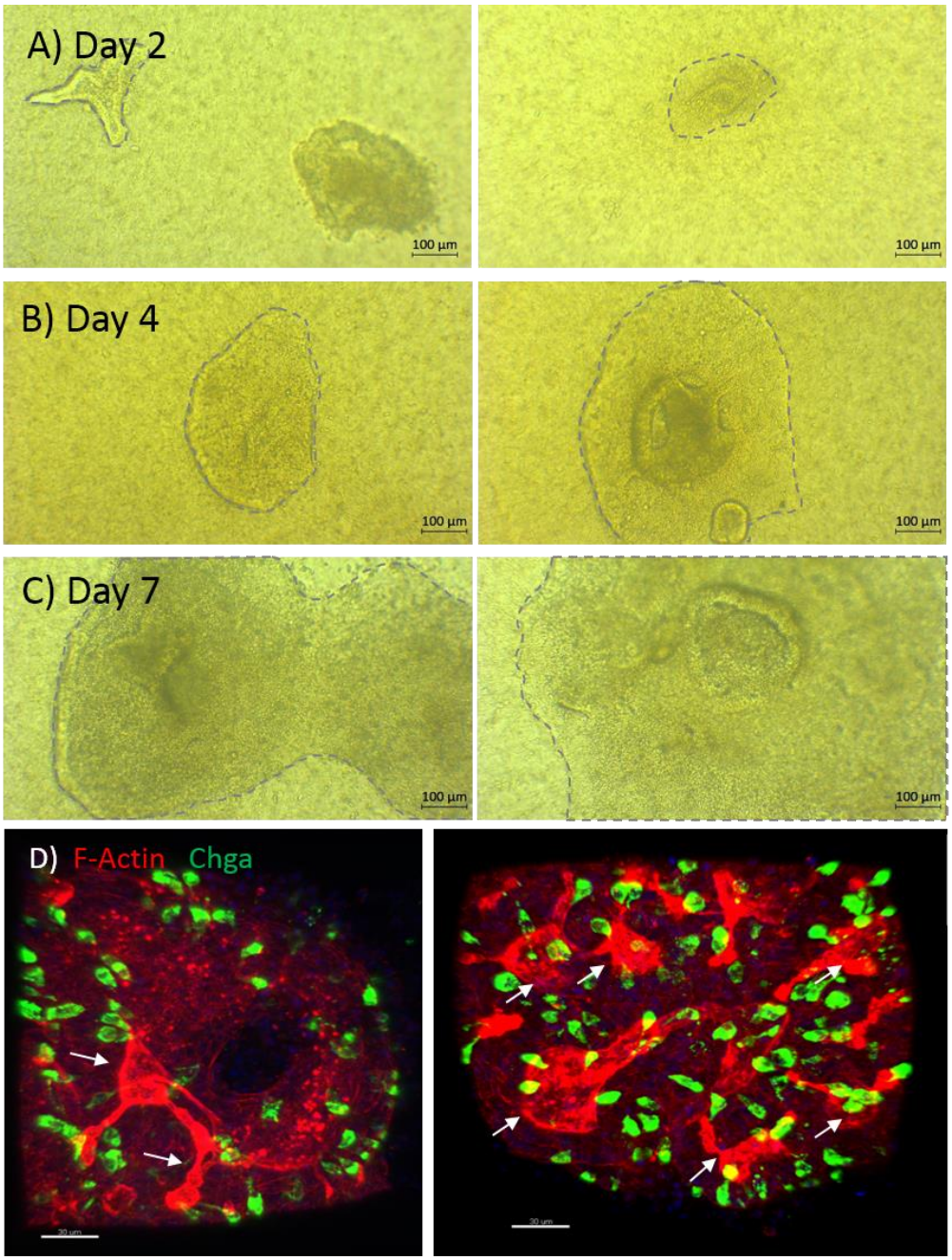

Figure 31) Bovine epithelial sheets can be cultured on rat tail collagen gels

Matrigel® grown organoids were passaged onto 2mg/mL collagen gels (A) Bovine organoid fragments show signs of flattening on the surface of collagen gels at day 2. (B) Growth of cells is observed by day 4, where the culture is becoming more sheet-like. (C) By day 7, epithelial sheets are established that are comparable in size to murine epithelial sheets as described in Fig. 4.3.1.1. (D) Bovine epithelial sheets retain enteroendocrine cell populations (green) as well as some 3D-like structures (denoted by white arrows). Scale bars (A-C) = 100µm, D = 20µm). Images are representative of two replicates.

Unlike murine epithelial monolayers that exhibit a flattened phenotype and cobblestoned f-actin staining pattern, bovine collagen-supported sheets do not appear uniformly flat. F-actin staining is generally enriched on the apical surface of polarized epithelia, and here we observed tubular structures with high F-actin expression which may be indicative of some luminal constructs retained within the bovine culture (**Figure 31 D**, white arrows).

Differences between the growth cycles of murine and bovine intestinal stem cells may account for the discrepancies in re-modelling of organoid models between species. The bovine epithelial model requires further optimisation to develop the monolayer phenotype, however these pilot results indicate that the collagen culture method can sustain growth of other mammalian species in addition to murine cultures which is a potential tool for the study of host-pathogen interactions in food-producing animal species. Further optimisation of this technique for bovine intestinal stem cell derived cultures is required to modify the structural arrangement to monolayer phenotype.

4.4 Discussion

In vivo, the small intestinal epithelium acts as a physical barrier to protect the host from enteric pathogens. In order to study host-pathogen interactions *in vitro*, we aim to recapitulate the *in vivo* environment as closely as possible however current models of the intestinal epithelium are limited. For infection studies, several characteristics of the gut must be considered which are desirable for an intestinal model; the presence of differentiated epithelial cell populations and the selective permeability of the epithelium regulated by polarised cells and cell-cell adhesion complexes. This chapter will discuss the development of a collagen-supported epithelial model, its ability to

mimic the *in vivo* epithelium, and also its limitations for the study of host-pathogen interactions.

Current models of the small intestine are limited, however the identification of LGR5+ intestinal stem cells has led to the development of 3D organoid cultures *in vitro.* Due to their ability to mimic the *in vivo* cellular diversity and structure, organoids are considered as promising tools for the study of enteric pathogens, but have not been fully optimized for this purpose. The enclosed conformation of organoid cultures restricts access to the relevant interface required to apply pathogens to study host-pathogen interactions. Ideally, microinjection can be used to penetrate organoid cultures to deliver pathogens without disrupting epithelial integrity (Wilson et al., 2014). However this technique requires specialised training and equipment, making it a less attractive and less accessible method for performing simple infection experiments. Moreover, microinjection of protozoan parasites has not yet been achieved in this model, which is likely due to difficulties with optimizing this method for large pathogens. Furthermore, microinjection is low throughput and laborious, yielding low volumes of biological material which limits the use of systems biology approaches.

Modification of 3D organoid culture techniques has established a semi-monolayer epithelial sheet supported by a collagen scaffold for the purposes of studying drug metabolism however the presence of differentiated epithelial cell types and polarization status is unknown (Jabaji et al., 2013). This model differs from classical organoid cultures by forming “open” conformational sheets with an exposed luminal surface. As this model is developed primarily for studying drug metabolism and not infection, here we adapt and characterize this model to assess the suitability for

infection studies by evaluating cellular diversity, polarisation and integrity of the epithelial sheet.

Two major epithelial cell types, Paneth cells and goblet cells, play important roles in supporting host immune defence against enteric pathogens. By confocal imaging, here we confirmed the presence of both Paneth and goblet cells within the collagen-supported epithelial sheets, which is supported by the detection of Paneth and goblet-associated proteins by label free mass spectrometry.

We demonstrate that several Paneth cell secretory antimicrobial peptides are detected within this epithelial model including α-defensins 2, 5, 20 and 24 by label free-mass spectrometry. Paneth cells play a major role in host defence and are characterised by large apical granules that occupy their cytoplasm. These long-lived cells are rich in secretory anti-microbial peptides which modulate the gut microbiota (Ayabe et al., 2000; Bevins and Salzman, 2011; Elphick and Mahida, 2005; Lisitsyn et al., 2012; Moal and Servin, 2006; van Es and Clevers, 2014). Importantly, intestinal defensins from Paneth cells confers resistance to enteric salmonellosis and *Shigella* infection (Fernandez et al., 2008; Salzman et al., 2003b). In addition to their role in immune defence, Paneth cells are important for the regulation of stem cell proliferation and Wnt signalling cascades in normal gut homeostasis which is important for epithelial cell turnover (Farin et al., 2012). *In vivo* Wnt signalling regulates the intestinal stem cell population by maintaining "stemness" and proliferative ability amongst these cells. Paneth cells provide essential signalling components such as Wnt3a and EGF to LGR5+ stem cells *in vitro*, and the removal of Paneth cells results in an ablation of the intestinal stem cell population (Toshiro Sato et al., 2011). For these reasons, the Paneth

cells play a major role in gut homeostasis and are an essential epithelial cell type required within an *in vitro* intestinal epithelial for self-regeneration.

Multiple mucus components and goblet cell markers were also detected via label free mass spectrometry within epithelial sheet cultures. In addition to intracellular MUC2 visualised by confocal imaging, we detected a variety of mucus components; alpha-enolase, anterior gradient protein 2 homolog, chloride intracellular channel protein 1, mucin-13 (MUC13) and zymogen granule membrane protein 16 (ZG16) (Bergstrom et al., 2014; Birchenough et al., 2015; Lenaerts et al., 2007; Moal and Servin, 2006; Park et al., 2009; Pelaseyed et al., 2014; Rodriguez-Pineiro et al., 2013; Roussa et al., 2010). Although multiple mucus components were detected here, within this thesis, the presence of a physical mucus layer has not yet been confirmed.

Due to the hydrated state of mucus, PFA fixing collapses the mucus and therefore does not preserve this feature of the model. The evaluation of the mucus barrier layer therefore requires examination through alternative means that do not involve this fixation method. We have identified two potential methods of evaluating this feature; either by exploiting fixation by Carnoy's fixation (reported to preserve mucus) or by two-photon imaging techniques (Coombes et al., 2013). Here, attempts to utilise Carnoy's fixation of epithelial sheets were unsuccessful, likely due to poor antibody compatibility with this method of preservation. Therefore for future characterisation, we suggest the development of an epithelial sheet model derived from the intestinal stem cells of fluorescent reporter mice such as ROSA$^{mT/mG}$ (The Jackson Laboratory, Maine, USA), overlaid with fluorescent beads to be live cell imaged. A similar technique has been previously exploited to demonstrate the presence of mucus on intestinal tissue explants by Coombes *et al.*, 2013.

The role of mucus for *Toxoplasma* invasion is currently unknown, however in related pathogens the mucus plays a significant role. In another apicomplexan *Cryptosporidium* spp, the parasite anchors onto the mucus layer to generate traction allowing it to penetrate host cells (Wilhelm and Yarovinsky, 2014; Yoshida et al., 2011). When the presence of a mucus layer is confirmed, live imaging techniques can be used to visualize *Toxoplasma* interaction with the mucus layer during early invasion events which may identify parasite behaviours that exploit the mucus layer in a similar manner to *Cryptosporidium* spp.

Several other important epithelial cell markers were also detected in our epithelial sheet model including enterocyte and microvilli markers; intestinal fatty-acid binding protein, villin-1, ezrin, plastin-1 and stem cell marker olfactomedin-4 (Coch and Leube, 2016; Grone et al., 1986; Hodin et al., 1997; Koo and Clevers, 2014; Saotome et al., 2004; Shinomiya, 2012; Yu et al., 2011). The detection of these markers within our cultures confirm the presence of a variety of differentiated epithelial cell types in culture that mimic the intestinal epithelium *in vivo.*

By confocal imaging, we have examined the distribution pattern of Paneth and goblet cells *in vitro.* Within four days of culture, organoid fragments formed epithelial sheets with uniform patterning throughout, however after 7 days incubation we observed some heterogeneity throughout the sheet. The central regions of the epithelial sheets were generally composed of smaller, and more tightly packed cells whereas the outer regions were composed of larger cells. Confocal analysis of these areas reveal clusters of Paneth cells distributed within the central regions only and goblet cell distributed sporadically throughout.

This observation is suggestive that the peripheral regions of the epithelial sheets are enterocyte like, and the inner regions of the sheet are crypt-like, which potentially mimics the intestinal patterning *in vivo*, where Paneth cells are clustered in the crypt domains, and goblet cells are distributed sporadically throughout the transit amplifying region and the villi. To support this observation, visualising the distribution of LGR5+ stem cells could confirm the localisation of proliferating stem cells in relation to Paneth cells within these central micro-domains. Due to a lack of validated commercial LGR5+ antibody, this objective was not achieved within this chapter and requires further examination. However the self-renewal of Matrigel® organoids, and the observable growth of sheets suggest that cell proliferation is functional.

Further to identifying the presence of differentiated epithelial cells, we quantified the populations of these cell types in the monolayer model and observed a lower proportion of Paneth and goblet cells when compared to Matrigel® grown 3D organoids. The 3D spatial arrangement and microenvironment is a unique feature of organoid cultures, and modification of this arrangement has evidently resulted in a diminished differentiated capacity. Recent work have demonstrated that the modification of static cell line cultures by the introduction of a microfluidic microenvironment can induce morphogenesis of 3D villus structures (Kim and Ingber, 2013). Adaptation of this epithelial monolayer model onto a microfluidic chamber may recover a proportion of differentiated cells lost through the removal of a 3D organoid structure without re-forming an enclosed luminal space. This however is not a requirement for the use of this model for basic science infection studies as the epithelium still retains differentiated cell types.

Having confirmed the presence of the Paneth and goblet cells *in vitro*, we also evaluated the epithelial polarisation of this model via confocal microscopy. The basolateral localisation of e-cadherin, and the apical enrichment of F-actin confirms the polarisation status of this epithelial sheet model. During early stage invasion, the expression of pathogen recognition proteins localized to either to apical or basal surfaces, such as TLRs, regulates the recognition of pathogens invading the epithelium, allowing the host to mount an appropriate immune response. Polarisation of the epithelium is therefore an important requirement of intestinal infection models.

In vivo, intercellular tight junctions maintain the separation of apical and basal domains, and also form a barrier to prevent excess transport of ions and molecules across the epithelium. The structural integrity of epithelial monolayers is maintained by the presence of these tight junctions, making this feature a desirable characteristic for intestinal infection models. Proteomic approaches were exploited to further examine the presence of absence of appropriate junctional proteins that make up the cell adhesion complexes; apical tight junctions, adherens junctions and desmosomes (Guttman and Finlay, 2009; Wells et al., 2014).

Tight junctions of the intestinal epithelium are multi-protein complexes composed of four integral transmembrane proteins; occludin, claudin, junctional adhesion molecule (JAM) and tricelluin that all interact with ZO proteins to form tight junctional structures (Lee, 2015; Mandell and Parkos, 2005). Within our samples, we detected JAM-A protein in one of our collagen epithelial biological replicates, ZO-1 also in one collagen epithelial replicate and ZO-2 in all collagen epithelial samples. However, none of these three tight junction proteins were detected in Matrigel® grown organoids, which will be discussed later.

Adherens junctions are involved with remodelling tight junctions during morphogenetic and wound healing processes, and are composed of cadherin adhesion receptors and cytoplasmic proteins (catenins). Two cadherin proteins were detected within epithelial sheets; e-cad (cadherin-1) and cadherin-17, in addition to two catenin proteins; catenin delta-1 and catenin alpha-1. E-cadherin is a major component of the epithelial adherens junction and removal of this protein in mice results in death within 24 hours of birth (Bondow et al., 2012). KO mice present with disrupted intestinal morphogenesis and the formation of abnormal adherens junctions leading to compromised intestinal barrier function (Bondow et al., 2012). Removal of e-cadherin also reduces the proportion of enterocytes within the small intestine, and increases the proportion of actively proliferating cells due to an inhibited level of nuclear activated β-catenin which as a result, alters Wnt signalling complexes. (Bondow et al., 2012). Thus e-cadherin is required for normal intestinal development.

Both catenin delta-1, (p120 catenin) and catenin alpha-1 that were readily detected in all epithelial samples are directly involved in intestinal homeostasis. Removal of p120 catenin in mice rapidly induces death within 21 days due to progressive mucosal erosion and intestinal bleeding (Smalley-Freed et al., 2010). Removal of p120 in immortalised cell lines generates low TEER monolayer cultures and amplifies immune cell engagement resulting in inflammation of the cells, thus this protein plays an essential role in barrier function and intestinal homeostasis (Smalley-Freed et al., 2010). P120 catenin binds and stabilises to cadherin proteins on the cell surface, and localises within the nucleus to activate transcription factors for gut homeostasis (Daugherty et al., 2014). A-catenin also attenuates transcription via inhibition of the Wnt signalling pathway, although it has been more thoroughly studied in the context of cellular junctions. A-catenin binds to filamentous actin to inhibit actin

polymerisation *in vitro* to modulate f-actin remodelling (Daugherty et al., 2014). Removal of α-catenin *in vitro* results in enhanced transcription thus demonstrating its role in the inhibition of the Wnt signalling pathway and gut homeostasis (Daugherty et al., 2014).

Hemidesmosome complexes facilitate adhesion of epithelial cells to basement membranes (Walko et al., 2015). Six hemidesmosome proteins were detected in collagen epithelial samples although not consistently; plectin, desmoglein-2, desmocollin, desmoplakin and two integrin subunits (α6 and β1) (Walko et al., 2015). (Walko et al., 2015). Integrin α6β4 and plectin form an essential component of the hemidesmosome complex to bind to extracellular laminin-332 and keratin intermediate filament network (Walko et al., 2015). Desmoplakin, has been shown to be essential for the formation of microvillus structures that compose the brush border of the intestinal epithelium and therefore its presence again indicates the correct homeostatic processes can be found within our model (Sumigray and Lechler, 2012).

In addition, we also examined the presence of relevant intestinal cytoskeletal proteins within our samples. Cytokeratin proteins are intermediate filament proteins located within the cytoskeleton of epithelial cells that generate networks of rigid but flexible junctions to retain the biological requirements of those cells; in the case of the intestine they regulate epithelial polarity (Herrmann et al., 2007). The expression of cytokeratins is anatomically specific and intermediate filaments are considered to play an important role in determining the development and growth of specific tissues and organs. These intermediate filaments anchor the components of the intestinal epithelium via hemidesmosome complexes (Herrmann et al., 2007; Walko et al., 2015). Murine intestinal epithelia express cytokeratins 7, 8, 18, 19 and 20 (Booth and

O'Shea, 2002; Gerbe et al., 2012; Helenius et al., 2016; Ku et al., 1999; Quinlan et al., 2006; Ren et al., 2011; Zhou et al., 2003), all of which were detected within both epithelial sheets and Matrigel®-grown organoids demonstrating tissue-specificity within this model. Furthermore, two other proteins of interest were detected; integrin β1 involved in maintaining cell polarisation (Beaulieu, 1992; Lee and Streuli, 2014; Yu et al., 2005) and intestinal-type alkaline phosphatase, a brush border enzyme which regulates intestinal homeostasis (Goldberg et al., 2008; Lallès, 2010).

Together, with confocal and proteomic data we demonstrate the presence of the appropriate junction complex proteins and structural proteins within the epithelial model. Although the presence of these proteins alone does not constitute the presence of tight junctional complexes, tight junctions mark the boundary of apical and basolateral membrane domains and thus regulate epithelial polarisation. As polarisation has been demonstrated in this model by confocal imaging, we can presume that some tight junctions must also exist to maintain this segregation of domains. Attempts were made to confirm ZO-1 distribution throughout the epithelial sheet, however due to technical issues with the antibody purchased this was not successful. Due to time constraints, it was not possible to examine the distribution of other tight junction proteins, such as JAMs, occludens and claudins, although this was considered. Further examination of this feature would be preferential to confirm the presence of appropriate tight junction complexes and the regulation of epithelial molecule transport.

The significance of developing this culture technique to generate differentiated and polarised epithelial sheets is hugely important for the study of zoonotic enteric pathogens, for which there are limited *in vitro* models. Only recently have we seen the

establishment of farm and companion animal organoid cultures of veterinary relevance which are still subject to restricted luminal access (Powell and Behnke, 2017) and our own unpublished data (manuscript in prep).

To demonstrate the validity of this culture technique for the development of epithelial sheets infection models, we also performed pilot studies to provide evidence of bovine epithelial sheet growth from bovine organoids. Here we generated a similar model to the murine epithelial sheet by culturing organoid fragments on rat tail collagen for 7 days. However, due to the poor availability of commercial bovine intestinal epithelial antibodies, this model has not yet been fully characterised at this time. Other characterisation methods such as qPCR could be used here to compare the expression of differentiated cell markers in these cultures to bypass a lack of validated bovine antibodies for imaging purposes. The findings here highlight two major characteristics of the epithelial sheet to support its use for infection studies, and demonstrate that this culture technique can be utilised in other mammalian species. However, several limitations of this model must also be considered.

Due to the small volume of biological material of both organoids and epithelial sheets, the use of mass spectrometry highlighted several discrepancies within the proteome data. We observed an absence of several marker proteins in Matrigel® organoids which were present in collagen-supported epithelial sheets; alpha-defensin 5, integrin alpha-6, integrin beta-4, plectin and zonula-occludens protein 2 (ZO-2). Zonula-occludens proteins and other tight junctional proteins were detected within 3D organoids previously (data not shown), which suggests that the sensitivity of mass spectrometry was not compatible with the size of these samples.

We also observed variation in the number of detectable proteins and the robustness of detection of specific cell markers across biological replicates. In contrast to studies of cell biology in immortalised cell line models which are easy to culture uniformly, the smaller scale of collagen epithelial sheet models makes obtaining large volumes of biological material difficult. This is complicated by difficulties with standardising seeding density of organoid fragments onto collagen gels. Matrigel®-grown 3D organoid cultures contain varying numbers of intestinal stem cells in each organoid. When fragmented, these produce aggregations of differing sizes which are then plated onto collagen gels making uneven sized starting cultures. As proliferation of the epithelial sheet is determined by number of stem cells present within each organoid fragment plated onto collagen, smaller fragments are likely to generate smaller epithelial sheets.

This natural variation within organoid cultures may account for some variability between protein returns of samples examined by mass spectrometry as several proteins were detected in some but not all replicates of either epithelial or 3D cultures including; alpha-defensin 2, alpha-defensin-24, mucin-2 fragments, mucin-13 and secretogranin-1. The sample size of these collagen sheets is therefore an important consideration for future work as detection of small protein changes are likely to be missed or not represented if the depth of analysis is shallow. For these reasons, future proteomic work involving epithelial sheets or organoid models should aim to increase the amount of biological material processed to maximise data gain.

To conclude, here we have established a modified culture technique to generate a collagen-supported epithelial sheet model. Using confocal microscopy and proteomic approaches, we have characterised this model for Paneth and goblet cell features

including the presence of anti-microbial peptide and mucus components. We have also demonstrated the validity of this culture technique by generating an equivalent bovine model. This provides supporting evidence of the use of these models for the generation of *in vitro* animal models for infection.

Chapter 5 – Optimisation of the Collagen-Supported Epithelial Sheet Model to Study Host Response to *Toxoplasma gondii* Infections

5.1 Introduction

Initial interactions between *Toxoplasma gondii* and host epithelial cells during early stage invasion are not well understood. The identification of *Toxoplasma* effector proteins has identified the mechanism of parasite internalization, however the host molecules involved in this process and mechanisms of epithelial transmigration have not been identified. Furthermore the host epithelial response to infection is poorly characterised.

Enteric apicomplexa cause diseases globally in a wide host range including humans, companion animals and farm animals. Generally, these infections are acute and self-limiting, however can become fatal if acquired by immunosuppressed patients. One of the most successful pathogens of economic importance is *T. gondii*. This parasite can infect virtually all mammalian cells and is thought to infect approximately 20% of the UK and US population, and between 50-80% in the Central and South American human population (Hill and Dubey, 2002; McAuley, 2014; NHS, 2015).

Progress in this field has been limited by a lack of suitable models for the study of early invasion host-pathogen interactions. Using the novel collagen-supported epithelial cell model developed in Chapter 4, we optimize a protocol to establish infection. Using this method, we performed infection studies to examine changes in the host-proteome in response to virulent type I and avirulent type III *Toxoplasma* strains during parasite invasion and replication with a view to identify targets for the development of novel therapeutics.

The majority of infections are asymptomatic or cause only mild flu-like symptoms, however if an infected person becomes immunosuppressed they may experience reactivation of latent infection leading to neurological or ocular disorders, and death (Carruthers and Suzuki, 2007; Hill and Dubey, 2002). Infection of hosts during pregnancy has devastating consequences, including spontaneous abortions in sheep, or congenital toxoplasmosis in humans resulting in developmental delay, microcephaly, seizures or late onset chorioretinitis (Gilbert et al., 2006; Kravetz and Federman, 2005). For these reasons, understanding the interactions during early stage invasion will help us to identify methods of disease prevention.

European and North American strains of *Toxoplasma* are defined as three clonal lineages; type I, type II and type III. Type I strains exhibit higher virulence in mice, have a long distance migration (LDM) phenotype *in vitro*, and transmigrate across the intestinal epithelial barrier more readily than type II or III strains (Fuentes et al., 2001; Howe et al., 1995; Saeij et al., 2005). Traditionally, type II strains are less virulent, and have been associated with human infections and the development of congenital infections in Europe and North America, whereas type III strains are typically associated with infections in animals (Carneiro et al., 2013; Fuentes et al., 2001; Howe et al., 1995). However, more recently, atypical strains have been described that do not conform to these rules. The mechanisms that determine pathogenesis of *Toxoplasma* are unclear, and the comparative study of virulent and avirulent strains may identify key determinants of pathogenesis.

To date, the invasion mechanisms of *Toxoplasma* have been studied both *in vitro* and *in vivo.* Several parasite effector proteins have been identified such as GPI-anchored surface antigens (SAGs), micronemal proteins (MICs) and rhoptry proteins (ROPs)

that interact with the host cell sequentially to regulate attachment and invasion (Grimwood *et al.,* 1996; Grimwood & Smith, 1996; Mineo *et al.,* 1993). However, the host-cell counterpart of many of these interactions is still unidentified. Furthermore, the mechanism by which *Toxoplasma* transmigrates across the intestinal epithelium is still not fully understood.

Generally the host intestinal epithelial response to infection is not well understood, although some features have been described. During early stage invasion, *Toxoplasma* parasites are reported to disrupt host tight junction proteins and exploit a paracellular route of migration across the intestinal epithelium (Barragan et al., 2005; Weight and Carding, 2012). However, much of this data comes from *in vitro* cell line assays, and parasites can be observed residing within epithelial cells *in vivo.* While production of cytokines and chemokines has been studies in intestinal epithelial cells following infection, we still understand very little about how the host protects itself from invasion, and how the parasite can modulate the host epithelial response for its own benefit.

Although *T. gondii* infections have been well studied using both murine *in vivo* and *in vitro* models, both methods have their limitations which has hindered our progress. *In vitro* models often rear simplistic results due to a lack of cell variation and thus a lack of complex host-pathogen physiology, and *in vivo* models pose technical challenges with maintaining the integrity of small intestinal tissues for procedures such as live cell imaging. Furthermore, due to the poor reproducibility and technical challenge of administering oral infections *in vivo*, often these invasions are established via intraperitoneal injections which do not mimic the natural route of infection.

Using our novel collagen-supported epithelial model, we will evaluate the use of label-free mass spectrometry to study *Toxoplasma* within the epithelial sheet model during early and late stage infection.

5.2 Materials and Methods

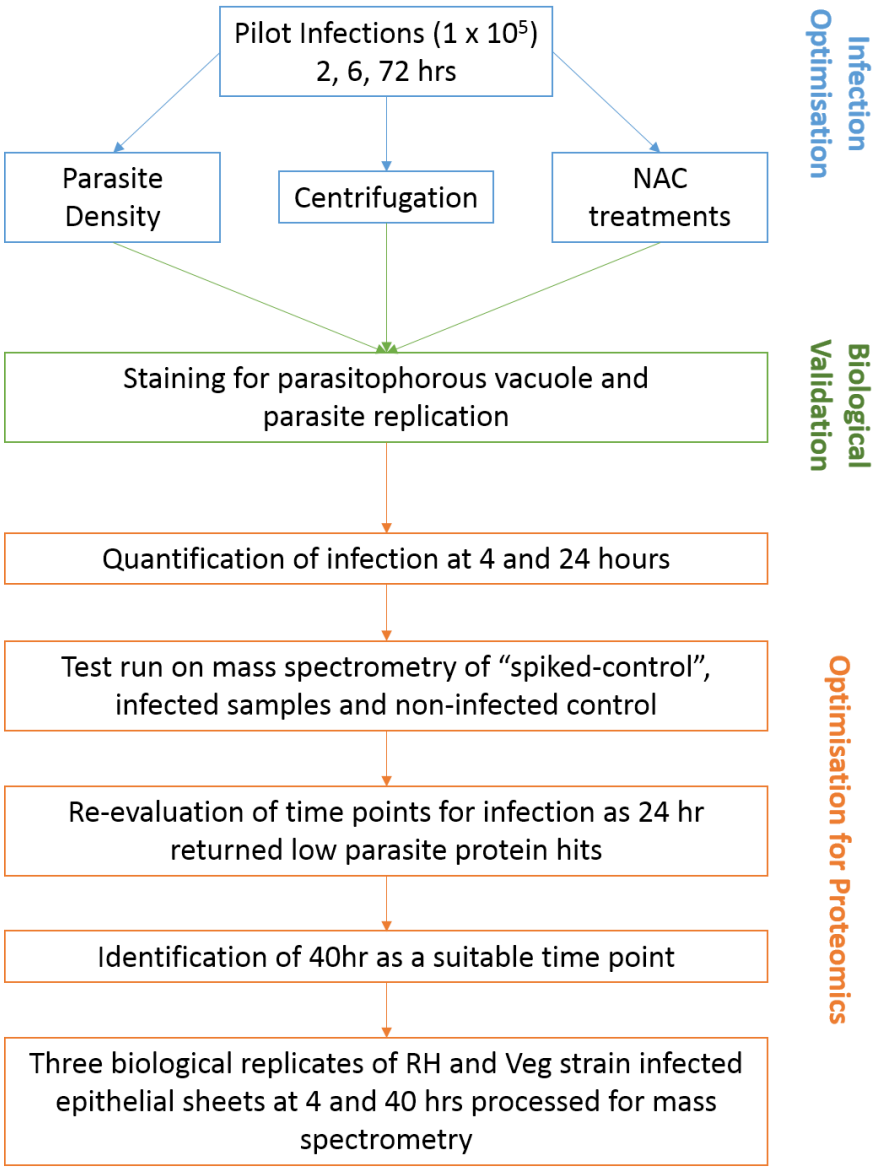

Figure 32) Workflow schematic outlining the optimisation of infection studies for quantitative label-free mass spectrometry

5.2.1 Collagen-Supported Epithelial Sheet Culture

Murine collagen-supported epithelial sheets were generated on rat tail collagen gels as described in Chapter 2. Day 7 Matrigel® grown organoid fragments were overlaid onto polymerised 2mg/mL rat tail collagen gels and allowed to adhere for 15 min at 37^{o}C and 5% CO_2. Complete organoid media was overlaid onto organoid fragments and cultured for 7 days, with complete media changed on day 4.

5.2.2 Culture of *Toxoplasma gondii* Parasites on Vero Cells

Both Type I RH and Type III Veg strains of *T. gondii* were cultured and maintained in Vero cell cultures as described in Chapter 2.3. *T. gondii* culture supernatant containing tachyzoites was used to passage stocks, and parasites were purified from Vero cells for infections using PD-10 desalting columns as described in Chapter 2.3.3.

For proteomics test run to determine the usefulness of including a "parasite-spiked" control, *Toxoplasma* were purified as above and pelleted by centrifugation. Parasites were de-activated by freezing at -20^{o}C for a minimum of 24 hours.

5.5.3. Infection of Epithelial Sheets with *Toxoplasma gondii* parasites

Epithelial sheets were infected as described in Chapter 2.4. Media was removed from day 7 epithelial sheets, and replaced with media containing parasites. Cultures were fixed at multiple time points with 4% paraformaldehyde (in PBS) for 60 min at room temperature, washed thrice in PBS and stored in PBS at 4^{o}C until staining.

To assess the potential role of mucus during the initial stages of infection, the effect of a pre-treatment with a mucolytic N-Acetyl L-Cysteine (NAC) (Sigma Aldrich) was assessed. At day 7, media was replaced with organoid media containing 0mM, 2mM,

5mM or 10mM NAC, and sheets were incubated for 60 minutes. NAC media was removed after incubation and replaced with complete media containing *T. gondii* tachyzoites. Samples were fixed for confocal imaging.

For optimisation of infection protocols, the effect of an additional centrifugation step following exposure to parasites was assessed. Infected epithelial sheets were either not centrifuged, or centrifuged at 100*xg* for 1 min prior to incubation. Cultures were fixed and stained for confocal imaging.

5.5.4. Antibody Staining and Confocal Imaging

Infected samples were stained and visualised by confocal imaging as described in Chapter 2.5. Epithelial sheets were stained with F-actin conjugated to Alexa Fluor 647 or rhodamine (Molecular Probes), DAPI and a mouse monoclonal *Toxoplasma gondii* antibody to SAG-1 (TP3, Abcam), and donkey anti-mouse Alexa Fluor 488 secondary.

Confocal images were acquired using Zen Black software on a Zeiss LSM880 upright confocal microscope using laser lines Diode (405), Argon (488), DPSS-5610 (561) and HeNe633 (633) and water immersion W-Plan Apochromat 40x/1.0 Dic objective or Plan-Apochromat 63x/1.0 oil DIC M27 (oil immersion) objective (all Zeiss) lens.

5.5.5. Quantification of Infection

Image analysis was performed in Imaris x64 v8.0.1 software as described in Chapter 2.6. The Imaris "spots" function was used to quantify the number of cells and parasites within any given sample. The Imaris "surface" function was used to mask intracellular parasites, and give an estimated number of intracellularly invaded parasites. Automation of these counts were manually checked and edited to increase the accuracy

of quantification. A minimum of three fields of view were used to quantify invasion by *T. gondii* for all experiments.

Quantification of images determined the rate of invasion at 24 hour, which we used to perform a test proteomic run with infected sheets, sheets spiked with deactivated parasites, and non-infected control.

5.5.6. Extracellular Parasite Removal and Collagenase Treatment for Proteomics

To minimise non-invading parasite proteins in infected samples, here a centrifugation step was evaluated for the proteomic sample preparation process. This optimisation was performed on 3D organoids as these were readily available.

Day 7 organoids were removed from Matrigel® by centrifugation, and re-suspended in PBS. Purified parasites were added at a density of 2 x 10^5 per sample and incubated with organoids for 60 min. Samples were spun at either 50*xg* or 25*xg* for either 3 or 1 min. A 10µL aliquot of the centrifuged supernatant, and cell pellet were taken for light microscopy where a parasite count was taken to determine the efficacy of centrifugation as a method of extracellular parasite removal (**Figure 29 A and B**). Parasite quantification in loose pellets and supernatant identified that 50*xg* and 25*xg* for 3 min removed 73% and 77% of parasites respectively (**Figure 29 B**).

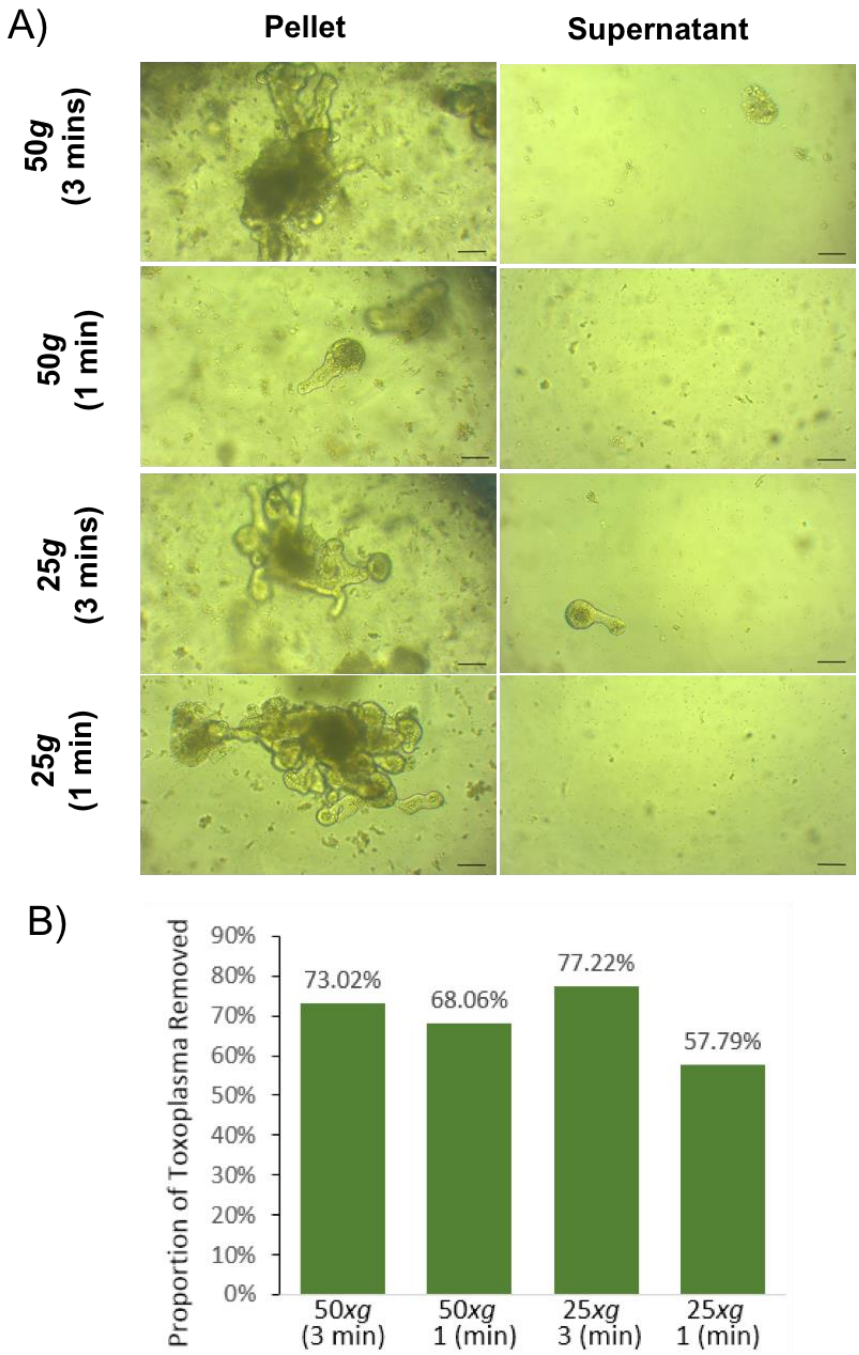

Figure 33) Removal of extracellular Toxoplasma gondii from 3D organoids can be achieved through centrifugation.

Organoid cultures were concentrated in four different conditions to remove *Toxoplasma* tachyzoites after incubating together for 1 hour. (A) Light microscopy images of cell pellets containing large organoid structures in centrifuged pellets, and parasites in supernatant. (B) Parasite count of supernatant and pellets determined the proportion of parasites removed through centrifugation at various speeds and time. This data is representative of a pilot experiment. Scale bars = 100µm.

Under these conditions, the removal of parasites was comparable. However due to the presence of organoid fragments in the supernatant of samples spun at 25*xg* for 3 min (**Figure 33 A**), this poses a risk of losing host cell material. For this reason, subsequent removal of parasites in samples for proteomics was performed via centrifugation at 50*xg* for 3 min to minimise the risk of losing biological material.

This spin out centrifugation was performed on infected epithelial sheets after collagenase treatment as described in Chapter 2.7.2. Isolated epithelial sheets were washed thrice with PBS and stored as a pellet for mass spectrometry peptide digest.

For the proteomics test run, de-activated toxoplasma were added to an uninfected epithelial sheet as a "parasite spiked" control. For this test run, single replicates of each were prepared. For the main host-pathogen interaction experiment, three biological replicates of day 7 *T. gondii* infected epithelial sheets were prepared

5.5.7 Peptide Digest and NanoLC MS ESI MS/MS Analysis

Sample peptide digest was performed as described in Chapter 2.7. Peptide mixtures (2µl) were analyzed by on-line nanoflow liquid chromatography by Dr Stuart Armstrong as described in Chapter 2.8. Raw data files were processed in Progenesis LC-MS (Version 4.1, Nonlinear Dynamics) as described in Chapter 2.8.

5.3 Results

Here we utilise the collagen-supported epithelial sheet model developed in Chapter 4 in a series of pilot infections to examine its biological capabilities to support protozoan parasite invasion and growth. Using confocal imaging and proteomic approaches, an infection protocol is optimised specifically for proteomic studies. Here this model is exploited to compare parasite-induced host protein response to *Toxoplasma gondii* RH

or Veg strain invasion and replication, against non-infected controls, with a view to identify targets for the development of novel therapeutics.

5.3.1 Collagen-Supported Epithelial Sheets are Susceptible to *T. gondii* Invasion and Parasite Replication

As the main objective of this thesis is to generate a novel model for the study of enteric pathogens, here we obtained evidence to support the use of our collagen-supported epithelial sheet model for infection studies by demonstrating susceptibility to invasion, and physiological compatibility with *T. gondii* replication.

We firstly evaluated the susceptibility of epithelial sheets to pathogen-invasion by applying *T. gondii* onto the apical surface of the epithelial sheet. However, due to the novelty of this model, the infectious dose for optimal invasion was unknown. The infectious dose chosen here was based on previous cell line infection studies performed by Mariwan Al-Bajalan (Al-Bajalan et al., 2017). During his doctoral studies, Mariwan infected 3-day post seeding HFF cells grown in T75 flasks with an infectious dose of 1×10^7 tachyzoites. As the collagen-supported epithelial model is cultured in 48-well plates with a $0.95cm^2$ surface area, the infectious dose was scaled down to represent a similar host-to-parasite cell ratio as closely as possible. We therefore applied 1×10^5 tachyzoites per well for the first pilot infection to determine whether the model was susceptible to invasion and parasite replication at 2, 6 and 72 hours infection.

Preliminary results show that collagen-grown epithelial sheets are susceptible to invasion as early as 2 hours post infection (p.i) (**Figure 34**).

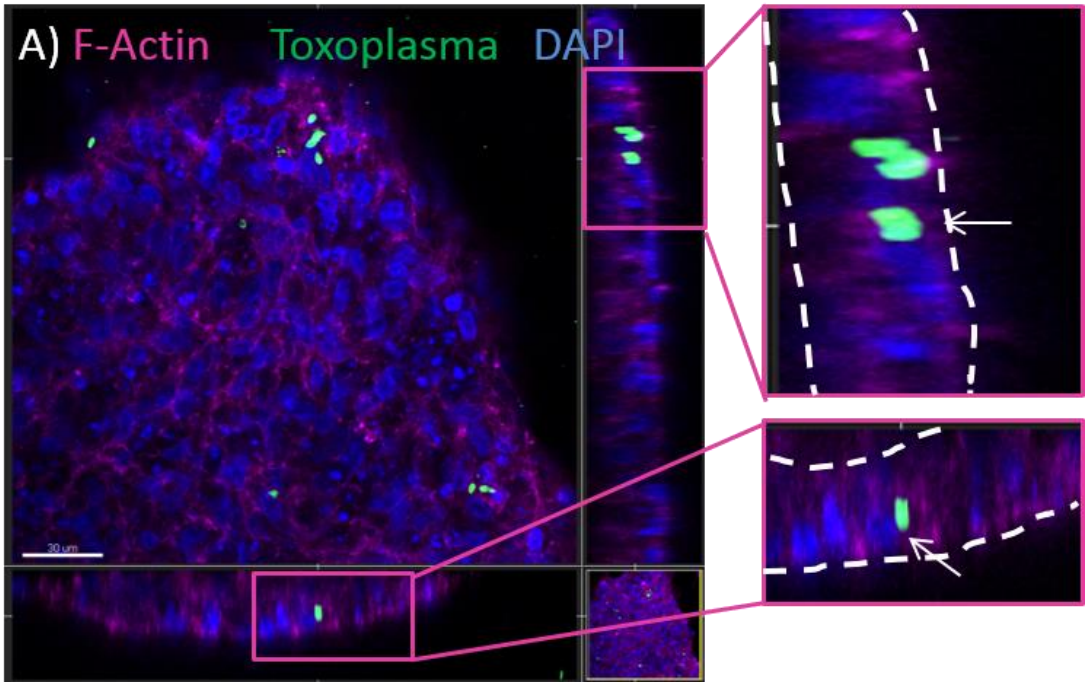

Figure 34) Collagen-supported epithelial sheets are susceptible to Toxoplasma gondii infection as early as 2 hours p.i

Collagen-supported epithelial sheets were infected for 2 hours with 1 x 10^5 *T. gondii* RH, fixed and processed or confocal microscopy. *Toxoplasma* were visualised by detection of AF488 fluorescence and parasite SAG-1 staining (green). Successful invasion was determined using Imaris (BitPlane) software. Images were analysed transversally to determine whether parasites were internalised based on F-actin staining (purple). Invasion was observed at 2 hours, as *T. gondii* parasites were embedded within the apical and basal surfaces of the epithelium as indicated by the arrows. Scale bars = 30µm.

Infection was determined using Imaris software using the "orthoslice" function to view the epithelium transversally. Parasites were deemed to be intracellular based on localisation between the basal and apical surfaces of the sheet, as defined by F-actin staining (dashed lines **Figure 34**).

T. gondii replicate within a PV formed upon successful invasion of host cells (Jacobs et al., 1998). To confirm successful invasion of the epithelial sheets by *T. gondii*, we stained for the *Toxoplasma* dense granule protein 7 (GRA7), which is secreted into PVs. The presence of GRA7 staining around individual tachyzoites confirmed the establishment of a PV following successful host cell invasion **(Figure 35)**.

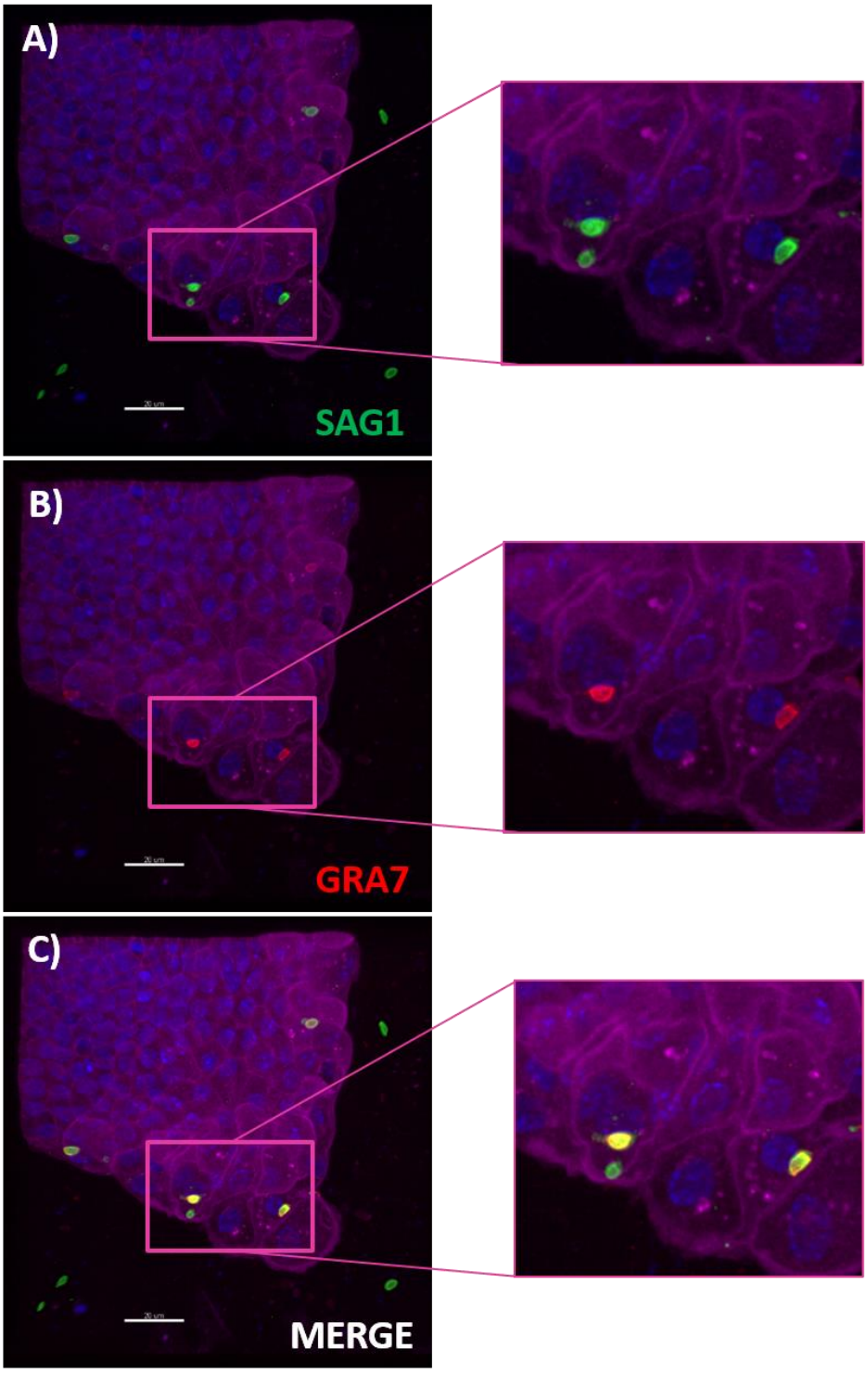

Figure 35) Toxoplasma dense granule (GRA7) is detectable on intracellular parasites at 4 hours p.i

Epithelial sheets were infected for 4 hours with 1 x 10^6 *T. gondii* RH, fixed and processed for confocal microscopy. (A) SAG1 staining (green) identifies both intracellular and extracellular parasites within the field of view, whereas (B) GRA7 (red) identifies intracellular parasites that have formed a parasitophorous vacuole at 4 hours p.i. Scale bars = 20µm.

At 6 and 72 hours following infection with $1x10^5$ parasites, we observed no signs of active replication (data not shown). However infection levels were in general very low. We therefore increased the infectious dose to 1×10^6 tachyzoites per well, and looked for evidence of parasite replication at 4 and 24 hours post infection. *In vitro, Toxoplasma* replication has been reported to occur as early as 4 hours post infection (Bommer, 1969). However, in our model, after 4 hours of incubation with *Toxoplasma* tachyzoites, parasite replication was not observed.

Nevertheless, when the incubation time was increased to 24 hours in subsequent experiments, we were able to observe the formation of rosettes characteristic of parasite replication (**Figure 36).**

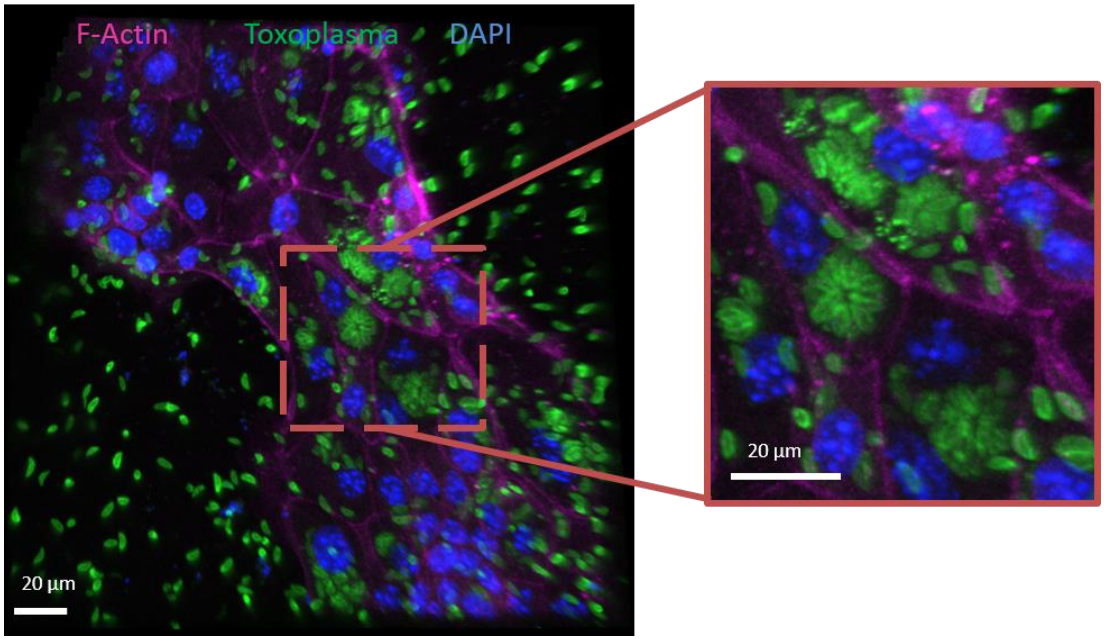

Figure 36) Collagen-supported epithelial sheets are capable of supporting parasite replication.

Collagen-supported epithelial sheets were infected for 24 hours with 1×10^6 *T. gondii* RH, fixed and processed for confocal microscopy by detecting parasite SAG1 via AF488 fluorescence. After 24 hours incubation with *T. gondii* tachyzoites, parasite replication was observed as denoted by the formation of intracellular rosettes. Scale bars = 20µm.

These results provide evidence to support the use of this novel model for the study of host-pathogen interactions as a) it is susceptible to infection, and b) can physiologically support pathogen growth and replication.

5.3.2 Increased Infectious Dose Increases Proportion of Invaded Cells at Early Time Points

To achieve the final objective of utilising the collagen-grown epithelial sheet model to study the host response to infection, we next performed a series of optimisation steps to maximise infection levels in our cultures, while minimising destruction of the monolayer.

Based on the findings of the pilot infections, it appeared that the initial infectious dose of parasites determined whether robust parasite replication was observed, irrespective of the duration of infection. Therefore, we evaluated three infectious doses to determine the optimal parasite density to determine the highest infection index achievable without inducing host cell damage during early invasion events.

Using Imaris image analysis software, the infections performed here were quantified as described in Chapter 2 to examine the proportion of host cells invaded, which will be referred to as the infection index. Unsurprisingly, increasing the infectious dose of parasites increases the infection index of collagen-supported epithelial sheets after 2 hours infection (**Figure 37**). The lowest infection index observed was at 2.2% in samples infected with 1×10^6 tachyzoites, which increases to 3.96% when doubling the infectious dose to 2×10^6 tachyzoites (**Figure 37**). At the highest infectious dose of 5×10^6 tachyzoites, an infection index of 5.47% was observed (**Figure 37**).

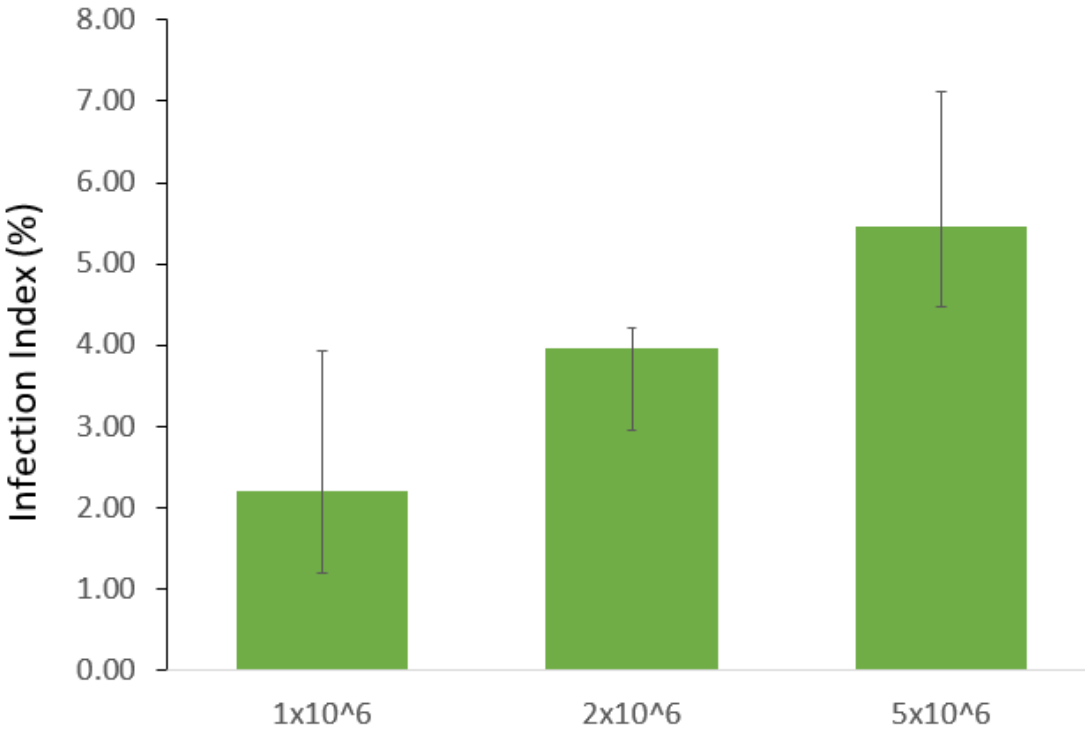

Figure 37) Increased infectious dose increases the proportion of cells invaded after 2 hours incubation

Epithelial sheets were infected for 2 hours with *T. gondii* RH, fixed and processed for confocal microscopy. Sheets were infected with either using 1 x 10^6, 2 x 10^6 or 5 x 10^6 *T. gondii* tachyzoites per well. Increasing parasite density increases the number of host cells infected after 2 hours of incubation with *T. gondii* RH. Bars represent standard error. The data presented here is representative of a single pilot experiment, with three confocal images quantified per density.

It should be noted here that the surface area coverage of collagen gels by the epithelial cells was variable between wells making it technically challenging to standardise MOI. To address this, we evaluated the relationship between the proportion of collagen gel covered by host cells, and the infection index observed. However, we found no relationship between the proportion of gel covered with epithelial sheet, and the eventual infection index, suggesting that the data does not need to be normalised to account for variation in gel coverage (**Figure 38**).

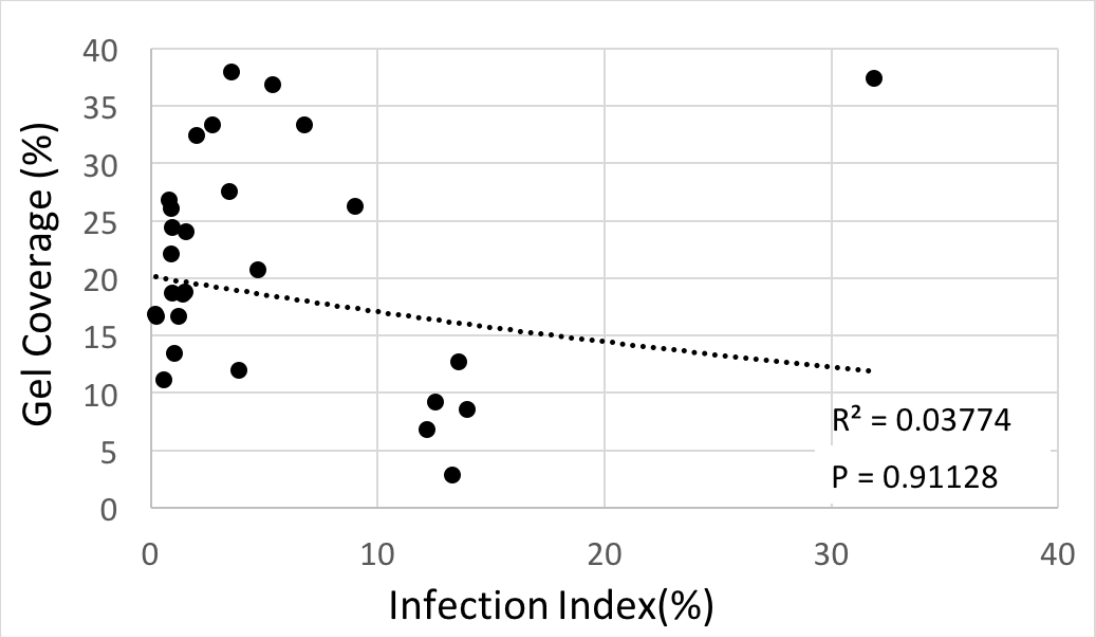

Figure 38) The surface area of epithelial sheets does not affect infection indices

Light microscopy images of infected gels were measured for surface area and percentage coverage of the collagen gel using ImageJ. The proportion of gel covered by the epithelial sheet does not affect the infection index as an outcome as determined by exponential regression analysis. Exponential regression analysis demonstrates a weak correlation between the percentage of collagen gel that the epithelial sheet occupies and the subsequent infection index ($R^2 = 0.03774$), however this finding is not statistically significant ($p = 0.91128$)

These findings suggest that a higher proportion of host cell infection can be achieved by increasing parasite density to $5x10^6$ tachyzoites per well. However epithelial sheets exposed to a high infectious dose appear to exhibit some signs of distress. In non-infected control samples, the epithelial F-actin appears robust with clearly defined intercellular and cell surface staining which is also observed at the lowest infectious dose of 1×10^6 tachyzoites per well (**Figure 39 A and B**).

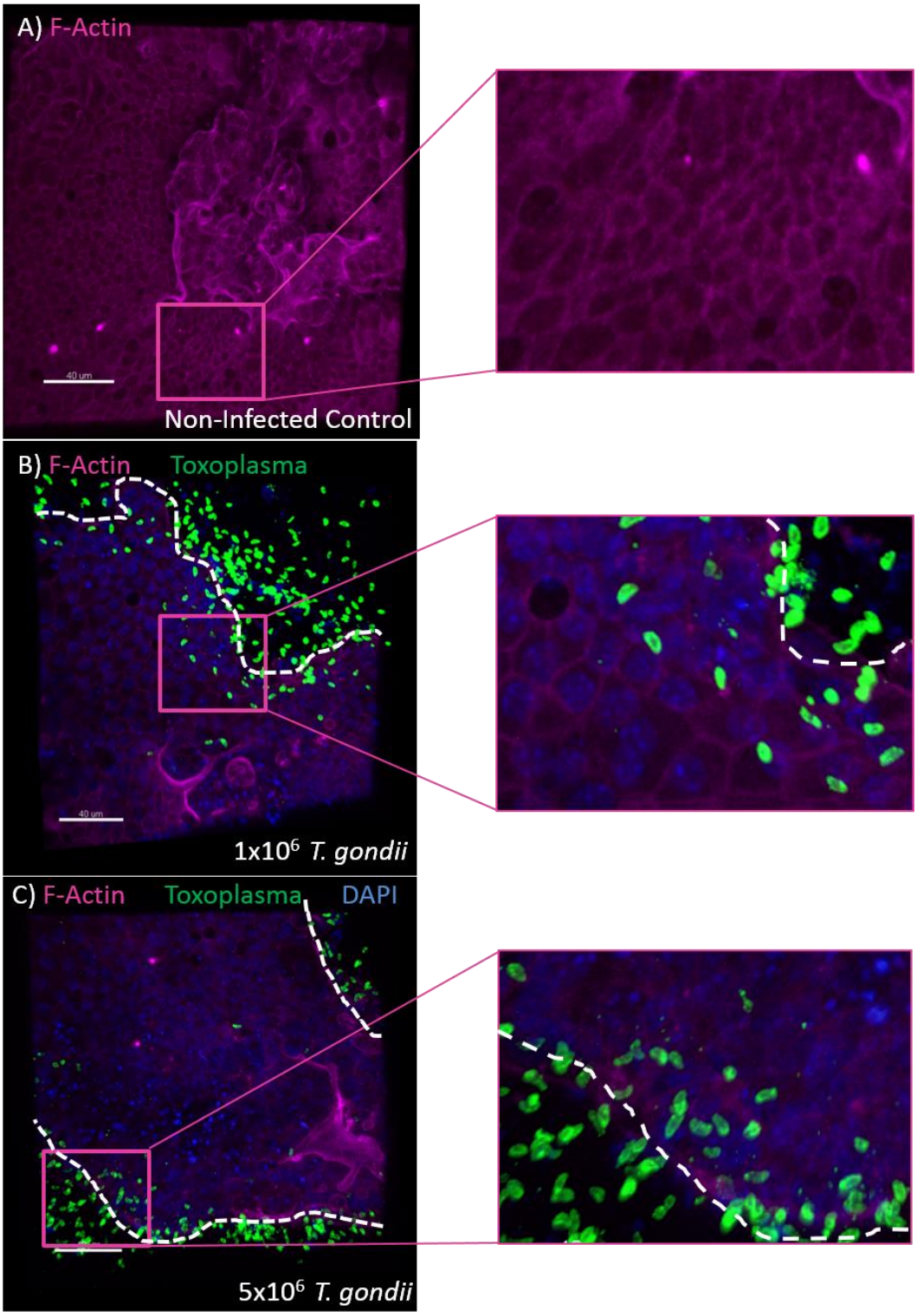

Figure 39) Increasing infectious dose disrupts epithelial integrity after 2 hours incubation

(A) Non-infected collagen-supported epithelial sheets show robust epithelial integrity, which is also reflected in (B) 1 x 10^6 tachyzoite infected sheets. (C) At a higher infectious dose of 5 x 10^6 tachyzoites, the epithelial sheet shows some visual signs of integrity loss. White dashed lines indicate perimeter of epithelial sheet. Scale bars = 40µm.

However at the highest infectious dose, the epithelial regions exposed to tachyzoites exhibits disrupted F-actin staining suggesting loss of integrity (**Figure 39 C**). Moreover, there is evidence of excess epithelial sloughing when compared to the morphology of the model at a lower infectious dose (**Figure 39 B and C**).

As the overall purpose of generating the collagen-supported epithelial model is to study host-pathogen interactions, it is crucial to generate high rates of host cell infection. For future infections, we hope to evaluate host-pathogen interactions during early invasion and during replication which we know takes place at around 24 hours. With these parameters in mind, although the highest infection index was observed by incubating collagen-supported epithelial sheets for 2 hours with 5 x 10^6 tachyzoites, the epithelial damage associated with this infectious dose makes it unsuitable for use in the future.

Although the lowest infectious dose resulting in the lowest rate of infection, the difference was not significant. The collagen-supported epithelial sheet also appears be have maintained epithelial integrity at the lower dose which will allow it to support replication during longer durations of infection. For this reason, we determined that 1 x 10^6 tachyzoites per well was a suitable infectious dose for future experimental work.

5.3.3. Parasite Aggregation Along The Epithelial Sheet Perimeter

While determining the optimal infectious dose, we noticed that large numbers of parasites aggregated along the epithelial sheet perimeter and uncovered surfaces of the collagen gel at 2 hours post infection (**Figure 39 B and C**). As the tachyzoites are applied directly to the collagen-supported epithelial sheet, it was assumed that parasites would be fairly uniformly distributed across the sample, even if they did not subsequently successfully invade the epithelial sheet.

Given that *T. gondii* can migrate across host cell surfaces using gliding motility, several non-exclusive explanations for this phenomenon were considered:

(1) While parasites may initially have settled evenly in the wells, impaired migration on collagen compared to on the epithelial surface may result in the observed distribution over time.
(2) Tachyzoites preferentially invade epithelial sheets at the perimeter, and are attracted to, or receive a "stop" signal, in these regions.
(3) The presence of a functional mucus layer is inhibiting parasite access to host cells.

In order to optimise infection of the epithelial sheets, we set out to address which of these scenarios might be operating, and whether we could create a more uniform distribution of parasites across the well.

5.3.4 The Perimeter-To-Surface Area Ratio Does Not Affect Infection Index

We next determined if tachyzoites might preferentially invade epithelial sheets at the perimeter. If this were true, we hypothesised that wells with higher perimeter to surface area ratios (i.e. those containing several smaller epithelial sheets), would show a greater proportion of invaded cells.

To evaluate this, light microscope images of infected collagen gels were acquired using GXCAM-Eclipse Camera (GT Vision, UK) and UCam Plus software. Light microscope images were analysed using ImageJ (NIH, USA) to generate measurements for length of perimeter and surface area of epithelial sheets on collagen gels. These measurements were used to generate an index of the perimeter-to-surface area, which was correlated with infection indices to evaluate the relationship between

the two measures. However, we found no relationship between the perimeter index and the eventual infection index, suggesting that the perimeter does not play a significant role in determining successful invasion, and is not the reason for the observed distribution in our cultures (**Figure 40**).

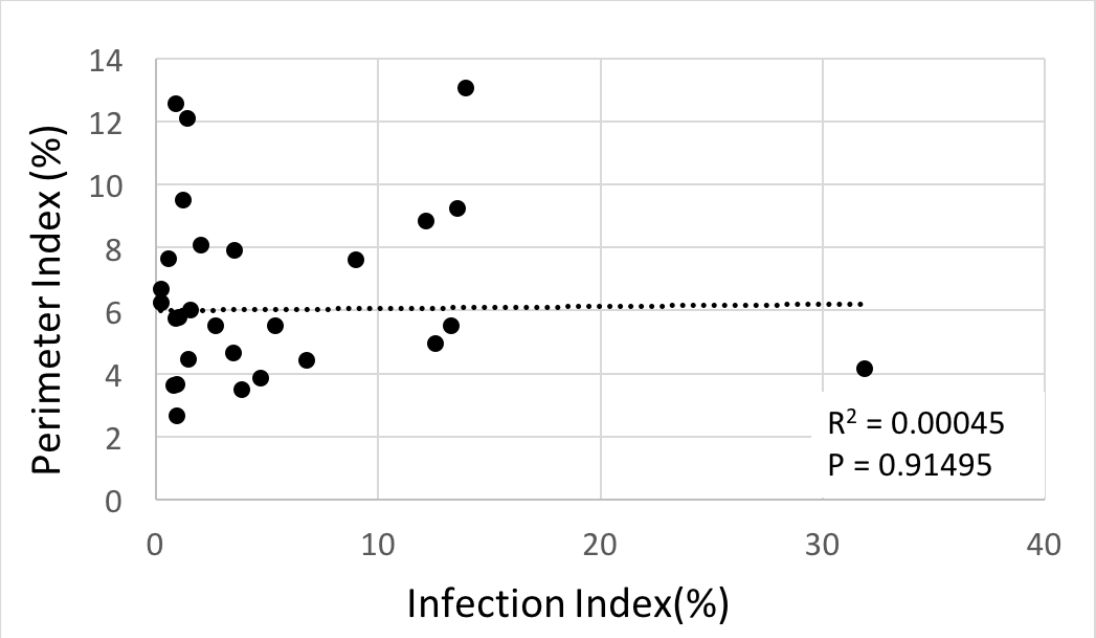

Figure 40) The perimeter index does not affect the infection index

Light microscopy images of infected gels were measured for epithelial sheet perimeter length using ImageJ. The perimeter-to-surface area index of epithelial sheets does not affect the infection index as an outcome as determined by linear regression analysis. Linear regression analysis demonstrates no correlation between the percentage of collagen gel that the epithelial sheet occupies and the subsequent infection index ($R^2 = 0.00045$) which was not statistically significant ($p = 0.91495$).

5.3.5 N-Acetyl L-Cysteine Treatment Does Not Increase Parasite Association to Host Cells

Having evaluated both the perimeter length-to-surface area ratio, and the distribution of parasites during early invasion, here we aim to address the role of a mucus barrier layer during early invasion.

Currently, the role of mucus in *Toxoplasma* invasion is unknown, and the presence of an intact mucus layer within this model has not been investigated. Here, we evaluate the use of a mucolytic compound, N-acetyl L-cysteine (NAC) to break down the mucus component, and assess the changes to parasite association with host cells.

Collagen-supported epithelial sheets were pre-treated with 0mM, 2mM, 5mM or 10mM NAC for 60 min prior to infection for a further 2 hours. Here we hypothesised that the addition of NAC will increase the parasite to host cell contact, which will be evaluated by calculating the infection index and the number of parasites associated with the epithelial sheet.

On first impressions, there were no visual changes to the distribution of tachyzoites after incorporating NAC pre-treatments prior to infections and parasites were still predominantly found at the perimeter of epithelial sheets (**Figure 41**).

Generally, the infection index was higher in non-NAC treated samples at 16.72%, except samples treated with 2mM NAC which resulted in an infection index of 24.42% (**Figure 42 A**). We also calculated the density of parasites associated with the epithelial sheet to account for parasites that may be in contact with the epithelial sheet, but had not yet invaded. Here a similar trend was observed – the association of parasites within the epithelial sheet was slightly increased following incubation with 2mM NAC, but reduced following incubation with 5mM or 10mM NAC (**Figure 42 B**).

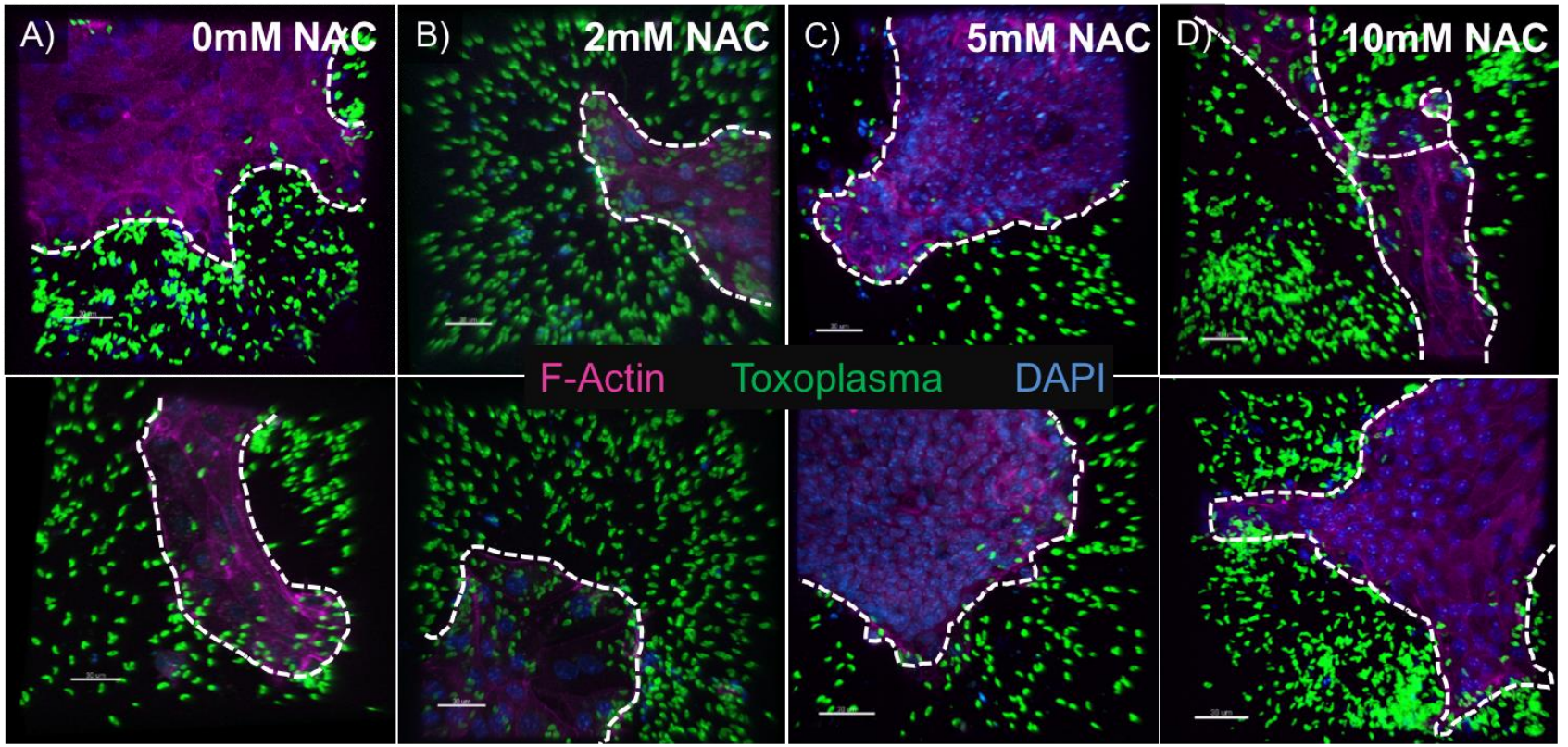

Figure 41) NAC pre-treatment does not alter the distribution of parasites across monolayer cultures after 2 hours incubation.

Epithelial sheets were pre-treated with 0mM, 2mmM, 5mM or 10mM NAC and infected with parasites for 2 hours. At 2 hour p.i, parasites (green) were still observed to be aggregating around the perimeter of epithelial sheets (purple) pre-treated with (A) 0mM, (B) 2mM, (C) 5mM and (D) 10mM. Images are representative of three fields of view in a single infection experiment. Dashed lines depict epithelial perimeters. Scale bars = 30µm

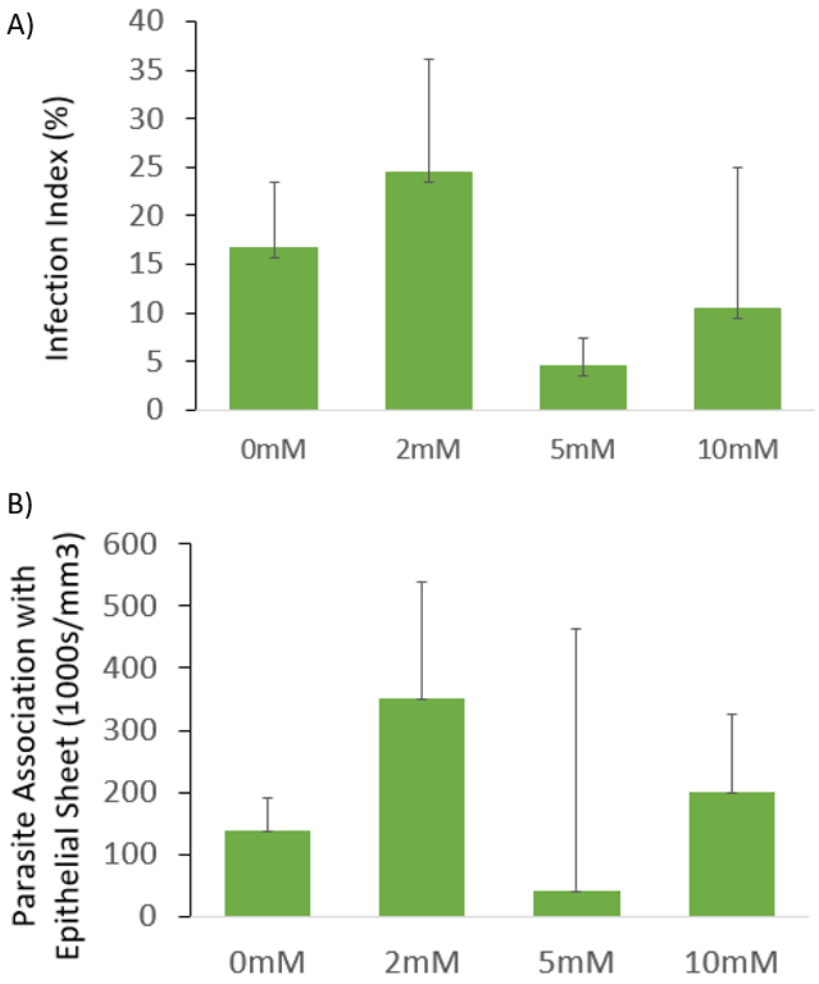

Figure 42) Pre-treatment with NAC does not increase the association of parasites to host cells

Epithelial sheets were pre-treated with either 0mM, 2mM, 5mM or 10mM NAC and infected with *T. gondii* tachyzoites for 2 hours. (A) Infection index was highest and lowest in 2mM and 10mM NAC pre-treatment respectively. (B) The number of parasites associated with epithelial sheets followed the same trend as the number of cells infected. The highest association was observed in 2mM NAC pre-treated sheets, and the lowest was in 5mM NAC pre-treated sheets. The bars represent standard error. The data presented here is representative of two experimental replicates.

The findings here suggest that either the mucus component does not play a significant role in determining the outcome of epithelial cell infection, or that an intact mucus barrier is absent within this model. Since we observed no dramatic improvement in the infection index with the use of NAC, and the biological impacts of introducing a

mucolytic treatment on parasite behavior and the host cell response is unknown, we decided not to incorporate this additional step into our protocol.

5.3.6 Centrifugation Does Not Affect Infection Index During Early Stage Invasion

Despite the absence of a clear explanation for the aggregative behaviour of tachyzoites around the epithelial sheets, and having found no clear evidence that a barrier exists to prevent invasion, we attempted to create a more uniform distribution of parasites in our cultures, with the hope to increase the infection index.

Established infection protocols of cell line cultures *in vitro* often exploit centrifugation to increase the contact of host cells and pathogen to encourage host cell invasion and synchronise infections. Within this model, tachyzoites are purified and re-suspended in organoid media which is then overlaid onto collagen-supported epithelial sheets. Here, we introduced an additional centrifugation at 100*xg* for 1 min after tachyzoites were added to epithelial sheets to promote direct contact with host cells and evaluate how parasites were settling onto the cultures. During this experiment samples were either spun, or not spun, and incubated for 30, 45 and 60 minutes before fixing.

Here, we examined the infection index and density of parasites associated with the epithelial sheet to evaluate the effect of centrifugation. At 30 and 45 minutes post infection, the infection index was higher in centrifuged samples, suggesting an improvement in the invasion rate with the addition of centrifugation (**Figure 43**, **A and B**).

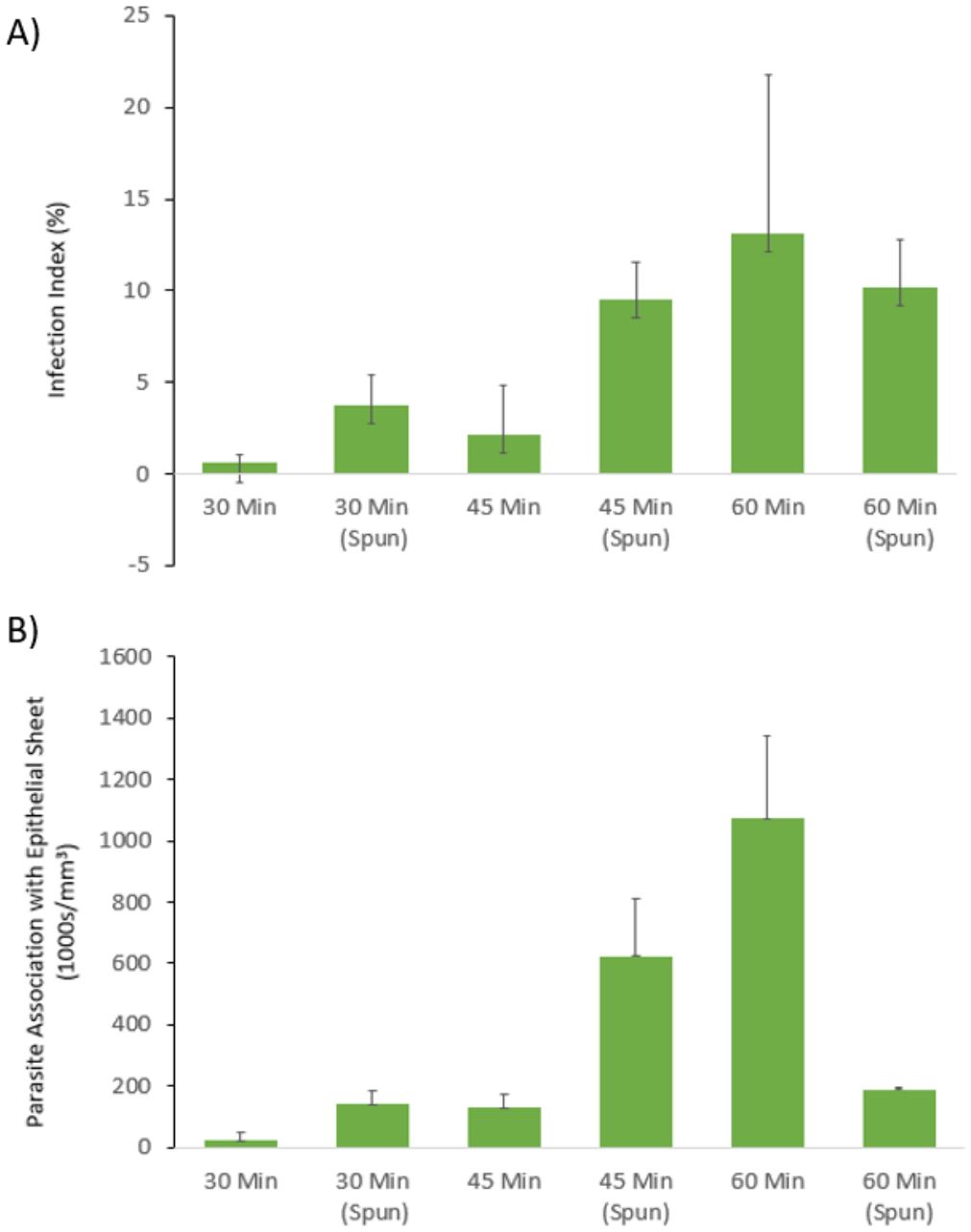

Figure 43) Centrifugation increases infection index and infectious potential at 30 and 45 min, but not at 60 min

Epithelial sheets were infected with *T. gondii* tachyzoites, and either centrifuged for 100*xg* for 1 min, or not. (A) Centrifugation increases the infection index at 30 and 45 min, but not at 60 min. (B) Centrifugation decreases the association index at 30 and 45 min, but not at 60 min. The bars represent standard error. The data represents a single pilot infection.

However, at 60 minutes post infection, this effect was lost, and the infection index in centrifuged samples was lower than in non-centrifuged samples (**Figure 43, A and B**). A similar pattern was observed when we calculated the density of parasites associated with the epithelial sheet (either invaded or attached to the apical surface). This data suggests that centrifugation initially brings more parasites in contact with the apical surface of the epithelial sheet, allowing invasion to occur more rapidly, but this does not result in higher infection rates at later time points (**Figure 43, A and B**).

For future study of host-pathogen interactions, it is unlikely that we will collect experimental data earlier than a 60 minute time point, and so the addition of centrifugation to our infection protocol will not improve the infection index and will not be incorporated.

Having determined that these optimisation steps described here do not increase the association of tachyzoites to host cells, we exploit this protocol to determine suitable parameters for proteomic studies.

Specifically, defining suitable time points to recapitulate biological events during early host cell invasion and parasite replication, and determining the minimal threshold of biological material required to generate enough proteome signal are crucial to the study design.

5.3.7 Selection of Time Points for Proteomic Studies

Preliminary data confirm that collagen-supported epithelial sheets are susceptible to invasion by, and support the replication of, *T. gondii.* Therefore our model provides an excellent tool to investigate the host epithelial cell response to infection at two key stages: early invasion and replication. However, unlike traditional cell line cultures

where infection protocols are established, the exact timing of these events in our model remain unknown. Here we performed a more detailed time-course to select appropriate time points for proteomics based analysis of the host response. For these experiments we utilised two parasite strains; virulent type I (RH) and avirulent type III (Veg) strain.

To select an early time-point, we first looked at infections following 1 and 4 hour incubation. Although infection was observed as early as 30 min in this model, the frequency of infection was low. Due to the asynchronous nature of parasite invasion, we decided to choose 1 hour as our early time point to maximise the observable number of invasion events for analysis. The four hour time-point was selected as previous work performed in cell lines by Xia *et al.* demonstrated that host cells exhibit large proteome changes at 4 hours post infection, indicating that the host response to infection is readily detectable at this time point (Xia et al., 2008)

Unsurprisingly, the infection index was lower in the avirulent Veg strain at both time points (**Figure 44**). At 1 hour incubation, the infection rate is low and the difference between the two strains is negligible, however differences becomes more evident by 4 hours resulting in 6.47% infection by Veg, and 8.20% infection by RH.

From these findings, we have tangible evidence that infection rates are lower at 1 hour p.i. than at 4 hour. p.i.. As previously observed, there was a marked lack of parasite replication at the 4 hour time-point, which suggests that the increase in infection index between 1 and 4 hours is attributable to new infection events occurring in an asynchronous manner. The occurrence of these new infection events make the 4 hour time-point suitable for the study of early invasion of host cells by *T. gondii*, while increasing the likelihood that parasite material and the host cell response will be detectable by mass spectrometry

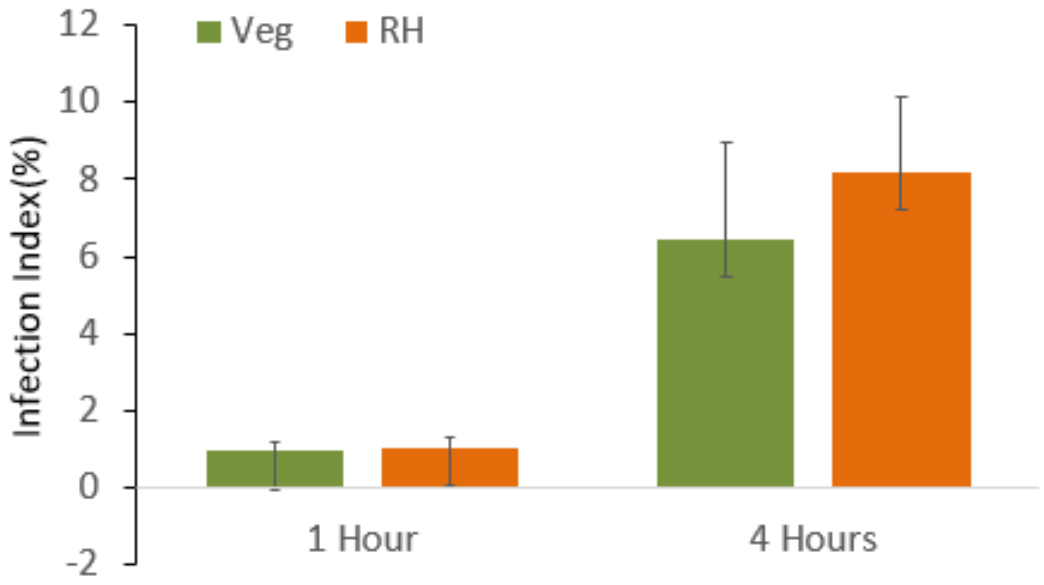

Figure 44) Infection after 1 Hour incubation with both RH and Veg is poor

After 1 hour incubation, infection rates in both Veg and RH infected samples is low. The infection rate increased following 4 hours infection, with RH exhibiting a higher infection index in these experiments. The bars represent standard error. Data representative of two biological replicates.

5.3.8 Replication Is Not Observed After 16 Hours Incubation with *T. gondii* RH or Veg Strains

Having identified a suitable time point to represent early stage invasion, next we proceeded to perform a time-course experiments to identify a suitable incubation period to assess parasite replication. Based on pilot studies, we had identified parasite replication within this model at 24 hours post infection, however have not yet determined if parasite replication occurs any earlier. Although replication is observed as early as 4 hours *in vitro*, previous infections of HFF cell lines report replication most commonly at approximately 16 hours. To assess whether the same interaction occurs within this model, here we performed a time-course experiment to quantify the presence of replication at 16, 24 and 40 hours post infection (**Figure 45**).

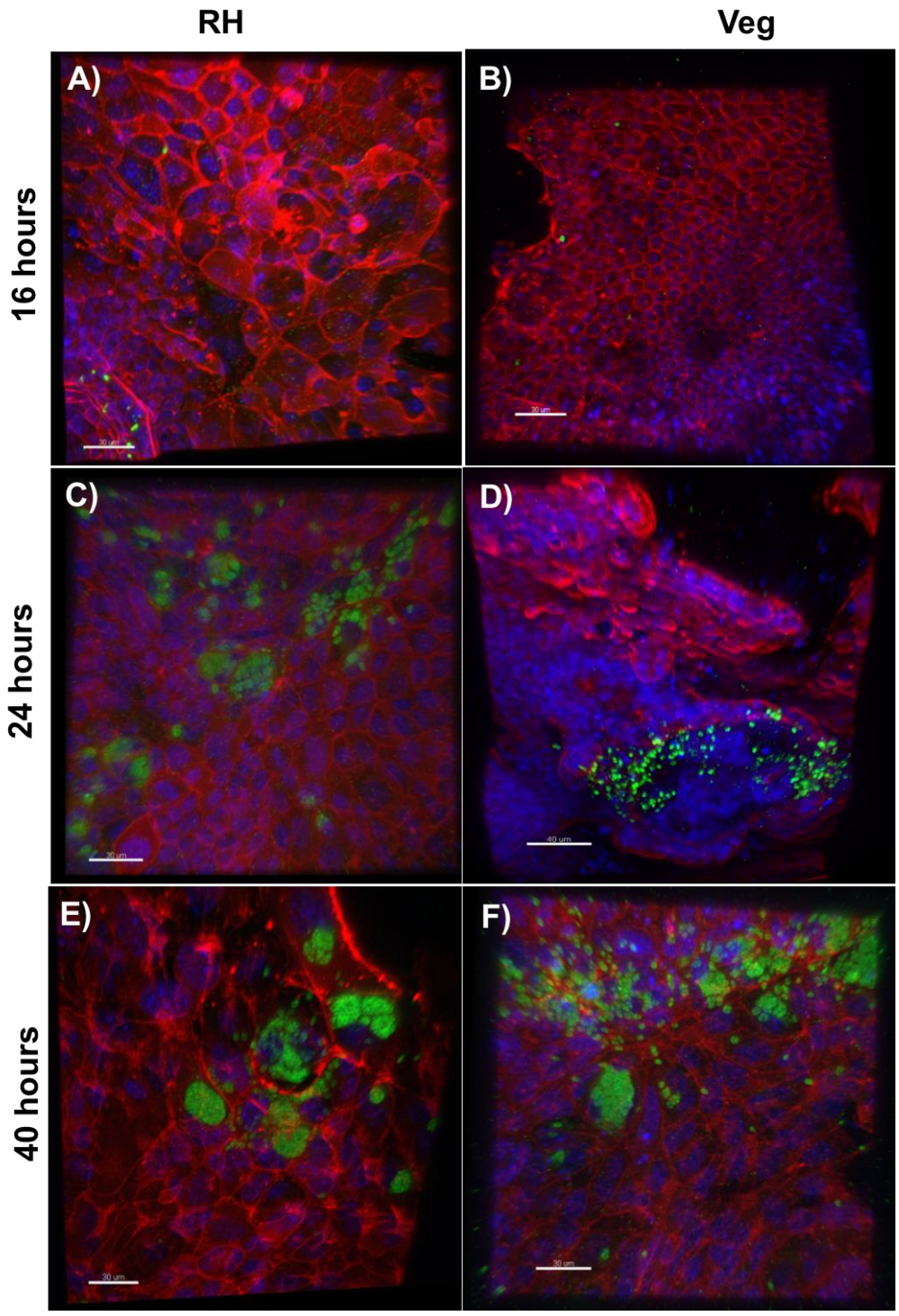

Figure 45) Replication does not after 16 hours infection with either T. gondii RH or Veg

Epithelial sheets were infected for 16, 24 and 40 hours, fixed and processed for confocal microscopy. Infection of epithelial model produces (A and B) no replication at 16 hours p.i., (C and D) some infection at 24 hours although with some regions of non-infected cells, and (E and F) more widespread infection throughout the sheet. Scale bars = 30µm except for (D) where scale bar = 40µm. Data representative of two biological replicates.

Initial observations based on confocal imaging suggest replication in RH but not Veg infected samples at 16 hours p.i. However, replication at this time point was limited to regions close to the perimeter of the sheet, whereas at 40 hours parasite replication was found to be more widespread.

To compare the differences in infection and replication between RH and Veg strains, we evaluated the infection index, and calculated the proportion of host cells that contain replicating parasites based on the presence of a minimum of three or more parasites clustered in an early rosette formation.

After incubation with RH and Veg tachyzoites for 16 hours, the proportion of infected cells is fairly low at 4.02% and 5.15% respectively (**Figure 46 A**). After 24 hours, this doubles in Veg infected samples, and triples in RH infected samples (**Figure 46 A**). By 40 hours, 18% and 41% of host cells become infected with Veg and RH respectively (**Figure 46 A**).

Confocal imaging identified no replication after 16 hours of incubation with either Veg or RH strains, and low level replication at 24 hours (**Figure 46** B). By 40 hours post infection, almost 5% of Veg-infected cells, and 8% of RH infected cells contained replicating parasites (**Figure 46 B**).

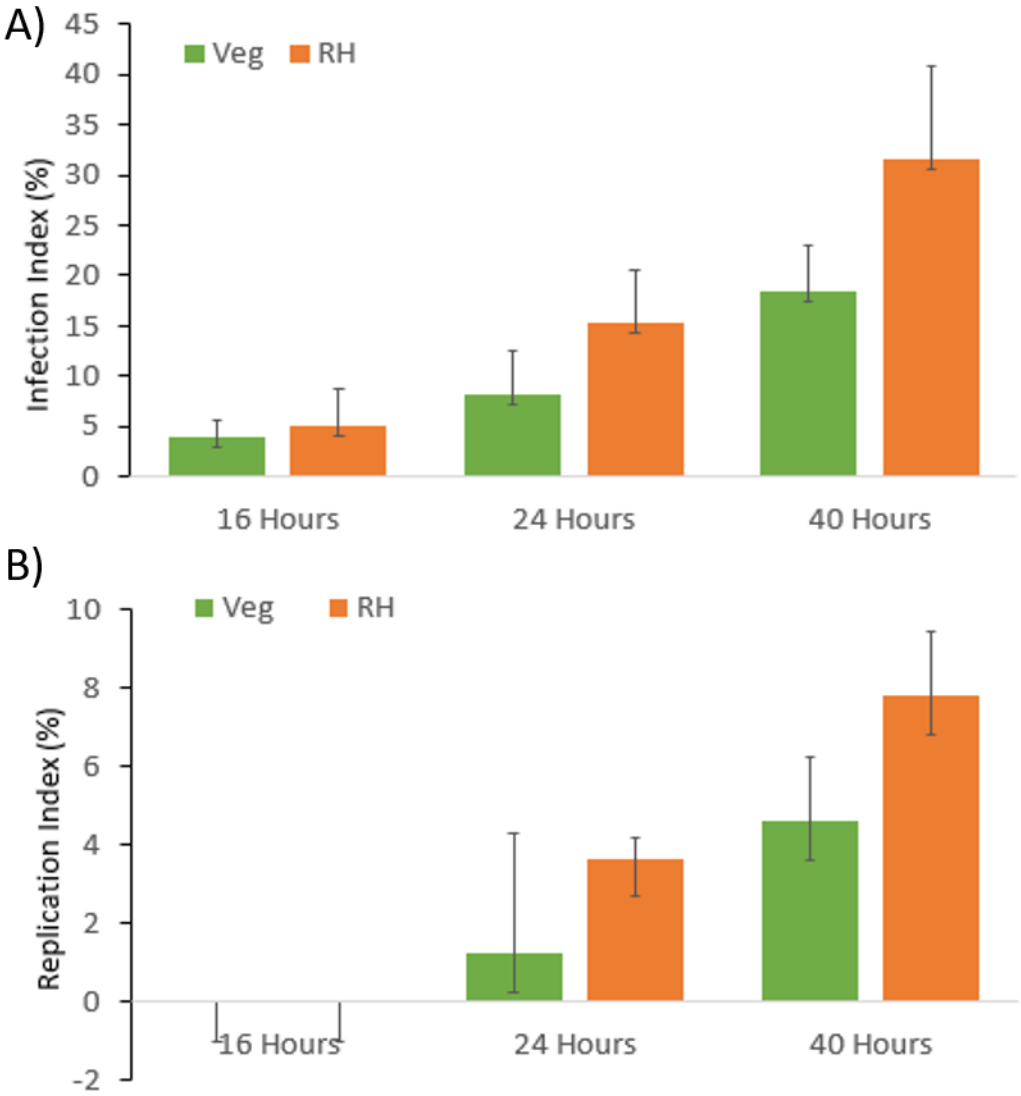

Figure 46) Parasite replication is not observed after 16 hours incubation

Epithelial sheets were infected for 16, 24 and 40 hours, fixed and processed for confocal microscopy. Analysis of images quantified these infections. (A) Infection of host cells increased with duration of time between 16 and 40 hours. (B) No replication events were observed at 16 hours. Replication was observed at 24 hours but at low levels in Veg-infected samples. By 40 hours, the proportion of cells containing replicating parasites had doubled from 24 hours. The bars represent standard error. Data representative of two biological replicates.

5.3.9 Label-Free Mass Spectrometry Detection of Parasite Proteins at 24 Hours Post-Infection

As *T. gondii* replication was not observed at 16 hour p.i., but was present after 24 hour infection, we performed a pilot infection to assess the sensitivity of label-free mass spectrometry for the detection of parasite proteins within the collagen-supported epithelial cell model.

The purpose of this pilot study was to evaluate the potential use of a parasite "spiked" control sample. Due to the complexity of parasite and host proteins present within infected samples, the incorporation of spiked controls into the experiment could potentially identify subsets of proteins modulated in response to host cell exposure to parasites, rather than simply just host cell proteins modulated in response to active infection. However, due to the small sample size of collagen-supported epithelial sheets, the sensitivity of mass spectrometry for protein detection in the model may be low. This pilot infection will assess the benefit of incorporating the parasite spiked control into the experimental design for future infection studies.

In chapter 4, we determined that 5 pooled-wells of collagen-supported epithelial sheets contained detectable host proteins, however the sensitivity of parasite protein detection in this model is not yet characterised. Moreover, due to the natural variability of cell numbers within this model observed in Chapter 4, here we decided to pool together 10-wells to increase the depth of protein detection for this pilot study.

797 total proteins were detected in the non-infected epithelial sheet sample, 1179 total proteins in the 24 hour RH-infected sample, and 1446 total proteins in the parasite spiked sample, with 667 proteins common in all three samples (**Figure 47**).

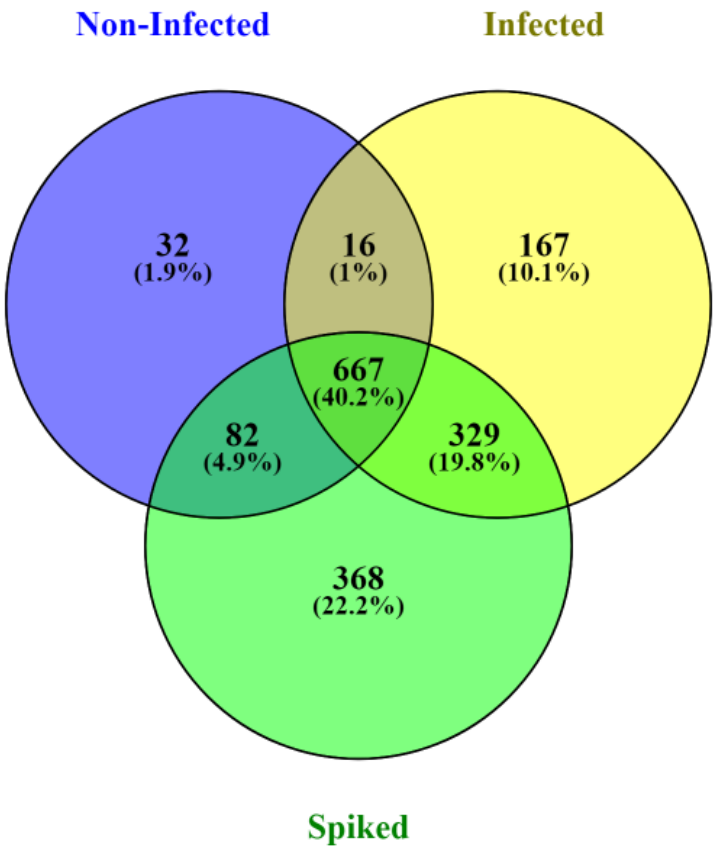

Figure 47) Venn diagram shows numbers of proteins detected in non-infected, 24 hour infected and spiked epithelial sheets

797 proteins in the non-infected sample (blue), 1179 proteins in the infected sample (yellow) and 1446 proteins in the spiked sample (green) were identified.

Non-infected and infected samples share 52.8% of proteins detected (**Figure 48 A**). The lowest number of proteins shared was between non-infected and parasite spiked samples at 50.1% (**Figure 48 B**), and the highest proportion of samples shared was between infected and spiked samples at 61.1% (**Figure 48 C**).

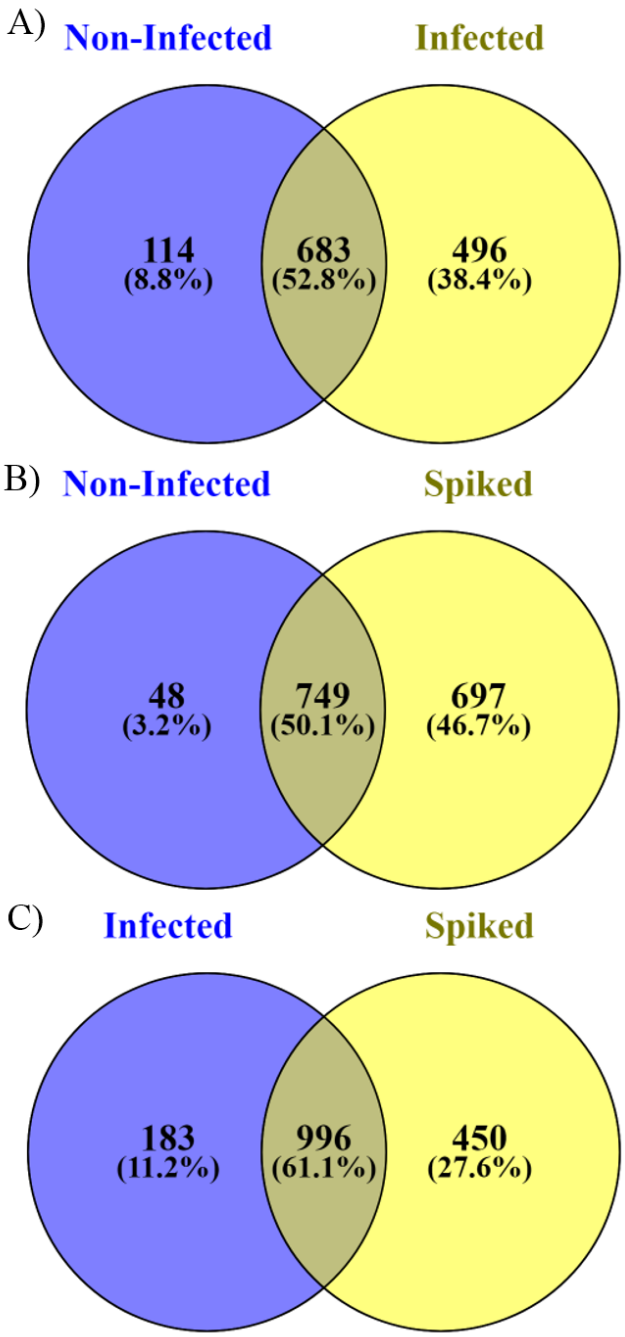

Figure 48) Venn diagram showing proteins detected by label-free mass spectrometry in non-infected, 24 hour RH infected and parasite spiked epithelial sheets

After removing single-peptide hits, we detected 797 proteins in non-infected, 1179 proteins in infected and 1446 proteins in parasite-spiked samples. **(A)** 683 **(**52.8%) proteins shared between non-infected and infected samples. **(B)** 749 (50.1%) proteins shared between non-infected and spiked samples. **(C)** 996 (61.1%) proteins shared between the infected and spiked samples. Results suggest that infected and spiked samples were most similar to one another, and non-infected and spiked samples were most different to one another.

Host proteins detected in each sample were analysed for similarities in molecular function and biological processes by gene ontology using Pantherdb (http://www.pantherdb.org/) (Mi et al., 2013). 22 proteins were excluded from the spiked control sample, 39 from the infected samples, and 3 proteins from the non-infected sample data set as they were either uncharacterised or not recognised by Pantherdb. Nine molecular function terms were associated with the proteins detected in all three samples (**Figure 49**). The proportion of proteins detected in each molecular function group was similar across samples. However some small differences were observed in the proportion of "catalytic activity" proteins which were slightly lower in non-infected samples, and "structural molecule activity" proteins which were slightly higher in non-infected samples (**Figure 49** purple bars).

Twelve biological processes were associated with proteins detected in the spiked (green bars) and non-infected (purple) sample, and thirteen biological processes were detected in the infected sample (orange) (**Figure 50**). The proportion of proteins detected in each of the biological processes groups was also similar across samples, with the exception of "cellular component organisation or biogenesis" in the non-infected sample, which had 1.2% and 1.4% more protein hits than spiked (green bars) and infected samples (orange bars) (**Figure 50** purple bars).

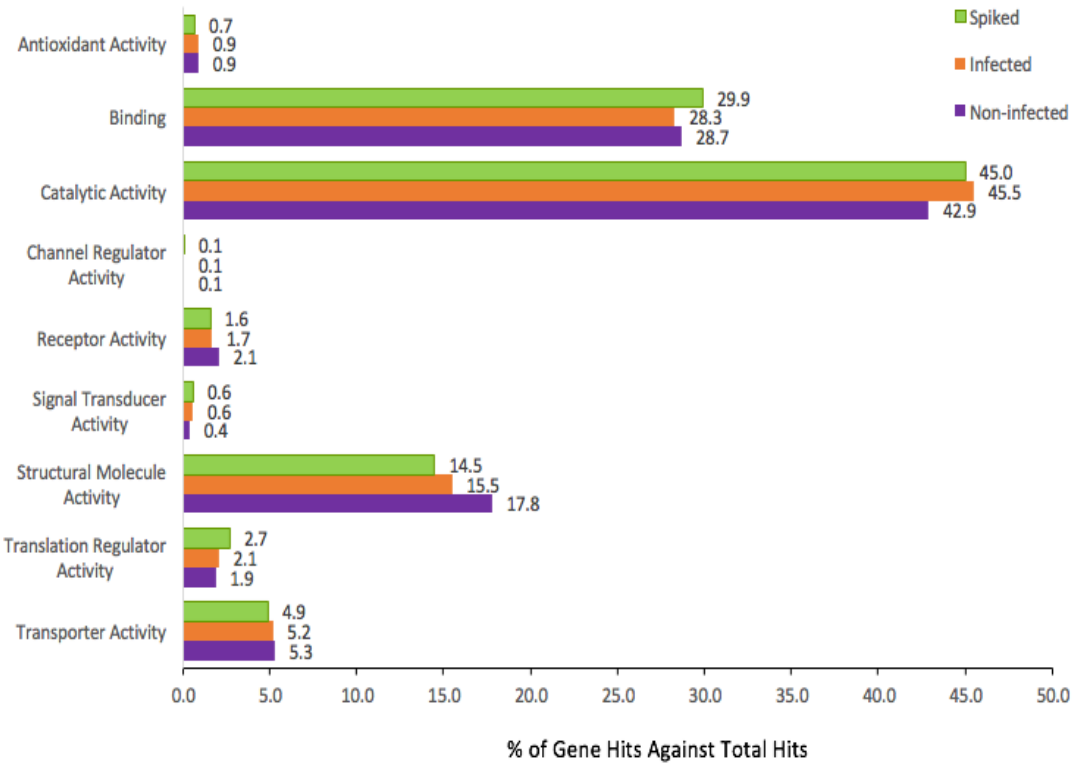

Figure 49) Comparison of molecular functions associated with proteins detected in pooled non-infected, 24 hour infected and spiked samples.

Single peptide proteins were removed from the data set and significant proteins were analysed in Panther DB Classification Tool (online; http://www.pantherdb.org/). 1446 proteins were input for the spiked control sample, with 22 unmapped ID's excluded. 1179 proteins were input for the infected sample, with 39 unmapped ID's excluded. 797 proteins were input for the non-infected sample, with 3 unmapped ID's excluded. Nine molecular functions were associated with spiked (green bars), infected (orange bars) and non-infected control (purple bars). The proportion of proteins associated with molecular function was similar across all three samples, with the exception of structural molecule activity which was slightly higher in non-infected samples, and catalytic activity which was slightly lower in non-infected samples.

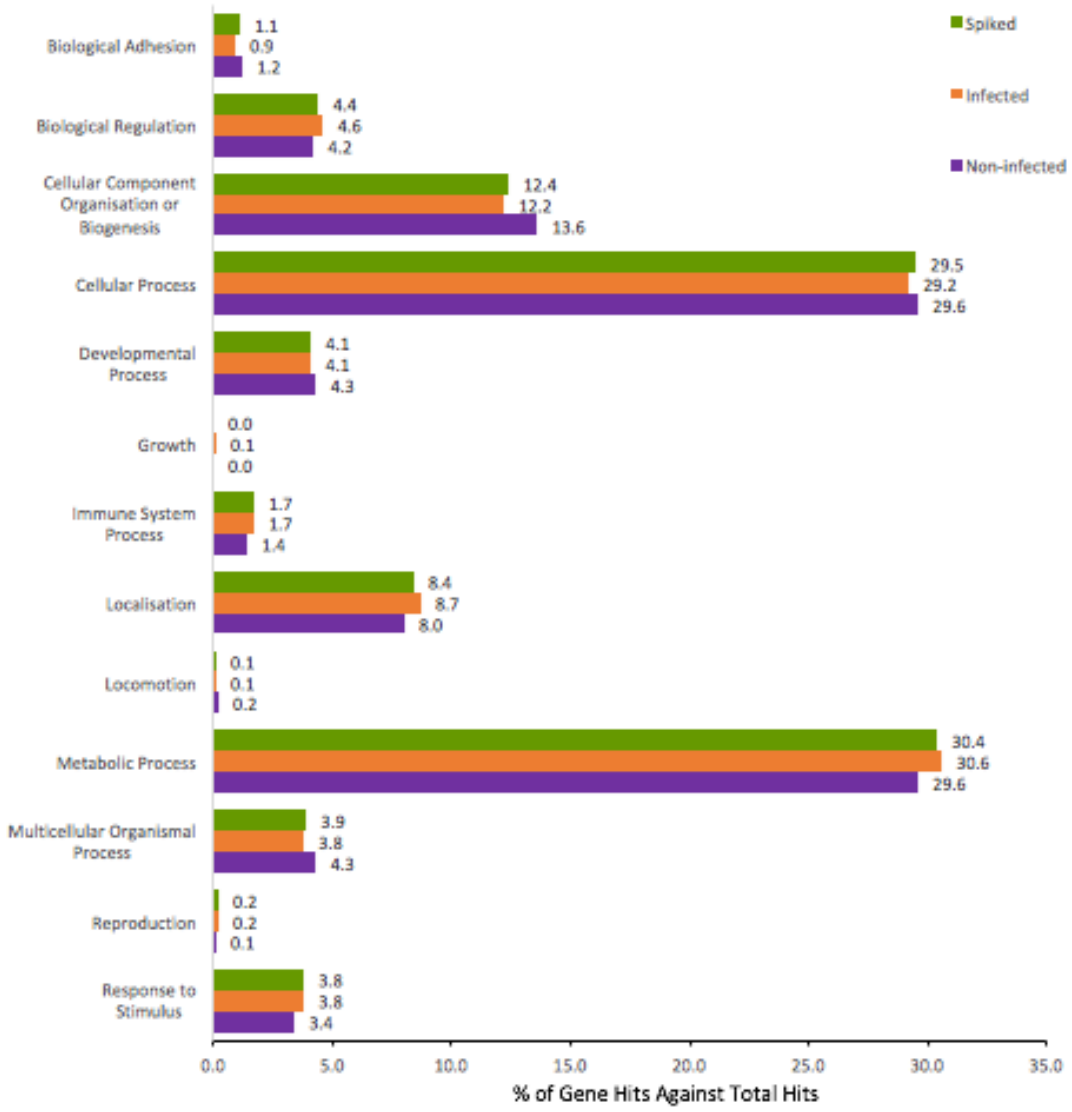

Figure 50) Comparison of biological processes associated with proteins detected in pooled non-infected, 24 hour infected and spiked samples

Single peptide proteins were removed from the data set and significant proteins were analysed in Panther DB Classification Tool (online; http://www.pantherdb.org1446 proteins were input for the spiked control sample, with 22 unmapped ID's excluded. 1179 proteins were input for the infected sample, with 39 unmapped ID's excluded. 797 proteins were input for the non-infected sample, with 3 unmapped ID's excluded. Twelve molecular functions were associated with spiked (green bars), and non-infected control (purple bars); and thirteen molecular functions were associated with the 24 hour infected (orange bars) sample. The proportion of proteins associated with biological processes were similar across all three samples, with the exception of cellular component organisation or biogenesis which was slightly higher in non-infected samples.

In the parasite-containing samples, 47 proteins were identified as parasite proteins in the 24 hour infected sample, and 24 in the parasite spiked sample, with 14 parasite proteins shared in both samples (**Table 12 - Table 14**).

Within infected epithelial sheets, multiple proteins involved with the actin-myosin complex involved in active invasion of host cells were detected (Boucher and Bosch, 2015).; TGME49_209030 actin (ACT1), TGME49_231630 alveolin containing intermediate filament (IMC4), TGME49_231640 alveolin containing intermediate filament (IMC1), TGME49_236040 fructose-1, 6-bisphosphate aldolase (F16BP/ FBP ALD), TGME49_2619190 glyceraldehyde-3-phosphate dehydrogenase (GAPDH2), TGME49_289690 glyceraldehyde-3-phopshate dehydrogenase (GAPDH1) and TGME49_293690 profilin (PRF) (**Table 12**).

Tachyzoite-stage specific parasite proteins were also identified within infected epithelial sheet samples (Hehl et al., 2015; Holmes et al., 2010; Lyons et al., 2002); TGME49_232350 lactate dehydrogenase (LDH1), TGME49_268850 enolase 2 (ENO2), TGME49_316400 alpha tubulin (TUBA1) and TGME49_318230 phosphoglycerate kinase (PGKI) (Highlighted in **Table 12***).*

Interestingly, we also detected 14-3-3 in infected samples, which has been reported as a mediator of DC hypermotility phenotype (Weidner et al., 2016).

In samples spiked with de-activated *T. gondii*, with the exception of ACT1, the proteins involved in maintaining the actin-myosin complex for cell invasion, and the tachyzoite specific proteins are absent (**Table 13**).

Table 12) 47 parasite proteins detected in 24 hour T. gondii RH infected epithelial sheets

TGME49_204400	ATPase synthase subunit alpha, putative
TGME49_209030	actin ACT1*
TGME49_210690	ribosomal protein RPS6
TGME49_211680	protein disulfide isomerase
TGME49_216880	guanine nucleotide-binding protein
TGME49_217890	alkyl hydroperoxide reductase/ Thiol specific antioxidant/ Mal allergen, putative
TGME49_219540	cytosolic tRNA-Ala synthetase
TGME49_221620	beta-tubulin, putative
TGME49_225930	triose-phosphate isomerase TPI-I
TGME49_226250	DEAD (Asp-Glu-Ala-Asp) box polypeptide DDX3X
TGME49_226960	phosphofructokinase PFKII
TGME49_231630	alveolin domain containing intermediate filament IMC4*
TGME49_231640	alveolin domain containing intermediate filament IMC1*
TGME49_232250	catalase
TGME49_232350	lactate dehydrogenase LDH1^{+}
TGME49_232940	heat shock protein HSP20
TGME49_233460	SAG-related sequence SRS29B
TGME49_235470	myosin A
TGME49_236040	fructose-1,6-bisphosphate aldolase*
TGME49_247350	thioredoxin domain-containing protein
TGME49_247550	heat shock protein HSP60
TGME49_248340	GTP-binding nuclear protein ran/tc4
TGME49_250770	eukaryotic initiation factor-4A, putative
TGME49_251810	translation initiation factor eIF-5A, putative
TGME49_259240	ribosomal protein RPS21
TGME49_261010	tat-binding family protein, putative
TGME49_261950	ATP synthase beta subunit ATP-B

* These proteins form part of, or interact with the parasite actin-myosin complex required for the successful invasion of host cells

$^{+}$ These are fast-multiplying tachyzoite specific

Table 8 Continued) 47 parasite proteins detected in 24 hour T. gondii RH infected epithelial sheets

TGME49_263090	14-3-3 protein
TGME49_266960	beta tubulin
TGME49_268850	enolase 2^{+}
TGME49_269190	glyceraldehyde-3-phosphate dehydrogenase GAPDH2*
TGME49_270510	asparaginyl-tRNA synthetase (NOB+tRNA synthase
TGME49_273090	cell division protein CDC48CY
TGME49_273760	heat shock protein HSP70
TGME49_286420	elongation factor 1-alpha (EF-1-ALPHA), putative
TGME49_288360	tryptophanyl-tRNA synthetase (TrpRS2)
TGME49_288380	heat shock protein HSP90
TGME49_289690	glyceraldehyde-3-phosphate dehydrogenase GAPDH1*
TGME49_293690	profilin PRF*
TGME49_295125	rhoptry protein ROP4
TGME49_308090	rhoptry protein ROP5
TGME49_310700	serine/threonine phosophatase PP1
TGME49_311720	chaperonin protein BiP
TGME49_313190	Rab18/RabC-family small GTPase
TGME49_316400	alpha tubulin TUBA1^{+}
TGME49_318230	phosphoglycerate kinase PGKI^{+}
TGME49_320050	ribosomal protein RPL5

* These proteins form part of, or interact with the parasite actin-myosin complex required for the successful invasion of host cells

$^{+}$ These are fast-multiplying tachyzoite specific

Table 13) 24 parasite proteins detected in epithelial sheets spiked with de-activated T. gondii RH

TGME49_204400	ATPase synthase subunit alpha, putative
TGME49_209030	actin ACT1
TGME49_211680	protein disulfide isomerase
TGME49_218260	histone H3.3
TGME49_221620	beta-tubulin, putative
TGME49_228210	26S proteasome regulatory subunit
TGME49_231970	pre-mRNA processing splicing factor PRP8
TGME49_233460	SAG-related sequence SRS29B
TGME49_242330	ribosomal protein RPS5
TGME49_248880	GTPase RAB7
TGME49_258130	Rab1 protein
TGME49_261010	tat-binding family protein, putative
TGME49_261950	ATP synthase beta subunit ATP-B
TGME49_266760	isocitrate dehydrogenase
TGME49_271050	SAG-related sequence SRS34A
TGME49_273090	cell division protein CDC48CY
TGME49_273760	heat shock protein HSP70
TGME49_276140	ADP ribosylation factor ARF1
TGME49_286420	elongation factor 1-alpha (EF-1-ALPHA), putative
TGME49_288380	heat shock protein HSP90
TGME49_289680	Ras-related protein Rab11
TGME49_308090	rhoptry protein ROP5
TGME49_311720	chaperonin protein BiP
TGME49_313190	Rab18/RabC-family small GTPase

Table 14) 14 parasite proteins shared in infected and spiked epithelial sheets	
TGME49_204400	ATPase synthase subunit alpha, putative
TGME49_209030	actin ACT1
TGME49_211680	protein disulfide isomerase
TGME49_221620	beta-tubulin, putative
TGME49_233460	SAG-related sequence SRS29B
TGME49_261010	tat-binding family protein, putative
TGME49_261950	ATP synthase beta subunit ATP-B
TGME49_273090	cell division protein CDC48CY
TGME49_273760	heat shock protein HSP70
TGME49_286420	elongation factor 1-alpha (EF-1-ALPHA), putative
TGME49_288380	heat shock protein HSP90
TGME49_308090	rhoptry protein ROP5
TGME49_311720	chaperonin protein BiP
TGME49_313190	Rab18/RabC-family small GTPase

Although relevant proteins for invasion were detected within 24 hour infected samples, the general number of parasite protein returns was low. Only 3.9% and 1.7% of proteins detected from infected and spiked controls were from *T. gondii*. Furthermore, there was variation in the number of host proteins identified across infected, spiked and non-infected control sample.

Although the 24 hour time point would be preferable as this represents early replication, the number parasite proteins detected in this pilot study indicate that the parasite load may be too low for detection and therefore will be unsuitable for proteomic studies.

Comparably, the 40 hour time point has a higher load of replicating parasites, and generally a higher rate of invasion than the 24 hour. For this reason, the larger proteomic study will incorporate 40 hours as a time point to study host cell responses during parasite replication.

5.3.10 Proteomic Analysis of Infections at 4 and 40 Hours with *T. gondii* RH and Veg

Following the optimisation of an infection protocol to study host-pathogen interactions via mass spectrometry, we determined the optimal time points for the study of *T. gondii* early stage invasion. Here, using quantitative label-free mass spectrometry, we evaluate the protein abundance changes of *T. gondii* infected epithelial sheets at 4 and 40 hours post-infection.

Three biological replicates of epithelial monolayer cultures were infected for 4 and 40 hours and either fixed for confocal imaging or stored for proteomics. Confocal imaging was used to confirm parasite invasion, and sample preparation was then performed for label-free mass spectrometry.

After removal of single peptides hits, 1909 proteins were identified. Of these proteins, 67 (3.5%) detected were *T. gondii* proteins. Using exclusion criteria of $p < 0.05$ and $\log_2$ fold change > 1.0, significantly up- and down-regulated proteins at 4 and 40 hours were identified (Supplementary Tables 1-6, Appendix B).

Comparison against non-infected control samples at each respective time point identified several differentially expressed proteins. After 4 hours incubation, of the detected host proteins, only 2 were down- and 3 were up-regulated by Veg infection (Supplementary Table 1, Appendix B), and 6 were down- and 1 was up-regulated by

RH infection compared to non-infected epithelial sheets (Supplementary Table 2, Appendix B).

After 40 hours incubation, of the host proteins, 22 were down- and 8 were up-regulated with Veg infection (Supplementary Tables 3 and 4, Appendix B), and 14 were down- and 11 proteins were up-regulated by RH infections compared to non-infected epithelial sheets (Supplementary Tables 5 and 6, Appendix B).

Comparison of Veg and RH parasite proteins at 4 and 40 hours identified very few differentially proteins between these time points (**Table 15**). A singular protein was significantly up-regulated from 4 to 40 hours by Veg infection; ribosomal protein RSP15 (TGME49_213350) (**Table 15**). Two proteins were significantly up-regulated from 4 to 40 hours by RH infection; ribosomal proteins RSP23 and RSP21 (TGME49_229670 and TGME_252240, respectively) (**Table 15**).

Table 15) Identification of significantly changed proteins between 4 and 40 hour infections of T. gondii Veg and RH Strain infections

Accession	Description	P Value	Log_2 Fold Change	Highest Condition
TGME49_213350	ribosomal protein RPS15 (RPS15)	0.04348	4.98828	VEG 40
TGME49_229670	ribosomal protein RPS23 (RPS23)	0.01938	14.32570	RH 40
TGME49_259240	ribosomal protein RPS21 (RPS21)	0.01564	Infinity	RH 40

5.3.11 A Subset of Host Proteins Was Similarly Modulated During RH and Veg Infections

3 host proteins were each up- or down-regulated by both Veg and RH strains after 40 hours incubation. Across both strains, there was an observable increase in the expression of host apolipoprotein A1 (APOA1), apolipoprotein A4 (APOA4) and chitinase-like protein 4 (CHIL4), and a downregulation in host ATP-binding cassette sub-family F member 2 (ABCF2), canalicular multispecific organic anion transporter 2 (ABCC3) and pleoptropic regulator 1 (PLRG1) (**Figure 51** and Supplementary Table 7, Appendix B).

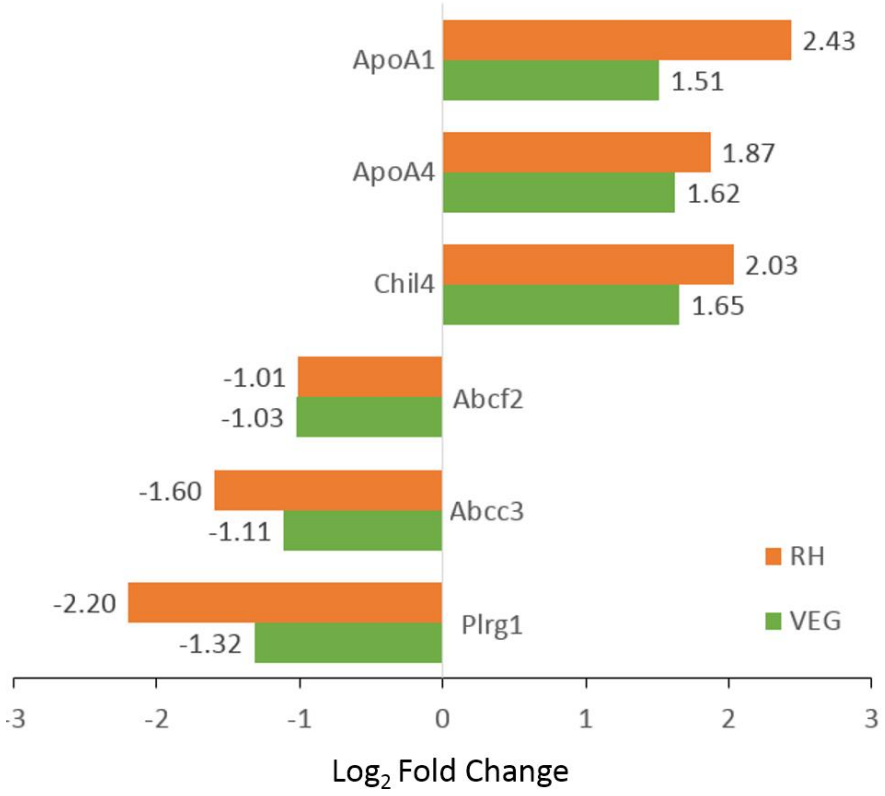

Figure 51) A sub-set of 6 proteins were similarly modulated after 40 hour incubation with T. gondii RH or Veg

Among the differentially expressed proteins, a sub-set of 6 proteins were commonly modulated at 40 hours infection with *Toxoplasma* RH and Veg parasites; APOA1, APOA4, CHIL4, ABCF2, ABCC3 and PLRG1.

CHIL4 is involved with neutrophil activity against helminth infections and the apolipoproteins are involved with lipid metabolism, PLRG1 is a regulator of cell proliferation and apoptosis, ABCC3 is involved with intracellular re-arrangement and ABCF2 is a cell protection factor.

5.3.12 Modulation of Host Cell Immune Responses by *T. gondii* Veg Strain

Here we examined the host-cell response to avirulent *T. gondii* Veg infection during invasion and replication at 4 and 40 hours respectively via quantitative label-free mass spectrometry.

At 4 hours post infection very few changes in protein abundance were detected, however we observed that in particular, mitochondrial single-stranded DNA-binding protein (SSBP1), host dual specificity mitogen-activated protein kinase 3 (MAP2K3) and PDZ and LIM domain protein 1 (PDLIM1) were up-regulated (Supplementary Table 1 Appendix B) following 4 hour incubation with parasites. Interestingly, at 4 hours we also detected a downregulation of apoa1 protein, involved with lipid biosynthesis which may act as a nutrient source during parasite scavenging.

After 40 hours incubation, 22 proteins were down- and 8 proteins were up-regulated with Veg infection compared to non-infected samples (Supplementary Tables 3 and 4, Appendix B).

Within the down-regulated proteins, in addition to the shared proteins described in chapter 5.3.11, modulation of host cell proliferation proteins was detected; serine/threonine-protein kinase vrk1 (VRK1), histone H1.1 (HIST1H1A) and PLRG1 (Table 3 Appendix B). A down-regulation of four mitochondrial proteins; 28S ribosomal protein S30 (MRPS30), ATP-dependent Clp protease proteolytic subunit

(CLPP), 39S ribosomal protein L55 (MRPL55) and acyl-coA synthetase family member 2 (ACSF2) was also observed (Supplementary Table 3 Appendix B).

Of the 8 up-regulated host proteins after 40 hours of Veg infection (compared to non-infected controls), in addition to the shared proteins described in chapter 5.3.11, kunitz-type protease inhibitor 2 (SPINT2) which plays a role in inhibition of apoptosis and serine palmitoyltransferase 1 (SPTLC1) involved with sphingolipid metabolism were up-regulated (Supplementary Table 4, Appendix B).

Here we also performed network analysis of detected proteins after both 4 and 40 hour infections to identify potential enriched functions within the data (**Figure 52** and **Figure 53**).

Network analysis of 4 hour Veg infections highlighted a change in small molecule biochemistry however the number of proteins identified within this network was low and many relationships were hypothetical, as denoted by dashed lines (**Figure 52**).

Network analysis of detected proteins using IPA software identified a general down-regulation of host cell signalling and cell-mediated immune responses after 40 hours (**Figure 53**). Here, this network also suggests a down-regulation of cytosolic host proteins by Veg tachyzoites after 40 hours incubation (**Figure 53**).

To conclude, we have identified a general down-regulation of host cell signalling and cell mediated immune responses during replication of Veg parasites at 40 hours post infection.

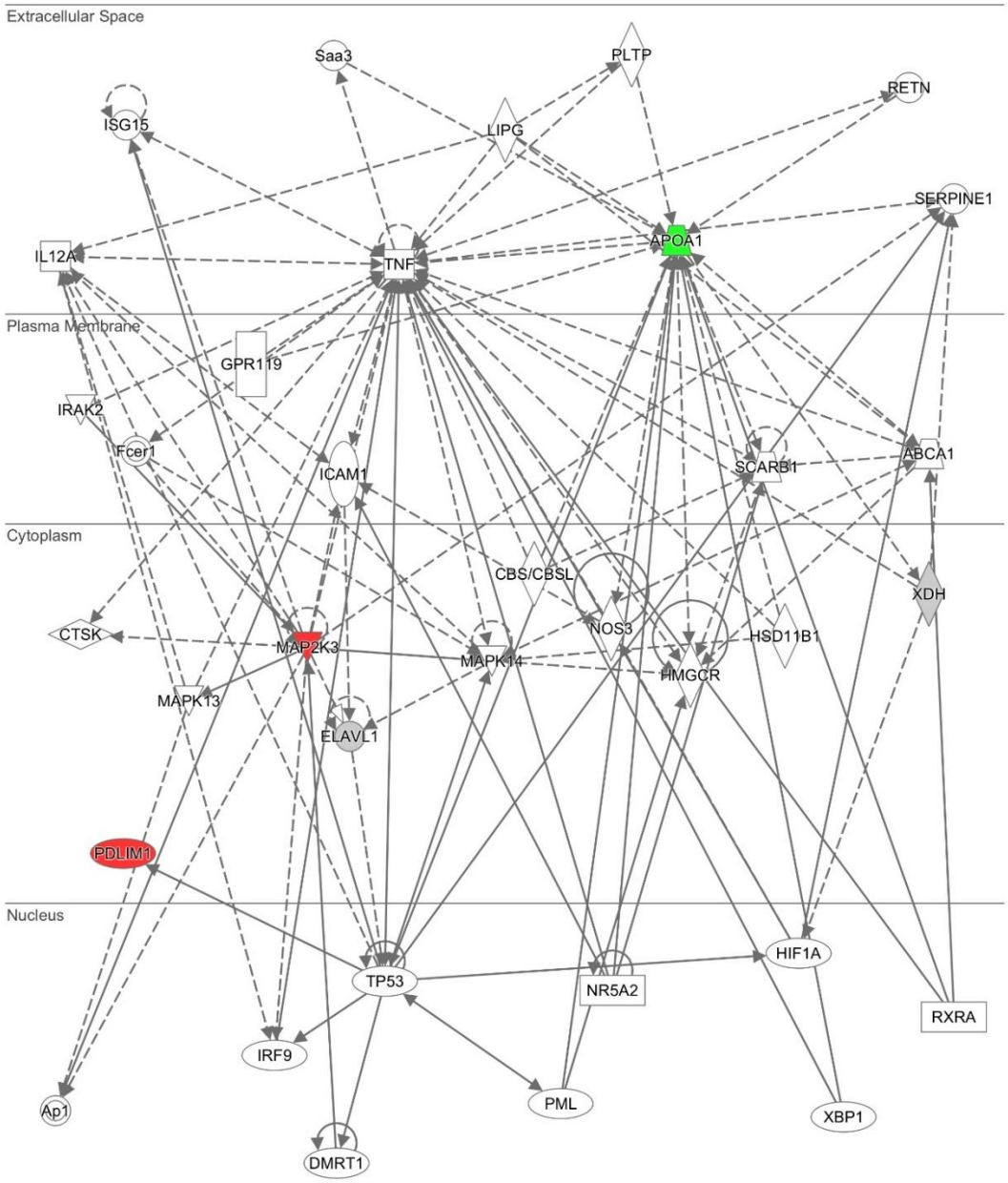

Figure 52) Host proteins with significant changes in abundance following 4 hour infections with Toxoplasma gondii Veg strain parasites map to a small molecular biochemistry and lipid metabolism network as determined by IPA software.

Within our dataset, 1 host protein was down-regulated (green), 2 host proteins were up-regulated (red) and 2 were detected but not significantly differentially expressed (grey).

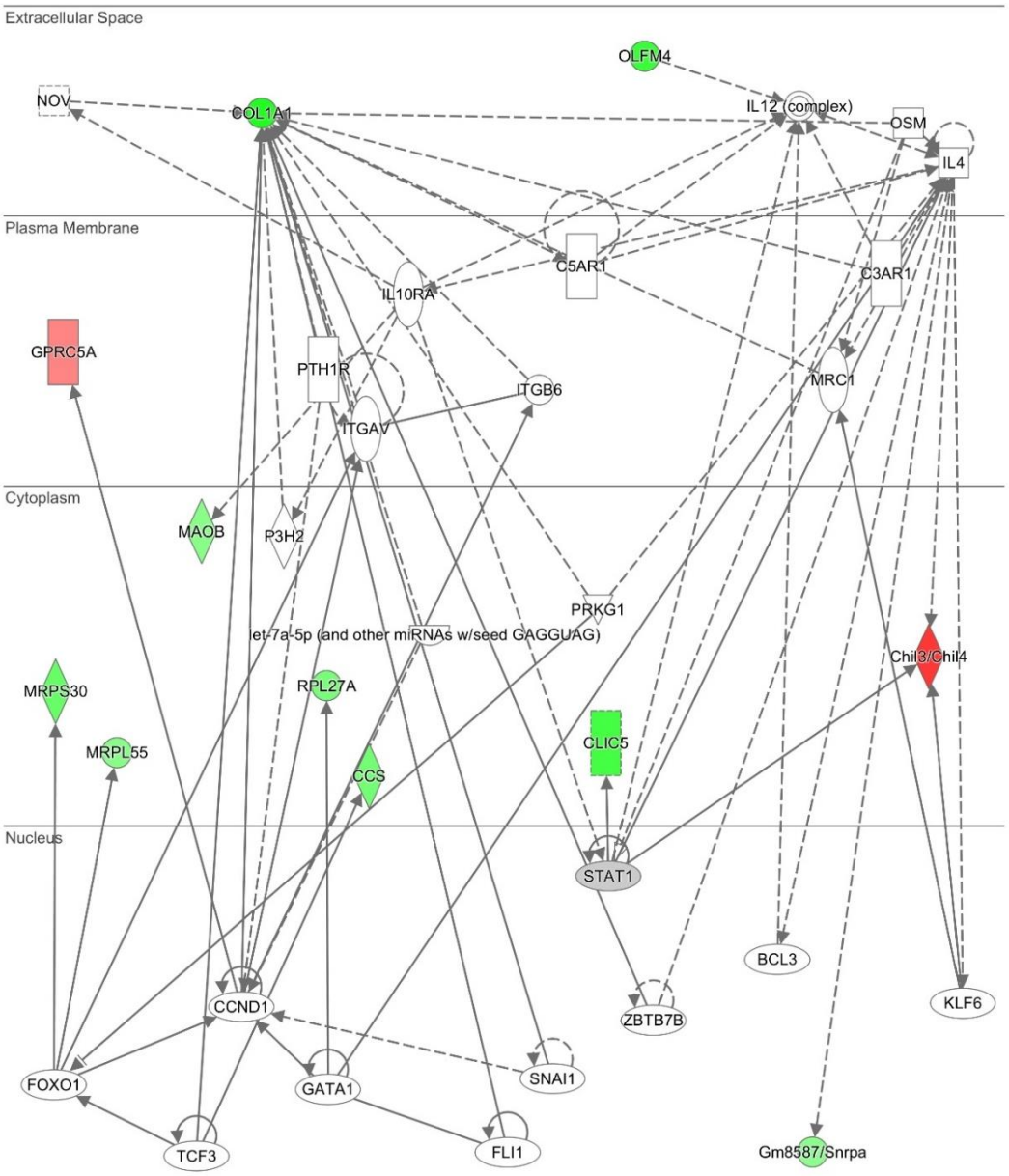

Figure 53) Host proteins with significant changes in abundance following 40 hour infections with Toxoplasma gondii Veg strain parasites map to a cell-cell signalling and cell-mediated immune response network as determined by IPA software.

Within our dataset, 9 host proteins were down-regulated (green) and 2 host proteins were up-regulated (red). Of the down-regulated proteins, 6 are localised within the host cell cytoplasm.

5.3.13 Modulation of Host Cell Lipid Metabolism by *T. gondii* RH Strain

Here we examined the host-cell response to virulent *T. gondii* RH infection during invasion and replication at 4 and 40 hours respectively via proteomic approaches. Surprisingly, although RH is more virulent than Veg, infection induced the modulation of fewer host cell proteins at both 4 and 40 hours incubation.

After 4 hours infection, we observed a down-regulation in sulfhydryl oxidase 1 (QSOX1) which plays a role in morphogenesis and tissue remodelling, and signal transducer and activator of transcription 1 (STAT1) (Supplementary Table 2 Appendix B) which is an important component of the IFN-γ pathway.

After 40 hours infection, 14 proteins were down- and 11 proteins were up-regulated by RH infections (Supplementary Tables 5 and 6, Appendix B).

Here, in addition to the shared proteins described in chapter 5.3.11, we observed a down-regulation of 2 salvage pathway proteins; l-fucose kinase (FUK) and sodium bicarbonate cotransporter 3 (SLC4A7), a barrier function protein cornifin a (SPRR1A) and 3 cell proliferation proteins; polyribonucleotide nucleotidyltransferase 1 (PNPT1), MMS19 nucleotide excision repair protein homolog (MMS19) and U6 snRNA-associated sm-like protein LSm7 (LSM7).

Of the up-regulated proteins, in addition to the shared proteins described in chapter 5.3.11, an anti-microbial peptide, alpha-defensin 22 (DEFA22), an isoprenoid biosynthesis protein, mevalonate kinase (MVK) and two intermicrovillar adhesion complex proteins; ankyrin repeat and SAM domain-containing protein 4B (ANKS4B) and cadherin-related family member 2 (CDHR2) were up-regulated (Supplementary Table 6, Appendix B).

Here we also performed network analysis of detected proteins after both 4 and 40 hour infections to identify potential enriched functions within the data.

Analysis of 4 hour RH infections highlight a change in tissue morphology network and stat1 signalling, however the number of proteins identified belonging to this network was low (**Figure 54** and **Figure 55**).

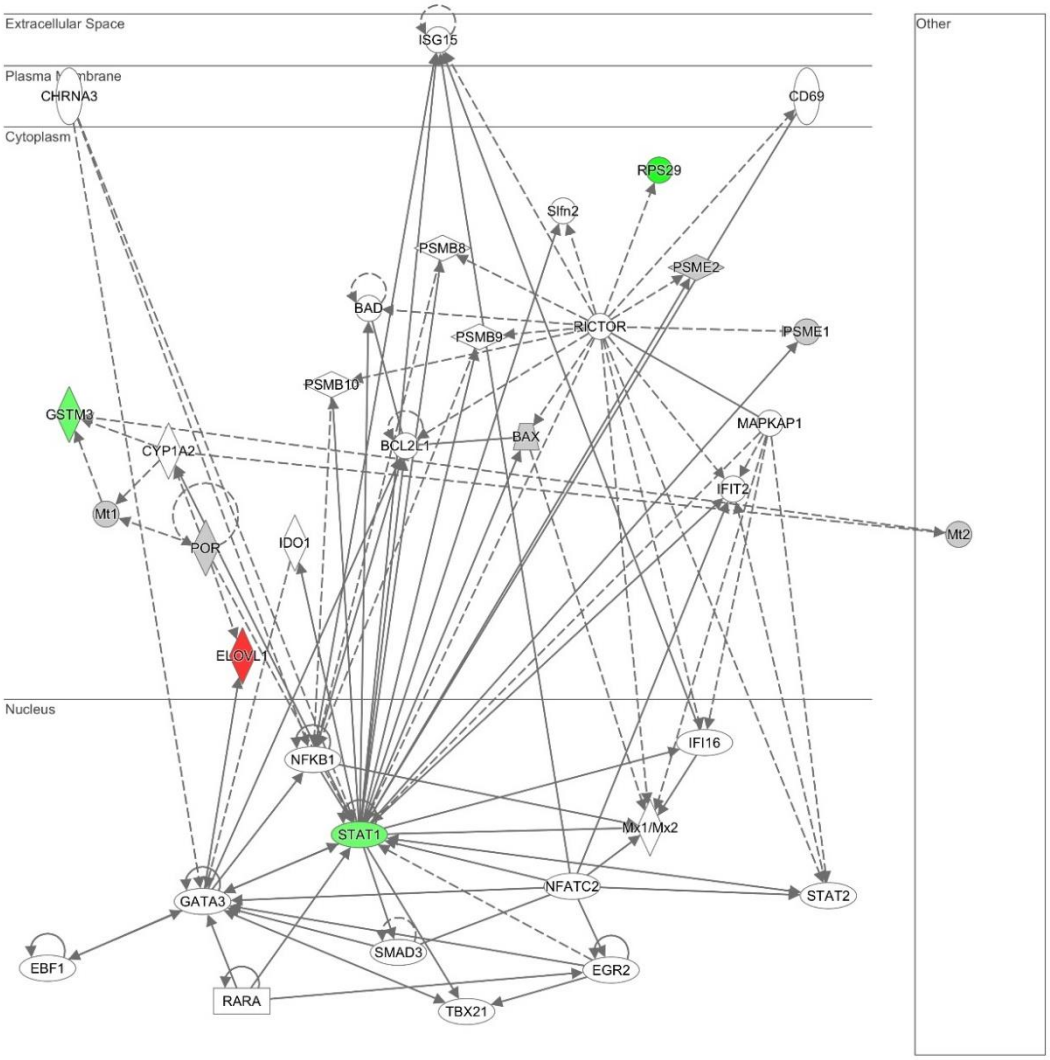

Figure 54) Host proteins with significant changes in abundance following 4 hour infection with Toxoplasma gondii RH strain map to a tissue morphology network as determined by IPA software.

Within our dataset, 3 host proteins were down- (green), 1 host protein was up-regulated (red) and 6 were detected but not significantly differentially expressed (grey).

Network analysis of detected proteins using IPA software identified an up-regulation in host cell lipid metabolism after 40 hour incubations with RH tachyzoites. Here this network identified 11 up-regulated proteins with a shared function involving lipid metabolism (**Figure 55**).

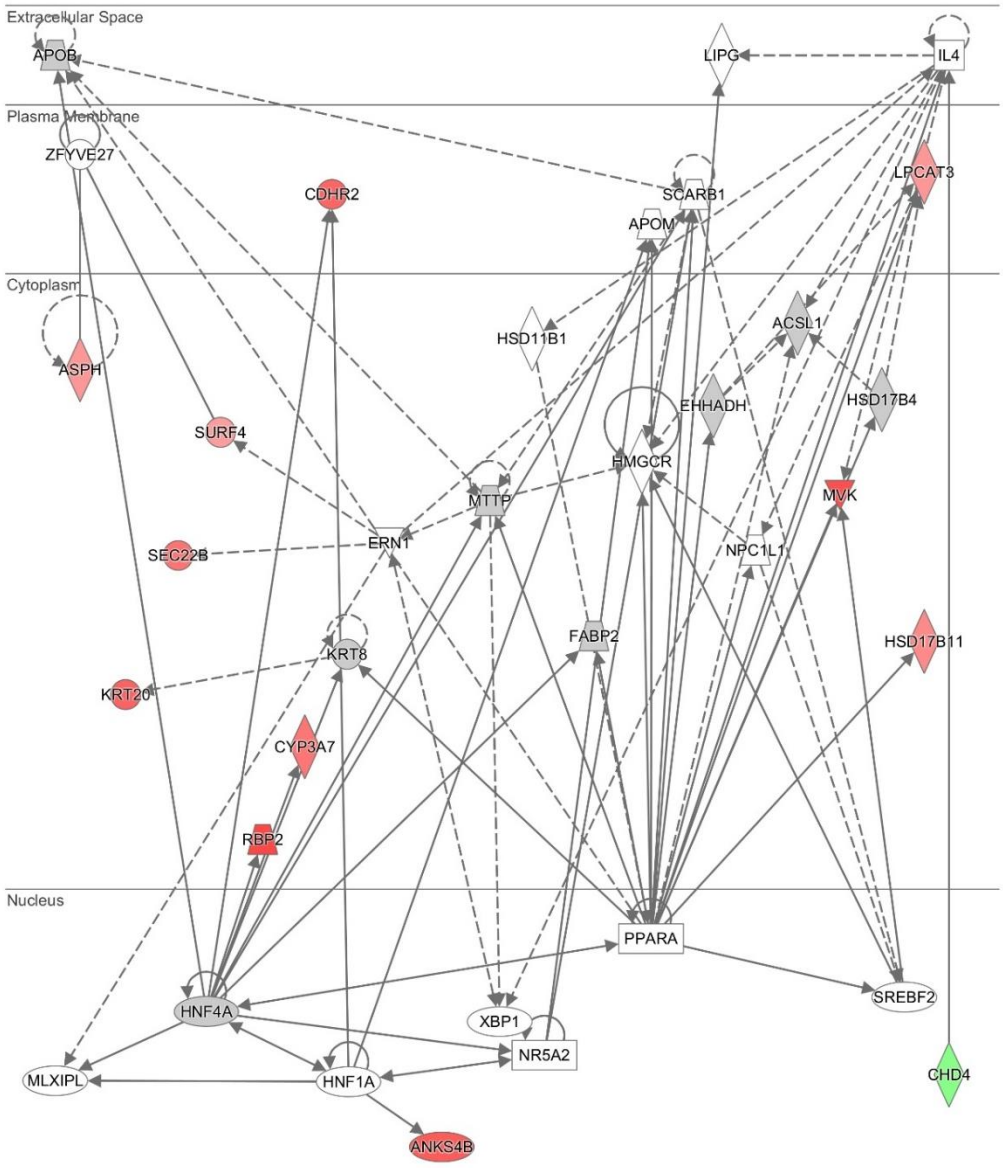

Figure 55) Host proteins with significant changes in abundance following 40 hour infection with Toxoplasma gondii RH strain map to a lipid metabolism network as determined by IPA software.

Within our dataset, 1 host protein was down-regulated (green), 11 host proteins were up-regulated (red) and 8 proteins were detected but not significantly differentially expressed.

To conclude, we have identified a lower number of host-proteins significantly differentially modulated by infection with RH than with Veg tachyzoites. However RH infection appears to modulate lipid metabolism to a higher extent than during Veg infections.

5.4.4 Discussion

Existing models of the small intestine are limited for the study of host responses to early stage invasion. Using the collagen-supported epithelial sheet model developed in chapter 4, we optimised an infection protocol to analyse changes in host proteome during active invasion and parasite replication by *T. gondii* RH and Veg strains.

T. gondii is widely considered to be capable of infecting almost all nucleated cells of warm-blooded vertebrates, and is easily maintained in cell culture. It was therefore surprising that very low infection rates were observed in our collagen-supported epithelial model.

During pilot infections, we observed that parasites were concentrated on uncovered regions of the collagen gel, at the perimeter of the epithelial sheets. We evaluated several optimization steps to create a more uniform distribution of parasites with the aim to increase invasion of host cells, however success was modest.

Complex *in vitro* models such as collagen-supported epithelial sheets may be comparatively more challenging than cell lines to infect due to the presence of Paneth and goblet cells that are known to play a role in host defence against pathogens. As the inner layer of colonic mucus is devoid of bacteria, and the composition of small intestinal mucus shares some similar proteins, the presence of these secreted mucus components in the collagen-supported epithelial model may contribute to the

inhibition of invasion here. However, this is not confirmed here as we only observed an increased invasion with one NAC treatment. Further work would be required to assess the presence of a mucus layer. Finally, type I *T. gondii* exhibit LDM phenotype and are thought to utilize a paracellular route of transmigration across the intestinal epithelium. However, we did not observe large numbers of parasites accumulating beneath epithelial sheets, which suggests that this is not responsible for the low levels of invasion reported here.

In vivo, T. gondii is thought to infect the tip of the villus (Coombes et al., 2013). However, it is currently unknown whether parasites preferentially invade enterocytes at the villus tip, or whether they are simply more accessible. In this collagen-supported epithelial model, we have not yet analysed whether *T. gondii* preferentially targets a specific epithelial cell type. However, the confirmed presence of a variety of fully differentiated epithelial cells makes this possible. Examining this aspect of invasion may uncover some interesting parasite biology to explain the discrepancies observed between this collagen-supported epithelial model and cell line models. Live cell imaging of parasite behavior using collagen-supported epithelial sheets generated from Cre-reported mice may also help us to understand these early stage interactions (Koshy et al., 2010).

Having determined suitable time points to represent early host cell invasion and parasite replication, we exploited quantitative label-free mass spectrometry to study the host cell response. During early stage invasion, very few significant changes in protein abundance were observed. Of note, STAT1 was decreased in abundance following infection with *T. gondii* RH strain. Previous studies have shown that all three

clonal lineages of *T. gondii* can block STAT1-mediated transcription when cells are infected prior to exposure to IFN-γ (Rosowski et al., 2014).

Although few changes were observed after 4 hour infection, at 40 hour post infection with both *T. gondii* strains we report changes in abundance of proteins involved with lipid metabolism and cell proliferation. *T. gondii* relies on scavenged host molecules for survival. The parasite is unable to synthesis its own cholesterol, and instead uses host cell cholesterol for survival. Moreover, despite being capable of synthesizing parasite lipoic acid, *Toxoplasma* are also reported to scavenge host lipoic acid and growth inhibition has been observed in lipoate-deficient conditions (Crawford et al., 2006).

In both RH and Veg strain infections, we report an increased abundance of APOA1 and APOA4 which are major components of high density lipoproteins and are involved in host cell lipid metabolism pathways (Schaefer et al., 1982). Furthermore, we show that a large proportion of the host cell proteins with significant changes in abundance after 40 hour infection with RH belong to a lipid metabolism network. For example, we also observed an increase in an isoprenoid biosynthesis protein, MVK, which agrees with previous transcriptomic studies that have reported increased transcription of glycolytic and mevalonate enzymes (Blader et al., 2001). Isoprenoids are organic compounds required in cell signalling and survival. Although apicomplexa can synthesis precursors within their apicoplast, *Toxoplasma* are still reliant on importing host cell isoprenoids for survival and so targeting of both host and parasite mevalonate pathways may be an appropriate therapy against apicomplexan infections (Li et al., 2013).

The observation of increased abundance of proteins involved in host lipid metabolism is consistent with nutrient scavenging required for parasite replication and survival, and may represent active modulation of host cell machinery by the parasite to aid its survival. Interestingly, although less proteins were changed in abundance in response to RH strain infection, more proteins involved with lipid metabolism were altered than in Veg infected cells. This finding indicates that the two lineages examined here differ in their ability to modulate host proteome response and deploy different strategies of parasite survival.

At 40 hours infection with Veg, we also observed an increased abundance of host SPINT2, involved with the inhibition of apoptosis. Along with the changes induced in host cell metabolism, the changes in the abundance of these proteins are characteristic of pro-parasite responses that are induced by *T. gondii* to ensure parasite survival (Spear et al., 2006). A number of studies have demonstrated that *T. gondii* modulates host apoptosis through multiple mechanisms, such as; blocking upstream signaling, interfering with caspase 8 processing and function and affecting the balance of pro- and anti-apoptotic BCL-2 family member proteins (Molestina, 2003; Nelson et al., 2008; Shapira et al., 2002; Vutova et al., 2007). This modulation of apoptotic processes is thought to enhance parasite survival.

Furthermore, we observed a modulation of host cell proliferation proteins (VRK1, HIST1H1A and PLRG1) by 40 hours in Veg but not RH infected samples (Kleinridders et al., 2009; Molitor and Traktman, 2013; Schober et al., 2011). Host cell cycle arrest has been previously reported in *T. gondii* infection (Brunet et al., 2008; Molestina et al., 2008; Nelson et al., 2008), however the roles of these three particular proteins in determining the outcome of infection are not yet known.

In addition to these pro-parasite infection induced changes in protein abundance, we also observed an increase in pro-host proteins as a result of infection. These are described as genes or proteins required by the host cell to defend against parasite invasion (Spear et al., 2006). Very few of these proteins were observed to have significant changes in abundance however after 40 hours RH infection we detected an increased abundance of host protection factor DEFA22. Mammalian alpha-defensins are antimicrobial peptides produced by intestinal Paneth cells and play a significant role in innate host defence. *In vivo,* the secretion of alpha-defensins in response to *Toxoplasma* is regulated in a TLR9 dependent manner (Foureau et al., 2010; Menendez et al., 2013). Generally, the alpha-defensins are significant in the tolerance of bacterial invasions (Salzman, 2010; Salzman et al., 2003a), and the modulation of related host cell β-defensin-2 is thought to be a host-evasion mechanism exploited by Type I *Toxoplasma* (Morampudi et al., 2011). However, the role of DEFA22 during *Toxoplasma* infection is not yet understood. Additional studies are required to determine the role of defa22 during *Toxoplasma* invasion events.

Clearly, evaluating host response in this epithelial sheet model by proteomic approaches demonstrates the ability to detect known characteristics of *T. gondii* infection including modulation of host cell lipid metabolism and an inhibition of host cell proliferation. However as discussed previously, the small volume of biological material and variability across wells limits the use of this model to study change in the parasite proteome. As a consequence, almost no changes in parasite protein abundance between the 4 and 40 hour infection time points were detected, making this model in its current form unsuitable for the study of parasite changes during infection. The inclusion of parasite spiked controls are generally included in cell line studies,

however due to the low expected number of protein hits based on pilot studies, this control was not used here.

For this model to produce enough parasite proteins for detection, it is recommended that this technique is up-scaled to larger sized wells from 30µL collagen domes in 48-well plates, to 24- or 12- well plates, and the number of replicates increased to generate a larger volume of experimental material for analysis. Due to time constraints this was not performed within this doctoral project, however the up-scaling of this technique is achievable with some minor adjustments to the culture and infection protocols.

To conclude, this chapter demonstrates the capabilities of this novel model to be used for infection studies, and highlights some improvements that can be implemented to improve this model. We have identified strain specific host proteome modifications, with Veg strain inducing host cell cycle arrest, whereas RH strain up-regulates host cell lipid metabolism. Furthermore, we have identified changes in abundance of DEFA22 that currently has an unknown role during *Toxoplasma* infection.

Chapter 6 – Summary and Forward Perspectives

The understanding of invasion mechanisms of enteric pathogens has primarily been elucidated via the use of *in vitro* and *in vivo* models of infection. However the early stage invasion events exploited by enteric pathogens is poorly understood due to a lack of suitable models. Since the identification of the intestinal stem cell marker, LGR5, 3D organoid models have been successfully established (Barker et al., 2012; Sato et al., 2009). These "mini-gut" models promise to be useful tools to study enteric pathogens.

Several areas of interest would benefit from the use of organoids; the study of Paneth and goblet cell for host defence and the study of early stage enteric protozoal invasion.

Paneth cells and goblet cells play significant roles in gut homeostasis and the regulation of gut microbiota (Farin et al., 2014; Fernandez et al., 2008; Salzman et al., 2010; Schulz and Pabst, 2013), however their specific interactions with enteric pathogens are largely still poorly understood. Due to their naturally low occurrence of these cell types *in vivo* and a lack of *in vitro* alternatives, the directed differentiation of organoid cultures to produce enriched Paneth and goblet cell populations has gained interest (Yin et al., 2014). These enriched organoid cultures have been characterised via molecular and transcriptomic approaches (Yin et al., 2014), however due to reported discrepancies between the transcript level and protein abundance in *vitro*, proteome analysis must also be performed to validate their use for infection studies (Xia et al., 2008).

Although these organoids are attractive tools for the study of host-pathogen interaction, a limiting characteristic of organoid cultures is their restricted luminal access which can only be bypassed via microinjection (Wilson et al., 2014; Zhang et

al., 2014). However, microinjection is not suitable for the establishment of protozoal infections due to challenges with optimizing this technique for larger protozoan parasites. The work presented in this doctoral thesis addresses these current limitations of organoids by demonstrating the amenability of enriched organoid cultures to proteomic analysis, presenting a novel modified protocol for the culture of differentiated and polarized epithelial monolayers, and, demonstrating the suitability of the model for the study of parasite induced host proteome changes via label free mass spectrometry and confocal microscopy.

In chapter 3, the establishment of 3D organoid cultures followed by modulation of differentiation pathways with the use of DAPT in combination of CHIR or IWP-2 drives epithelial cells toward the Paneth cell or goblet cell lineages. Quantitative label-free mass spectrometry was used for the comparative study of Paneth and goblet-enriched organoid proteome compared to non-treated controls. The main challenge concerned with the combination of these techniques was low volume of organoid material for mass spectrometry. By pooling multiple wells of organoid samples, the number of proteins detected were sufficient to perform comparative analysis. Evaluation of enriched Paneth and goblet cell organoid proteomes via label free mass spectrometry has demonstrated the ability to successfully combine these two technologies. These enriched organoids contained an increased abundance of proteins associated with secretory cells, mucus components (in goblet enriched) and MMP7 (in Paneth enriched). We also identified a protein, DNAJC3, that had not previously been described in Paneth cells, but that was increased in abundance in Paneth-skewed cultures, and enriched within Paneth cells by IHC. A potential role for DNAJC3 in Paneth cell differentiation or function deserves further exploration.

The findings here demonstrate the success of using proteomic approaches to study organoid cultures, specifically to investigate the host defence functions of Paneth and goblet cells *in vitro*. The enriched organoid cultures in this 3D conformation are still limited for infection studies due to their restricted luminal access, leading to the work performed in chapter 4.

In chapter 4, the modification of organoid cultures led to the establishment of differentiated and polarized intestinal epithelial monolayers *in vitro* as a method to bypass restricted luminal access of 3D organoid cultures. The effect of organoid modification on cell arrangement, cell differentiation and sheet polarization was addressed. The distribution of Paneth and goblet cells suggest a presence of differentiated micro-domains within the inner regions of the epithelial sheets which may mimic the crypt like domains *in vivo.* Quantification of these cells in epithelial sheets confirms the retention of these populations in the novel model after 8 days in culture, albeit at a lower rate than 3D organoids. The collagen-supported epithelial sheets also showed features consistent with polarization, which is important for the correct localization and function of pathogen recognition receptors *in vivo,* and thus is an important feature of intestinal infection models *in vitro.*

Analysis of organoid models by mass spectrometry revealed a variability in the numbers of proteins detected across different pooled epithelial sheet and 3D organoid samples. The disruption of organoids during passage is non-uniform and the number of crypt buds re-embedded in this process is difficult to standardize. As a result, we faced challenges with seeding the same number of intestinal stem cells per well resulting in discrepancies in the size of epithelial sheets between samples. This in turn impacts the robustness of using mass spectrometry on small samples, as the availability

of biological material is low. Moving forward, the experimental design of infection studies must be carefully considered to ensure sufficient biological material is available for detection of large numbers of proteins by mass spectrometry.

The development of this model benefits the field of infection biology by providing an alternative model to the use of immortalized cell line cultures to study enteric infections. These findings led to the use of this epithelial model to study early stage invasion of murine intestinal epithelial cells by *Toxoplasma gondii*.

In chapter 5, the collagen-supported epithelial model was exploited to study the host response to early invasion and *Toxoplasma gondii* replication. Confocal microscopy was used to examine the progression of infection over time, revealing a lag in host cell invasion and parasite proliferation in comparison to reported observations in cell line infections, likely due to the presence of Paneth and goblet cells that have important roles in host defence. Generally during pilot infection assays, invasion of host cells was low during early stage invasion, resulting in poor detection of parasite proteins during mass spectrometry test runs. Consequently, observations of significant parasite proteome changes were limited within this system without up-scaling the volume of experimental material, however this was not achievable within the time frame of this project. The time and labour required to generate additional experimental replicates and a larger number of wells was a major drawback in this investigation but could be incorporated into future studies. Regardless of this challenge, this study demonstrated that proteins involved in host cell cycling, apoptosis, cell mediated immune response and lipid metabolism were modulated in response to *Toxoplasma* infections. These findings agree with current literature of *T. gondii* invasion (Al-Bajalan et al., 2017; Blader et al., 2001; Butcher et al., 2001; Guiton et al., 2017; Nelson et al., 2008), to

provide supporting evidence for use of label free mass spectrometry with this model to study parasite-induced host proteome changes, even during short term infections. Within this chapter we also show that Veg and RH strain infections elicit distinct modifications in the abundance of host cell proteins.

This doctoral thesis has addressed some of the structural limitations of current intestinal models for the study of enteric pathogens. The development of an *in vitro* epithelial monolayer model widens the scope for future study of host-pathogen interactions by providing an alternative *in vitro* model to cell lines. Moving forward, several lines of investigation could be considered based on the findings reported here.

Firstly, the transmigration of parasites across the host epithelium has not yet been fully described *in vivo* although some mechanisms have been described (Barragan and Sibley, 2002; Weight et al., 2015). The poor suitability of existing models limited the ability to study these early stage events, however, the establishment of the novel epithelial model provides the means to apply live imaging techniques *in vitro* to visualize the parasite invasion of a fully differentiation and polarized epithelial monolayer in real time.

Secondly, during natural infections, bradyzoite and sporozoite forms of *Toxoplasma* are ingested to infect the intestinal epithelium. Due to difficulties obtaining bradyzoite and sporozoite stages of *Toxoplasma*, infections in this thesis were performed with tachyzoite stages that can be cultured *in vitro*. Although current literature has demonstrated that sporozoites and tachyzoites have some shared characteristics and express a core set of proteins for host cell invasion, these proteins are expressed at different abundancies (Guiton et al., 2017), and stage specific parasite proteins have also been identified (Dubey et al., 1998; Schwarz et al., 2005). Therefore expanding

the model to the study of other parasite stages would provide insights into the host-pathogen communication mechanisms during early stage invasion and potentially identify relevant parasite molecular signaling pathways that could be exploited for the development of novel therapeutics.

Thirdly, having determined that 3D organoids can be successfully characterised by mass spectrometry following drug-skewing, this technology could be adapted to generate Paneth or goblet-enriched epithelial sheets with the view to study defence functions in response to microbial stimulation.

Lastly, the development of this model to generate a co-culture model which integrates intraepithelial lymphocytes, or other immune cell populations, would be beneficial for the study of more complex interactions. To date, the development of organoid co-cultures has been limited. A recently study utilized organoid cultures for the expansion of intraepithelial lymphocytes, however an infection model has yet to be developed (Nozaki et al., 2016).

The development of a collagen-supported epithelial sheet in this doctoral thesis has established a novel *in vitro* tool to study *T. gondii* host-pathogen interactions via quantitative label-free mass spectrometry and confocal microscopy, and can be extrapolated to include other enteric pathogens. This thesis has also highlighted several routes of investigation in which further work is required to elucidate the complexities of host-pathogen interaction for the identification of appropriate vaccine targets or signaling pathways for the development of therapeutics.

References

Abreu, M.T., 2010. Toll-like receptor signalling in the intestinal epithelium : how bacterial recognition shapes intestinal function. Nat. Rev. 10, 131–143.

Aikawa, M., Miller, L.H., Johnson, J., Rabbege, J., 1978. Erythrocyte entry by malarial parasites. A moving junction between erythrocyte and parasite. J. Cell Biol. 77, 72–82. https://doi.org/10.1083/jcb.77.1.72

Al-Bajalan, M.M.M., Xia, D., Armstrong, S., Randle, N., Wastling, J.M., 2017. Toxoplasma gondii and Neospora caninum induce different host cell responses at proteome-wide phosphorylation events; a step forward for uncovering the biological differences between these closely related parasites. Parasitol. Res. [Epub ahea. https://doi.org/10.1007/s00436-017-5579-7

Alday, H., Doggett, J., 2017. Drugs in development for toxoplasmosis: advances, challenges, and current status. Drug Des. Devel. Ther. 11, 273–293. https://doi.org/10.2147/DDDT.S60973

Anderson-white, B.R., Ivey, F.D., Cheng, K., Szatanek, T., Lorestani, A., Beckers, C.J., Ferguson, D.J.P., Sahoo, N., Gubbels, J., 2012. A family of intermediate filament-like proteins is sequentially assembled into the cytoskeleton of Toxoplasma gondii. Cell Micrioblogy 13, 18–31. https://doi.org/10.1111/j.1462-5822.2010.01514.x.A

Anderson, J.M., Van Itallie, C.M., 2009. Physiology and function of the tight junction. Cold Spring Harb. Perspect. Biol. 1, 1–16. https://doi.org/10.1101/cshperspect.a002584

Andersson-Rolf, A., Fink, J., Mustata, R.C., Koo, B., 2014. A Video Protocol of Retroviral Infection in Primary Intestinal Organoid Culture. J. Vis. Exp. 90, e51765. https://doi.org/10.3791/51765 (2014).

Arrieta, M.C., Bistritz, L., Meddings, J.B., 2006. Alterations in intestinal permeability. Gut 55, 1512–1520. https://doi.org/10.1136/gut.2005.085373

Augustine, P.C., 2001. Cell: Sporozoite interactions and invasion by apicomplexan parasites of the genus Eimeria. Int. J. Parasitol. 31, 1–8. https://doi.org/10.1016/S0020-7519(00)00150-8

Ayabe, T., Satchell, D.P., Tanabe, H., Wilson, C.L., Hagen, S.J., Ouellette, A.J., Pesendorfer, P., 2002. POST-TRANSLATION MODIFICATION AND DEGRADATION : Activation of Paneth Cell α -Defensins in Mouse Small Intestine Activation of Paneth Cell ␣ -Defensins in Mouse Small Intestine *. https://doi.org/10.1074/jbc.M109410200

Ayabe, T., Satchell, D.P., Wilson, C.L., Parks, W.C., Selsted, M.E., Ouellette, A.J., 2000. Secretion of microbicidal alpha-defensins by intestinal Paneth cells in response to bacteria. Nat. Immunol. 1, 113–8. https://doi.org/10.1038/77783

Bansal, D., Ave, P., Kerneis, S., Frileux, P., Boché, O., Baglin, A.C., Dubost, G., Leguern, A.-S., Prevost, M.-C., Bracha, R., Mirelman, D., Guillén, N., Labruyère, E., 2009. An ex-vivo Human Intestinal Model to Study Entamoeba histolytica Pathogenesis. PLoS Negl. Trop. Dis. 3, e551.

Bargieri, D., Lagal, V., Andenmatten, N., Tardieux, I., Meissner, M., Ménard, R., 2014. Host Cell Invasion by Apicomplexan Parasites: The Junction Conundrum. PLoS

Pathog. 10, 1–9. https://doi.org/10.1371/journal.ppat.1004273

Barker, N., van Es, J.H., Kuipers, J., Kujala, P., van den Born, M., Cozijnsen, M., Haegebarth, A., Korving, J., Begthel, H., Peters, P.J., Clevers, H., 2007. Identification of Stem Cells in Small Intestine and Colon by Marker Gene Lgr5. Nature 449, 1003–1007. https://doi.org/10.1038/nature06196

Barker, N., van Oudenaarden, A., Clevers, H., 2012. Identifying the stem cell of the intestinal crypt: strategies and pitfalls. Cell Stem Cell 11, 452–60. https://doi.org/10.1016/j.stem.2012.09.009

Barragan, A., Brossier, F., Sibley, L.D., 2005. Transepithelial migration of Toxoplasma gondii involves an interaction of intercellular adhesion molecule 1 (ICAM-1) with the parasite adhesin MIC2. Cell. Microbiol. 7, 561–568. https://doi.org/10.1111/j.1462-5822.2005.00486.x

Barragan, A., Sibley, L.D., 2002. Transepithelial migration of Toxoplasma gondii is linked to parasite motility and virulence. J. Exp. Med. 195, 1625–1633. https://doi.org/10.1084/jem.20020258

Beaulieu, J.-F., 1992. Differential expression of the VLA family of integrins along the crypt-villus axis in the human small intestine. J. Cell Sci. 102, 427–36.

Berenreiterová, M., Flegr, J., Kuběna, A.A., Němec, P., 2011. The distribution of Toxoplasma gondii cysts in the brain of a mouse with latent toxoplasmosis: Implications for the behavioral manipulation hypothesis. PLoS One 6, e28925. https://doi.org/10.1371/journal.pone.0028925

Bergstrom, J.H., Berg, K.A., Rodriguez-Pineiro, A.M., Stecher, B., Johansson, M.E. V, Hansson, G.C., 2014. AGR2, an endoplasmic reticulum protein, is secreted into the gastrointestinal mucus. PLoS One 9, e104186. https://doi.org/10.1371/journal.pone.0104186

Bergstrom, K.S.B., Guttman, J.A., Rumi, M., Ma, C., Bouzari, S., Khan, M.A., Gibson, D.L., Vogl, A.W., Vallance, B.A., 2008. Modulation of intestinal goblet cell function during infection by an attaching and effacing bacterial pathogen. Infect. Immun. 76, 796–811. https://doi.org/10.1128/IAI.00093-07

Bergstrom, K.S.B., Kissoon-Singh, V., Gibson, D.L., Ma, C., Montero, M., Sham, H.P., Ryz, N., Huang, T., Velcich, A., Finlay, B.B., Chadee, K., Vallance, B.A., 2010. Muc2 protects against lethal infectious colitis by disassociating pathogenic and commensal bacteria from the colonic mucosa. PLoS Pathog. 6, e1000902. https://doi.org/10.1371/journal.ppat.1000902

Bevins, C.L., Salzman, N.H., 2011. Paneth cells, antimicrobial peptides and maintenance of intestinal homeostasis. Nat. Rev. Microbiol. 9, 356–368. https://doi.org/10.1038/nrmicro2546

Birchenough, G.M.H., Johansson, M.E., Gustafsson, J.K., Bergström, J.H., Hansson, G.C., 2015. New developments in goblet cell mucus secretion and function. Mucosal Immunol. 8, 712–719. https://doi.org/10.1038/mi.2015.32

Birchmeier, W., 2011. Stem cells: Orphan receptors find a home. Nature 476, 287–288. https://doi.org/10.1038/476287a

Black, M.W., Boothroyd, J.C., 2000. Lytic cycle of Toxoplasma gondii. Microbiol. Mol. Biol. Rev. 64, 607–623. https://doi.org/10.1128/MMBR.64.3.607-623.2000

Blader, I.J., Manger, I.D., Boothroyd, J.C., 2001. Microarray Analysis Reveals

Previously Unknown Changes in Toxoplasma gondii-infected Human Cells. J. Biol. Chem. 276, 24223–24231.

Bommer, W., 1969. The life cycle of virulent toxoplasma in cell cultures. Aust. J. Exp. Biol. Med. Sci. 47, 505–12.

Bonapaz, R.D.S., Hermes-Uliana, C., Nascimento Santos, F.D., da Silva, A. V, Araujo, E.J.D.A., SantAna, D.D.M.G., 2010. Effect of Infection with Toxoplasma gondii Oocyts on the Intestinal Wall and the Mysenteric Plexus of Chicken (Gallus gallus). Pesqui. Veterinária Bras. 30, 787–792.

Bondow, B.J., Faber, M.L., Wojta, K.J., Walker, E., Battle, M.A., 2012. E-cadherin is required for intestinal morphogenesis in the mouse. Dev. Biol. 371, 1–12. https://doi.org/10.1016/j.ydbio.2012.06.005.E-cadherin

Booth, C., O'Shea, J., 2002. Chapter 10. Isolation and Culture of Intestinal Epithelial Cells, Culture of Epithelial Cells, Second Edition. Wiley-Liss, Inc. https://doi.org/10.1002/0471221201.ch10

Boucher, L.E., Bosch, J., 2015. The apicomplexan glideosome and adhesins - Structures and function. J. Struct. Biol. 190, 93–114. https://doi.org/10.1016/j.jsb.2015.02.008

Boyle, E.C., Brown, N.F., Finlay, B.B., 2006. Salmonella enterica serovar Typhimurium effectors SopB, SopE, SopE2 and SipA disrupt tight junction structure and function. Cell. Microbiol. 8, 1946–1957. https://doi.org/10.1111/j.1462-5822.2006.00762.x

Briceño, M.P., Nascimento, L.A.C., Nogueira, N.P., Barenco, P.V.C., Ferro, E.A.V., Rezende-Oliveira, K., Goulart, L.R., Alves, P.T., Barbosa, B. de F., Lima, W.R., Silva, N.M., 2016. *Toxoplasma gondii* Infection Promotes Epithelial Barrier Dysfunction of Caco-2 Cells. J. Histochem. Cytochem. 64, 459–469. https://doi.org/10.1369/0022155416656349

Briske-Anderson, M.J., Finley, J.W., Newman, S.M., 1997. The influence of culture time and passage number on the morphological and physiological development of Caco-2 cells. Proc. Soc. Exp. Biol. Med. 214, 248–257. https://doi.org/10.3181/00379727-214-44093

Brunet, J., Pfaff, A.W., Abidi, A., Unoki, M., Nakamura, Y., Guinard, M., Klein, J.P., Candolfi, E., Mousli, M., 2008. Toxoplasma gondii exploits UHRF1 and induces host cell cycle arrest at G2 to enable its proliferation. Cell. Microbiol. 10, 908–920. https://doi.org/10.1111/j.1462-5822.2007.01093.x

Bry, L., Falk, P., Huttner, K., Ouellette, A., Midtvedt, T., Gordon, J.I., 1994. Paneth cell differentiation in the developing intestine of normal and transgenic mice. Proc. Natl. Acad. Sci. U. S. A. 91, 10335–10339. https://doi.org/10.1073/pnas.91.22.10335

Butcher, B.A., Fox, B.A., Rommereim, L.M., Kim, S.G., Maurer, K.J., Yarovinsky, F., Herbert, D.R., Bzik, D.J., Denkers, E.Y., 2011. Toxoplasma gondii rhoptry kinase rop16 activates stat3 and stat6 resulting in cytokine inhibition and arginase-1-dependent growth control. PLoS Pathog. 7, e1002236. https://doi.org/10.1371/journal.ppat.1002236

Butcher, B.A., Kim, L., Johnson, P.F., Denkers, E.Y., 2001. Toxoplasma gondii tachyzoites inhibit proinflammatory cytokine induction in infected macrophages by preventing nuclear translocation of the transcription factor NF-kappa B. J. Immunol. 167, 2193–201. https://doi.org/10.4049/jimmunol.167.4.2193

Cadwell, K., Liu, J.Y., Brown, S.L., Miyoshi, H., Loh, J., Lennerz, J.K., Kishi, C., Kc, W., Carrero, J.A., Hunt, S., Stone, C.D., Brunt, E.M., Xavier, R.J., Sleckman, B.P., Li, E., Mizushima, N., Stappenbeck, T.S., Virgin IV, H.W., 2008. A key role for autophagy and the autophagy gene Atg16l1 in mouse and human intestinal Paneth cells. Nature 456, 259–263.

Carey, K.L., Jongco, A.M., Kim, K., Ward, G.E., 2004. The Toxoplasma gondii Rhoptry Protein ROP4 Is Secreted Into The Parasitophorous Vacuole and Becomes Phosphorylated in Infected Cells. Eukaryot. Cell 3, 1320–1330. https://doi.org/10.1128/EC.3.5.1320

Carneiro, A.C.A.V., Andrade, G.M., Costa, J.G.L., Pinheiro, B.V., Vasconcelos-Santos, D.V., Ferreira, A.M., Su, C., Januário, J.N., Vitor, R.W.A., 2013. Genetic characterization of Toxoplasma gondii revealed highly diverse genotypes for isolates from newborns with congenital toxoplasmosis in Southeastern Brazil. J. Clin. Microbiol. 51, 901–907. https://doi.org/10.1128/JCM.02502-12

Carruthers, V., Boothroyd, J.C., 2007. Pulling together: an integrated model of Toxoplasma cell invasion. Curr. Opin. Microbiol. 10, 83–89.

Carruthers, V.B., Sibley, L.D., 1997. Sequential protein secretion from three distinct organelles of Toxoplasma gondii accompanies invasion of human fibroblasts. Eur. J. Cell Biol. 73, 114–23.

Carruthers, V.B., Suzuki, Y., 2007. Effects of Toxoplasma gondii infection on the brain. Schizophr. Bull. 33, 745–751. https://doi.org/10.1093/schbul/sbm008

Centres for Disease Control and Prevention, 2017. Foodborne Germs and Illnesses | Food Safety | CDC [WWW Document]. Centres Dis. Control Prev. URL https://www.cdc.gov/foodsafety/foodborne-germs.html (accessed 9.18.17).

Chen, B., Dodge, M.E., Tang, W., Lu, J., Ma, Z., Fan, C.-W., Wei, S., Hao, W., Kilgore, J., Williams, N.S., Roth, M.G., Amatruda, J.F., Chen, C., Lum, L., 2009. Small molecule-mediated disruption of Wnt-dependent signaling in tissue regeneration and cancer. Nat Chem Biol 5, 100–107. https://doi.org/10.1038/nchembio.137.Small

Citi, S., Cordenonsi, M., 1998. Tight junction proteins. Biochim. Biophys. Acta 1448, 1–11.

Clevers, H., 2006. Wnt/β-Catenin Signaling in Development and Disease. Cell 127, 469–480. https://doi.org/10.1016/j.cell.2006.10.018

Clevers, H., Nusse, R., 2012. Wnt/β-Catenin Signaling and Disease. Cell 149, 1192–1205.

Clevers, H.C., Bevins, C.L., 2013. Paneth Cells : Maestros of the Small Intestinal Crypts. Annu. Rev. Physiol 75, 289–311. https://doi.org/10.1146/annurev-physiol-030212-183744

Clough, B., Frickel, E.M., 2017. The Toxoplasma Parasitophorous Vacuole: An Evolving Host–Parasite Frontier. Trends Parasitol. 33, 473–488. https://doi.org/10.1016/j.pt.2017.02.007

Coch, R.A., Leube, R.E., 2016. Intermediate Filaments and Polarization in the Intestinal Epithelium. Cells 5, 1–18. https://doi.org/10.3390/cells5030032

Cohen, E., Ophir, I., Shaul, Y.B., 1999. Induced differentiation in HT29, a human colon adenocarcinoma cell line. J. Cell Sci. 2666, 2657–66.

Collazo, C.M., Galán, J.E., 1997. The invasion-associated type-III protein secretion system in Salmonella--a review. Gene 192, 51–59. https://doi.org/S0378-1119(96)00825-6 [pii]

Cook, A.J.C., Gilbert, R.E., Buffolano, W., Zufferey, J., Petersen, E., Jenum, P.A., Foulon, W., Semprini, A.E., Dunn, D.T., 2000. Sources of toxoplasma infection in pregnant women: European multicentre case-control study. European Research Network on Congenital Toxoplasmosis. BMJ 321, 142–147. https://doi.org/10.1136/bmj.321.7254.142

Coombes, J.L., Charsar, B.A., Han, S., Halkias, J., Chan, S.W., Koshy, A.A., Striepen, B., Robey, E.A., 2013. Motile invaded neutrophils in the small intestine of Toxoplasma gondii-infected mice reveal a potential mechanism for parasite spread. Proc. Natl. Acad. Sci. 110, E1913–E1922.

Coopman, P., Djiane, A., 2016. Adherens Junction and E-Cadherin complex regulation by epithelial polarity. Cell. Mol. Life Sci. 73, 3535–3553. https://doi.org/10.1007/s00018-016-2260-8

Crawford, M.J., Thomsen-Zieger, N., Ray, M., Schachtner, J., Roos, D.S., Seeber, F., 2006. Toxoplasma gondii scavenges host-derived lipoic acid despite its de novo synthesis in the apicoplast. EMBO J. 25, 3214–22. https://doi.org/10.1038/sj.emboj.7601189

Da Huang, W., Sherman, B.T., Lempicki, R.A., 2009. Systematic and integrative analysis of large gene lists using DAVID bioinformatics resources. Nat. Protoc. 4, 44–57.

Daugherty, R.L., Serebryannyy, L., Yemelyanov, A., Flozak, A.S., Yu, H.-J., Kosak, S.T., DeLanerolle, P., Gottardi, C.J., 2014. Alpha-catenin is an inhibitor of transcription. Proc. Natl. Acad. Sci. 111, 5260–5265. https://doi.org/10.1073/pnas.1308663111

de Graaf, I.A.M., Olinga, P., de Jager, M.H., Merema, M.T., de Kanter, R., van de Kerkhof, E.G., Groothuis, G.M.M., 2010. Preparation and incubation of precision-cut liver and intestinal slices for application in drug metabolism and toxicity studies. Nat. Protoc. 5, 1540–1551.

de Kanter, R., Tuin, A., van de Kerkhof, E., Martignoni, M., Draaisma, A.L., de Jager, M.H., de Graaf, I.A.M., Meijer, D.K.F., Groothuis, G.M.M., 2005. A new technique for preparing precision-cut slices from small intestine and colon for drug biotransformation studies. J. Pharmacol. Toxicol. Methods 51, 65–72.

de Sousa Abreu, R., Penalva, L.O., Marcotte, E.M., Vogel, C., 2009. Global signatures of protein and mRNA expression levels. Mol. Biosyst. 5, 1512–1526. https://doi.org/10.1039/b908315d

Dehmer, J.J., Garrison, A.P., Speck, K.E., Dekaney, C.M., van Landeghem, L., Sun, X., Henning, S.J., Helmrath, M.A., 2011. Expansion of intestinal epithelial stem cells during murine development. PLoS One 6, e27070. https://doi.org/10.1371/journal.pone.0027070

Deng, L., Feng, J., Broaddus, R.R., 2010. The novel estrogen-induced gene EIG121 regulates autophagy and promotes cell survival under stress. Cell Death Dis. 1, e32. https://doi.org/10.1038/cddis.2010.9

Derouin, F., Piketty, C., Chastang, C., Chau, F., Rouveix, B., Pocidalo, J.J., 1991. Anti-Toxoplasma effects of dapsone alone and combined with pyrimethamine.

Antimicrob. Agents Chemother. 35, 252–255. https://doi.org/10.1128/AAC.35.2.252.Updated

Devenish, J.A., Schiemann, D.A., 1981. HeLa cell infection by Yersinia enterocolitica: Evidence for lack of intracellular multiplication and development of a new procedure for quantitative expression of infectivity. Infect. Immun. 32, 48–55.

Drewry, L.L., Sibley, L.D., 2015. Toxoplasma Actin Is Required for Efficient Host Cell Invasion. MBio 6, e00557-15. https://doi.org/10.1128/mBio.00557-15.Editor

Du, J., An, R., Chen, L., Shen, Y., Chen, Y., Cheng, L., Jiang, Z., Zhang, A., Yu, L., Chu, D., Shen, Y., Luo, Q., Chen, H., Wan, L., Li, M., Xu, X., Shen, J., 2014. Toxoplasma gondii virulence factor rop18 inhibits the host nf-kb pathway by promoting p65 degradation. J. Biol. Chem. 289, 12578–12592. https://doi.org/10.1074/jbc.M113.544718

Dubey, J.P., Gamble, H.R., Hill, D., Sreekumar, C., Romand, S., Thulliez, P., 2002. High Prevalence of Viable Toxoplasma Gondii Infection in Market Weight Pigs From a Farm in Massachusetts. J. Parasitol. 88, 1234–1238. https://doi.org/10.1645/0022-3395(2002)088[1234:HPOVTG]2.0.CO;2

Dubey, J.P., Lindsay, D.S., Speer, C.A., 1998. Structures of Toxoplasma gondii tachyzoites, bradyzoites, and sporozoites and biology and development of tissue cysts. Clin. Microbiol. Rev. 11, 267–299.

Dukes, J.D., Whitley, P., Chalmers, A.D., 2011. The MDCK variety pack: choosing the right strain. BMC Cell Biol. 12, 43. https://doi.org/10.1186/1471-2121-12-43

Dunn, J.D., Ravindran, S., Kim, S.K., Boothroyd, J.C., 2008. The Toxoplasma gondii dense granule protein GRA7 is phosphorylated upon invasion and forms an unexpected association with the rhoptry proteins ROP2 and ROP4. Infect. Immun. 76, 5853–5861. https://doi.org/10.1128/IAI.01667-07

Dupont, C.D., Christian, D.A., Hunter, C.A., 2013. Immune reponse and immunopathology during toxoplasmosis. Semin. Immunopathol. 34, 793–813. https://doi.org/10.1007/s00281-012-0339-3.Immune

Egarter, S., Andenmatten, N., Jackson, A.J., Whitelaw, J.A., Pall, G., Black, J.A., Ferguson, D.J.P., Tardieux, I., Mogilner, A., Meissner, M., 2014. The toxoplasma acto-myoA motor complex is important but not essential for gliding motility and host cell invasion. PLoS One 9, e91819. https://doi.org/10.1371/journal.pone.0091819

El Hajj, H., Lebrun, M., Arold, S.T., Vial, H., Labesse, G., Dubremetz, J.F., 2007. ROP18 is a rhoptry kinase controlling the intracellular proliferation of Toxoplasma gondii. PLoS Pathog. 3, e14. https://doi.org/10.1371/journal.ppat.0030014

Elphick, D.A., Mahida, Y.R., 2005. Paneth cells: their role in innate immunity and inflammatory disease. Gut 54, 1802–9. https://doi.org/10.1136/gut.2005.068601

Erickson, N.A., Nystrom, E.E.L., Mundhenk, L., Arike, L., Glauben, R., Heimesaat, M.M., Fischer, A., Bereswill, S., Birchenough, G.M.H., Gruber, A.D., Johansson, M.E.V., 2015. The goblet cell protein Clca1 (Alias mClca3 or Gob-5) is not required for intestinal mucus synthesis, structure and barrier function in naive or DSS-Challenged Mice. PLoS One 10, 1–22. https://doi.org/10.1371/journal.pone.0131991

Ermund, A., Gustafsson, J.K., Hansson, G.C., Keita, Å. V., 2013a. Mucus properties and goblet cell quantification in mouse, rat and human ileal Peyer's patches. PLoS

One 8, e83688. https://doi.org/10.1371/journal.pone.0083688

Ermund, A., Schutte, A., Johansson, M.E. V, Gustafsson, J.K., Hansson, G.C., 2013b. Studies of mucus in mouse stomach, small intestine, and colon. I. Gastrointestinal mucus layers have different properties depending on location as well as over the Peyer's patches. AJP Gastrointest. Liver Physiol. 305, G341–G347. https://doi.org/10.1152/ajpgi.00046.2013

Es, J.H. Van, Jay, P., Gregorieff, A., Gijn, M.E. Van, Jonkheer, S., Hatzis, P., Thiele, A., Born, M. Van Den, Begthel, H., Brabletz, T., Taketo, M.M., Clevers, H., 2005. Wnt signalling induces maturation of Paneth cells in intestinal crypts. Nat. Cell Biol. 7, 381–386. https://doi.org/10.1038/ncb1240

Esteban-Redondo, I., Innes, E.A., 1997. Toxoplasma gondii infection in sheep and cattle. Comp. Immunol. Microbiol. Infect. Dis. 20, 191–196. https://doi.org/10.1016/S0147-9571(96)00039-2

Fahy, G.M., Guan, N., de Graaf, I.A.M., Tan, Y., Griffin, L., Groothuis, G.M.M., 2013. Cryopreservation of precision-cut tissue slices. Xenobiotica 43, 113–132.

Farin, H.F., Karthaus, W.R., Kujala, P., Rakhshandehroo, M., Schwank, G., Vries, R.G.J., Kalkhoven, E., Nieuwenhuis, E.E.S., Clevers, H., 2014. Paneth cell extrusion and release of antimicrobial products is directly controlled by immune cell-derived IFN-γ. J. Exp. Med. 211, 1393–405. https://doi.org/10.1084/jem.20130753

Farin, H.F., van Es, J.H. Van, Clevers, H., 2012. Redundant Sources of Wnt Regulate Intestinal Stem Cells and Promote Formation of Paneth Cells. Gastroenterology 143, 1518–1529.

Fayer, R., Trout, J.M., Graczyk, T.K., Lewis, E.J., 2000. Prevalence of Cryptosporidium, Giardia and Eimeria infections in post- weaned and adult cattle on three Maryland farms. Vet. Parasitol. 93, 103–112. https://doi.org/10.1016/S0304-4017(00)00356-3

Fernandez, M.-I., Regnault, B., Mulet, C., Tanguy, M., Jay, P., Sansonetti, P.J., Pédron, T., 2008. Maturation of paneth cells induces the refractory state of newborn mice to Shigella infection. J. Immunol. 180, 4924–4930. https://doi.org/180/7/4924 [pii]

Fevr, T., Robine, S., Louvard, D., Huelsken, J., 2007. Wnt/β-Catenin Is Essential for Intestinal Homeostasis and Maintenance of Intestinal Stem Cells. Mol. Cell. Biol. 27, 7551–7559.

Finkbeiner, S.R., Spence, J.R., 2013. A Gutsy Task: Generating Intestinal Tissue from Human Pluripotent Stem Cells. Dig. Dis. Sci. 58, 1176–1184.

Finlay, B.B., Gumbiner, B., Falkow, S., 1988. Penetration of Salmonella through a polarized Madin-Darby canine kidney epithelial cell monolayer. J. Cell Biol. 107, 221–30.

Fletcher, S.M., Stark, D., Harkness, J., Ellis, J., 2012. Enteric protozoa in the developed world: A public health perspective. Clin. Microbiol. Rev. 25, 420–449. https://doi.org/10.1128/CMR.05038-11

Food Standards Agency, 2017. Food alerts [WWW Document]. URL https://www.food.gov.uk/enforcement/alerts?keyword=&page=3 (accessed 3.3.17).

Foureau, D.M., Mielcarz, D.W., Menard, L.C., Schulthess, J., Werts, C., Vasseur, V., Ryffel, B., Kasper, L.H., Buzoni-Gatel, D., 2010. TLR9-dependent induction of

intestinal alpha-defensins by Toxoplasma gondii. J. Immunol. 184, 7022–7029. https://doi.org/10.4049/jimmunol.0901642

France, M.M., Turner, J.R., 2017. The mucosal barrier at a glance. J. Cell Sci. 130, 307–314. https://doi.org/10.1242/jcs.193482

Fuentes, I., Rubio, J.M., Rami, C., Alvar, J., 2001. Genotypic Characterization of Toxoplasma gondii Strains Associated with Human Toxoplasmosis in Spain : Direct Analysis from Clinical Samples. J. Clin. Microbiol. 39, 1566–70. https://doi.org/10.1128/JCM.39.4.1566

Ganz, T., Gabayan, V., Liao, H.I., Liu, L., Oren, A., Graf, T., Cole, A.M., 2003. Increased inflammation in lysozyme M-deficient mice in response to Micrococcus luteus and its peptidoglycan. Blood 101, 2388–2392. https://doi.org/10.1182/blood-2002-07-2319

Garcia-Réguet, N., Lebrun, M., Fourmaux, M.N., Mercereau-Puijalon, O., Mann, T., Beckers, C.J.M., Samyn, B., Van Beeumen, J., Bout, D., Dubremetz, J.F., 2000. The microneme protein MIC3 of Toxoplasma gondii is a secretory adhesin that binds to both the surface of the host cells and the surface of the parasite. Cell. Microbiol. 2, 353–364. https://doi.org/10.1046/j.1462-5822.2000.00064.x

Garcia, M.I., Ghiani, M., Lefort, A., Libert, F., Strollo, S., Vassart, G., 2009. LGR5 deficiency deregulates Wnt signaling and leads to precocious Paneth cell differentiation in the fetal intestine. Dev. Biol. 331, 58–67.

Gatkowska, J., Wieczorek, M., Dziadek, B., Dzitko, K., Dlugonska, H., 2012. Behavioral changes in mice caused by Toxoplasma gondii invasion of brain. Parasitol. Res. 111, 53–58. https://doi.org/10.1007/s00436-011-2800-y

Gatton, M.L., Martin, L.B., Cheng, Q., 2004. Evolution of Resistance to Sulfadoxine-Pyrimethamine in Plasmodium falciparum. Antimicrob. Agents Chemother. 48, 2116–2123. https://doi.org/10.1128/AAC.48.6.2116

Gerbe, F., Legraverend, C., Jay, P., 2012. The intestinal epithelium tuft cells: specification and function. Cell. Mol. life Sci. 69, 2907–17. https://doi.org/10.1007/s00018-012-0984-7

Ghazalpour, A., Bennett, B., Petyuk, V.A., Orozco, L., Hagopian, R., Mungrue, I.N., Farber, C.R., Sinsheimer, J., Kang, H.M., Furlotte, N., Park, C.C., Wen, P.Z., Brewer, H., Weitz, K., Camp, D.G., Pan, C., Yordanova, R., Neuhaus, I., Tilford, C., Siemers, N., Gargalovic, P., Eskin, E., Kirchgessner, T., Smith, D.J., Smith, R.D., Lusis, A.J., 2011. Comparative analysis of proteome and transcriptome variation in mouse. PLoS Genet. 7, e1001393. https://doi.org/10.1371/journal.pgen.1001393

Gianella, R.A., Washington, O., Gemski, P., Formal, S.B., 1973. Invasion of HeLa Cells by Salmonella Typhimurium: A model for Study of Invasiveness of Salmonella. J. Infect. Dis. 128, 69–75.

Gilbert, R., Tan, H.K., Cliffe, S., Guy, E., Stanford, M., 2006. Symptomatic toxoplasma infection due to congenital and postnatally acquired infection. Arch. Dis. Child. 91, 495–8. https://doi.org/10.1136/adc.2005.088385

Gilmore, A.P., 2005. Anoikis. Cell Death Differ. 12, 1473–1477. https://doi.org/10.1038/sj.cdd.4401723

Giuffrida, P., Biancheri, P., MacDonald, T.T., 2014. Proteases and small intestinal barrier function in health and disease. Curr. Opin. Gastroenterol. 30, 1–7.

Glasner, C., Albiger, B., Buist, G., Tambi?? Andra??evi??, A., Canton, R., Carmeli, Y., Friedrich, A.W., Giske, C.G., Glupczynski, Y., Gniadkowski, M., Livermore, D.M., Nordmann, P., Poirel, L., Rossolini, G.M., Seifert, H., Vatopoulos, A., Walsh, T., Woodford, N., Donker, T., Monnet, D.L., Grundmann, H., Koraqi, A., Apfalter, P., Glupczynski, Y., Markovi??, T., Strateva, T., Pieridou-Bagatzouni, D., Hrabak, J., Hammerum, A.M., Coignard, B., Kaase, M., T??th, ??kos, Hardarson, H., Wee Boo, T., Pantosti, A., Raka, L., Balode, A., Miciuleviciene, J., Perrin-Weniger, M., Nestorova, N., Mijovi??, G., Bijlmer, H., Samuelsen, ??rjan, Zabicka, D., Cani??a, M., Kaftandzieva, A., Damian, M., Wiuff, C., Jelesi??, Z., Nik??, M., Pir??, M., Oteo, J., Giske, C.G., Endimiani, A., G??r, D., 2013. Carbapenemase-producing Enterobacteriaceae in Europe: A survey among national experts from 39 countries, February 2013. Eurosurveillance 18, 1–7. https://doi.org/10.2807/1560-7917.ES2013.18.28.20525

Godl, K., Johansson, M.E.V., Lidell, M.E., Mörgelin, M., Karlsson, H., Olson, F.J., Gum, J.R., Kim, Y.S., Hansson, G.C., 2002. The N terminus of the MUC2 mucin forms trimers that are held together within a trypsin-resistant core fragment. J. Biol. Chem. 277, 47248–47256. https://doi.org/10.1074/jbc.M208483200

Gold, D.A., Kaplan, A.D., Lis, A., Bett, G.C.L., Rosowski, E.E., Cirelli, K.M., Bougdour, A., Sidik, S.M., Beck, J.R., Lourido, S., Egea, P.F., Bradley, P.J., Hakimi, M., Rasmusson, R.L., Saeij, J.P.J., 2015. The Toxoplasma dense granule proteins GRA17 and GRA23 mediate the movement of small molecules between the host and the parasitophorous vacuole. Cell Host Microbe 17, 642–652. https://doi.org/10.1016/j.chom.2015.04.003.The

Goldberg, R.F., Austen, W.G., Zhang, X., Munene, G., Mostafa, G., Biswas, S., McCormack, M., Eberlin, K.R., Nguyen, J.T., Tatlidede, H.S., Warren, H.S., Narisawa, S., Millan, J.L., Hodin, R.A., 2008. Intestinal alkaline phosphatase is a gut mucosal defense factor maintained by enteral nutrition. Proc. Natl. Acad. Sci. 105, 3551–3556. https://doi.org/10.1073/pnas.0712140105

Goldman, M., Carver, R.K., Sulzer, A.J., 1958. Reproduction of Toxoplasma gondii by Internal Budding. J. Parasitol. 44, 161–171.

Goodman, A.G., Fornek, J.L., Medigeshi, G.R., Perrone, L.A., Peng, X., Dyer, M.D., Proll, S.C., Knoblaugh, S.E., Carter, V.S., Korth, M.J., Nelson, J.A., Tumpey, T.M., Katze, M.G., 2009. p58IPK: A novel "CIHD" member of the host innate defense response against pathogenic virus infection. PLoS Pathog. 5, e1000438. https://doi.org/10.1371/journal.ppat.1000438

Gopal, R., Birdsell, D., Monroy, F.P., 2011. Regulation of chemokine responses in intestinal epithelial cells by stress and Toxoplasma gondii infection. Parasite Immunol. 33, 12–24. https://doi.org/10.1111/j.1365-3024.2010.01248.x

Gregg, B., Taylor, B.C., John, B., Tait-Wojno, E.D., Girgis, N.M., Miller, N., Wagage, S., Roos, D.S., Hunter, C.A., 2013. Replication and distribution of Toxoplasma gondii in the small intestine after oral infection with tissue cysts. Infect. Immun. 81, 1635–1643.

Grivel, J.-C., Margolis, L., 2009. Use of human tissue explants to study human infectious agents. Nat. Protoc. 4, 256–269.

Grone, H.J., Weber, K., Helmchen, U., Osborn, M., 1986. Villin-a marker of brush border differentiation and cellular origin in human renal cell carcinoma. Am J Pathol 124, 294–302.

Grover, P.K., Hardingham, J.E., Cummins, A.G., 2010. Stem cell marker olfactomedin 4: critical appraisal of its characteristics and role in tumorigenesis. Cancer Metastasis Rev. 29, 761–775.

Gubbels, M.J., Wieffer, M., Striepen, B., 2004. Fluorescent protein tagging in Toxoplasma gondii: Identification of a novel inner membrane complex component conserved among Apicomplexa. Mol. Biochem. Parasitol. 137, 99–110. https://doi.org/10.1016/j.molbiopara.2004.05.007

Guiton, P.S., Sagawa, J.M., Fritz, H.M., Boothroyd, J.C., 2017. An in vitro model of intestinal infection reveals a developmentally regulated transcriptome of Toxoplasma sporozoites and a NFkB-like signature in infected host cells. PLoS One 12, e0173018. https://doi.org/10.1371/journal.pone.0173018

Guo, M., Dubey, J.P., Hill, D., Buchanan, R.L., Gamble, H.R., Jones, J.L., Pradhan, A.K., 2015. Prevalence and risk factors for Toxoplasma gondii infection in meat animals and meat products destined for human consumption. J. Food Prot. 78, 457–476. https://doi.org/10.4315/0362-028X.JFP-14-328

Gutierrez-Aguillar, M., Baines, C.P., 2013. Physiological and pathological roles of mitochondrial SLC25 carriers. J. Biol. Chem. 454, 371–386. https://doi.org/10.1042/BJ20121753.

Guttman, J.A., Finlay, B.B., 2009. Tight junctions as targets of infectious agents. Biochim. Biophys. Acta 1788, 832–841. https://doi.org/10.1016/j.bbamem.2008.10.028

Haegebarth, A., Clevers, H., 2009. Wnt Signaling, Lgr5, and Stem Cells in the Intestine and Skin. Am. J. Pathol. 174, 715–21. https://doi.org/10.2353/ajpath.2009.080758

Hansson, G.C., 2012. Role of mucus layers in gut infection and inflammation. Curr. Opin. Microbiol. 15, 57–62. https://doi.org/10.1016/j.mib.2011.11.002

Haramis, A.G., Begthel, H., van der Born, M., van Es, J., Jonkheer, S., Offerhaus, G.J., Clevers, H., 2004. De Novo Crypt Formation and Juvenile Polyposis on BMP Inhibition in Mouse Intestine. Science (80-.). 303, 1684–1686.

Harding, C.R., Egarter, S., Gow, M., Jiménez-Ruiz, E., Ferguson, D.J.P., Meissner, M., 2016. Gliding Associated Proteins Play Essential Roles during the Formation of the Inner Membrane Complex of Toxoplasma gondii. PLoS Pathog. 12, e1005403. https://doi.org/10.1371/journal.ppat.1005403

He, X.C., Zhang, J., Tong, W.-G., Tawfik, O., Ross, J., Scoville, D.H., Tian, Q., Zeng, X., He, X., Wiedemann, L.M., Mishina, Y., Li, L., 2004. BMP Signaling Inhibits Intestinal Stem Cell Self-Renewal Through Suppression of Wnt-B-Catenin Signaling. Nat. Genet. 36, 1117–21. https://doi.org/10.1038/ng1430

Hehl, A.B., Basso, W.U., Lippuner, C., Ramakrishnan, C., Okoniewski, M., Walker, R.A., Grigg, M.E., Smith, N.C., Deplazes, P., 2015. Asexual expansion of Toxoplasma gondii merozoites is distinct from tachyzoites and entails expression of non-overlapping gene families to attach, invade, and replicate within feline enterocytes. BMC Genomics 16, 66. https://doi.org/10.1186/s12864-015-1225-x

Helenius, T.O., Antman, C.A., Asghar, M.N., Nyström, J.H., Toivola, D.M., 2016. Keratins Are Altered in Intestinal Disease-Related Stress Responses. Cells 5, 35. https://doi.org/10.3390/cells5030035

Herrmann, H., Bär, H., Kreplak, L., Strelkov, S. V., Aebi, U., 2007. Intermediate filaments: from cell architecture to nanomechanics. Nat. Rev. Mol. Cell Biol. 8,

562–573. https://doi.org/10.1038/nrm2197

Hill, D., Dubey, J.P., 2002. Toxoplasma gondii: Transmission, diagnosis, and prevention. Clin. Microbiol. Infect. 8, 634–640. https://doi.org/10.1046/j.1469-0691.2002.00485.x

Hodin, R.A., Shei, A., Meng, S., 1997. Transcriptional activation of the human villin gene during enterocyte differentiation. J. Gastrointest. Surg. 1, 433–8; discussion 438.

Hoelzer, K., Pouillot, R., Dennis, S., 2012. Animal models of listeriosis : a comparative review of the current state of the art and lessons learned. Vet. Res. 43, 18. https://doi.org/10.1186/1297-9716-43-18

Hollenbeck, J.E., 2016. Interaction of the role of Concentrated Animal Feeding Operations (CAFOs) in Emerging Infectious Diseases (EIDS). Infect. Genet. Evol. 38, 44–46. https://doi.org/10.1016/j.meegid.2015.12.002

Holmes, M., Liwak, U., Pricop, I., Wang, X., Tomavo, S., Ananvoranich, S., 2010. Silencing of tachyzoite enolase 2 alters nuclear targeting of bradyzoite enolase 1 in Toxoplasma gondii. Microbes Infect. 12, 19–27. https://doi.org/10.1016/j.micinf.2009.09.010

Howe, D.K., Sibley, L.D., Howe, D.K., Sibley, L.D., 1995. Toxoplasma gondii Comprises of Parasite Three Clonal Lineages : Correlation with Human Disease Genotype. J. Infect. Dis. 172, 1561–6.

Hutchinson, J.P., Wear, a. R., Lambton, S.L., Smith, R.P., Pritchard, G.C., 2011. Survey to determine the seroprevalence of Toxoplasma gondii infection in British sheep flocks. Vet. Rec. 169, 582–587. https://doi.org/10.1136/vr.d5764

Huynh, M.H., Carruthers, V.B., 2006. Toxoplasma MIC2 is a major determinant of invasion and virulence. PLoS Pathog. 2, 0753–0762. https://doi.org/10.1371/journal.ppat.0020084

Ilani, T., Alon, A., Grossman, I., Horowitz, B., Kartvelishvily, E., Cohen, S.R., Fass, D., 2013. A secreted disulfide catalyst controls extracellular matrix composition and function. Science (80-.). 341, 74–6. https://doi.org/10.1126/science.1238279

Itzkovitz, S., Lyubimova, A., Blat, I.C., Maynard, M., van Es, J., Lees, J., Jacks, T., Clevers, H., van Oudenaarden, A., 2011. Single-molecule transcript counting of stem-cell markers in the mouse intestine. Nat. Cell Biol. 14, 106–114. https://doi.org/10.1038/ncb2384

Jabaji, Z., Sears, C.M., Brinkley, G.J., Lei, N.Y., Joshi, V.S., Wang, J., Lewis, M., Stelzner, M., Martín, M.G., Dunn, J.C.Y., 2013. Use of Collagen Gel as an Alternative Extracellular Matrix for the In Vitro and In Vivo Growth of Murine Small Intestinal Epithelium. Tissue Eng. Part C Methods 19, 961–969.

Jacobs, D., Dubremetz, J.F., Loyens, A., Bosman, F., Saman, E., 1998. Identification and heterologous expression of a new dense granule protein (GRA7) from Toxoplasma gondii. Mol. Biochem. Parasitol. 91, 237–249. https://doi.org/10.1016/S0166-6851(97)00204-1

Jankovic, D., Kullberg, M.C., Hieny, S., Caspar, P., Collazo, C.M., Sher, A., 2002. In the absence of IL-12, CD4+ T cell responses to intracellular pathogens fail to default to a Th2 pattern and are host protective in an IL-10-/- setting. Immunity 16, 429–439. https://doi.org/10.1016/S1074-7613(02)00278-9

Jensen, J., Pedersen, E.E., Galante, P., Hald, J., Heller, R.S., Ishibashi, M., Kageyama, R., Guillemot, F., Serup, P., Madsen, O.D., 2000. Control of endodermal endocrine development by Hes-1. Nat. Genet. 24, 36–44. https://doi.org/10.1038/71657

Jewett, T.J., Sibley, L.D., 2003. Aldolase forms a bridge between cell surface adhesins and the actin cytoskeleton in apicomplexan parasites. Mol. Cell 11, 885–894. https://doi.org/10.1016/S1097-2765(03)00113-8

Johansson, M.E. V, Hansson, G.C., 2014. Is the intestinal goblet cell a major immune cell? Cell Host Microbe 15, 251–252. https://doi.org/10.1016/j.chom.2014.02.014

Johansson, M.E. V, Sjövall, H., Hansson, G.C., 2013. The gastrointestinal mucus system in health and disease. Nat. Rev. Gastroenterol. Hepatol. 10, 352–61. https://doi.org/10.1038/nrgastro.2013.35

Jones, E.J., Korcsmaros, T., Carding, S.R., 2016. Mechanisms and pathways of Toxoplasma gondii transepithelial migration. Tissue Barriers 5, e1273865. https://doi.org/10.1080/21688370.2016.1273865

Kaltungo, B.Y., Musa, I.W., 2013. A Review of Some Protozoan Parasites Causing Infertility in Farm Animals. ISRN Trop. Med. 2013, 1–6. https://doi.org/10.1155/2013/782609

Kanda, T., Fujii, H., Tani, T., Murakami, H., Suda, T., Sakai, Y., Ono, T., Hatakeyama, K., 1996. Intestinal fatty acid-binding protein is a useful diagnostic marker for mesenteric infarction in humans. Gastroenterology 110, 339–343. https://doi.org/10.1053/gast.1996.v110.pm8566578

Kang, E., Yousefi, M., Gruenheid, S., 2016. R-Spondins Are Expressed by the Intestinal Stroma and are Differentially Regulated during Citrobacter rodentium- and DSS-Induced Colitis in Mice. PLoS One 11, e0152859. https://doi.org/10.1371/journal.pone.0152859

Kihlstrom, E., 1977. Infection of HeLa cells with Salmonella typhimurium 395 MS and MR10 bacteria. Infect. Immun. 17, 290–295.

Kim, H.J., Ingber, D.E., 2013. Gut-on-a-Chip microenvironment induces human intestinal cells to undergo villus differentiation. Integr. Biol. 5, 1130–40. https://doi.org/10.1039/c3ib40126j

Kim, K., Wagle, M., Tran, K., Zhan, X., Dixon, M.A., Liu, S., Gros, D., Korver, W., Yonkovich, S., Tomasevic, N., Binnerts, M., Abo, A., 2008. R-Spondin Family Members Regulate the Wnt Pathway by a Common Mechanism. Molecuiar Biol. Cell 19, 2588–2596. https://doi.org/10.1091/mbc.E08

Kim, S., Takayama, S., 2015. Organ-on-a-chip and the kidney. Kidney Res. Clin. Pract. 34, 165–169. https://doi.org/10.1016/j.krcp.2015.08.001

Kirk, M.D., Pires, S.M., Black, R.E., Caipo, M., Crump, J.A., Devleesschauwer, B., Dopfer, D., Fazil, A., Fischer-Walker, C.L., Hald, T., Hall, A.J., Keddy, K.H., Lake, R.J., Lanata, C.F., Torgerson, P.R., Havelaar, A.H., Angulo, F.J., 2015. World Health Organization Estimates of the Global and Regional Disease Burden of 22 Foodborne Bacterial, Protozoal, and Viral Diseases, 2010: A Data Synthesis. PLoS Med. 12, e1001921. https://doi.org/10.1371/journal.pmed.1001921

Kleinlützum, D., Weaver, G., Schley, D., 2013. Within-group contact of cattle in dairy barns and the implications for disease transmission. Res. Vet. Sci. 95, 425–429. https://doi.org/10.1016/j.rvsc.2013.06.006

Kleinridders, A., Pogoda, H.-M., Irlenbusch, S., Smyth, N., Koncz, C., Hammerschmidt, M., Brüning, J.C., 2009. PLRG1 is an essential regulator of cell proliferation and apoptosis during vertebrate development and tissue homeostasis. Mol. Cell. Biol. 29, 3173–3185. https://doi.org/10.1128/MCB.01807-08

Klotz, C., Aebischer, T., Seeber, F., 2012. Stem cell-derived cell cultures and organoids for protozoan parasite propagation and studying host–parasite interaction. Int. J. Med. Microbiol. 302, 203–209.

Knight, P.A., Griffith, S.E., Pemberton, A.D., Pate, J.M., Guarneri, L., Anderson, K., Talbot, R.T., Smith, S., Waddington, D., Fell, M., Archibald, A.L., Burgess, S.T., Smith, D.W., Miller, H.R., Morrison, I.W., 2011. Novel gene expression responses in the ovine abomasal mucosa to infection with the gastric nematode Teladorsagia circumcincta. Vet. Res. 42, 78. https://doi.org/10.1186/1297-9716-42-78

Kohbata, S., Yokoyama, H., Yabuuchi, E., 1986. Cytopathogenic effect of Salmonella typhi GIFU 10007 on M cells of murine ileal Peyer's patches in ligated ileal loops: an ultrastructural study. Microbiol Immunol 30, 1225–1237. https://doi.org/10.1111/j.1348-0421.1986.tb03055.x

Kohler, H., Sakaguchi, T., Hurley, B.P., Kase, B.J., Reinecker, H., Mccormick, B.A., Sakaguchi, T., Bp, H., Bj, K., H-c, R., 2007. Salmonella enterica serovar Typhimurium regulates intercellular junction proteins and facilitates transepithelial neutrophil and bacterial passage. Am J Physiol Gastrointest Liver Physiol 293, G178–G187. https://doi.org/10.1152/ajpgi.00535.2006.

Köksal, Z.Ş., Yanik, K., Bilgin, K., Yılmaz, E.M., Hokelek, M., 2016. In vivo efficacy of drugs against Toxoplasma gondii combined with Immunomodulators. Jpn. J. Infect. Dis. 69, 113–117. https://doi.org/10.7883/yoken.JJID.2015.023

Koo, B.-K., Clevers, H., 2014. Stem cells marked by the R-spondin receptor Lgr5. Gastroenterology 147, 289–302.

Koo, B.-K., Stange, D.E., Sato, T., Karthaus, W., Farin, H.F., Huch, M., van Es, J.H., Clevers, H., 2012. Controlled gene expression in primary Lgr5 organoid cultures. Nat. Methods 9, 81–83.

Kopan, R., Ilagan, M.X.G., 2009. The Canonical Notch Signaling Pathway: Unfolding the Activation Mechanism. Cell 137, 216–233. https://doi.org/10.1016/j.cell.2009.03.045

Korinek, V., Barker, N., Moerer, P., van Donselaar, E., Huls, G., Peters, P.J., Clevers, H., 1998. Depletion of Epithelial Stem-Cell Compartments in the Small Intestine of Mice Lacking Tcf-4. Nat. Genet. 19, 379–383. https://doi.org/10.1038/1270

Korth, M.J., Lara, J.C., Moseley, S.L., 1994. Epithelial cell invasion by bovine septicemic Escherichia coli. Infect. Immun. 62, 41–47.

Koshy, A.A., Fouts, A.E., Lodoen, M.B., Alkan, O., M, H., Boothroyd, J.C., 2010. Toxoplasma secreting Cre recombinase for analysis of host parasite interactions. October 7, 307–309. https://doi.org/10.1038/nmeth.1438.Toxoplasma

Kravetz, J.D., Federman, D.G., 2005. Toxoplasmosis in pregnancy. Am. J. Med. 118, 212–216. https://doi.org/10.1016/j.amjmed.2004.08.023

Ku, N.O., Zhou, X., Toivola, D.M., Omary, M.B., 1999. The cytoskeleton of digestive epithelia in health and disease. Am. J. Physiol. 277, G1108–G1137.

Kuhnert, F., Davis, C.R., Wang, H.T., Chu, P., 2004. Essential requirement for Wnt

signaling in proliferation of adult small intestine and colon revealed by adenoviral expression of Dickkopf-1, in: Proceedings of the National Academy of Sciences. pp. 266–271.

Labruyere, E., Lingnau, M., Mercier, C., Sibley, L.D., 1999. Differential membrane targeting of the secretory proteins GRA4 and GRA6 within the parasitophorous vacuole formed by Toxoplasma gondii. Mol. Biochem. Parasitol. 102, 311–324. https://doi.org/10.1016/S0166-6851(99)00092-4

Ladwein, M., Pape, U., Schmidt, D., Schno, M., Fiedler, S., Langbein, L., Franke, W.W., Moldenhauer, G., Zo, M., 2005. The cell – cell adhesion molecule EpCAM interacts directly with the tight junction protein claudin-7 309, 345–357. https://doi.org/10.1016/j.yexcr.2005.06.013

Laliberte, J., Carruthers, V., 2008. Host cell manipulation by the human pathogen Toxoplasma gondii. Cell. Mol. life Sci. 65, 1900–1915. https://doi.org/10.1007/s00018-008-7556-x.Host

Lallès, J.P., 2010. Intestinal alkaline phosphatase: Multiple biological roles in maintenance of intestinal homeostasis and modulation by diet. Nutr. Rev. 68, 323–332. https://doi.org/10.1111/j.1753-4887.2010.00292.x

Larson, L.K.R., Spickler, A.R., 2013. Zoonotic Campylobacteriosis, Center of Food Security and Public Heath.

Law, R.J., Gur-arie, L., Rosenshine, I., Finlay, B.B., 2013. In Vitro and In Vivo Model Systems for Studying Enteropathogenic Escherichia coli Infections. Cold Spring Harb. Perspect. Med. 3, a009977. https://doi.org/10.1101/cshperspect.a009977

Lazzeri, E., Peired, A., Ballerini, L., Lasagni, L., 2012. Adult Stem Cells in Tissue Homeostasis and Disease. Curr. Front. Perspect. Cell Biol. 379–404. https://doi.org/10.5772/33941

Lebrun, M., Michelin, A., El Hajj, H., Poncet, J., Bradley, P.J., Vial, H., Dubremetz, J.F., 2005. The rhoptry neck protein RON4 relocalizes at the moving junction during Toxoplasma gondii invasion. Cell. Microbiol. 7, 1823–1833. https://doi.org/10.1111/j.1462-5822.2005.00646.x

Lee, J.L., Streuli, C.H., 2014. Integrins and epithelial cell polarity. J. Cell Sci. 127, 3217–3225. https://doi.org/10.1242/jcs.146142

Lee, S.H., 2015. Intestinal Permeability Regulation by Tight Junction: Implication on Inflammatory Bowel Diseases. Intest. Res. 13, 11–18. https://doi.org/10.5217/ir.2015.13.1.11

Lenaerts, K., Bouwman, F.G., Lamers, W.H., Renes, J., Mariman, E.C., 2007. Comparative proteomic analysis of cell lines and scrapings of the human intestinal epithelium. BMC Genomics 8, 91. https://doi.org/10.1186/1471-2164-8-91

Li, Z.H., Ramakrishnan, S., Striepen, B., Moreno, S.N.J., 2013. Toxoplasma gondii Relies on Both Host and Parasite Isoprenoids and Can Be Rendered Sensitive to Atorvastatin. PLoS Pathog. 9, e1003665. https://doi.org/10.1371/journal.ppat.1003665

Limon, G., Beauvais, W., Dadios, N., Villena, I., Cockle, C., Blaga, R., Guitian, J., 2017. Cross-Sectional Study of Toxoplasma gondii Infection in Pig Farms in England. Foodborne Pathog. Dis. 14, 269–281. https://doi.org/10.1089/fpd.2016.2197

Lisitsyn, N. a, Bukurova, Y. a, Nikitina, I.G., Krasnov, G.S., Sykulev, Y., Beresten, S.F., 2012. Enteric alpha defensins in norm and pathology. Ann. Clin. Microbiol. Antimicrob. 11, 1–6. https://doi.org/10.1186/1476-0711-11-1

Liu, Q., Singla, L.D., Zhou, H., 2012. Vaccines against Toxoplasma gondii. Status, challenges and future directions. Hum. Vaccin. Immunother. 8, 1305–1308.

Logan, C.Y., Nusse, R., 2004. The Wnt Signaling Pathway in Development and Disease. Annu. Rev. Cell Dev. Biol. 20, 781–810.

Loonen, L.M., Stolte, E.H., Jaklofsky, M.T., Meijerink, M., Dekker, J., van Baarlen, P., Wells, J.M., 2014. REG3γ-deficient mice have altered mucus distribution and increased mucosal inflammatory responses to the microbiota and enteric pathogens in the ileum. Mucosal Immunol. 7, 939–947. https://doi.org/10.1038/mi.2013.109

Lu, S., Gough, A.W., Bobrowski, W.F., Stewart, B.H., 1996. Transport properties are not altered across Caco-2 cells with heightened TEER despite underlying physiological and ultrastructural changes. J. Pharm. Sci. 85, 270–273. https://doi.org/10.1021/js950269u

Lupindu, A.M., Dalsgaard, A., Msoffe, P.L.M., Ngowi, H.A., Mtambo, M.M., Olsen, J.E., 2015. Transmission of antibiotic-resistant Escherichia coli between cattle, humans and the environment in peri-urban livestock keeping communities in Morogoro, Tanzania. Prev. Vet. Med. 118, 477–482. https://doi.org/10.1016/j.prevetmed.2014.12.005

Lyons, R.E., McLeod, R., Roberts, C.W., 2002. Toxoplasma gondii tachyzoite–bradyzoite interconversion. Trends Parasitol. 18, 198–201. https://doi.org/10.1016/S1471-4922(02)02248-1

Macartney, K.K., Baumgart, D.C., Carding, S.R., Brubaker, J.O., Offit, P. a, 2000. Primary murine small intestinal epithelial cells, maintained in long-term culture, are susceptible to rotavirus infection. J. Virol. 74, 5597–5603. https://doi.org/10.1128/JVI.74.12.5597-5603.2000

MacCallum, A.J., Harris, D., Haddock, G., Everest, P.H., 2006. Campylobacter jejuni-infected human epithelial cell lines vary in their ability to secrete interleukin-8 compared to in vitro-infected primary human intestinal tissue. Microbiology 152, 3661–3665. https://doi.org/10.1099/mic.0.29234-0

Mahé, M.M., Aihara, E., Schumacher, M. a, Zavros, Y., Marshall, H., Helmrath, M. a, Sato, T., Shroyer, N.F., 2014. Establishment of gastrointestinal epithelial organoids. Curr. Protoc. Mouse Biol. 217–240. https://doi.org/10.1002/9780470942390.mo130179.Establishment

Mandell, K.J., Parkos, C.A., 2005. The JAM family of proteins. Adv. Drug Deliv. Rev. 57, 857–867. https://doi.org/10.1016/j.addr.2005.01.005

Martin, H.M., Campbell, B.J., Hart, C.A., Mpofu, C., Nayar, M., Singh, R., Englyst, H., Williams, H.F., Rhodes, J.M., 2004. Enhanced Escherichia coli adherence and invasion in Crohn's disease and colon cancer. Gastroenterology 127, 80–93.

McAuley, J.B., 2014. Congenital toxoplasmosis. J. Pediatric Infect. Dis. Soc. 3, 30–35. https://doi.org/10.1093/jpids/piu077

McBerry, C., Egan, C.E., Rani, R., Yang, Ny., Wu, D., Boespflug, N., Boon, L., Butcher, B., Mirpuri, J., Hogan, S.P., Denkers, E.Y., Aliberti, J., Herbert, D.R., 2012. Trefoil factor 2 negatively regulates Type 1 immunity agaisnt Toxoplasma gondii. J Immunol 189, 3078–3084. https://doi.org/10.4049/jimmunol.1103374

McCool, D.J., Marcon, M.A., Forstner, J.F., Forstner, G.G., 1990. The T84 human colonic adenocarcinoma cell line produces mucin in culture and releases it in response to various secretagogues. Biochem. J. 267, 491–500.

Menendez, A., Willing, B.P., Montero, M., Wlodarska, M., So, C.C., Bhinder, G., Vallance, B.A., Finlay, B.B., 2013. Bacterial stimulation of the TLR-MyD88 pathway modulates the homeostatic expression of ileal paneth cell a-defensins. J. Innate Immun. 5, 39–49. https://doi.org/10.1159/000341630

Mennechet, F.J.D., Kasper, L.H., Rachinel, N., Li, W., Vandewalle, A., Buzoni-gatel, D., 2002. Lamina Propria CD4 + T Lymphocytes Synergize with Murine Intestinal Epithelial Cells to Enhance Proinflammatory Response Against an Intracellular Pathogen. J. Immunol. 168, 2988–2996. https://doi.org/10.4049/jimmunol.168.6.2988

Mercier, C., Cesbron-Delauw, M.F., 2015. Toxoplasma secretory granules : one population or more ? Trends Parasitol. 31, 1–12. https://doi.org/10.1016/j.pt.2014.12.002

Mercurio, A.M., Rabinovitz, I., Shaw, L.M., 2001. The alpha 6 beta 4 integrin and epithelial cell migration. Curr. Opin. Cell Biol. 13, 541–5. https://doi.org/10.1016/S0955-0674(00)00249-0

Mi, H., Muruganujan, A., Casagrande, J.T., Thomas, P.D., 2013. Large-scale gene function analysis with the PANTHER classification system. Nat. Protoc. 8, 1551–66. https://doi.org/10.1038/nprot.2013.092

Milano, J., McKay, J., Dagenais, C., Foster-Brown, L., Pognan, F., Gadient, R., Jacobs, R.T., Zacco, A., Greenberg, B., Ciaccio, P.J., 2004. Modulation of notch processing by gamma-secretase inhibitors causes intestinal goblet cell metaplasia and induction of genes known to specify gut secretory lineage differentiation. Toxicol. Sci. 82, 341–58. https://doi.org/10.1093/toxsci/kfh254

Mital, J., Meissner, M., Soldati, D., Ward, G.E., 2005. Conditional Expression of Toxoplasma gondii Apical Membrane Antigel-1 (TgAMA1) Demonstrates that TgAMA1 Plays a Critical Role in Host Cell Invasion. Mol. Biol. Cell 16, 4341–4349.

Miyazono, K., Maeda, S., Imamura, T., 2005. BMP Receptor Signaling: Transcriptional Targets, Regulation of Signals, and Signaling Cross-Talk. Cytokine Growth Factor Rev. 16, 251–263. https://doi.org/10.1016/j.cytogfr.2005.01.009

Moal, V.L.-L., Servin, A.L., 2006. The Front Line of Eneteric Host Defense against Unwelcome Intrusion of Harmful Microorgansims: Mucins, Antimicrobial Peptides and Microbiota. Clin. Microbiol. Rev. 19, 315–337. https://doi.org/10.1128/CMR.19.2.315

Molestina, R.E., 2003. Activation of NF- B by Toxoplasma gondii correlates with increased expression of antiapoptotic genes and localization of phosphorylated I B to the parasitophorous vacuole membrane. J. Cell Sci. 116, 4359–4371. https://doi.org/10.1242/jcs.00683

Molestina, R.E., El-guendy, N., Sinai, A.P., 2008. Infection with Toxoplasma gondii results in dysregulation of the host cell cycle. Cell. Microbiol. 10, 1153–1165. https://doi.org/10.1111/j.1462-5822.2008.01117.x

Molitor, T.P., Traktman, P., 2013. Molecular genetic analysis of VRK1 in mammary epithelial cells: depletion slows proliferation in vitro and tumor growth and

metastasis in vivo. Oncogenesis 2, e48. https://doi.org/10.1038/oncsis.2013.11

Montgomery, R.K., Breault, D.T., 2008. Small intestinal stem cell markers. J. Anat. 213, 52–8. https://doi.org/10.1111/j.1469-7580.2008.00925.x

Montoya, J.G., Liesenfeld, O., 2004. Toxoplasmosis. Lancet 363, 1965–1976. https://doi.org/10.1016/S0140-6736(04)16412-X

Moon, C., Vandussen, K.L., Miyoshi, H., Stappenbeck, T.S., 2013. Development of a primary mouse intestinal epithelial cell monolayer culture system to evaluate factors that modulate IgA transcytosis 7, 818–828. https://doi.org/10.1038/mi.2013.98

Morampudi, V., Braun, M.Y., D'Souza, S., 2011. Modulation of early ??-defensin-2 production as a mechanism developed by type I Toxoplasma gondii to evade human intestinal immunity. Infect. Immun. 79, 2043–2050. https://doi.org/10.1128/IAI.01086-10

Morrissette, N.S., Sibley, L.D., 2002. Cytoskeleton of apicomplexan parasites. Microbiol. Mol. Biol. Rev. 66, 21–38. https://doi.org/10.1128/MMBR.66.1.21

MSD Animal Health, 2017. Toxovax® - Product Overview [WWW Document]. URL http://www.msd-animal-health.co.nz/products/toxovax/020_product-overview.aspx (accessed 9.19.17).

Munday, B.L., Dubey, J.P., 1986. Serology of experimental toxoplasmosis in pregnant ewes and their foetuses. Aust. Vet. J. 63, 353–355. https://doi.org/10.1111/j.1751-0813.1986.tb02894.x

Muza-Moons, M.M., Schneeberger, E.E., Hecht, G.A., 2004. Enteropathogenic Escherichia coli infection leads to appearance of aberrant tight junctions strands in the lateral membrane of intestinal epithelial cells. Cell. Microbiol. 6, 783–793. https://doi.org/10.1111/j.1462-5822.2004.00404.x

Nakamura, T., Tsuchiya, K., Watanabe, M., 2007. Crosstalk Between Wnt and Notch Signal ing in Intestinal Epithelial Cell Fate Decision. J. Gastroenterol. 42, 705–10. https://doi.org/10.1007/s00535-007-2087-z

Nakase, Y., Hagiwara, A., Nakamura, T., Kin, S., Nakashima, S., Yoshikawa, T., Fukuda, K., Kuriu, Y., Miyagawa, K., Sakakura, C., Otsuji, E., Shimizu, Y., Ikada, Y., Yamagishi, H., 2006. Tissue Engineering of Small Intestinal Tissue Using Collagen Sponge Scaffolds Seeded with Smooth Muscle Cells. Tissue Eng. 12, 403–412.

Nataro, J.P., Hicks, S., Phillips, A.D., Vial, P.A., Sears, C.L., Nataro, J.P., Hicks, S., Phillips, A.D., Vial, P.A., 1996. T84 cells in culture as a model for enteroaggregative Escherichia coli T84 Cells in Culture as a Model for Enteroaggregative Escherichia coli Pathogenesis 64, 4761–4768.

Neal, J.T., Kuo, C.J., 2016. Organoids as Models for Neoplastic Transformation. Annu. Rev. Pathol. Mech. Dis 11, 199–220. https://doi.org/10.1146/annurev-pathol-012615-044249

Nelson, M.M., Jones, A.R., Carmen, J.C., Sinai, A.P., Burchmore, R., Wastling, J.M., 2008. Modulation of the host cell proteome by the intracellular apicomplexan parasite Toxoplasma gondii. Infect. Immun. 76, 828–844. https://doi.org/10.1128/IAI.01115-07

NHS, 2015. Toxoplasmosis - NHS Choices.

Nichols, G.L., 2000. Food-borne protozoa. Br. Med. Bull. 55, 209–235.

Nozaki, K., Mochizuki, W., Matsumoto, Y., Matsumoto, T., Fukuda, M., Mizutani, T., Watanabe, M., Nakamura, T., 2016. Co-culture with intestinal epithelial organoids allows efficient expansion and motility analysis of intraepithelial lymphocytes. J. Gastroenterol. 51, 206–213. https://doi.org/10.1007/s00535-016-1170-8

Oliveros, J.C., 2007. Venny. An interactive tool for comparing lists with Venn diagrams [WWW Document]. URL http://bioinfogp.cnb.csic.es/tools/venny/index.html

Ong, Y.C., Reese, M.L., Boothroyd, J.C., 2010. Toxoplasma Rhoptry Protein 16 (ROP16) subverts host function by direct tyrosine phosphorylation of STAT6. J. Biol. Chem. 285, 28731–28740. https://doi.org/10.1074/jbc.M110.112359

Ormestad, M., 2006. Foxf1 and Foxf2 control murine gut development by limiting mesenchymal Wnt signaling and promoting extracellular matrix production. Development 133, 833–843.

Oshima, T., Miwa, H., 2016. Gastrointestinal mucosal barrier function and diseases. J. Gastroenterol. 51, 768–778. https://doi.org/10.1007/s00535-016-1207-z

Palmieri, F., 2004. The mitochondrial transporter family (SLC25): Physiological and pathological implications. Pflugers Arch. Eur. J. Physiol. 447, 689–709. https://doi.org/10.1007/s00424-003-1099-7

Park, S.-W., Zhen, G., Verhaeghe, C., Nakagami, Y., Nguyenvu, L.T., Barczak, A.J., Killeen, N., Erle, D.J., 2009. The protein disulfide isomerase AGR2 is essential for production of intestinal mucus. Proc. Natl. Acad. Sci. 106, 6950–6955. https://doi.org/10.1073/pnas.0808722106

Peeters, T., Vantrappen, G., 1975. The Paneth cell: a source of intestinal lysozyme. Gut 16, 553–558. https://doi.org/10.1136/gut.16.7.553

Peignon, G., Durand, A., Cacheux, W., Ayrault, O., Terris, B., Laurent-Puig, P., Shroyer, N.F., Van Seuningen, I., Honjo, T., Perret, C., Romagnolo, B., 2011. Complex interplay between β-catenin signalling and Notch effectors in intestinal tumorigenesis. Gut 60, 166–76. https://doi.org/10.1136/gut.2009.204719

Pelaseyed, T., Berstrom, J.H., Gustafsson, J.K., Ermund, A., Birchenough, G.M.H., Schutte, A., Post, S., Svensson, F., Rodriguez-Pineiro, A.M., Nystrom, E.E.L., Wising, C., Johansson, M.E. V, Hansson, G.C., 2014. The mucus and mucins of the goblet cells and enterocytes provide the first defense line of the gastrointestinal tract and interact with the immune system 8–20.

Pickering, L.K., 2004. Antimicrobial resistance among enteric pathogens. Semin. Pediatr. Infect. Dis. 15, 71–77. https://doi.org/10.1053/j.spid.2004.01.009

Pin, C., Watson, A.J.M., Carding, S.R., 2012. Modelling the spatio-temporal cell dynamics reveals novel insights on cell differentiation and proliferation in the small intestinal crypt. PLoS One 7, e37115. https://doi.org/10.1371/journal.pone.0037115

Pizarro-Cerda, J., Kuhbacher, A., Cossart, P., 2015. Entry of Listeria monocytogenes in Mammalian Epithelial Cells: An Updated Review. Cold Spring Harb. Perspect. Med. 2, a010009.

Powell, R.H., Behnke, M.S., 2017. WRN conditioned media is sufficient for in vitro propagation of intestinal organoids from large farm and small companion animals. Biol. Open 6, 698–705.

Quinlan, J.M., Yu, W.-Y., Hornsey, M. a, Tosh, D., Slack, J.M.W., 2006. In vitro culture of embryonic mouse intestinal epithelium: cell differentiation and introduction of reporter genes. BMC Dev. Biol. 6, 24. https://doi.org/10.1186/1471-213X-6-24

Ramadoss, P., Abraham, B.J., Tsai, L., Zhou, Y., Costa-E-Sousa, R.H., Ye, F., Bilban, M., Zhao, K., Hollenberg, A.N., 2014. Novel mechanism of positive versus negative regulation by thyroid hormone receptor β1 (TRβ1) identified by genome-wide profiling of binding sites in mouse liver. J. Biol. Chem. 289, 1313–1328. https://doi.org/10.1074/jbc.M113.521450

Ramesh, N., Mortazavi, S., Unniappan, S., 2015. Nesfatin-1 stimulates glucagon-like peptide-1 and glucose-dependent insulinotropic polypeptide secretion from STC-1 cells in vitro. Biochem. Biophys. Res. Commun. 462, 124–130. https://doi.org/10.1016/j.bbrc.2015.04.100

Ranga, A., Gjorevski, N., Lutolf, M.P., 2014. Drug discovery through stem cell-based organoid models. Adv. Drug Deliv. Rev. 69–70, 19–28.

Rees, J.R., Pannier, A., Mcnees, A., Shallow, S., Angulo, F.J., Vugia, D.J., 2004. Persistent Diarrhea , Arthritis , and Other Complications of Enteric Infections : A Pilot Survey Based on California FoodNet Surveillance , 1998 – 1999 3756, 1998–1999.

Ren, H.J., Cui, J., Wang, Z.Q., Liu, R.D., 2011. Normal mouse intestinal epithelial cells as a model for the in vitro invasion of trichinella spiralis infective larvae. PLoS One 6, e27010. https://doi.org/10.1371/journal.pone.0027010

Revenu, C., Ubelmann, F., Hurbain, I., El-Marjou, F., Dingli, F., Loew, D., Delacour, D., Gilet, J., Brot-Laroche, E., Rivero, F., Louvard, D., Robine, S., 2012. A new role for the architecture of microvillar actin bundles in apical retention of membrane proteins. Mol. Biol. Cell 23, 324–336. https://doi.org/10.1091/mbc.E11-09-0765

Robert-Gangneux, F., Dardé, M.L., 2012. Epidemiology of and diagnostic strategies for toxoplasmosis. Clin. Microbiol. Rev. 25, 264–296. https://doi.org/10.1128/CMR.05013-11

Roberts, C.L., Keita, A. V, Duncan, S.H., O'Kennedy, N., Söderholm, J.D., Rhodes, J.M., Campbell, B.J., Soderholm, J.D., 2010. Translocation of Crohn's disease Escherichia coli across M-cells: contrasting effects of soluble plant fibres and emulsifiers. Gut 59, 1331–1339. https://doi.org/10.1136/gut.2009.195370

Rodriguez-Pineiro, A.M., Bergström, J.H., Ermund, A., Gustafsson, J.K., Schutte, A., Johansson, M.E.V., Hansson, G.C., 2013. Studies of mucus in mouse stomach, small intestine, and colon. II. Gastrointestinal mucus proteome reveals Muc2 and Muc5ac accompanied by a set of core proteins. Am. J. Physiol. Gastrointest. Liver Physiol. 305, G348-56. https://doi.org/10.1152/ajpgi.00047.2013

Roobol, A., Roobol, J., Bastide, A., Knight, J.R.P., Willis, A.E., Smales, C.M., 2015. p58IPK is an inhibitor of the eIF2α kinase GCN2 and its localization and expression underpin protein synthesis and ER processing capacity. Biochem. J. 465, 213–25. https://doi.org/10.1042/BJ20140852

Rosowski, E.E., Lu, D., Julien, L., Rodda, L., Gaiser, R.A., Jensen, K.D.C., Saeij, J.P.J., 2011. Strain-specific activation of the NF-κB pathway by GRA15, a novel *Toxoplasma gondii* dense granule protein. J. Exp. Med. 208, 195–212. https://doi.org/10.1084/jem.20100717

Rosowski, E.E., Nguyen, Q.P., Camejo, A., Spooner, E., Saeija, J.P.J., 2014. Toxoplasma gondii inhibits gamma interferon (IFN-γ)-and IFN-β-induced host cell STAT1 transcriptional activity by increasing the association of STAT1 with DNA. Infect. Immun. 82, 706–719. https://doi.org/10.1128/IAI.01291-13

Rothfuchs, A.G., Trumstedt, C., Mattei, F., Schiavoni, G., Hidmark, A., Wigzell, H., Rottenberg, M.E., 2006. STAT1 Regulates IFN- - and IFN- -Dependent Control of Infection with Chlamydia pneumoniae by Nonhemopoietic Cells. J. Immunol. 176, 6982–6990. https://doi.org/10.4049/jimmunol.176.11.6982

Roussa, E., Wittschen, P., Wolff, N. a, Torchalski, B., Gruber, A.D., Thévenod, F., 2010. Cellular distribution and subcellular localization of mCLCA1/2 in murine gastrointestinal epithelia. J. Histochem. Cytochem. 58, 653–68. https://doi.org/10.1369/jhc.2010.955211

Roxas, J.L., Koutsouris, A., Bellmeyer, A., Tesfay, S., Royan, S., Falzari, K., Harris, A., Cheng, H., Rhee, K.J., Hecht, G., 2010. Enterohemorrhagic E. coli alters murine intestinal epithelial tight junction protein expression and barrier function in a Shiga toxin independent manner. Lab. Invest. 90, 1152–68. https://doi.org/10.1038/labinvest.2010.91

Rusu, D., Loret, S., Peulen, O., Mainil, J., Dandrifosse, G., 2005. Immunochemical, biomolecular and biochemical characterization of bovine epithelial intestinal primocultures. BMC Cell Biol. 6, 42. https://doi.org/10.1186/1471-2121-6-42

Saeij, J.P.J., Boyle, J.P., Boothroyd, J.C., 2005. Differences among the three major strains of Toxoplasma gondii and their specific interactions with the infected host. Trends Parasitol. 21, 476–481.

Salzman, N.H., 2010. Paneth cell defensins and the regulation of the microbiome: détente at mucosal surfaces. Gut Microbes 1, 401–6. https://doi.org/10.4161/gmic.1.6.14076

Salzman, N.H., Chou, M.M., de Jong, H., Liu, L., Porter, E.M., Paterson, Y., 2003a. Enteric salmonella infection inhibits Paneth cell antimicrobial peptide expression. Infect Immun 71, 1109–1115. https://doi.org/10.1128/IAI.71.3.1109

Salzman, N.H., Ghosh, D., Huttner, K., Paterson, Y., Bevins, C., 2003b. Protection against enteric salmonellosis in transgenic mice expressing a human intestinal defensin. Nature 422, 522–526. https://doi.org/10.1038/nature01520

Salzman, N.H., Hung, K., Haribhai, D., Chu, H., Karlsson-Sjöberg, J., Amir, E., Teggatz, P., Barman, M., Hayward, M., Eastwood, D., Stoel, M., Zhou, Y., Sodergren, E., Weinstock, G.M., Bevins, C.L., Williams, C.B., Bos, N. a, 2010. Enteric defensins are essential regulators of intestinal microbial ecology. Nat. Immunol. 11, 76–83. https://doi.org/10.1038/ni.1825

Sambuy, Y., De Angelis, I., Ranaldi, G., Scarino, M.L., Stammati, a., Zucco, F., 2005. The Caco-2 cell line as a model of the intestinal barrier: Influence of cell and culture-related factors on Caco-2 cell functional characteristics. Cell Biol. Toxicol. 21, 1–26. https://doi.org/10.1007/s10565-005-0085-6

Saotome, I., Curto, M., McClatchey, A.I., 2004. Ezrin is essential for epithelial organization and villus morphogenesis in the developing intestine. Dev. Cell 6, 855–864. https://doi.org/10.1016/j.devcel.2004.05.007

Sato, T., Es, J.H., Snippert, H.J., Stange, D.E., Vries, R.G., Born, M., Barker, N., Shroyer, N.F., Wetering, M., Clevers, H., van Es, J.H., van den Born, M., van de

Wetering, M., 2011. Paneth cells constitute the niche for Lgr5 stem cells in intestinal crypts. Nature 469, 415–418.

Sato, T., Stange, D.E., Ferrante, M., Vries, R.G.J., van Es, J.H., van den Brink, S., van Houdt, W.J., Pronk, A., van Gorp, J., Siersema, P.D., Clevers, H., 2011. Long-term Expansion of Epithelial Organoids From Human Colon, Adenoma, Adenocarcinoma, and Barrett's Epithelium. Gastroenterology 141, 1762–1772.

Sato, T., Vries, R.G., Snippert, H.J., Wetering, M., Barker, N., Stange, D.E., Es, J.H., Abo, A., Kujala, P., Peters, P.J., Clevers, H., van de Wetering, M., van Es, J.H., 2009. Single Lgr5 stem cells build crypt-villus structures in vitro without a mesenchymal niche. Nature 459, 262–265.

Saxena, K., Blutt, S.E., Ettayebi, K., Zeng, X., Broughman, J.R., Crawford, S.E., Karandikar, U.C., Sastri, N.P., Conner, M.E., Opekun, A.R., Graham, D.Y., Qureshi, W., Sherman, V., Foulke-abel, J., In, J., Kovbasnjuk, O., Zachos, N.C., Donowitz, M., Estes, K., 2016. Human Intestinal Enteroids : a New Model To Study Human Rotavirus Infection , Host Restriction , and Pathophysiology. J. Virol 90, 43–56. https://doi.org/10.1128/JVI.01930-15.Editor

Schaefer, E.J., Zech, L.A., Jenkins, L.L., Bronzert, T.J., Rubalcaba, E.A., Lindgren, F.T., Aamodt, R.L., Brewer, H.B., 1982. Human apolipoprotein A-l and A 4 metabolism. J. Lipid Res. 23, 850–62.

Schober, C.S., Aydiner, F., Booth, C.J., Seli, E., Reinke, V., 2011. The kinase VRK1 is required for normal meiotic progression in mammalian oogenesis. Mech. Dev. 128, 178–90. https://doi.org/10.1016/j.mod.2011.01.004

Schonhoff, S.E., Giel-Moloney, M., Leiter, A.B., 2004. Minireview: Development and differentiation of gut endocrine cells. Endocrinology 145, 2639–44. https://doi.org/10.1210/en.2004-0051

Schulz, O., Pabst, O., 2013. Antigen sampling in the small intestine. Trends Immunol. 34, 155–61. https://doi.org/10.1016/j.it.2012.09.006

Schwarz, J.A., Fouts, A.E., Cummings, C.A., Ferguson, D.J.P., Boothroyd, J.C., 2005. A novel rhoptry protein in Toxoplasma gondii bradyzoites and merozoites. Mol. Biochem. Parasitol. 144, 159–166.

Senarathna, G., Crowe, A., 2015. The influence of passage number for Caco2 cell models when evaluating P-gp mediated drug transport. Pharmazie 70, 798–803. https://doi.org/10.1691/ph.2015.5106

Shapira, S., Speirs, K., Gerstein, a, Caamano, J., Hunter, C. a, 2002. Suppression of NF-kappaB activation by infection with Toxoplasma gondii. J. Infect. Dis. 185 Suppl, S66–S72. https://doi.org/10.1086/338000

Shinomiya, H., 2012. Plastin family of actin-bundling proteins: its functions in leukocytes, neurons, intestines, and cancer. Int. J. Cell Biol. 2012, 213492. https://doi.org/10.1155/2012/213492

Siissalo, S., Laitinen, L., Koljonen, M., Vellonen, K.S., Kortejärvi, H., Urtti, A., Hirvonen, J., Kaukonen, A.M., 2007. Effect of cell differentiation and passage number on the expression of efflux proteins in wild type and vinblastine-induced Caco-2 cell lines. Eur. J. Pharm. Biopharm. 67, 548–554. https://doi.org/10.1016/j.ejpb.2007.03.017

Simonovic, I., Rosenberg, J., Koutsouris, A., Hecht, G., 2000. Enteropathogenic Escherichia coli dephosphorylates and dissociates occludin from intestinal

epithelial tight junctions. Cell. Microbiol. 2, 305–315. https://doi.org/10.1046/j.1462-5822.2000.00055.x

Singh, S., Alam, M.M., Pal-Bhowmick, I., Brzostowski, J.A., Chitnis, C.E., 2010. Distinct external signals trigger sequential release of apical organelles during erythrocyte invasion by malaria parasites. PLoS Pathog. 6, e1000746. https://doi.org/10.1371/journal.ppat.1000746

Sixt, M., Lämmermann, T., 2011. Chapter 11: In Vitro Analysis of Chemotactic Leukocyte Migration in 3D Environments, in: Methods in Molecular Biology. Humana Press, Totowa, NJ, pp. 149–165.

Smalley-Freed, W.G., Efimov, A., Burnett, P.E., Short, S.P., Davis, M.A., Gumucio, D.L., Washington, M.K., Coffey, R.J., Reynolds, A.B., 2010. P120-Catenin Is Essential for Maintenance of Barrier Function and Intestinal Homeostasis in Mice. J. Clin. Invest. 120, 1824–1835. https://doi.org/10.1172/JCI41414

Smith, J.E., 1995. A ubiquitous intracellular parasite: The cellular biology of Toxoplasma gondii. Int. J. Parasitol. 25, 1301–1309. https://doi.org/10.1016/0020-7519(95)00067-C

Smith, T., Wolff, K.A., Nguyen, L., 2013. Molecular biology of drug resistance in Mycobacterium tuberculosis. Curr. Top. Microbiol. Immunol. 374, 53–80. https://doi.org/10.1007/82_2012_279.

Sommer, C. a, Mostoslavsky, G., 2014. RNA-Seq Analysis of Enteroendocrine Cells Reveals a Role for FABP5 in the Control of GIP Secretion. Mol. Endocrinol. 28, 1855–65. https://doi.org/10.1210/me.2014-1194

Sommer, F., Adam, N., Johansson, M.E. V, Xia, L., Hansson, G.C., Backhed, F., 2014. Altered mucus glycosylation in core 1 O-glycan-deficient mice affects microbiota composition and intestinal architecture. PLoS One 9, e85254. https://doi.org/10.1371/journal.pone.0085254

Spear, W., Chan, D., Coppens, I., Johnson, R.S., Giaccia, A., Blader, I.J., 2006. The host cell transcription factor hypoxia-inducible factor 1 is required for Toxoplasma gondii growth and survival at physiological oxygen levels. Cell. Microbiol. 8, 339–352. https://doi.org/10.1111/j.1462-5822.2005.00628.x

Specian, R.D., Oliver, M.G., 1991. Functional biology of intestinal goblet cells. Am J Physiol 260, C183-93.

Spence, J.R., Mayhew, C.N., Rankin, S.A., Kuhar, M.F., Vallance, J.E., Tolle, K., Hoskins, E.E., Kalinichenko, V. V, Wells, S.I., Zorn, A.M., Shroyer, N.F., Wells, J.M., 2010. Directed differentiation of human pluripotent stem cells into intestinal tissue in vitro. Nature 470, 105–109.

Stark, D., Barratt, J.L.N., Van Hal, S., Marriott, D., Harkness, J., Ellis, J.T., 2009. Clinical significance of enteric protozoa in the immunosuppressed human population. Clin. Microbiol. Rev. 22, 634–650. https://doi.org/10.1128/CMR.00017-09

Stelzner, M., Helmrath, M., Dunn, J.C.Y., Henning, S.J., Houchen, C.W., Kuo, C., Lynch, J., Li, L., Magness, S.T., Martin, M.G., Wong, M.H., Yu, J., 2012. A nomenclature for intestinal in vitro cultures. Am. J. Physiol. Gastrointest. Liver Physiol. 302, G1359-63. https://doi.org/10.1152/ajpgi.00493.2011

Stepp, M.A., Spurr-Michaud, S., Tisdale, A., Elwell, J., Gipson, I.K., 1990. Alpha 6 beta 4 integrin heterodimer is a component of hemidesmosomes. Proc. Natl. Acad.

Sci. 87, 8970–8974. https://doi.org/10.1073/pnas.87.22.8970

Straub, K.W., Peng, E.D., Hajagos, B.E., Tyler, J.S., Bradley, P.J., 2011. The moving junction protein RON8 facilitates firm attachment and host cell invasion in Toxoplasma gondii. PLoS Pathog. 7, e1002007. https://doi.org/10.1371/journal.ppat.1002007

Su, M.-C., Yuan, R.-H., Lin, C.-Y., Jeng, Y.-M., 2008. Cadherin-17 is a useful diagnostic marker for adenocarcinomas of the digestive system. Mod. Pathol. 21, 1379–1386. https://doi.org/10.1038/modpathol.2008.107

Sumigray, K.D., Lechler, T., 2012. Desmoplakin controls microvilli length but not cell adhesion or keratin organization in the intestinal epithelium. Mol. Biol. Cell 23, 792–799. https://doi.org/10.1091/mbc.E11-11-0923

SYROCOT, 2007. Effectiveness of prenatal treatment for congenital toxoplasmosis: a meta-analysis of individual patients' data. Lancet 369, 115–122. https://doi.org/10.1016/S0140-6736(07)60072-5

Tafazoli, F., Magnusson, K., Zheng, L., 2003. Disruption of Epithelial Barrier Integrity by Salmonella enterica Serovar Typhimurium Requires Geranylgeranylated Proteins Disruption of Epithelial Barrier Integrity by Salmonella enterica Serovar Typhimurium Requires Geranylgeranylated Proteins 71, 872–881. https://doi.org/10.1128/IAI.71.2.872

Takeda, N., Jain, R., LeBoeuf, M.R., Wang, Q., Lu, M.M., Epstein, J.A., 2011. Interconversion Between Intestinal Stem Cell Populations in Distinct Niches. Science (80-.). 334, 1420–1424. https://doi.org/10.1126/science.1213214

Takeichi, M., 2014. Dynamic contacts: rearranging adherens junctions to drive epithelial remodelling. Nat. Rev. Mol. Cell Biol. 15, 397–410. https://doi.org/10.1038/nrm3802

Tarr, P.I., Gordon, C. a., Chandler, W.L., 2005. Shiga-toxin-producing Escherichia coli and haemolytic uraemic syndrome. Lancet 365, 1073–1086. https://doi.org/10.1016/S0140-6736(05)71144-2

Taupin, D., Podolsky, D.K., 2003. Trefoil factors: initiators of mucosal healing. Nat. Rev. Mol. Cell Biol. 4, 721–32. https://doi.org/10.1038/nrm1203

Tenter, A.M., Heckeroth, A.R., Weiss, L.M., 2000. Toxoplasma gondii: From animals to humans. Int. J. Parasitol. 30, 1217–1258. https://doi.org/10.1016/S0020-7519(00)00124-7

Tian, H., Biehs, B., Sauvage, F.J. De, Klein, O.D., Tian, H., Biehs, B., Chiu, C., Siebel, C.W., Wu, Y., Costa, M., Sauvage, F.J. De, 2015. Opposing Activities of Notch and Wnt Signaling Regulate Intestinal Stem Cells and Gut Homeostasis Report Opposing Activities of Notch and Wnt Signaling Regulate Intestinal Stem Cells and Gut Homeostasis. CellReports 11, 33–42. https://doi.org/10.1016/j.celrep.2015.03.007

Torrey, E.F., Yolken, R.H., 2003. Toxoplasma gondii and Schizophrenia. Emerg. Infect. Dis. 9, 1375–1380. https://doi.org/10.3201/eid0911.030143

Turck, N., Lefebvre, O., Gross, I., Gendry, P., Kedinger, M., Simon-Assmann, P., Launay, J.F., 2006. Effect of laminin-1 on intestinal cell differentiation involves inhibition of nuclear nucleolin. J. Cell. Physiol. 206, 545–555. https://doi.org/10.1002/jcp.20501

Ungell, A.-L., Nylander, S., Bergstrand, S., Sjöberg, Å., Lennernäs, H., 1998. Membrane Transport of Drugs in Different Regions of the Intestinal Tract of the Rat. J. Pharm. Sci. 87, 360–366. https://doi.org/10.1021/js970218s

van de Kerkhof, E.G., de Graaf, I.A.M., de Jager, M.H., Meijer, D.K.F., Groothuis, G.M.M., 2005. Characterization of rat small intestinal and colon precision-cut slices as an in vitro system for drug metabolism and induction studies. Drug Metab. Dispos. 33, 1613–1620.

Van De Kerkhof, E.G., Ungell, A.L.B., Sjöberg, Å.K., De Jager, M.H., Hilgendorf, C., De Graaf, I.A.M., Groothuis, G.M.M., 2006. Innovative methods to study human intestinal drug metabolism in vitro: Precision-cut slices compared with Ussing chamber preparations. Drug Metab. Dispos. 34, 1893–1902. https://doi.org/10.1124/dmd.106.011148

van Es, J.H., Clevers, H., 2014. Paneth cells. Curr. Biol. 24, R547-8. https://doi.org/10.1016/j.cub.2014.04.049

Van Huizen, R., Martindale, J.L., Gorospe, M., Holbrook, N.J., 2003. P58IPK, a novel endoplasmic reticulum stress-inducible protein and potential negative regulator of eIF2α signaling. J. Biol. Chem. 278, 15558–15564. https://doi.org/10.1074/jbc.M212074200

van Roy, F., Berx, G., 2008. The cell-cell adhesion molecule E-cadherin. Cell. Mol. Life Sci. 65, 3756–88. https://doi.org/10.1007/s00018-008-8281-1

VanDussen, K.L., Carulli, A.J., Keeley, T.M., Patel, S.R., Puthoff, B.J., Magness, S.T., Tran, I.T., Maillard, I., Siebel, C., Kolterud, Å., Grosse, A.S., Gumucio, D.L., Ernst, S. a., Tsai, Y., Dempsey, P.J., Samuelson, L.C., Kolterud, A., Grosse, A.S., Gumucio, D.L., Ernst, S. a., Tsai, Y., Dempsey, P.J., Samuelson, L.C., 2012. Notch Signaling Modulates Proliferation and Differentiation of Intestinal Crypt Base Columnar Stem Cells. Development 497, 488–497. https://doi.org/10.1242/dev.070763

Vandussen, K.L., Marinshaw, J.M., Shaikh, N., Miyoshi, H., Moon, C., Tarr, P.I., Ciorba, M.A., Stappenbeck, T.S., 2014. Development of an enhanced human gastrointestinal epithelial culture system to facilitate patient-based assays. https://doi.org/10.1136/gutjnl-2013-306651

Vutova, P., Wirth, M., Hippe, D., Gross, U., Schulze-Osthoff, K., Schmitz, I., Lüder, C.G.K., 2007. Toxoplasma gondii inhibits Fas/CD95-triggered cell death by inducing aberrant processing and degradation of caspase 8. Cell. Microbiol. 9, 1556–1570. https://doi.org/10.1111/j.1462-5822.2007.00893.x

Wald, F.A., Oriolo, A.S., Llanos Casanova, M., Salas, P.J.I., 2005. Dominant maternal-effect mutations causing embryonic lethality in Caenorhabditis elegans. Molecuiar Biol. Cell 16, 4096–4107. https://doi.org/10.1091/mbc.E05

Walker, C.R., Hautefort, I., Dalton, J.E., Overweg, K., Egan, C.E., Bongaerts, R.J., Newton, D.J., Cruickshank, S.M., Andrew, E.M., Carding, S.R., 2013. Intestinal intraepithelial lymphocyte-enterocyte crosstalk regulates production of bactericidal angiogenin 4 by paneth cells upon microbial challenge. PLoS One 8, e84553. https://doi.org/10.1371/journal.pone.0084553

Walko, G., Castañón, M.J., Wiche, G., 2015. Molecular architecture and function of the hemidesmosome. Cell Tissue Res. 360, 363–378. https://doi.org/10.1007/s00441-014-2061-z

Walton, K.D., Whidden, M., Kolterud, A., Shoffner, S., Czerwinski, M.J., Kushwaha, J., Parmar, N., Chandhrasekhar, D., Freddo, a. M., Schnell, S., Gumucio, D.L., 2015. Villification in the mouse: Bmp signals control intestinal villus patterning. Development 143, 734–764. https://doi.org/10.1242/dev.130112

Wang, R.N., Green, J., Wang, Z., Deng, Y., Qiao, M., Peabody, M., Zhang, Q., Ye, J., Yan, Z., Denduluri, S., Idowu, O., Li, M., Shen, C., Hu, A., Haydon, R.C., Kang, R., Mok, J., Lee, M.J., Luu, H.L., Shi, L.L., 2014. Bone Morphogenetic Protein (BMP) signaling in development and human diseases. Genes Dis. 1, 87–105. https://doi.org/10.1016/j.gendis.2014.07.005

Wang, S., Liu, J., Li, L., Wice, B.M., 2004. Individual Subtypes of Enteroendocrine Cells in the Mouse Small Intestine Exhibit Unique Patterns of Inositol 1,4,5-trisphosphate Receptor Expression. J. Histochem. Cytochem. 52, 53–63. https://doi.org/10.1177/002215540405200106

Wang, Y.-H., Trucksis, M., McElwee, J.J., Wong, P.H., Maciolek, C., Thompson, C.D., Prueksaritanont, T., Garrett, G.C., Declercq, R., Vets, E., Willson, K.J., Smith, R.C., Klappenbach, J. a, Opiteck, G.J., Tsou, J. a, Gibson, C., Laethem, T., Panorchan, P., Iwamoto, M., Shaw, P.M., Wagner, J. a, Harrelson, J.C., 2012. UGT2B17 genetic polymorphisms dramatically affect the pharmacokinetics of MK-7246 in healthy subjects in a first-in-human study. Clin. Pharmacol. Ther. 92, 96–102. https://doi.org/10.1038/clpt.2012.20

Wang, Y., DiSalvo, M., Gunasekara, D.B., Dutton, J., Proctor, A., Lebhar, M.S., Williamson, I.A., Speer, J., Howard, R.L., Smiddy, N.M., Bultman, S.J., Sims, C.E., Magness, S.T., Allbritton, N.L., 2017. Self-renewing Monolayer of Primary Colonic or Rectal Epithelial Cells. Cell. Mol. Gastroenterol. Hepatol. 4, 165–182.e7. https://doi.org/10.1016/j.jcmgh.2017.02.011

Wang, Z.X., Zhou, C.X., Elsheikha, H.M., He, S., Zhou, D.H., Zhu, X.Q., 2017. Proteomic differences between developmental stages of Toxoplasma gondii revealed by iTRAQ-based quantitative proteomics. Front. Microbiol. 8, 1–15. https://doi.org/10.3389/fmicb.2017.00985

Weeks, C.S., Tanabe, H., Cummings, J.E., Crampton, S.P., Sheynis, T., Jelinek, R., Vanderlick, T.K., Cocco, M.J., Ouellette, A.J., 2006. Matrix metalloproteinase-7 activation of mouse paneth cell pro-alpha-defensins: SER43 down arrow ILE44 proteolysis enables membrane-disruptive activity. J. Biol. Chem. 281, 28932–42. https://doi.org/10.1074/jbc.M602041200

Weidner, J.M., Kanatani, S., Uchtenhagen, H., Varas-Godoy, M., Schulte, T., Engelberg, K., Gubbels, M.J., Sun, H.S., Harrison, R.E., Achour, A., Barragan, A., 2016. Migratory activation of parasitized dendritic cells by the protozoan Toxoplasma gondii 14-3-3 protein. Cell. Microbiol. 18, 1537–1550. https://doi.org/10.1111/cmi.12595

Weight, C.M., Carding, S.R., 2012. The protozoan pathogen Toxoplasma gondii targets the paracellular pathway to invade the intestinal epithelium. Ann. N. Y. Acad. Sci. 1258, 135–142.

Weight, C.M., Jones, E.J., Horn, N., Wellner, N., Carding, S.R., 2015. Elucidating pathways of Toxoplasma gondii invasion in the gastrointestinal tract: involvement of the tight junction protein occludin. Microbes Infect. 17, 698–709. https://doi.org/10.1016/j.micinf.2015.07.001

Wells, J.M., Brummer, R.J., Derrien, M., MacDonald, T., Troost, F., Cani, P.D.,

Theodorou, V., Dekker, J., Meheust, A., de Vos, W.M., Mercenier, A., Nauta, A., Garcia-Rodenas, C.L., 2014. The Regulation of Gut Barrier Function and Potential Biomarkers. Br. J. Nutr. 312, G171–G193. https://doi.org/10.1152/ajpgi.00048.2015

WHO, 2014. Antimicrobial resistance. Global Report on Surveillance. Bull. World Health Organ. 61, 383–94. https://doi.org/10.1007/s13312-014-0374-3

Wilhelm, C.L., Yarovinsky, F., 2014. Apicomplexan infections in the gut. Parasite Immunol. 36, 409–420. https://doi.org/10.1111/pim.12115

Williams, E.C., Janmey, P.A., Johnson, R.B., Mosher, D.F., 1983. Fibronectin. Effect of disulfide bond reduction on its physical and functional properties. J. Biol. Chem. 258, 5911–5914.

Wilson, C.L., 1999. Regulation of Intestinal -Defensin Activation by the Metalloproteinase Matrilysin in Innate Host Defense. Science (80-.). 286, 113–117. https://doi.org/10.1126/science.286.5437.113

Wilson, S.S., Tocchi, a, Holly, M.K., Parks, W.C., Smith, J.G., 2014. A small intestinal organoid model of non-invasive enteric pathogen-epithelial cell interactions. Mucosal Immunol. 8, 1–10. https://doi.org/10.1038/mi.2014.72

Wlodarska, M., Thaiss, C.A., Nowarski, R., Henao-Mejia, J., Zhang, J.P., Brown, E.M., Frankel, G., Levy, M., Katz, M.N., Philbrick, W.M., Elinav, E., Finlay, B.B., Flavell, R.A., 2014. NLRP6 inflammasome orchestrates the colonic host-microbial interface by regulating goblet cell mucus secretion. Cell 156, 1045–1059. https://doi.org/10.1016/j.cell.2014.01.026

Wolfe, M.S., 1992. Giardiasis. Clin. Microbiol. Rev. 5, 93–100. https://doi.org/10.1128/CMR.5.1.93

World Health Organisation, 2015. WHO estimates of the global burden of foodborne diseases 268 p.

Wu, W., Jamshidi, N., Eraly, S.A., Liu, H.C., Bush, K.T., Palsson, B.O., Nigam, S.K., 2013. Multispecific drug transporter Slc22a8 (Oat3) regulates multiple metabolic and signaling pathways. Drug Metab. Dispos. 41, 1825–1834. https://doi.org/10.1124/dmd.113.052647

Xia, D., Sanderson, S.J., Jones, A.R., Prieto, J.H., Yates, J.R., Bromley, E., Tomley, F.M., Lal, K., Sinden, R.E., Brunk, B.P., Roos, D.S., Wastling, J.M., 2008. The proteome of Toxoplasma gondii: integration with the genome provides novel insights into gene expression and annotation. Genome Biol. 9, R116.1-R116.18. https://doi.org/10.1186/gb-2008-9-7-r116

Yan, K.S., Chia, L. a, Li, X., Ootani, A., Su, J., Lee, J.Y., Su, N., Luo, Y., Heilshorn, S.C., Amieva, M.R., Sangiorgi, E., Capecchi, M.R., Kuo, C.J., 2012. The Intestinal Stem Cell Markers Bmi1 and Lgr5 Identify Two Functionally Distinct Populations. Proc. Natl. Acad. Sci. U. S. A. 109, 466–71. https://doi.org/10.1073/pnas.1118857109

Yang, Q., Bermingham, N. a, Finegold, M.J., Zoghbi, H.Y., 2001. Requirement of Math1 for Secretory Cell Lineage Committment in the Mouse Intestine. Science 294, 2155–2158. https://doi.org/10.1126/science.1065718

Yin, X., Farin, H.F., van Es, J.H., Clevers, H., Langer, R., Karp, J.M., 2014. Niche-independent high-purity cultures of Lgr5+ intestinal stem cells and their progeny. Nat. Methods 11, 106–112.

Yin, Y., Bijvelds, M., Dang, W., Xu, L., Van Der Eijk, A.A., Knipping, K., Tuysuz, N., Dekkers, J.F., Wang, Y., De Jonge, J., Sprengers, D., Van Der Laan, L.J.W., Beekman, J.M., Ten Berge, D., Metselaar, H.J., De Jonge, H., Koopmans, M.P.G., Peppelenbosch, M.P., Pan, Q., 2015. Modeling rotavirus infection and antiviral therapy using primary intestinal organoids. Antiviral Res. 123, 120–131. https://doi.org/10.1016/j.antiviral.2015.09.010

Yoshida, N., Tyler, K.M., Llewellyn, M.S., 2011. Invasion mechanisms among emerging food-borne protozoan parasites. Trends Parasitol. 27, 459–466. https://doi.org/10.1016/j.pt.2011.06.006

Yu, J., Peng, S., Luo, D., March, J.C., 2012. In vitro 3D human small intestinal villous model for drug permeability determination. Biotechnol. Bioeng. 109, 2173–2178. https://doi.org/10.1002/bit.24518

Yu, L., Wang, L., Chen, S., 2011. Olfactomedin 4, a novel marker for the differentiation and progression of gastrointestinal cancers. Neoplasma 58, 9–13.

Yu, W., Datta, A., Leroy, P., O'Brien, L.E., Mak, G., Jou, T., Matlin, K.S., Mostov, K.E., Zegers, M.M.P., 2005. B1-Integrin Orients Epithelial Polarity via Rac1 and Laminin. Mol. Biol. Cell 16, 433–445. https://doi.org/10.1091/mbc.E04-05-0435

Zachos, N.C., Kovbasnjuk, O., Foulke-abel, J., In, J., Blutt, S.E., Jonge, H.R. De, Estes, M.K., 2016. Human Enteroids / Colonoids and Intestinal Organoids Functionally Recapitulate and Pathophysiology. J. Biol. Chem. 291, 3759–3766. https://doi.org/10.1074/jbc.R114.635995

Zhang, J., Li, L., 2005. BMP signaling and stem cell regulation. Dev. Biol. 284, 1–11. https://doi.org/10.1016/j.ydbio.2005.05.009

Zhang, Y.-G., Wu, S., Xia, Y., Sun, J., 2014. Salmonella-infected crypt-derived intestinal organoid culture system for host-bacterial interactions. Physiol. Rep. 2, e12147–e12147. https://doi.org/10.14814/phy2.12147

Zhou, D.-H., Wang, Z.-X., Zhou, C.-X., He, S., Elsheikha, H.M., Zhu, X.-Q., 2017. Comparative proteomic analysis of virulent and avirulent strains of Toxoplasma gondii reveals strain-specific patterns. Oncotarget 8, 80481–80491. https://doi.org/10.18632/oncotarget.19077

Zhou, Q., Toivola, D.M., Feng, N., Greenberg, H.B., Franke, W.W., Omary, M.B., 2003. Kerain 20 Helps Maintain Intermediate Filament Organization in Intestinal Epithelia. Mol. Biol. Cell 14, 2959–2971. https://doi.org/10.1091/mbc.E03

Zhu, Y., Huang, Y.F., Kek, C., Bulavin, D. V., 2013. Apoptosis differently affects lineage tracing of lgr5 and bmi1 intestinal stem cell populations. Cell Stem Cell 12, 298–303. https://doi.org/10.1016/j.stem.2013.01.003

Zietek, T., Rath, E., Haller, D., Daniel, H., 2015. Intestinal organoids for assessing nutrient transport, sensing and incretin secretion. Sci. Rep. 5, 16831. https://doi.org/10.1038/srep16831

Appendix A – Chapter 3 Supplementary Tables and Figures

Supplementary Table 1) Top 20 proteins up- and down-regulated in DAPT/CHIR (Paneth Skewed) organoids

Protein Identifier	Protein Name	Protein Function	Subcellular Location	Q Value	P Value	Log2 Fold Change
P54869	3-hydroxy-3-methylglutaryl-CoA synthase 2 (mitochondrial) (HMGCS2)	Condenses acetyl-CoA with acetoacetyl-CoA to form HMG-CoA, which is the substrate for HMG-CoA reductase.	Cytoplasm	0.00953	0.00032	▲2.436
P81117	Nucleobindin-2 (NUCB2)	Calcium-binding protein. May have a role in calcium homeostasis.	Nucleus	0.01100	0.00076	▲2.432
Q64459	Cytochrome P450 3A11 (CYP3A11); CYP3A5	Catalyzes erythromycin N-demethylation, nifedipine oxidation and testosterone 6 beta-hydroxylation.	Cytoplasm	0.00972	0.00027	▲2.103
Q64458	Cytochrome P450 2C29 (CYP2C29); CYP2C8	Metabolizes arachidonic acid to produce 14,15-cis-epoxyeicosatrienoic acid (EET).	Cytoplasm	0.00464	0.00008	▲2.069
Q9D816	Cytochrome P450 2C55 (CYP2C55); CYP2C18	Metabolizes arachidonic acid mainly to 19-hydroxyeicosatetraenoic acid (HETE).	Cytoplasm	0.00980	0.00041	▲1.896
Q10738	*Matrilysin (MMP7)	Degrades casein, gelatins of types I, III, IV, and V, and fibronectin.	Extracellular Space	0.01169	0.00093	▲1.785

* Differentiated cell marker of Paneth cells

Supplementary Table 1 Continued) Top 20 proteins up- and down-regulated in DAPT/CHIR (Paneth Skewed) organoids						
Protein Identifier	**Protein Name**	**Protein Function**	**Subcellular Location**	**Q Value**	**P Value**	**Log2 Fold Change**
P19324	Serpin H1 (SERPINH1)	Binds specifically to collagen. Could be involved as a chaperone in the biosynthetic pathway of collagen.	Extracellular Space	0.04760	0.01640	▲1.737
O55071	Cytochrome P450 2B19 (CYP2B19)	In liver microsomes, this enzyme is involved in an NADPH-dependent electron transport pathway. It oxidizes a variety of structurally unrelated compounds, including steroids, fatty acids, and xenobiotics.	Cytoplasm	0.00942	0.00026	▲1.685
P02088	Hemoglobin, Beta Adult Major Chain (HBB-B1)	Involved in oxygen transport from the lung to the various peripheral tissues.	Extracellular Space	0.01660	0.01820	▲1.683
P26339	Chromogranin-A (CHGA)	Secretory protein	Cytoplasm	0.00049	<0.00001	▲1.665
P35441	Thrombospondin 1 (THBS1)	Adhesive glycoprotein that mediates cell-to-cell and cell-to-matrix interactions.	Extracellular Space	0.00944	0.00031	▲1.561
P12791	Cytochrome P450 2B10 (CYP2B10); CYP2B6	In liver microsomes, this enzyme is involved in an NADPH-dependent electron transport pathway. It oxidizes a variety of structurally unrelated compounds, including steroids, fatty acids, and xenobiotics.	Cytoplasm	0.00560	0.00011	▲1.523

Supplementary Table 1 Continued) Top 20 proteins up- and down-regulated in DAPT/CHIR (Paneth Skewed) organoids						
Protein Identifier	**Protein Name**	**Protein Function**	**Subcellular Location**	**Q Value**	**P Value**	**Log2 Fold Change**
P52825	Cartinine (CPT2)	Catalytic activity; Palmitoyl-CoA + L-carnitine = CoA + L-palmitoylcarnitine.	Cytoplasm	0.02090	0.00302	▲1.509
Q05421	Cytochrome P450 2E1 (CYP2E1)	Metabolizes several precarcinogens, drugs, and solvents to reactive metabolites.	Cytoplasm	0.02870	0.00593	▲1.499
O88310	Intelectin-1 (ITLN1)	May play a role in the defense system against microorganisms. May specifically recognize carbohydrate chains of pathogens and bacterial components containing galactofuranosyl residues, in a calcium-dependent manner.	Plasma Membrane	0.00470	0.00008	▲1.490
Q78KK3	Solute Carrier Family 22 Member 18 (SLC22A18)	May act as a transporter of organic cations based on a proton efflux antiport mechanism.	Plasma Membrane	0.01150	0.00087	▲1.463
Q91VE0	Solute Carrier Family 27 Member 4 (SLC27A4)	Involved in translocation of long-chain fatty acids (LFCA) across the plasma membrane. Appears to be the principal fatty acid transporter in small intestinal enterocytes. Plays a role in the formation of the epidermal barrier.	Plasma Membrane	0.03860	0.00109	▲1.407

Supplementary Table 1 Continued) Top 20 proteins up- and down-regulated in DAPT/CHIR (Paneth Skewed) organoids

Protein Identifier	Protein Name	Protein Function	Subcellular Location	Q Value	P Value	Log2 Fold Change
Q80W94	2-Acylglycerol O-Acyltransferase (MOGAT2)	Catalyzes the formation of diacylglycerol from 2-monoacylglycerol and fatty acyl-CoA.	Cytoplasm	0.01150	0.00856	▲1.406
A2AFS3	Protein KIAA1324 (KIAA1324)	May protect cells from cell death by inducing cytosolic vacuolization and upregulating the autophagy pathway.	Plasma Membrane; Endosome; Golgi Apparatus; Lyosome	0.01060	0.00588	▲1.361
P16014	Chromogranin B/Secretogranin (CHGB)	Neuroendocrine secretory granule protein, which may be the precursor for other biologically active peptides.	Extracellular Space	0.01050	0.00048	▲1.347
Q3UW53	Protein Niban (FAM129A)	Regulates phosphorylation of a number of proteins involved in translation regulation including EIF2A, EIF4EBP1 and RPS6KB1.	Cytoplasm	0.00942	0.00030	▼4.544
Q8K2Z4	Condensin Complex Subunit 1 (NCAPD2)	RIKEN cDNA 5330417C22 gene.	Nucleus	0.02830	0.00566	▼2.296

Supplementary Table 1 Continued) Top 20 proteins up- and down-regulated in DAPT/CHIR (Paneth Skewed) organoids						
Protein Identifier	**Protein Name**	**Protein Function**	**Subcellular Location**	**Q Value**	**P Value**	**Log2 Fold Change**
Q8BHB9	Chloride Intracellular Channel Protein 6 (CLIC6)	May insert into membranes and form chloride ion channels. May play a critical role in water-secreting cells, possibly through the regulation of chloride ion transport.	Plasma Membrane	0.00464	0.00006	▼2.221
O70310	N-Myristoyltransferase 1 (NMT1)	Adds a myristoyl group to the N-terminal glycine residue of certain cellular proteins.	Cytoplasm	0.00250	0.00423	▼2.185
Q3UZZ4	^Olfactomedin-4 (OLFM4)	Facilitates cell adhesion, most probably through interaction with cell surface lectins and cadherin. May promote proliferation of pancreatic cancer cells by favoring the transition from the S to G2/M phase.	Extracellular Space	0.00391	0.00004	▼2.138
P45377	Aldose Reductase-Related Protein 2 (AKR1B10)	Catalytic activity; Alditol + $NAD(P)^+$ = aldose + NAD(P)H.	Cytoplasm	0.02050	0.00284	▼1.997
^ Stem cell marker of Lgr5+ intestinal stem cells						

Supplementary Table 1 Continued) Top 20 proteins up- and down-regulated in DAPT/CHIR (Paneth Skewed) organoids						
Protein Identifier	**Protein Name**	**Protein Function**	**Subcellular Location**	**Q Value**	**P Value**	**Log2 Fold Change**
P02798	Metallothionein-2 (MT2)	Metallothioneins have a high content of cysteine residues that bind various heavy metals; these proteins are transcriptionally regulated by both heavy metals and glucocorticoids.	Other	0.03757	0.01050	▼1.890
Q62189	U1 Small Nuclear Ribonucleoprotein A (SNRPA)	Component of the spliceosomal U1 snRNP, which is essential for recognition of the pre-mRNA 5' splice-site and the subsequent assembly of the spliceosome.	Nucleus	0.03413	0.009180	▼1.681
P51432	Phospholipase C, Beta 3 (Phosphatidylinositol-specific) (PLCB3)	The production of the second messenger molecules diacylglycerol (DAG) and inositol 1,4,5-trisphosphate (IP3) is mediated by activated phosphatidylinositol-specific phospholipase C enzymes.	Cytoplasm	0.00782	0.00182	▼1.631

Supplementary Table 1 Continued) Top 20 proteins up- and down-regulated in DAPT/CHIR (Paneth Skewed) organoids						
Protein Identifier	**Protein Name**	**Protein Function**	**Subcellular Location**	**Q Value**	**P Value**	**Log2 Fold Change**
Q4VAA2	Protein CDV3 (CDV3)	Uncharacterised	Cytoplasm	0.01145	0.00081	▼1.616
P62960	Y Box Binding Protein 1 (YBX1)	Mediates pre-mRNA alternative splicing regulation. The secreted form acts as an extracellular mitogen and stimulates cell migration and proliferation.	Nucleus	0.00980	0.00413	▼1.608
P61290	Proteasome Activator Complex Subunit 3 (PSME3)	Subunit of the 11S REG-gamma (also called PA28-gamma) proteasome regulator, a doughnut-shaped homoheptamer which associates with the proteasome.	Cytoplasm	0.03230	0.00510	▼1.544
Q8VCN5	Cystathionine (CTH)	Catalyzes the last step in the trans-sulfuration pathway from methionine to cysteine.	Cytoplasm	0.00955	0.00033	▼1.519
Q61753	D-3-Phosphoglycerate Dehydrogenase (PHGDH)	Catalytic activity associated with amino-acid biosynthesis and L-serine biosynthesis	Cytoplasm	0.00392	0.00042	▼1.510

Supplementary Table 1 Continued) Top 20 proteins up- and down-regulated in DAPT/CHIR (Paneth Skewed) organoids						
Protein Identifier	**Protein Name**	**Protein Function**	**Subcellular Location**	**Q Value**	**P Value**	**Log2 Fold Change**
Q8CAY6	Acetyl-CoA Acetyltransferase (ACAT2)	Catalytic activity; 2 acetyl-CoA = CoA + acetoacetyl-CoA.	Cytoplasm	0.01380	0.00142	▼1.501
Q61166	Microtubule-Associated Protein RP/EB Family Member 1 (MAPRE1)	Binds to the plus end of microtubules and regulates the dynamics of the microtubule cytoskeleton. Promotes cytoplasmic microtubule nucleation and elongation. May be involved in spindle function by stabilizing microtubules and anchoring them at centrosomes.	Cytoplasm	0.02110	0.00319	▼1.354
Q9CQM9	Glutaredoxin 3 (GLRX3)	Has an essential function in embryogenesis.	Cytoplasm	0.01380	0.00142	▼1.334
Q9ER72	Cysteine-tRNA Ligase, Cytoplasmic (CARS)	Catalytic activity; ATP + L-cysteine + tRNA(Cys) = AMP + diphosphate + L-cysteinyl-tRNA(Cys).	Cytoplasm	0.02060	0.00291	▼1.330
P17918	Proliferating Cell Nuclear Antigen (PCNA)	Auxiliary protein of DNA polymerase delta and is involved in the control of eukaryotic DNA replication by increasing the polymerase's processibility during elongation of the leading strand.	Nucleus	0.01170	0.00093	▼1.326
Q62433	Protein NDRG1 (NDRG1)	Stress-responsive protein involved in hormone responses, cell growth, and differentiation.	Nucleus	0.03220	0.00772	▼1.287

Supplementary Table 2) Top 20 proteins up- and down-regulated in DAPT/IWP-2 (Goblet Skewed) organoids

Protein Identifier	Protein Name	Protein Function	Subcellular Location	Q Value	P Value	Log2 Fold Change
Q9D7Z6	*Calcium-Activated Chloride Channel Regulator 1 (CLCA1)	Known component of small intestinal mucus. May be involved in the regulation of mucus production and/or secretion by goblet cells.	Plasma Membrane	0.00347	0.00044	▲3.328
P02772	*Alpha-fetoprotein (AFP)	Binds estrogens, fatty acids and metals.	Extracellular Space	0.00866	0.00366	▲2.939
P26339	*Chromogranin-A (CHGA)	Pancreastatin strongly inhibits glucose induced insulin release from the pancreas.	Cytoplasm	0.01349	0.00103	▲2.859
P19324	Serpin H1 (SERPINH1)	Binds specifically to collagen. Could be involved as a chaperone in the biosynthetic pathway of collagen.	Extracellular Space	0.04147	0.01470	▲2.846
P09240	*Cholecystokinin (CCK)	Induces gall bladder contraction and the release of pancreatic enzymes in the gut.	Extracellular Space	0.01682	0.00158	▲2.828
Q64459	Cytochrome P450 3A11 (CYP3A11); CYP3A5	Catalyzes erythromycin N-demethylation, nifedipine oxidation and testosterone 6 beta-hydroxylation.	Cytoplasm	0.00867	0.00035	▲2.810
P20152	Vimentin (VIM)	Class-III intermediate filaments found in various non-epithelial cells.	Cytoplasm	0.01043	0.00053	▲2.481
Q62395	*Trefoil Factor 3 (TFF3)	Involved in the maintenance and repair of the intestinal mucosa.	Extracellular Space	0.04095	0.01430	▲2.383

* Differentiated cell markers of goblet/enteroendocrine cells

Supplementary Table 2 Continued) Top 20 proteins up- and down-regulated in DAPT/IWP-2 (Goblet Skewed) organoids

Protein Identifier	Protein Name	Protein Function	Subcellular Location	Q Value	P Value	Log2 Fold Change
P48756	Gastric inhibitory polypeptide (GIP)	*Potent stimulator of insulin secretion and relatively poor inhibitor of gastric acid secretion.	Extracellular Space	0.01174	0.00066	▲2.360
Q8K0C5	Zymogen granule membrane protein 16 (ZG16)	May play a role in protein trafficking	Extracellular Matrix; Extracellular Matrix	0.03616	0.01062	▲2.266
P16110	Galectin-3 (LGALS3)	Together with DMBT1, required for terminal differentiation of columnar epithelial cells during early embryogenesis.	Extracellular Space	0.00431	0.01620	▲2.199
Q99P58	+ Ras-Related Protein Rab-27B (RAB27B)	May be involved in targeting uroplakins to urothelial apical membranes.	Cytoplasm	0.04033	0.01320	▲2.139
Q8BND5	Sulfhydryl oxidase 1 (QSox1)	Catalyzes the oxidation of sulfhydryl groups in peptide and protein thiols to disulfides with the reduction of oxygen to hydrogen peroxide. May contribute to disulfide bond formation in a variety of secreted proteins	Extracellular Space;Golgi Apparatus; Endoplasmic Reticulum; Extracellular Vesicular Exosome	0.03340	0.00794	▲2.095

* Differentiated cell markers of goblet/enteroendocrine cells
+ Proteins associated with secretion in other organs

Supplementary Table 2 Continued) Top 20 proteins up- and down-regulated in DAPT/IWP-2 (Goblet Skewed) organoids

Protein Identifier	Protein Name	Protein Function	Subcellular Location	Q Value	P Value	Log2 Fold Change
P16014	* Chromogranin-B (CHGB); Secretogranin-1	Neuroendocrine secretory granule protein, which may be the precursor for other biologically active peptides.	Extracellular Space	0.02089	0.00235	▲2.039
Q78KK3	Solute Carrier Family 22 Member 18 (SLC22A18)	May act as a transporter of organic cations based on a proton efflux antiport mechanism.	Plasma Membrane	0.00866	0.00031	▲1.902
O88312	*Anterior Gradient Protein 2 (AGR2)	Required for MUC2 post-transcriptional synthesis and secretion.	Extracellular Space	0.04257	0.00153	▲1.857
P52624	Uridine Phopshorylase 1 (UPP1)	Catalyzes the reversible phosphorylytic cleavage of uridine and deoxyuridine to uracil and ribose- or deoxyribose-1-phosphate.	Cytoplasm	0.02203	0.00333	▲1.825
Q9JJX6	P2X Purino Receptor (P2RX4)	Receptor for ATP that acts as a ligand-gated ion channel.	Plasma Membrane	0.00256	0.00459	▲1.758
Q64133	Amine Oxidase (Flavin-Containing) A (MAOA)	Catalyzes the oxidative deamination of biogenic and xenobiotic amines and has important functions in the metabolism of neuroactive and vasoactive amines in the central nervous system and peripheral tissues.	Cytoplasm	0.00578	0.00009	▲1.754
Q9R112	Sulfide:Quinone Oxidoreductase, Mitochonrdrial (SQRDL)	Catalyzes the oxidation of hydrogen sulfide with the help of a quinone, such as ubiquinone, giving rise to thiosulfate and ultimately to sulfane (molecular sulfur) atoms.	Cytoplasm	0.00866	0.00032	▲1.709

* Differentiated cell markers of goblet/enteroendocrine cells

Supplementary Table 2 Continued) Top 20 proteins up- and down-regulated in DAPT/IWP-2 (Goblet Skewed) organoids

Protein Identifier	Protein Name	Protein Function	Subcellular Location	Q Value	P Value	Log2 Fold Change
Q9R112	Sulfide:Quinone Oxidoreductase, Mitochonrdrial (SQRDL)	Catalyzes the oxidation of hydrogen sulfide with the help of a quinone, such as ubiquinone, giving rise to thiosulfate and ultimately to sulfane (molecular sulfur) atoms.	Cytoplasm	0.00866	0.00032	▲1.709
E9Q1P8	Interferon Regulatory Factor 2-Binding Protein 2 (IRF2BP2)	Acts as a transcriptional corepressor in a IRF2-dependent manner, this repression is not mediated by histone deacetylase activities.	Cytoplasm Nucleoplasm Nucleus	0.00203	0.003313	▼2.588
Q3UZZ4	^Olfactomedin-4 (OLFM4)	Facilitates cell adhesion, most probably through interaction with cell surface lectins and cadherin. May promote proliferation of pancreatic cancer cells by favoring the transition from the S to G2/M phase.	Extracellular Space	0.02152	0.00001	▼2.337
P34022	Ran-Binding Protein 3 (RANBP3)	May act in an intracellular signaling pathway which may control the progression through the cell cycle by regulating the transport of protein and nucleic acids across the nuclear membrane.	Nucleus	0.02179	0.00615	▼2.297

* Stem cell marker

Supplementary Table 2 Continued) Top 20 proteins up- and down-regulated in DAPT/IWP-2 (Goblet Skewed) organoids

Protein Identifier	Protein Name	Protein Function	Subcellular Location	Q Value	P Value	Log2 Fold Change
Q8K2Z4	Non-SMC Condensin 1 Complex, Subunit D2 (NCAPD2)	Regulatory subunit of the condensin complex, a complex required for conversion of interphase chromatin into mitotic-like condense chromosomes. The condensin complex probably introduces positive supercoils into relaxed DNA in the presence of type I topoisomerases and converts nicked DNA into positive knotted forms in the presence of type II topoisomerases. May target the condensin complex to DNA via its C-terminal domain (By similarity)	Nucleus	0.02180	0.00305	▼2.179
P26350	Prothymosin alpha (PTMA)	Prothymosin alpha may mediate immune function by conferring resistance to certain opportunistic infections.	Nucleus	0.02125	0.00266	▼2.091
P34022	Ran-specific GTPase-activating protein (RANBP1)	Inhibits GTP exchange on Ran. Forms a Ran-GTP-RANBP1 trimeric complex. Increase GTP hydrolysis induced by the Ran GTPase activating protein RANGAP1.	Axon Cytoplasm Centrosome Nucleus	0.00866	0.00014	▼2.034

Supplementary Table 2 Continued) Top 20 proteins up- and down-regulated in DAPT/IWP-2 (Goblet Skewed) organoids

Protein Identifier	Protein Name	Protein Function	Subcellular Location	Q Value	P Value	Log2 Fold Change
Q99LT0	Protein Dpy-30 Homolog (DPY30)	In embryonic stem (ES) cells, plays a crucial role in the differentiation potential, particularly along the neural lineage, regulating gene induction and histone H3 'Lys-4' methylation at key developmental loci, including that mediated by retinoic acid.	Nucleus Golgi Apparatus	0.01358	0.00109	▼2.013
P62960	Y Box Binding Protein 1 (YBX1)	Mediates pre-mRNA alternative splicing regulation. The secreted form acts as an extracellular mitogen and stimulates cell migration and proliferation.	Nucleus	0.02540	0.00436	▼2.012
Q8BT18	Serine/Arginine Repetitive Matrix Protein 2 (SRRM2)	Uncharacterised Protein	Membrane	0.02951	0.00657	▼1.947
Q8BTM8	Filamin A (FLNA)	Promotes orthogonal branching of actin filaments and links actin filaments to membrane glycoproteins.	Cytoplasm	0.00884	0.00040	▼1.877
Q60973	Retinoblastoma Binding Protein 7 (RBBP7)	Core component of several complexes which regulate chromatin metabolism.	Nucleus	0.00347	0.00004	▼1.857
P46061	Ran GTP-ase-Activating Protein 1 (RANGAP1)	GTPase activator for the nuclear Ras-related regulatory protein Ran, converting it to the putatively inactive GDP-bound state.	Nucleus	0.02932	0.00629	▼1.856

Supplementary Table 2 Continued) Top 20 proteins up- and down-regulated in DAPT/IWP-2 (Goblet Skewed) organoids						
Protein Identifier	**Protein Name**	**Protein Function**	**Subcellular Location**	**Q Value**	**P Value**	**Log2 Fold Change**
Q8BG22	Calcium-Activated Chloride Channel Regulator 2 (CLCA2)	Plays a role in modulating chloride current across the plasma membrane in a calcium-dependent manner, and cell adhesion.	Plasma Membrane	0.02104	0.00244	▼1.828
Q80X41	Serine/Threonine Protein Kinase (VRK1)	Serine/threonine kinase involved in Golgi disassembly during the cell cycle.	Nucleus	0.01350	0.00101	▼1.811
Q9QYR9	Acyl-coenzyme A Thioesterase 2, Mitochondrial (ACOT2)	Enzyme that catalyzes the hydrolysis of acyl-CoAs to the free fatty acid and coenzyme A (CoASH).	Cytoplasm	0.01500	0.00127	▼1.792
Q99LP6	GrpE Protein Homolog 1 (GRPEL1)	Essential component of the PAM complex, a complex required for the translocation of transit peptide-containing proteins from the inner membrane into the mitochondrial matrix in an ATP-dependent manner.	Mitochondrion Matrix	0.03594	0.01024	▼1.780
Q9CQF3	Cleavage and Polyadenylation Specificity Factor Subunit 5 (NUDT21)	Component of the cleavage factor Im (CFIm) complex that plays a key role in pre-mRNA 3'-processing.	Nucleus	0.04090	0.01420	▼1.766
Q91VK1	Basic Leucine Zipper (BZW2)	May be involved in neuronal differentiation.	Cytoplasm	0.03490	0.00908	▼1.757

Supplementary Table 2 Continued) Top 20 proteins up- and down-regulated in DAPT/IWP-2 (Goblet Skewed) organoids

Protein Identifier	Protein Name	Protein Function	Subcellular Location	Q Value	P Value	Log2 Fold Change
P51432	Phospholipase C, Beta 3 (PLCB3)	The production of the second messenger molecules diacylglycerol (DAG) and inositol 1,4,5-trisphosphate (IP3) is mediated by activated phosphatidylinositol-specific phospholipase C enzymes.	Cytoplasm	0.00518	0.00007	▼1.747
P84228	Histone H3.2 (HIST1H3B)			0.04314	0.01627	▼1.745

Supplementary Table 3) 17 Proteins were Uniquely Up-Regulated in DAPT & CHIR (Paneth Skew) organoids

Protein Identifier	Protein Name	FC (log2)	Q value
Q9D816	Cytochrome P450 2C55 (CYP2C55)	▲1.896	0.01
Q10738	Matrilysin (MMP7)	▲1.785	0.012
P35441	Thrombospondin-1 (THBS1)	▲1.561	0.009
P52825	Carnitine O-palmitoyltransferase 2, mitochondrial (CPT2)	▲1.509	0.021
Q05421	Cytochrome P450 2E1 (CYP2E1	▲1.499	0.029
O88310	Intelectin-1a (ITLN1)	▲1.49	0.005
O88310	Intelectin-1a (ITLN1)	▲1.49	0.005
P14824	Annexin A6 (ANXA6)	▲1.256	0.021
Q91ZE0	Trimethyllysine dioxygenase, mitochondrial (TMLHE)	▲1.195	0.015
Q9FYw3	DnaJ homolog subfamily C member 3 (DNAJC3)	▲1.137	0.031
Q921G7	Electron transfer flavoprotein-ubiquinone oxidoreductase, mitochondrial (ETFDH)	▲1.108	0.037
Q9QZ88	Vacuolar protein sorting-associated protein 29 (VPS29)	▲1.09	0.039
Q9JMC8	Band 4.1-like protein 4B (EPB41L4B)	▲1.081	0.028
P50396	Rab GDP dissociation inhibitor alpha (GDI1)	▲1.07	0.023
P09528	Ferritin heavy chain (FTH1)	▲1.069	0.027
Q3TDQ1	Dolichyl-diphosphooligosaccharide--protein glycosyltransferase subunit STT3B (STT3B)	▲1.062	0.032
Q9D379	Epoxide hydrolase 1 (EPHX1)	▲1.013	0.004
Q791V5	Mitochondrial carrier homolog 2 (MTCH2)	▲1.008	0.020

Supplementary Table 4) 20 Proteins were Uniquely Down-regulated in DAPT & CHIR (Paneth Skew) organoids

Protein Identifier	Protein Name	FC (log2)	Q value
Q3UW53	Protein Niban (FAM129A)	▼4.544	0.009
P02798	Metallothionein-2 (MT2)	▼1.890	0.038
Q8BKS9	Pumilio domain-containing protein KIAA0020 (KIAA0020)	▼1.439	0.043
Q9CQM9	Glutaredoxin-3 (GLRX3)	▼1.334	0.014
Q62433	Protein NDRG1 (NDRG1)	▼1.287	0.032
Q8BTY2	Sodium bicarbonate cotransporter 3 (SLC4A7)	▼1.258	0.032
P53996	Cellular nucleic acid-binding protein (CNBP)	▼1.247	0.025
Q80SU7	Interferon-induced very large GTPase 1 (GVIN1)	▼1.238	0.017
P97864	Caspase-7 (CASP7)	▼1.208	0.003
Q8K354	Carbonyl reductase [NADPH] 3 (CBR3)	▼1.178	0.015
P83882	60S ribosomal protein L36a (RPL36A)	▼1.169	0.039
Q8CII2	Cell division cycle protein 123 homolog (CDC123)	▼1.167	0.041
Q920E5	Farnesyl pyrophosphate synthase (FDPS)	▼1.142	0.005
O70475	UDP-glucose 6-dehydrogenase (UGDH)	▼1.080	0.004
P24270	Catalase (CAT)	▼1.063	0.010
P62264	40S ribosomal protein S14 (RPS14)	▼1.054	0.011
P24472	Glutathione S-transferase A4 (GSTA4)	▼1.041	0.019
O55111	Desmoglein-2 (DSG2)	▼1.039	0.005
Q99JX4	Eukaryotic translation initiation factor 3 subunit M (EIF3M)	▼1.039	0.025

Supplementary Table 5) 42 Proteins were Uniquely Up-Regulated in DAPT & IWP-2 (Goblet/Enteroendocrine) organoids

Protein Identifier	Protein Name	FC (log2)	Q Value
Q9D7Z6	Calcium-activated chloride channel regulator 1 (CLCA1)	▲3.33	0.00347
P02772	Alpha-fetoprotein (AFP)	▲2.94	0.00866
P09240	Cholecystokinin (CCK)	▲2.83	0.01683
P20152	Vimentin (VIM)	▲2.48	0.01043
Q62395	Trefoil factor 3 (TFF3)	▲2.38	0.04095
P48756	Gastric inhibitory polypeptide (GIP)	▲2.36	0.01174
Q8K0C5	Zymogen granule membrane protein 16 (ZG16)	▲2.27	0.03616
P16110	Galectin-3 (LGALS3)	▲2.20	0.04314
Q99P58	Ras-related protein Rab-27B (RAB27B)	▲2.14	0.04034
Q8BND5	Sulfhydryl oxidase 1 (QSOX1)	▲2.09	0.0334
O88312	Anterior gradient protein 2 homolog (AGR2)	▲1.86	0.04257
P52624	Uridine phosphorylase 1 (UPP1)	▲1.83	0.02204
Q9JJX6	P2X purinoceptor 4 (P2RX4)	▲1.76	0.02562
Q91Y74	CMP-N-acetylneuraminate-beta-galactosamide-alpha-2,3-sialyltransferase 4 (ST3GAL4)	▲1.56	0.02204
P12791	Cytochrome P450 2B10 (CYP2B10)	▲1.55	0.01732
P03921	NADH-ubiquinone oxidoreductase chain 5 (MTND5)	▲1.50	0.03385
P97742	Carnitine O-palmitoyltransferase 1, liver isoform (CPT1A)	▲1.49	0.03385
A2ASS6	Titin (TTN)	▲1.48	0.02332
P56528	ADP-ribosyl cyclase 1 (CD38)	▲1.41	0.04424
P63239	Neuroendocrine convertase 1 (PCSK1)	▲1.37	0.03162
Q9D8V0	Minor histocompatibility antigen H13 (HM13)	▲1.35	0.00866
O88451	Retinol dehydrogenase 7 (RDH7)	▲1.30	0.03687
Q8R1M8	Mucosal pentraxin (MPTX1)	▲1.29	0.03487

* Differentiated cell markers of goblet/enteroendocrine cells

+ Proteins associated with secretion in other organs

Supplementary Table 5 Continued) 42 Proteins were Uniquely Up-Regulated in DAPT & IWP-2 (Goblet/Enteroendocrine) organoids

Protein Identifier	Protein Name	FC (log2)	Q Value
Q9CQX2	Cytochrome b5 type B (CYB5B)	▲1.26	0.04134
P35276	Ras-related protein Rab-3D (RAB3D)	▲1.25	0.02708
P17665	Cytochrome c oxidase subunit 7C, mitochondrial (COX7C)	▲1.23	0.04378
P56391	Cytochrome c oxidase subunit 6B1 (COX6B1)	▲1.22	0.02089
P17717	UDP-glucuronosyltransferase 2B17 (UGT2B17)	▲1.21	0.01349
Q8BW75	Amine oxidase [flavin-containing] B (MAOB)	▲1.2	0.04034
Q91W97	Putative hexokinase HKDC1 (HKDC1)	▲1.2	0.01349
Q61847	Meprin A subunit beta (MEP1B)	▲1.19	0.03891
Q64521	Glycerol-3-phosphate dehydrogenase, mitochondrial (GPD2)	▲1.18	0.04085
Q8BSY0	Aspartyl/asparaginyl beta-hydroxylase (ASPH)	▲1.17	0.0430
P46978	Dolichyl-diphosphooligosaccharide--protein glycosyltransferase subunit STT3A (STT3A)	▲1.17	0.03557
Q8BU33	Acetolactate synthase-like protein (ILVBL)	▲1.15	0.02104
Q9D8B4	NADH dehydrogenase [ubiquinone] 1 alpha subcomplex subunit 11 (NDUFA11)	▲1.14	0.03595
Q64464	Cytochrome P450 3A13 (CYP3A13)	▲1.10	0.02908
P58021	Transmembrane 9 superfamily member 2 (TM9SF2)	▲1.09	0.03595
Q8R0X7	Sphingosine-1-phosphate lyase 1 (SGPL1)	▲1.08	0.04633
O88428	Bifunctional 3'-phosphoadenosine 5'-phosphosulfate synthase 2 (PAPSS2)	▲1.03	0.03487
Q9Z2A7	Diacylglycerol O-acyltransferase 1 (DGAT1)	▲1.02	0.01387
Q791V5	Mitochondrial Carrier Homolog 2 (MTCH2)	▲1.00	0.0275

Supplementary Table 6) 120 Proteins were Uniquely Down-Regulated in DAPT & IWP-2 (Goblet/Enteroendocrine) organoids			
Protein Identifier	**Protein Name**	**FC (log2)**	**Q Value**
E9Q1P8	Interferon regulatory factor 2-binding protein 2 (IRF2BP2)	▼2.59	0.02204
Q9CT10	Ran-binding protein 3 (RANBP3)	▼2.30	0.02908
P62960	Nuclease-sensitive element-binding protein 1 (YBX1)	▼2.01	0.02540
Q99LT0	Protein dpy-30 homolog (DPY30)	▼2.01	0.01359
Q8BTI8	Serine/arginine repetitive matrix protein 2 (SRRM2)	▼1.95	0.02951
Q8BTM8	Filamin-A (FLNA)	▼1.88	0.00884
P46061	Ran GTPase-activating protein 1 (RANGAP1)	▼1.86	0.02936
Q60973	Histone-binding protein RBBP7 (RBBP7)	▼1.86	0.00347
Q80X41	Serine/threonine-protein kinase VRK1 (VRK1)	▼1.81	0.01349
Q8CGP1	Histone H2B type 1-K (HIST1H2BK)	▼1.77	0.02539
Q9CQF3	Cleavage and polyadenylation specificity factor subunit 5 (NUDT21)	▼1.77	0.04088
Q91VK1	Basic leucine zipper and W2 domain-containing protein 2 (BZW2)	▼1.76	0.03487
P51432	1-phosphatidylinositol 4,5-bisphosphate phosphodiesterase beta-3 (PLCB3)	▼1.75	0.00518
P84228	Histone H3.2 (HIST1H3B)	▼1.74	0.04314
P34884	Macrophage migration inhibitory factor (MIF)	▼1.73	0.03843
Q61233	Plastin-2 (LCP1)	▼1.71	0.02042
P30681	High mobility group protein B2 (HMGB2)	▼1.68	0.02180
P61327	Protein mago nashi homolog (MAGOH)	▼1.68	0.02204
Q8VCN5	Cystathionine gamma-lyase (CTH)	▼1.63	0.00854
Q01320	DNA topoisomerase 2-alpha (TOP2A)	▼1.61	0.02786
Q8CD91	SPARC-related modular calcium-binding protein 2 (SMOC2)	▼1.59	0.00866
O08583	THO complex subunit 4 (ALYREF)	▼1.58	0.04017
* Stem cell marker			

Supplementary Table 6 Continued) 120 Proteins were Uniquely Down-Regulated in DAPT & IWP-2 (Goblet/Enteroendocrine) organoids			
Protein Identifier	**Protein Name**	**FC (log2)**	**Q Value**
P31786	Acyl-CoA-binding protein (DBI)	▼1.56	0.03944
Q3UHX2	28 kDa heat- and acid-stable phosphoprotein (PDAP1)	▼1.54	0.04088
Q62189	U1 small nuclear ribonucleoprotein A (SNRPA)	▼1.54	0.00884
Q4VAA2	Protein CDV3 (CDV3)	▼1.52	0.04300
Q60829	Protein phosphatase 1 regulatory subunit 1B (PPP1R1B)	▼1.51	0.02153
Q60972	Histone-binding protein RBBP4 (RBBP4)	▼1.51	0.02332
P46664	Adenylosuccinate synthetase isozyme 2 (ADSS)	▼1.47	0.01349
P43275	Histone H1.1 (HIST1H1A)	▼1.47	0.02641
Q9CR41	Huntingtin-interacting protein K (HYPK)	▼1.47	0.00621
Q99020	Heterogeneous nuclear ribonucleoprotein A/B (HNRNPAB)	▼1.44	0.01551
P17742	Peptidyl-prolyl cis-trans isomerase A (PPIA)	▼1.43	0.04980
Q5SW19	Clustered mitochondria protein homolog (CLUH)	▼1.43	0.04660
Q64433	10 kDa heat shock protein, mitochondrial (HSPE1)	▼1.42	0.02180
P17751	Triosephosphate isomerase (TPI1)	▼1.41	0.02180
P17182	Alpha-enolase (ENO1)	▼1.41	0.01359
P06151	L-lactate dehydrogenase A chain (LDHA)	▼1.41	0.04604
P51859	Hepatoma-derived growth factor (HDGF)	▼1.39	0.03557
Q9DAW9	Calponin-3 (CNN3)	▼1.38	0.02933
Q99JR8	SWI/SNF-related matrix-associated actin-dependent regulator of chromatin subfamily D member 2 (SMARCD2)	▼1.37	0.04538
P99027	60S acidic ribosomal protein P2 (RPLP2)	▼1.37	0.04085
Q9DBJ1	Phosphoglycerate mutase 1 (PGAM1)	▼1.37	0.02344
P06745	Glucose-6-phosphate isomerase (GPI)	▼1.35	0.01732

Supplementary Table 6 Continued) 120 Proteins were Uniquely Down-Regulated in DAPT & IWP-2 (Goblet/Enteroendocrine) organoids			
Protein Identifier	**Protein Name**	**FC (log2)**	**Q Value**
Q8R4N0	Citrate lyase subunit beta-like protein, mitochondrial (CLYBl)	▼1.35	0.04085
O35226	26S proteasome non-ATPase regulatory subunit 4 (PSMD4)	▼1.34	0.04019
Q9CY58	Plasminogen activator inhibitor 1 RNA-binding protein (SERBP1)	▼1.33	0.01732
P70168	Importin subunit beta-1 (KPNB1)	▼1.33	0.01349
P97386	DNA ligase 3 (LIG3)	▼1.32	0.04758
P47791	Glutathione reductase, mitochondrial (GSR)	▼1.31	0.00989
Q9DCL9	Multifunctional protein ADE2 (PAICS)	▼1.31	0.00866
Q61133	Glutathione S-transferase theta-2 (GSTT2)	▼1.31	0.04034
P56959	RNA-binding protein FUS (FUS)	▼1.28	0.00866
Q8R2K1	Fucose mutarotase (FUOM)	▼1.28	0.02180
Q8CIG8	Protein arginine N-methyltransferase 5 (PRMT5)	▼1.26	0.02126
Q61029	Lamina-associated polypeptide 2, isoforms beta/delta/epsilon/gamma (TMPO)	▼1.26	0.04314
Q04447	Creatine kinase B-type (CKB)	▼1.25	0.01683
P62862	40S ribosomal protein S30 (FAU)	▼1.24	0.04088
P70698	CTP synthase 1 (CTPS1)	▼1.24	0.04701
P49717	DNA replication licensing factor MCM4 (MCM4)	▼1.23	0.02951
Q9CR16	Peptidyl-prolyl cis-trans isomerase D (PPID)	▼1.23	0.00866
P47968	Ribose-5-phosphate isomerase (RPIA)	▼1.22	0.03142
Q9Z2N8	Actin-like protein 6A (ACTL6A)	▼1.22	0.03687
P62075	Mitochondrial import inner membrane translocase subunit Tim13 (TIMM13)	▼1.21	0.03487
Q9R190	Metastasis-associated protein MTA2 (MTA2)	▼1.21	0.04085
P57016	Ladinin-1 (LAD1)	▼1.20	0.02126
P38647	Stress-70 protein, mitochondrial (HSPA9)	▼1.19	0.01551

Supplementary Table 6 Continued) 120 Proteins were Uniquely Down-Regulated in DAPT & IWP-2 (Goblet/Enteroendocrine) organoids			
Protein Identifier	**Protein Name**	**FC (log2)**	**Q Value**
Q9CQ65	S-methyl-5'-thioadenosine phosphorylase (MTAP)	▼1.19	0.03648
P61982	14-3-3 protein gamma (YWHAG)	▼1.19	0.03812
P11499	Heat shock protein HSP 90-beta (HSP90AB1)	▼1.18	0.04314
Q8BH04	Phosphoenolpyruvate carboxykinase [GTP], mitochondrial (PCK2)	▼1.18	0.00866
Q9JKB1	Ubiquitin carboxyl-terminal hydrolase isozyme L3 (UCHL3)	▼1.18	0.04538
Q8CGK3	Lon protease homolog, mitochondrial (LONP1)	▼1.17	0.02540
P62897	Cytochrome c, somatic (CYCS)	▼1.17	0.01315
Q9ERK4	Exportin-2 (CSE1L)	▼1.16	0.04701
Q9CZX8	40S ribosomal protein S19 (RPS19)	▼1.15	0.03595
P63242	Eukaryotic translation initiation factor 5A-1 (EIF5A)	▼1.15	0.02180
P49722	Proteasome subunit alpha type-2 (PSMA2)	▼1.15	0.02907
Q9R1P0	Proteasome subunit alpha type-4 (PSMA4)	▼1.15	0.03487
Q91YR9	Prostaglandin reductase 1 (PTGR1)	▼1.14	0.02922
Q99LX0	Protein DJ-1 (PARK7)	▼1.14	0.02584
P54728	UV excision repair protein RAD23 homolog B (RAD23B)	▼1.14	0.04727
P27612	Phospholipase A-2-activating protein (PLAA)	▼1.14	0.04065
Q9CWZ3	RNA-binding protein 8A (RBM8A)	▼1.13	0.04321
Q99KP6	Pre-mRNA-processing factor 19 (PRPF19)	▼1.13	0.04701
Q9QXG4	Acetyl-coenzyme A synthetase, cytoplasmic (ACSS2)	▼1.12	0.02126
P07901	Heat shock protein HSP 90-alpha (HSP90AA1)	▼1.11	0.02863
Q64737	Trifunctional purine biosynthetic protein adenosine-3 (GART)	▼1.10	0.01550
B1AZI6	THO complex subunit 2 (THOC2)	▼1.10	0.03616
P97855	Ras GTPase-activating protein-binding protein 1 (G3BP1)	▼1.10	0.02584

Supplementary Table 6 Continued) 120 Proteins were Uniquely Down-Regulated in DAPT & IWP-2 (Goblet/Enteroendocrine) organoids			
Protein Identifier	**Protein Name**	**FC (log2)**	**Q Value**
Q7TPV4	Myb-binding protein 1A (MYBBP1A)	▼1.09	0.02332
P80317	T-complex protein 1 subunit zeta (CCT6A)	▼1.09	0.02562
Q9CZ30	Obg-like ATPase 1 (OLA1)	▼1.09	0.01349
Q01768	Nucleoside diphosphate kinase B (NME2)	▼1.09	0.03462
Q9R1T2	SUMO-activating enzyme subunit 1 (SAE1)	▼1.09	0.04538
Q9CPU0	Lactoylglutathione lyase (GLO1)	▼1.08	0.01551
P70670	Nascent polypeptide-associated complex subunit alpha, muscle-specific form (NACA)	▼1.08	0.02951
Q60864	Stress-induced-phosphoprotein 1 (STIP1)	▼1.08	0.01315
Q8C1A5	Thimet oligopeptidase (THOP1)	▼1.08	0.00866
Q93092	Transaldolase (TALDO1)	▼1.07	0.04538
P28352	DNA-(apurinic or apyrimidinic site) lyase (APEX1)	▼1.07	0.04134
P26638	Serine--tRNA ligase, cytoplasmic (SARS)	▼1.06	0.03385
P70296	Phosphatidylethanolamine-binding protein 1 (PEBP1)	▼1.06	0.04300
Q9Z2U1	Proteasome subunit alpha type-5 (PSMA5)	▼1.06	0.03291
O08709	Peroxiredoxin-6 (PRDX6)	▼1.05	0.02483
Q9JHU9	Inositol-3-phosphate synthase 1 (ISYNA1)	▼1.05	0.04315
Q99L45	Eukaryotic translation initiation factor 2 subunit 2 (EIF2S2)	▼1.05	0.02180
P49312	Heterogeneous nuclear ribonucleoprotein A1 (HNRNPA1)	▼1.04	0.04134
P05202	Aspartate aminotransferase, mitochondrial (GOT2)	▼1.04	0.04314
P63017	Heat shock cognate 71 kDa protein (HSPA8)	▼1.04	0.04538
Q61316	Heat shock 70 kDa protein 4 (HSPA4)	▼1.03	0.03698
Q8BGD9	Eukaryotic translation initiation factor 4B (EIF4B)	▼1.03	0.03595
Q9CQI6	Coactosin-like protein (COTL1)	▼1.03	0.04085

Supplementary Table 6 Continued) 120 Proteins were Uniquely Down-Regulated in DAPT & IWP-2 (Goblet/Enteroendocrine) organoids			
Protein Identifier	**Protein Name**	**FC (log2)**	**Q Value**
Q9R1P3	Proteasome subunit beta type-2 (PSMB2)	▼1.03	0.03023
Q7TNC4	Putative RNA-binding protein Luc7-like 2 (LUC7L2)	▼1.02	0.04538
Q9WUP7	Ubiquitin carboxyl-terminal hydrolase isozyme L5 (UCHL5)	▼1.02	0.02708
P63085	Mitogen-activated protein kinase 1 (MAPK1)	▼1.01	0.04727
Q09143	High affinity cationic amino acid transporter 1 (SLC7A1)	▼1.00	0.04321
Q99MD9	Nuclear autoantigenic sperm protein (NASP)	▼1.00	0.02344
Q9EPL8	Importin-7 (IPO7)	▼1.00	0.03487

Supplementary Table 7) 18 proteins are up-regulated in both Paneth and Goblet cell enteroid cultures following drug skew treatment including several secretory proteins such as secretogranin-1 and chromogranin-a.

Protein Identifier	Protein Name	Q Value	P Value	Log2 Fold Change	Group
A2AFS3	UPF0577 protein KIAA1324 (KIAA1324)	0.01058	0.00059	▲1.361	Paneth
		0.00867	0.00023	▲1.532	Goblet
O55071	Cytochrome P450 2B19 (CYP2B19)	0.00942	0.00025	▲1.685	Paneth
		0.00578	0.00008	▲1.387	Goblet
P12791	Cytochrome P450 2B10 (CYP2B10)	0.00560	0.00011	▲1.523	Paneth
		0.01732	0.00173	▲1.554	Goblet
P16014	Secretogranin-1 (CHGB)	0.01048	0.00048	▲1.347	Paneth
		0.02089	0.00235	▲2.039	Goblet
P19324	Serpin H1 (SERPINH1)	0.04760	0.01641	▲1.737	Paneth
		0.01466	0.0415	▲2.846	Goblet
P21447	Multidrug resistance protein 1A (ABCB1A)	0.00942	0.00026	▲1.084	Paneth
		0.00101	0.00000	▲1.070	Goblet
P26339	Chromogranin-A (CHGA)	0.00050	0.00007	▲1.665	Paneth
		0.01350	0.00103	▲2.859	Goblet
P81117	Nucleobindin-2 (NUCB2)	0.01101	0.00076	▲2.432	Paneth
		0.00347	0.00004	▲1.675	Goblet
Q62425	NADH dehydrogenase [ubiquinone] 1 alpha subcomplex subunit 4 (NDUFA4)	0.00612	0.00013	▲1.336	Paneth
		0.01732	0.00175	▲1.510	Goblet
Q64133	Amine oxidase [flavin-containing] A (MAOA)	0.01095	0.00073	▲1.210	Paneth
		0.00578	0.00009	▲1.755	Goblet

Supplementary Table 7 Continued) 18 proteins are up-regulated in both Paneth and Goblet cell enteroid cultures following drug skew treatment including several secretory proteins such as secretogranin-1 and chromogranin-a.					
Protein Identifier	**Protein Name**	**Q Value**	**P Value**	**Log2 Fold Change**	**Group**
Q64458	Cytochrome P450 2C29 (CYP2C29)	0.00464	0.00007	▲2.069	Paneth
		0.03943	0.01246	▲1.441	Goblet
Q64459	Cytochrome P450 3A11 (CYP3A11)	0.00942	0.00027	▲2.103	Paneth
		0.00866	0.00035	▲2.810	Goblet
Q78KK3	Solute carrier family 22 member 18 (SLC22A18)	0.01151	0.00087	▲1.463	Paneth
		0.00866	0.000310	▲1.902	Goblet
Q80W94	2-acylglycerol O-acyltransferase 2 (MOGAT2)	0.01151	0.00086	▲1.406	Paneth
		0.01174	0.00065	▲1.259	Goblet
Q8BND5	Sulfhydryl oxidase 1 (QSOX1)	0.02204	0.00338	▲1.533	Paneth
		0.03340	0.00793	▲2.095	Goblet
Q8CFJ7	Solute carrier family 25 member 45 (SLC25A45)	0.01106	0.00058	▲1.329	Paneth
		0.02790	0.00567	▲1.078	Goblet
Q91VE0	Long-chain fatty acid transport protein 4 (SLC27A4)	0.03360	0.01094	▲1.407	Paneth
		0.02951	0.00656	▲1.372	Goblet
Q9R112	Sulfide:quinone oxidoreductase, mitochondrial (SQRDL)	0.02794	0.00536	▲1.137	Paneth
		0.00867	0.00033	▲1.710	Goblet

Supplementary Table 8) 45 proteins are down-regulated in both Paneth and Goblet cell enteroid cultures following drug skew treatment including stem cell marker olfactomedin-4 (olfm4).

Protein Identifier	Protein Name	Q Value	P Value	Log2 Fold Change	Group
E9Q1P8	Interferon regulatory factor 2-binding protein 2 (IRF2BP2)	0.01048 0.02204	0.00053 0.00331	▼1.920 ▼2.590	Paneth Goblet
O70435	Proteasome subunit alpha type-3 (PSMA3)	0.02726 0.01194	0.00510 0.00069	▼1.129 ▼1.400	Paneth Goblet
P05064	Fructose-bisphosphate aldolase A (ALDOA)	0.03113 0.02104	0.00734 0.00246	▼1.175 ▼1.450	Paneth Goblet
P09411	Phosphoglycerate kinase 1 (PGK1)	0.02909 0.02125	0.00626 0.00261	▼1.118 ▼1.220	Paneth Goblet
P17918	Proliferating cell nuclear antigen (PCNA)	0.01169 0.01359	0.00093 0.00110	▼1.326 ▼1.620	Paneth Goblet
P26350	Prothymosin alpha (PTMA)	0.01597 0.02126	0.01457 0.00266	▼1.271 ▼2.090	Paneth Goblet
P26645	Myristoylated alanine-rich C-kinase substrate (MARCKS)	0.04938 0.04980	0.01780 0.02249	▼1.034 ▼1.540	Paneth Goblet
P28656	Nucleosome assembly protein 1-like 1 (NAP1L1)	0.01086 0.00951	0.00063 0.00046	▼1.105 ▼1.630	Paneth Goblet
P34022	Ran-specific GTPase-activating protein (RANBP1)	0.01238 0.00866	0.00165 0.00025	▼1.194 ▼2.030	Paneth Goblet
P35979	60S ribosomal protein L12 (RPL12)	0.00429 0.04617	0.00304 0.01938	▼1.025 ▼1.110	Paneth Goblet

Supplementary Table 8 Continued) 45 proteins are down-regulated in both Paneth and Goblet cell enteroid cultures following drug skew treatment including stem cell marker olfactomedin-4 (olfm4).

Protein Identifier	Protein Name	Q Value	P Value	Log2 Fold Change	Group
P38647	Stress-70 protein, mitochondrial (HSPA9)	0.00392	0.00004	▼1.114	Paneth
		0.01551	0.00138	▼1.190	Goblet
P40142	Transketolase (TKT)	0.01260	0.00110	▼1.173	Paneth
		0.02562	0.00464	▼1.620	Goblet
P47915	60S ribosomal protein L29 (RPL29)	0.01380	0.00138	▼1.103	Paneth
		0.02562	0.00464	▼1.020	Goblet
P51432	1-phosphatidylinositol 4,5-bisphosphate phosphodiesterase beta-3 (PLCB3)	0.00782	0.00018	▼1.631	Paneth
		0.00518	0.00007	▼1.750	Goblet
P52293	Importin subunit alpha-1 (KPNA2)	0.02502	0.00422	▼1.167	Paneth
		0.03385	0.00836	▼1.360	Goblet
P54227	Stathmin (STMN1)	0.03089	0.00710	▼1.017	Paneth
		0.00347	0.00003	▼1.650	Goblet
P59325	Eukaryotic translation initiation factor 5 (EIF5)	0.01405	0.00146	▼1.257	Paneth
		0.02678	0.00503	▼1.080	Goblet
P61290	Proteasome activator complex subunit 3 (PSME3)	0.03228	0.00779	▼1.544	Paneth
		0.02180	0.02180	▼1.700	Goblet
P62960	Nuclease-sensitive element-binding protein 1 (YBX1)	0.00980	0.00041	▼1.608	Paneth
		0.02540	0.00436	▼2.010	Goblet
Q3UZZ4	Olfactomedin-4 (OLFM4)	0.00391	0.00003	▼2.138	Paneth
		0.00033	0.00006	▼2.340	Goblet
Q4VAA2	Protein CDV3 (CDV3)	0.01145	0.00081	▼1.616	Paneth
		0.04300	0.01575	▼1.520	Goblet

Supplementary Table 8 Continued) 45 proteins are down-regulated in both Paneth and Goblet cell enteroid cultures following drug skew treatment including stem cell marker olfactomedin-4 (olfm4).

Protein Identifier	Protein Name	Q Value	P Value	Log2 Fold Change	Group
Q5SW19	Clustered mitochondria protein homolog (CLUH)	0.01095	0.00069	▼1.728	Paneth
		0.04660	0.01981	▼1.430	Goblet
Q61074	Protein phosphatase 1G (PPM1G)	0.02502	0.00427	▼1.137	Paneth
		0.04701	0.20214	▼1.070	Goblet
Q61166	Microtubule-associated protein RP/EB family member 1 (MAPRE1)	0.02107	0.00319	▼1.354	Paneth
		0.02180	0.00308	▼1.530	Goblet
Q61753	D-3-phosphoglycerate dehydrogenase (PHGDH)	0.00391	0.00004	▼1.510	Paneth
		0.00866	0.00026	▼1.470	Goblet
Q62189	U1 small nuclear ribonucleoprotein A (SNRPA)	0.03413	0.00918	▼1.681	Paneth
		0.00884	0.00042	▼1.540	Goblet
Q62351	Transferrin receptor protein 1 (TFRC)	0.01163	0.00089	▼1.159	Paneth
		0.03166	0.00740	▼1.010	Goblet
Q64152	Transcription factor BTF3 (BTF3)	0.00278	0.00001	▼1.265	Paneth
		0.00866	0.00036	▼1.380	Goblet
Q7TMY8	E3 ubiquitin-protein ligase HUWE1 (HUWE1)	0.02055	0.00286	▼1.148	Paneth
		0.04859	0.02161	▼1.460	Goblet
Q8BG22	Calcium-activated chloride channel regulator 2 (CLCA2)	0.03455	0.00939	▼1.174	Paneth
		0.02104	0.00244	▼1.830	Goblet
Q8BHB9	Chloride intracellular channel protein 6 (CLIC6)	0.00464	0.00006	▼2.221	Paneth
		0.02855	0.00586	▼1.620	Goblet

Supplementary Table 8 Continued) 45 proteins are down-regulated in both Paneth and Goblet cell enteroid cultures following drug skew treatment including stem cell marker olfactomedin-4 (olfm4).

Protein Identifier	Description	Q Value	P Value	Log2 Fold Change	Group
Q8BW96	Calcium/calmodulin-dependent protein kinase type 1D (CAMK1D)	0.01169	0.00094	▼1.261	Paneth
		0.03915	0.01229	▼1.320	Goblet
Q8CAY6	Acetyl-CoA acetyltransferase, cytosolic (ACAT2)	0.013802	0.00142	▼1.501	Paneth
		0.01936	0.00203	▼1.640	Goblet
Q8CI11	Guanine nucleotide-binding protein-like 3 (GNL3)	0.013802	0.00141	▼1.108	Paneth
		0.00302	0.00001	▼1.370	Goblet
Q8K2Z4	Condensin complex subunit 1 (NCAPD2)	0.02830	0.00566	▼2.296	Paneth
		0.02178	0.00305	▼2.180	Goblet
Q8VCN5	Cystathionine gamma-lyase (CTH)	0.00955	0.00033	▼1.519	Paneth
		0.00854	0.00018	▼1.630	Goblet
Q99K85	Phosphoserine aminotransferase (PSAT1)	0.00942	0.00030	▼1.126	Paneth
		0.00101	0.00000	▼1.150	Goblet
Q99LP6	GrpE protein homolog 1, mitochondrial (GRPEL1)	0.03006	0.00652	▼1.224	Paneth
		0.03595	0.01024	▼1.780	Goblet
Q9CT10	Ran-binding protein 3 (RANBP3)	0.01202	0.00101	▼2.104	Paneth
		0.02908	0.00616	▼2.300	Goblet
Q9CY58	Plasminogen activator inhibitor 1 RNA-binding protein (SERBP1)	0.01048	0.00054	▼1.058	Paneth
		0.01732	0.00166	▼1.330	Goblet
Q9D2C2	Protein SAAL1 (SAAL1)	0.04176	0.01310	▼1.263	Paneth
		0.03444	0.00860	▼1.420	Goblet

Supplementary Table 8 Continued) 45 proteins are down-regulated in both Paneth and Goblet cell enteroid cultures following drug skew treatment including stem cell marker olfactomedin-4 (olfm4).

Protein Identifier	Description	Q Value	P Value	Log2 Fold Change	Group
Q9DB15	39S ribosomal protein L12, mitochondrial (MRPL12)	0.01095	0.00073	▼1.156	Paneth
		0.01174	0.00067	▼1.220	Goblet
Q9DCL9	Multifunctional protein ADE2 (PAICS)	0.03303	0.00853	▼1.094	Paneth
		0.00866	0.00036	▼1.310	Goblet
Q9ER72	Cysteine--tRNA ligase, cytoplasmic (CARS)	0.02060	0.00291	▼1.330	Paneth
		0.01349	0.00101	▼1.590	Goblet
Q9QYR9	Acyl-coenzyme A thioesterase 2, mitochondrial (ACOT2)	0.01145	0.00081	▼1.101	Paneth
		0.01501	0.00127	▼1.790	Goblet

Appendix B – Chapter 5 Supplementary Tables and Figures

Supplementary Table 9) 6 significantly differentially expressed proteins following 4 hr infection with T. gondii Veg					
Accession	**P Value**	**Log_2 fold change**	**Highest mean condition**	**Lowest mean condition**	**Description**
P11930	0.04265	▼2.41595	NI 4 Hour	Veg 4 Hour	Nucleoside diphosphate-linked moiety X motif 19 (NUDT19)
Q00623	0.04501	▼1.12368	NI 4 Hour	Veg 4 Hour	Apolipoprotein A-I (APOA1)
Q9CYR0	0.04862	▲2.74808	Veg 4 Hour	NI 4 Hour	Single-stranded DNA-binding protein, mitochondrial (SSBP1)
O09110	0.01667	▲1.42508	Veg 4 Hour	NI 4 Hour	Dual specificity mitogen-activated protein kinase kinase 3 (MAP2K3)
O70400	0.00892	▲1.12391	Veg 4 Hour	NI 4 Hour	PDZ and LIM domain protein 1 (PDLIM1)

Supplementary Table 10) 7 significantly differentially expressed proteins following 4 hr infection with T. gondii RH					
Accession	**P Value**	**Log_2 fold change**	**Highest mean condition**	**Lowest mean condition**	**Description**
Q8BND5	0.02580	▼3.14181	NI 4 Hour	RH 4 Hour	Sulfhydryl oxidase 1 (QSOX1)
P62274	0.01610	▼2.15817	NI 4 Hour	RH 4 Hour	40S ribosomal protein S29 (RPS29)
Q8VCA8	0.03860	▼1.23863	NI 4 Hour	RH 4 Hour	Secernin-2 (SCRN2)
P97370	0.00184	▼1.16750	NI 4 Hour	RH 4 Hour	Sodium/potassium-transporting ATPase subunit beta-3 (ATP1B3)
P48774	0.01928	▼1.02345	NI 4 Hour	RH 4 Hour	Glutathione S-transferase Mu 5 (GSTM5)
P42225	0.03891	▼1.00922	NI 4 Hour	RH 4 Hour	Signal transducer and activator of transcription 1 (STAT1)
Q9JLJ5	0.02658	▲1.63966	RH 4 Hour	NI 4 Hour	Elongation of very long chain fatty acids protein 1 (ELOVL1)

Supplementary Table 11) 22 significantly down-regulated host proteins following 40 hr infection with T. gondii Veg

Accession	P Value	Log_2 fold change	Highest mean condition	Lowest mean condition	Description
P11087	0.01317	▼2.56163	NI 40 Hours	Veg 40 Hours	Collagen alpha-1(I) chain (COL1A1)
Q80X41	0.03638	▼2.18669	NI 40 Hours	Veg 40 Hours	Serine/threonine-protein kinase VRK1 (VRK1)
Q61074	0.04837	▼2.13302	NI 40 Hours	Veg 40 Hours	Protein phosphatase 1G (PPM1G)
P43275	0.02111	▼1.90468	NI 40 Hours	Veg 40 Hours	Histone H1.1 (HIST1H1A)
Q3UZZ4	0.04411	▼1.77315	NI 40 Hours	Veg 40 Hours	Olfactomedin-4 (OLFM4)
Q8BXK9	0.03322	▼1.68080	NI 40 Hours	Veg 40 Hours	Chloride intracellular channel protein 5 (CLIC5)
Q5SW19	0.01377	▼1.61416	NI 40 Hours	Veg 40 Hours	Clustered mitochondria protein homolog (CLUH)
Q9D0G0	0.01831	▼1.35600	NI 40 Hours	Veg 40 Hours	28S ribosomal protein S30, mitochondrial (MRPS30)
Q922V4	0.02939	▼1.31806	NI 40 Hours	Veg 40 Hours	Pleiotropic regulator 1 (PLRG1)
Q8R0I0	0.04483	▼1.24742	NI 40 Hours	Veg 40 Hours	Angiotensin-converting enzyme 2 (ACE2)
Q9WU84	0.02672	▼1.23968	NI 40 Hours	Veg 40 Hours	Copper chaperone for superoxide dismutase (CCS)
Q64674	0.01018	▼1.23267	NI 40 Hours	Veg 40 Hours	Spermidine synthase (SRM)

Supplementary Table 11 Continued) 22 significantly down-regulated host proteins following 40 hr infection with T. gondii Veg					
Accession	**P Value**	**Max fold change**	**Highest mean condition**	**Lowest mean condition**	**Description**
P14115	0.02075	▼1.21573	NI 40 Hours	Veg 40 Hours	60S ribosomal protein L27a (RPL27A)
P24547	0.04824	▼1.12300	NI 40 Hours	Veg 40 Hours	Inosine-5'-monophosphate dehydrogenase 2 (IMPDH2)
B2RX12	0.00696	▼1.11254	NI 40 Hours	Veg 40 Hours	Canalicular multispecific organic anion transporter 2 (ABCC3)
O88696	0.04252	▼1.07706	NI 40 Hours	Veg 40 Hours	ATP-dependent Clp protease proteolytic subunit, mitochondrial (CLPP)
Q9CZ83	0.01364	▼1.06303	NI 40 Hours	Veg 40 Hours	39S ribosomal protein L55, mitochondrial (MRPL55)
Q8BW75	0.03560	▼1.06091	NI 40 Hours	Veg 40 Hours	Amine oxidase [flavin-containing] B (MAOB)
Q99LE6	0.03232	▼1.02520	NI 40 Hours	Veg 40 Hours	ATP-binding cassette sub-family F member 2 (ABCF2)
Q62189	0.03506	▼1.02444	NI 40 Hours	Veg 40 Hours	U1 small nuclear ribonucleoprotein A (SNRPA)
Q8VDN2	0.02246	▼1.01081	NI 40 Hours	Veg 40 Hours	Sodium/potassium-transporting ATPase subunit alpha-1 (ATP1A1)
Q8VCW8	0.04813	▼1.00025	NI 40 Hours	Veg 40 Hours	Acyl-CoA synthetase family member 2, mitochondrial (ACSF2)

Supplementary Table 12) 8 significantly up-regulated host proteins following 40 hr infection with T. gondii Veg					
Accession	**P Value**	**Log_2 fold change**	**Highest mean condition**	**Lowest mean condition**	**Description**
O35704	0.00651	▲1.91999	Veg 40 Hours	NI 40 Hours	Serine palmitoyltransferase 1 (SPTLC1)
Q91Z98	0.01299	▲1.65462	Veg 40 Hours	NI 40 Hours	Chitinase-like protein 4 (CHIL4)
P06728	0.01094	▲1.62479	Veg 40 Hours	NI 40 Hours	Apolipoprotein A-IV (APOA4)
Q00623	0.01880	▲1.51152	Veg 40 Hours	NI 40 Hours	Apolipoprotein A-I (APOA1)
Q9WU03	0.03012	▲1.27395	Veg 40 Hours	NI 40 Hours	Kunitz-type protease inhibitor 2 (SPINT2)
Q8VHF2	0.03767	▲1.11234	Veg 40 Hours	NI 40 Hours	Cadherin-related family member 5 (CDHR5)
O70439	0.02158	▲1.02476	Veg 40 Hours	NI 40 Hours	Syntaxin-7 (STX7)
Q8BHL4	0.02495	▲1.01771	Veg 40 Hours	NI 40 Hours	Retinoic acid-induced protein 3 (GPRC5A)

Supplementary Table 13) 14 significantly down-regulated proteins following 40 hr infection with T. gondii RH

Accession	P Value	Log_2 fold change	Highest mean condition	Lowest mean condition	Description
Q922V4	0.00185	▼2.19892	NI 40 Hours	RH 40 Hours	Pleiotropic regulator 1 (PLRG1)
Q7TMC8	0.01778	▼1.83413	NI 40 Hours	RH 40 Hours	L-fucose kinase (FUK)
Q8BTY2	0.01167	▼1.73019	NI 40 Hours	RH 40 Hours	Sodium bicarbonate cotransporter 3 (SLC4A7)
B2RX12	0.00254	▼1.60019	NI 40 Hours	RH 40 Hours	Canalicular multispecific organic anion transporter 2 (ABCC3)
Q8K1R3	0.00856	▼1.41438	NI 40 Hours	RH 40 Hours	Polyribonucleotide nucleotidyltransferase 1, mitochondrial (PNPT1)
Q62266	0.01148	▼1.25045	NI 40 Hours	RH 40 Hours	Cornifin-A (SPRR1A)
Q9D071	0.03740	▼1.17241	NI 40 Hours	RH 40 Hours	MMS19 nucleotide excision repair protein homolog (MMS19)
Q8BHG1	0.03159	▼1.15852	NI 40 Hours	RH 40 Hours	Nardilysin (NRDC)
P07744	0.00241	▼1.13182	NI 40 Hours	RH 40 Hours	Keratin, type II cytoskeletal 4 (KRT4)
Q9D024	0.02041	▼1.09104	NI 40 Hours	RH 40 Hours	Coiled-coil domain-containing protein 47 (CCDC47)
Q9CQQ8	0.03781	▼1.07536	NI 40 Hours	RH 40 Hours	U6 snRNA-associated Sm-like protein LSm7 (LSM7)
Q6PDQ2	0.04810	▼1.04153	NI 40 Hours	RH 40 Hours	Chromodomain-helicase-DNA-binding protein 4 (CHD4)

Supplementary Table 13 Continued) 14 significantly down-regulated proteins following 40 hr infection with T. gondii RH					
Accession	**P Value**	**Log_2 fold change**	**Highest mean condition**	**Lowest mean condition**	**Description**
P0C0S6; TGME49_300200	0.02624	▼1.02445	NI 40 Hours	RH 40 Hours	Histone H2A.Z (H2AFZ)
Q99LE6	0.02574	▼1.00862	NI 40 Hours	RH 40 Hours	ATP-binding cassette sub-family F member 2 (ABCF2)

Supplementary Table 14) 11 significantly up-regulated proteins following 40 hr infection with T. gondii RH

Accession	P Value	Log_2 fold change	Highest mean condition	Lowest mean condition	Description
Q00623	0.00999	▲2.43261	RH 40 Hours	NI 40 Hours	Apolipoprotein A-I (APOA1)
Q91Z98	0.01045	▲2.03083	RH 40 Hours	NI 40 Hours	Chitinase-like protein 4 (CHIL4)
Q6Q473	0.02806	▲1.87577	RH 40 Hours	NI 40 Hours	Calcium-activated chloride channel regulator 4A (CLCA4A)
P06728	0.04176	▲1.86969	RH 40 Hours	NI 40 Hours	Apolipoprotein A-IV (APOA4)
O70318	0.00781	▲1.30632	RH 40 Hours	NI 40 Hours	Band 4.1-like protein 2 (EPB41L2)
Q08652	0.02998	▲1.29869	RH 40 Hours	NI 40 Hours	Retinol-binding protein 2 (RBP2)
Q9R008	0.02756	▲1.22539	RH 40 Hours	NI 40 Hours	Mevalonate kinase (MVK)
Q8C1N8	0.00736	▲1.20815	RH 40 Hours	NI 40 Hours	Alpha-defensin 22 (DEFA22)
Q8K3X6	0.04827	▲1.12850	RH 40 Hours	NI 40 Hours	Ankyrin repeat and SAM domain-containing protein 4B (ANKS4B)
Q9D312	0.02482	▲1.05905	RH 40 Hours	NI 40 Hours	Keratin, type I cytoskeletal 20 (KRT20)
E9Q7P9	0.04759	▲1.03794	RH 40 Hours	NI 40 Hours	Cadherin-related family member 2 (CDHR2)

Supplementary Table 15) 6 significantly up- or down-regulated proteins shared between 40 hour Veg and RH incubated epithelial sheets

Accession	Description	P Value	Log_2 fold change	Condition
Q922V4	Pleiotropic regulator 1 (PLRG1)	0.02939	▼1.31806	Veg 40 Hours
		0.00185	▼2.19892	RH 40 Hours
B2RX12	Canalicular multispecific organic anion transporter 2 (ABCC3)	0.00696	▼1.11254	Veg 40 Hours
		0.00254	▼1.60019	RH 40 Hours
Q99LE6	ATP-binding cassette sub-family F member 2 (ABCF2)	0.03232	▼1.02520	Veg 40 Hours
		0.02574	▼1.00862	RH 40 Hours
Q91Z98	Chitinase-like protein 4 (CHIL4)	0.01299	▲1.65462	Veg 40 Hours
		0.01045	▲2.03083	RH 40 Hours
P06728	Apolipoprotein A-IV (APOA4)	0.01094	▲1.62479	Veg 40 Hours
		0.04176	▲1.86969	RH 40 Hours
Q00623	Apolipoprotein A-I (APOA1)	0.01880	▲1.51152	Veg 40 Hours
		0.00999	▲2.43261	RH 40 Hours